GL01314

Heat Flow

METHOD FOR DETERMINING TERRESTRIAL HEAT FLOW IN OIL FIELDS

HUMBERTO DA SILVA CARVALHO* AND VICTOR VACQUIER‡

A method of determining terrestrial heat flow in oil fields from bottom-hole temperatures, electric logs, and thermal conductivity of core samples has been tried in six Recôncavo Basin oil fields in Brazil. The average heat-flow value so determined for the Recôncavo Basin is 1.10 ± 0.15 microcalories/cm²sec. The technique can be used for calculating heat flow in continental areas elsewhere. A more significant outcome of our experiment is that it demonstrates an inexpensive method of obtaining terrestrial heat-flow values in the sedimentary basins of the world.

INTRODUCTION

Geothermal heat in all likelihood provides the energy for the motion of crustal plates on the earth, causing spreading of the ocean floor and the building of mountains on the continents (Le Pichon et al, 1973; Bullard, 1975). It also provides the conditions necessary for the maturation of hydrocarbons in sediments. From compilations of heat-flow values in igneous terrains it was shown by Polyak and Smirnov (1968) that heat flow decreases with the age of the basement rocks from an average of 1.7 microcalories per cm²sec (HFU) in the Cenozoic to 0.9 HFU in the Precambrian. From analysis of surface igneous rocks, we know that the heat-producing radioactive elements in igneous rocks have been concentrated toward the surface, probably by selective crystallization, for if the rest of the earth's mantle contained the same concentration of them, our planet would have melted long ago. The decrease of heat flow with the age of the basement rocks is interpreted as caused by the erosion of the surface layers, which are more radioactive than the rocks below. Where the basement rocks lie too deep for sampling, the age of the basement can be crudely estimated from the value of the heat flow.

Because of the slow speed of propagation of heat conduction, the present heat flow measured close to the earth's surface may reflect tectonic conditions in the geologic past. It is conceivable that subduction zones no longer present might show up in the distribution of heat flow, similar to what we now see in the seas of Japan and Okhotsk. This might be the case of the Borderland Province off the coast of southern California, where according to the chronology of lineated magnetic anomalies subduction stopped about 20 m.y. ago (Atwater and Menard, 1970), but where the heat flow is still high (Lee and Henyey, 1975).

On a larger scale, we now have an adequate coverage of heat flow in the world oceans, but on land the distribution of values is irregular and the only regularity observed so far is the previously mentioned dependence of heat flow on the age of plutonic rocks. A better heat-flow coverage of areas of geologic interest could be had from oil field data.

METHOD

In connection with an attempt to measure heat flow in Bolivia, R. E. Warren (personal communication, 1969) suggested a method for determining heat flow without making special measurements in wells. Heat flow is the product of the temperature gradient times the thermal conductivity. The former can be obtained from the bottom-hole temperatures (BHT). In an oil field, BHT's are usually measured at sufficiently different depths,

Manuscript received by the Editor May 24, 1976; revised manuscript received October 11, 1976.
* Universidade Federal da Bahia, Salvador, Bahia, Brazil.
‡ Scripps Institution of Oceanography, La Jolla, CA 92093

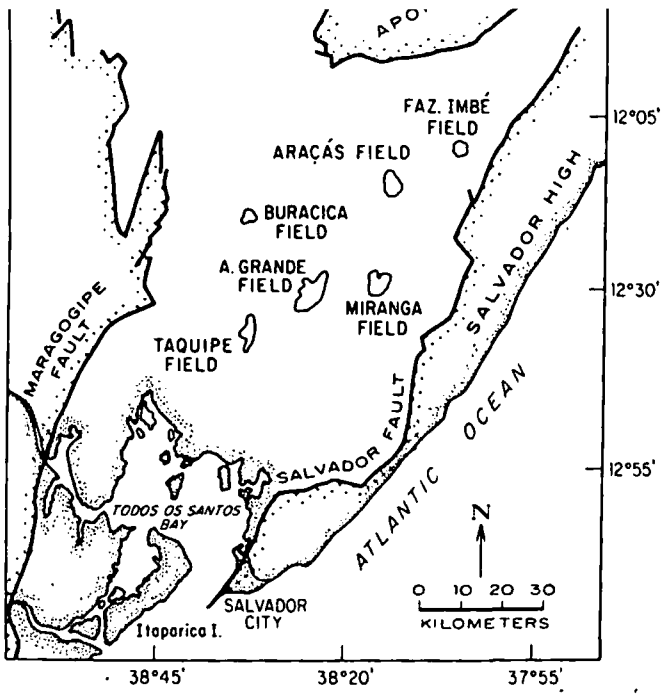

FIG. 1. Recôncavo Basin in eastern Brazil.

so that by averaging the measurements in, say, 100 wells, and by making appropriate corrections the temperature gradient can be determined to a precision of about 10 percent. Because of the current interest in formation temperature in connection with the maturation of hydrocarbons (e.g., Tissot et al, 1971), methods for correcting BHT's for the disturbing effects of drilling have been devised (Evans and Coleman, 1974; Dowdle and Cobb, 1974). These corrections have not been applied to our data.

The thermal conductivity was obtained from electric logs and measurements on core samples, in the depth interval where the BHT's were obtained. From well logs and inspection of the core samples, the specimens were classified into five categories: oil-saturated sandstone, water-saturated sandstone, shale, siltstone, and limestone. Cylindrical specimens 48.0 mm in diameter and about 38.1 mm long were drilled out of the original cores and impregnated under vacuum with oil or water at the core laboratory of Petrobrás. Thermal conductivity of the samples was measured in a divided-bar apparatus which was calibrated with combinations of discs of fused and crystalline quartz of the same dimensions as the rock specimens. The average temperature of the warm and cold ends of the divided bar was adjusted to the room temperature of the air-conditioned geophysical laboratory of applied geophys-

needed for the specimen to come sufficiently close to temperature equilibrium to about 20 minutes. Measurements on the same samples could be repeated to a few percent. The average thermal conductivity for each category was calculated. Measurements on specimens from all the fields were lumped together. It was assumed that the character of the stratigraphy was sufficiently uniform in the Recôncavo Basin to use these average values for the calculation of the effective thermal conductivity in the six oil fields for which we determined the temperature gradient. In each field, electric logs from a number of wells were selected for calculating the average thermal conductivity. On the electric log, the rock-type was obtained from the self-potential trace. The resistivity trace differentiated between oil- and water-saturated sandstone. Experience has shown that the petrology of the measured specimens should also be determined by laboratory methods. We determined the fraction of the total thickness of the interval covered by the BHT's in the field that is occupied by each category of rock. This value was then multiplied by the reciprocal of its average thermal conductivity. The reciprocal of the sum of

AGE		LITHOLOGY	THICKNESS (METERS)
TERTIARY	PLIOCENE	SANDSTONE	50
	MIOCENE	GREEN SHALE, THIN LIMESTONE	20
EARLY CRETACEOUS	APTIAN	SANDSTONE CONGLOMERATE	70
	WEALDEN	SANDSTONE RED SHALE GREEN & BLACK SHALE SANDSTONE	MAX. 2,800
		SHALE, SILTSTONE SANDSTONE LIMESTONE	MAX. 1,700
		GRAY & GREEN SHALE LENTICULAR SANDSTONE FRACTURED SHALE THIN LIMESTONE SANDSTONE	300 to 2,100
		GREEN & MARDON SHALE	MAX 180
JURASSIC (?)	PURBECKIAN (?)	SANDSTONE	MAX. 460
		RED SHALE SANDSTONE RED SHALE, EVAPORITE	MAX. 695

FIG. 2. Generalized stratigraphy of the Recôncavo Basin.

conductivity of the field was obtained by averaging the results obtained by this procedure for all of the chosen wells, from 8 to 20 per field.

GEOLOGIC SETTING

The geologic and generalized stratigraphy of the Recôncavo Basin are shown in Figures 1 and 2. The oil fields we worked with are shown in Figure 1. The basin is located on the Atlantic coast near the city of Salvador in the state of Bahía. It is an intracratonic half-graben filled with Jurassic, Cretaceous, and Tertiary sediments (Figure 1). The geographic limits of the basin are placed arbitrarily at the Precambrian Aporá salient on the north and at Itaparica Island to the south. On the west it is bounded by the Maragogipe fault system, and on the east by the Salvador horst block. The basin is characterized by a system of faulted blocks, the main faults striking northeast and northwest. Basement rock on all sides of the basin is early Precambrian migmatite and granulite of sedimentary and igneous origin (Ghignone and de Andrade, 1970).

DATA AND RESULTS

Figures 3 through 8 present the BHT's plotted against depth. The points on these graphs are represented by the center of single-digit numbers indicating the number of wells yielding the plotted temperature at the same depth. Thus a "4" means four different wells gave the same temperature at the same depth at the center of the digit 4. Some wells had BHT's recorded at two or more different depths, but in most wells only one temperature was measured. The points on Figures 3–8 scatter enough to produce the rather large standard deviations in the fourth column of Table 1. In future work of this kind, an attempt should be

Dowdle and Cobb, 1974; Bullard, 1947). Drilling tends to lower the measured temperature in the deeper horizons, thus decreasing the measured temperature gradient with respect to the true gradient. Therefore, in our data, Araçás, Fazenda Imbé, and Miranga, the fields where wells reach down to 3 km should have given lower gradients than the other three fields. The numbers of the second column of Table 1 do not substantiate this expectation but seem unrelated to the depth range.

The thermal conductivity measurements on cores were carried out by the divided-bar thermal conductivity apparatus, as described previously under "Method". In Table 2, the third column gives the mean values for the conductivity of the five rock-types of the stratigraphic section. The measurements are much more accurate than the classification into rock-types, which is crude. Occasionally the well log, the mineralogical examination with hand lens, and the conductivity value failed to agree and the sample had to be discarded. The small number of shale specimens is unfortunate, but that was all we could get.

Returning now to Table 1, the fifth column gives the mean conductivity calculated as previously explained under "Method" (above), from the average stratigraphy given by the number of well logs in column 6 and the conductivities of the third column of Table 2. The small spread of the numbers indicates that the lithology of the six fields is close to being the same. The standard deviation of these numbers (column 7) also shows good internal consistency but does not give the accuracy of the conductivity determination because of the uncertainties of the values in Table 2. These uncertainties would thus affect the conductivity values of column 5 by almost the same multiplying factor.

Table 1. Summary of gradient, conductivity, and heat flow in the Recôncavo Basin.[1]

Field	Gradient, °C/km	No. of BHT	Standard deviation, °C/km	Mean conductivity, cal/cm sec °C	No. of logs	Standard deviation, cal/cm sec °C	Heat flow	Standard deviation
							cal/cm² sec	
Araçàs	20.4	149	3.0	5.94×10^{-3}	15	0.06×10^{-3}	1.21×10^{-6}	0.18×10^{-6}
Àgua Grande	19.6	231	3.1	5.78	20	0.08	1.13	0.18
Buracica	15.0	138	3.1	5.81	10	0.06	0.87	0.18
Fazenda Imbè	21.3	42	4.6	5.71	8	0.06	1.22	0.26
Miranga	15.6	235	3.2	5.82	20	0.08	0.91	0.19
Taquipe	21.4	123	2.7	5.86	8	0.08	1.25	0.15

[1] Average heat flow: 1.10 ± 0.15 microcal/cm² sec.

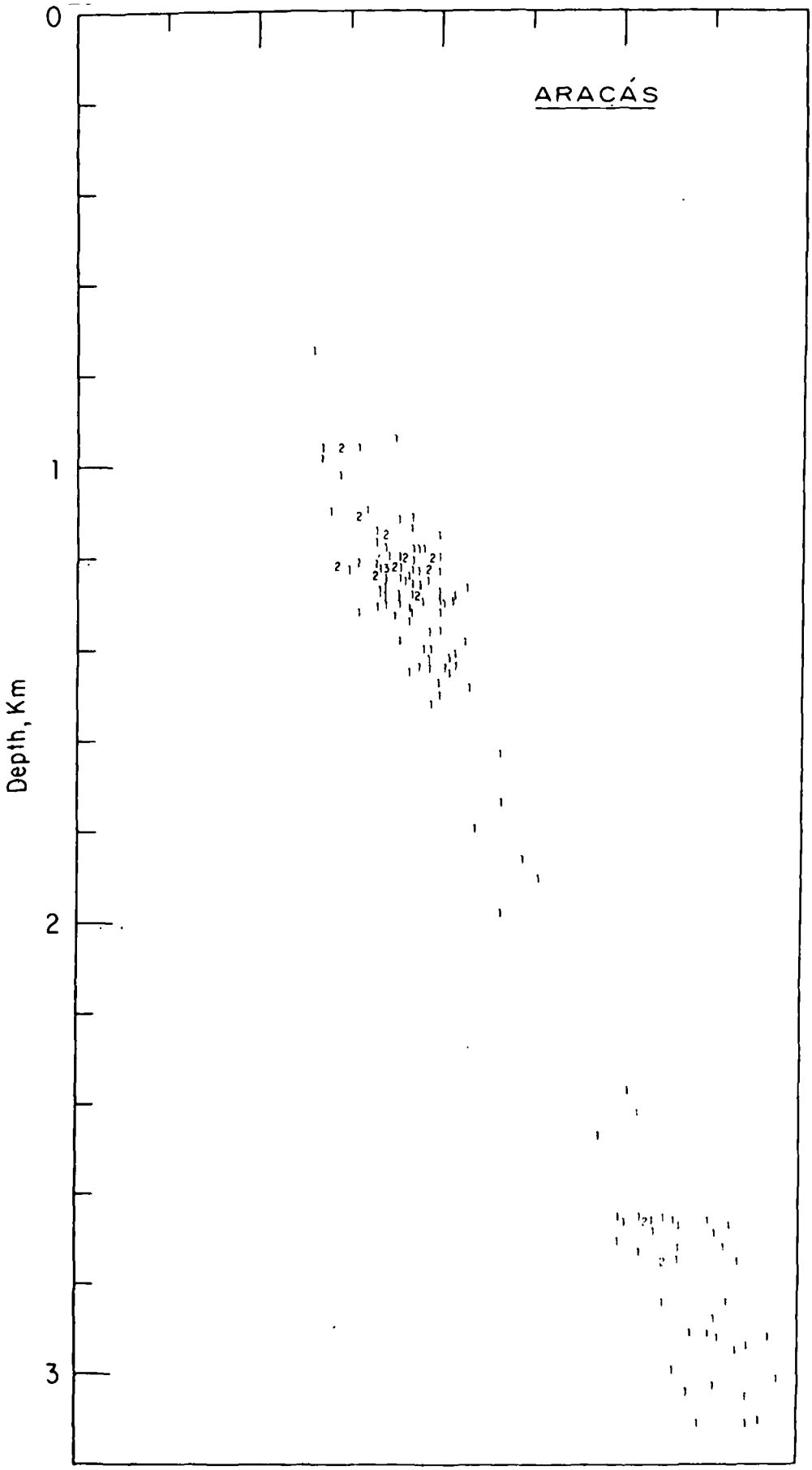

FIG. 3. Bottom-hole temperatures plotted against depth in Araçás field.

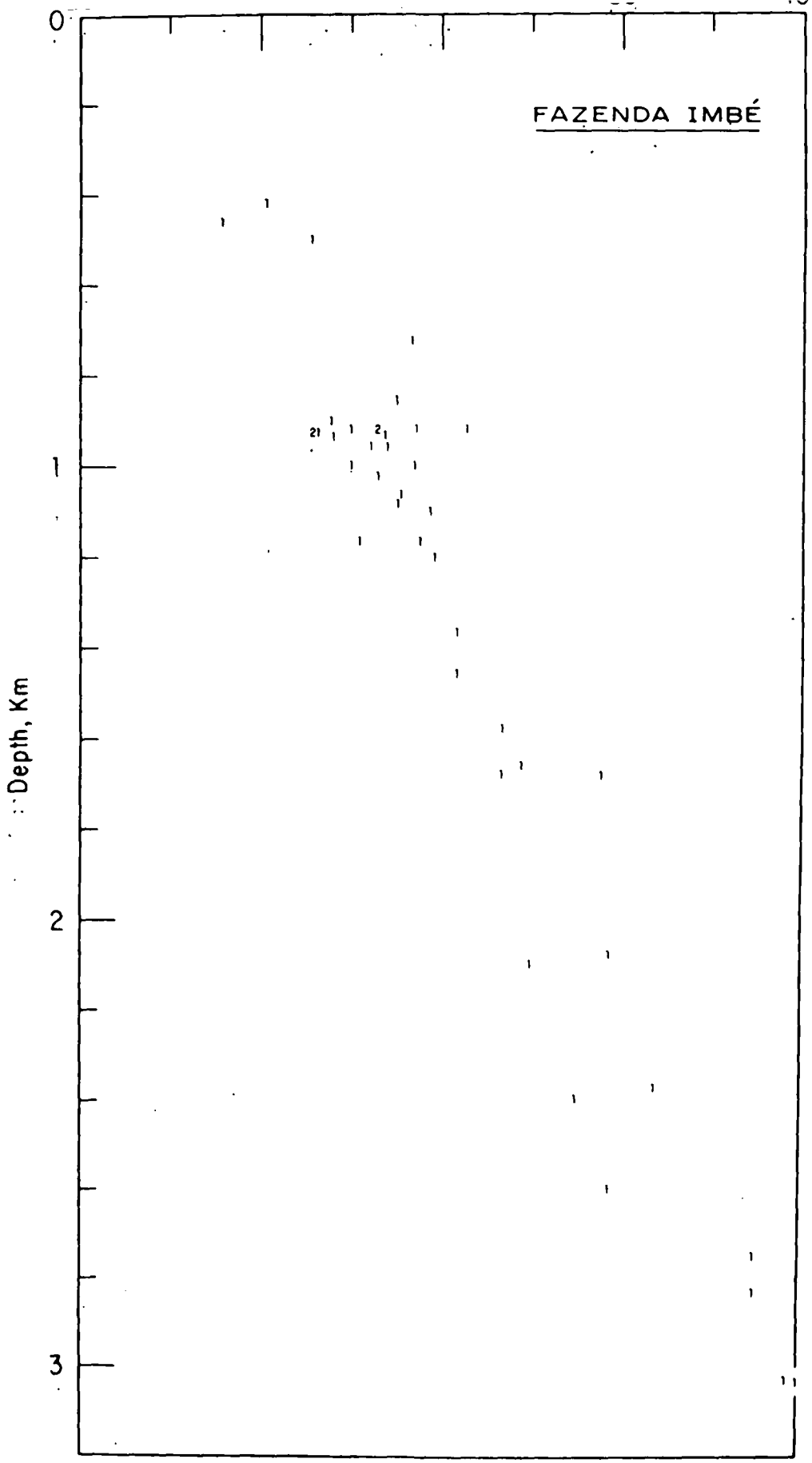

FIG. 4. Bottom-hole temperatures plotted against depth in Fazenda Imbé field.

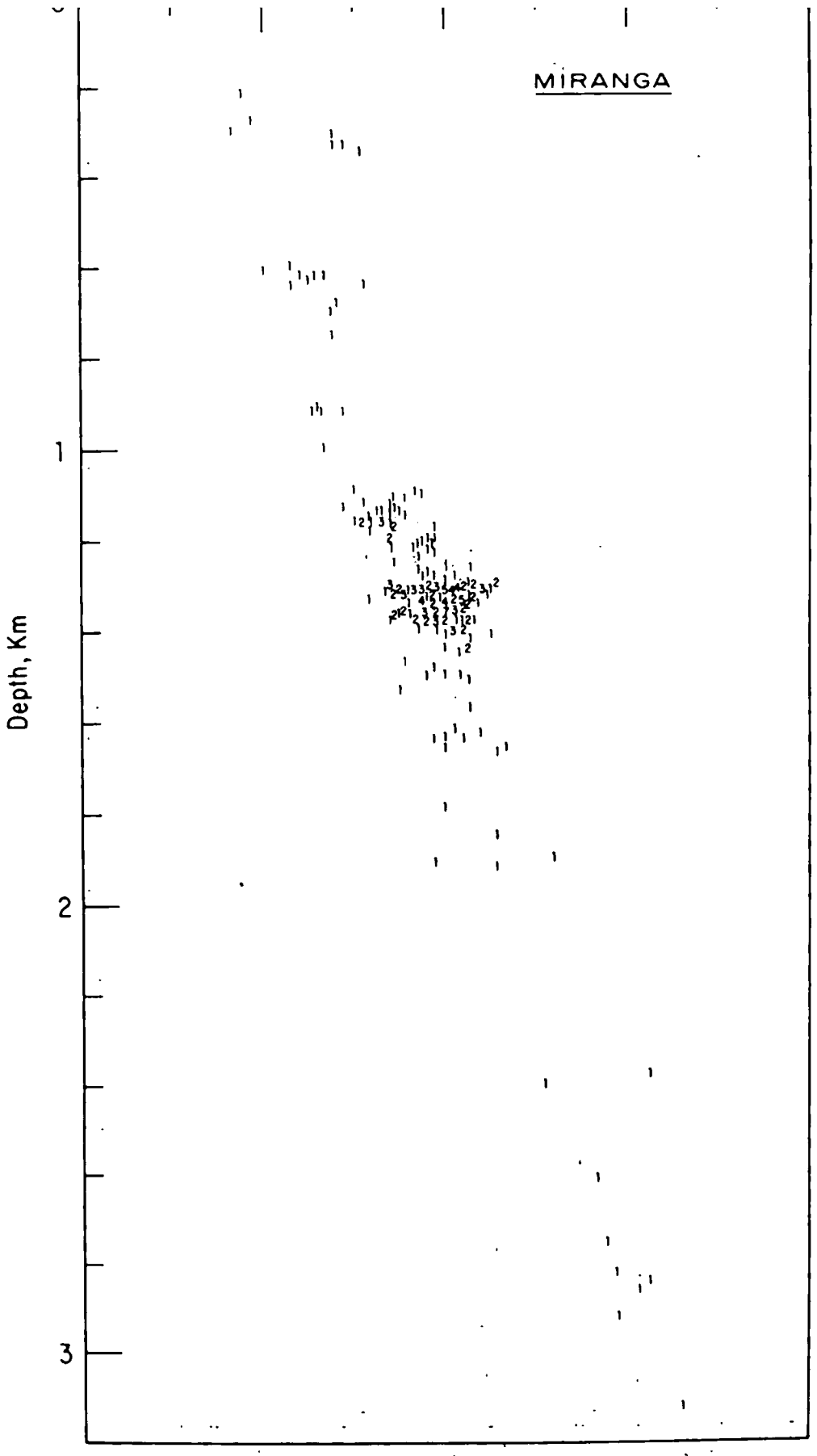

FIG. 5. Bottom-hole temperatures plotted against depth in Miranga field.

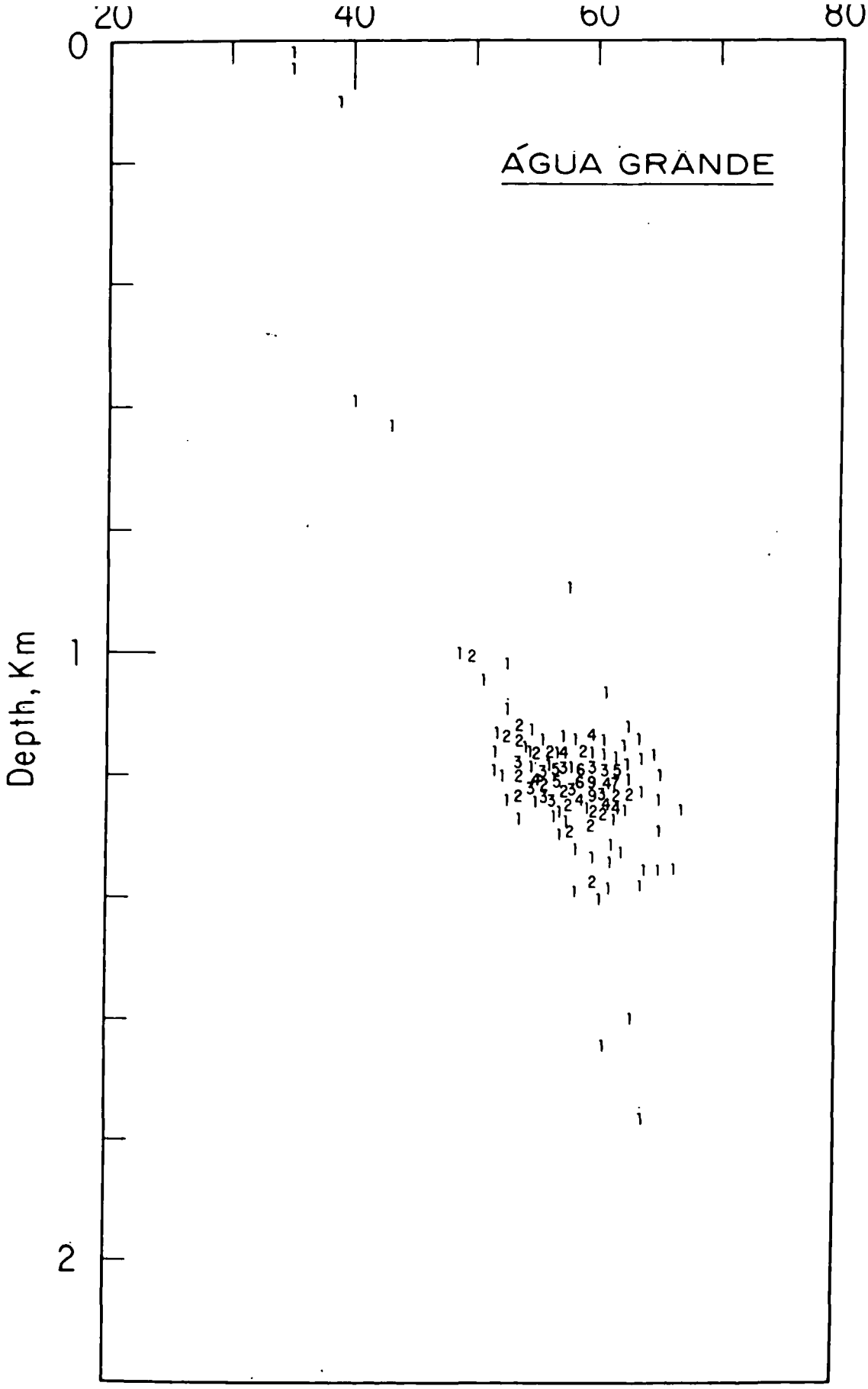

FIG. 6. Bottom-hole temperatures plotted against depth in Água Grande field.

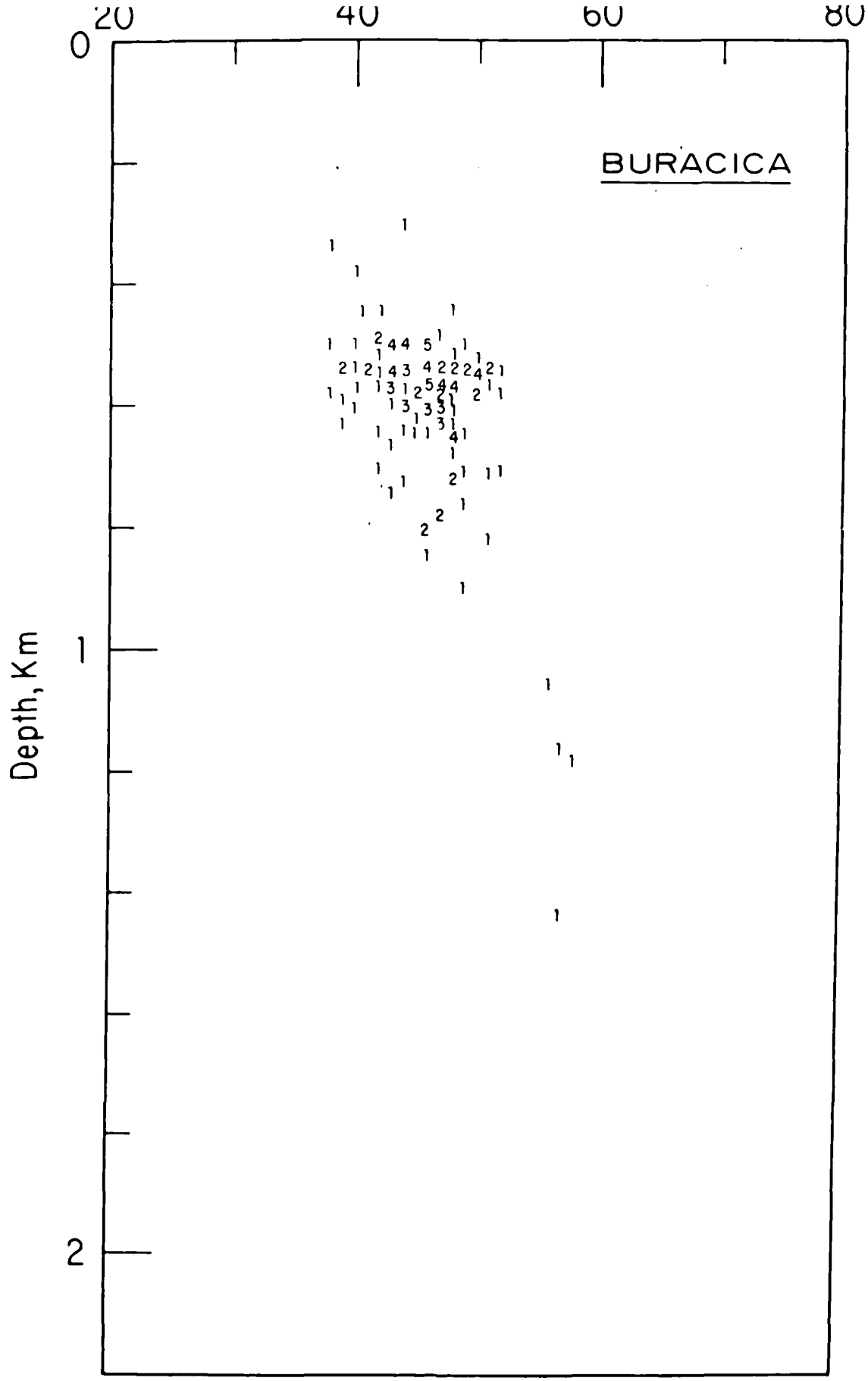

FIG. 7. Bottom-hole temperatures plotted against depth in Buracica field.

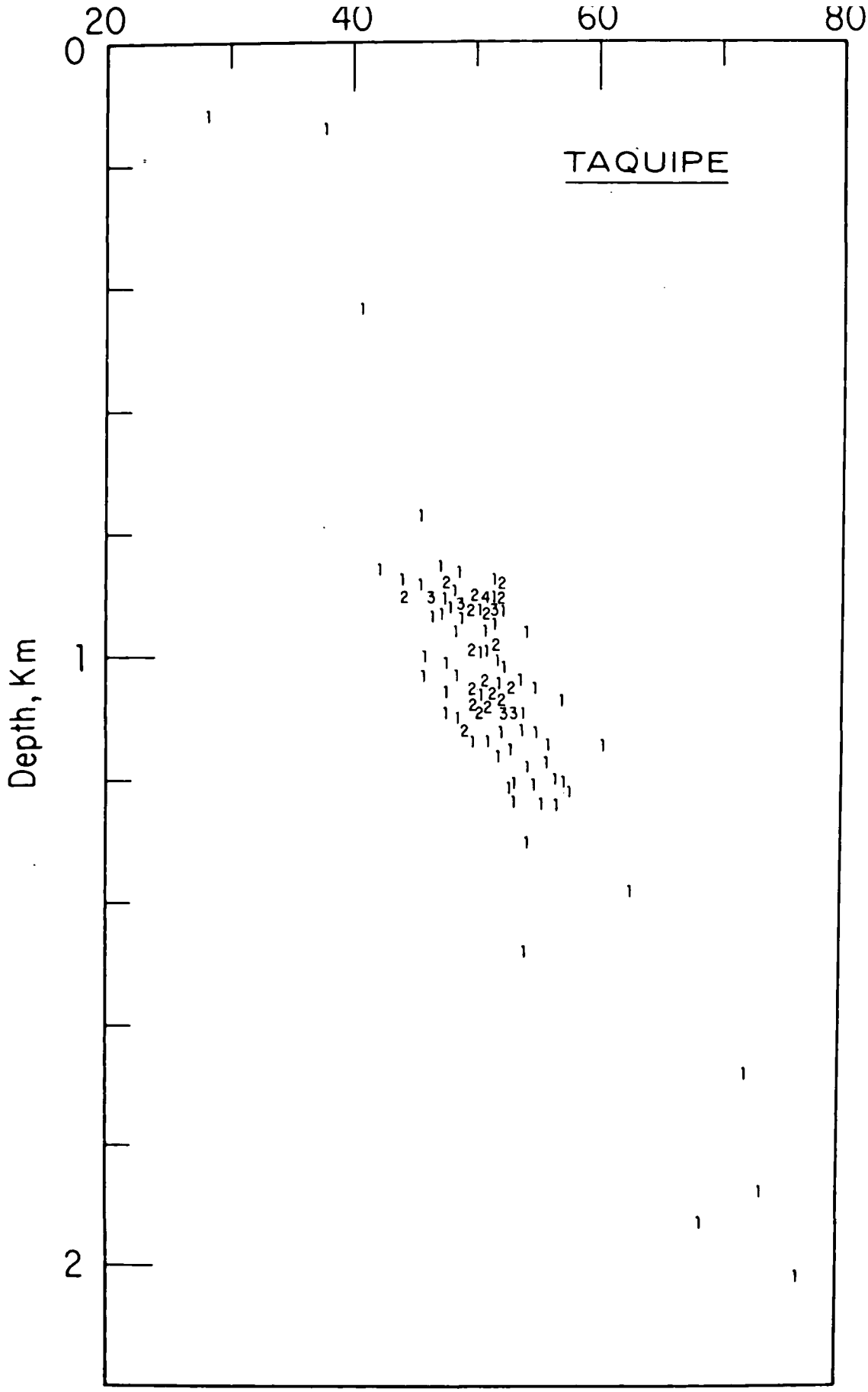

FIG. 8. Bottom-hole temperatures plotted against depth in Taquipe field.

Sandstone	water	7.98×10^{-3}	20	1.83×10^{-3}
Sandstone	oil	6.58	35	1.26
Siltstone	—	5.76	20	0.98
Shale	—	5.22	6	**
Limestone	—	6.00*	—	—

* Estimated.
** Range: 4.47 – 5.06 – 7.84 – 4.27 – 4.58 – 5.11.

The differences in the heat-flow values for the individual fields are mainly due to the values of the temperature gradient, which may be related to the depth to the basement and to shale diapirs in Recôncavo Basin. The low value of heat flow we obtained for the Miranga field may be due to a combination of both of these causes. The field is located on a thick shale diapir in a basement depression. Ghignone and de Andrade (1969) in their Figure 4 (giving isopach contours on the top of Lower Ilhas and Candeias formations) show Miranga field on the 2500 m contour, whereas the other fields except Buracica lie between the 1000 m and the 1500 m contours and, in general, have higher values of heat flow. Unfortunately the value for Buracica is discordant. Presumably it should give the highest heat flow value because it lies within the 500 m contour on top of the Lower Ilhas and Candeias formations. Actually, its value came out the lowest of the six. The poor distribution of BHT's and depth for this field (Figure 7) may be responsible for this discrepancy.

The mean value of the heat flow we got in the Recôncavo Basin is $1.10 \pm 0.15 \cdot 10^{-6}$cal/cm^{2}sec. It is a reasonable value for the floor of the basin which must have subsided in the Jurassic when the South Atlantic Ocean began to form. A more significant outcome of our experiment is that it demonstrates an inexpensive method of obtaining terrestrial heat-flow values in the sedimentary basins of the world.

ACKNOWLEDGMENTS

We thank the Management of Petrobrás for the use of their computer facility and core laboratory. We are also grateful to Petrobrás geologist Luís Passos for guiding us through the files, the core warehouses, as well as the geology of the fields, and Hernani Chavez for processing the temperature data through the computer. We thank Prof. Dr. Carlos A. Dias, coordinator of the Programa de Pesquisa e Posgraduação em Geofísica, Universidade Federal da Bahía, Salvador, Bahía, Brazil, who invited one of us (V. V.) to spend nine months of his sabbatical leave in 1973–74 at the University of Bahía. This work was financed entirely by the Conselho Nacional de Desenvolvimento Cientifico e Technológico, CNPq, Brazil.

REFERENCES

Atwater, T., and Menard, H. W., 1970, Magnetic lineations in the NE Pacific: Earth Plan. Sci. Lett., v. 7, p. 445–450.

Bullard E. C., 1947, The time necessary for a bore hole to attain temperature equilibrium: Roy. Astron. Soc. Geophys. Suppl., v. 5, p. 125–130.

——— 1975, Overview of plate tectonics, *in* Petroleum and global tectonics: A. G. Fischer and S. Judson Eds., Princeton Univ. Press, p. 16.

Dowdle, W. L., and Cobb, W. M., 1974, Estimatiion of static formation temperatures from well logs: Paper no. SPE5036, SPE AIME.

Evans, T. R., and Coleman, N. C., 1974, North Sea geothermal gradients: Nature, v. 247, p. 28–30.

Ghignone, J. I., and de Andrade, G., 1970, General geology and major oil fields of the Reconcavo Basin, Brazil, *in* Geology of giant petroleum fields: M. T. Halbouty, Ed., AAPG Mem. 14, p. 337–358.

Lee, T., and Henyey, T. L., 1975, Heat flow through the Southern California borderland: J. Geophys. Res., v. 80, p. 3733–3743.

Le Pichon, X., Francheteau, J., and Bonnin, J., 1973, Plate tectonics: Amsterdam, Elsevier, p. 18.

Polyak, B. G., and Smirnov, Ya. B., 1968, Relationship between terrestrial heat flow and the tectonics of continents: Geotectonics, p. 205–213.

Tissot, B., Califet-Debyser, Y., Deroo, G., and Oudin, J. L., 1971, Origin and evolution of hydrocarbons in early Toarcian shales, Paris Basin, France: AAPG Bull., v. 55, p. 2177–2193.

GEOPHYSICS, VOL. 49, NO. 4 (APRIL 1984); P. 453–466, 11 FIGS., 2 TABLES.

Heat flow in the Uinta Basin determined from bottom hole temperature (BHT) data

David S. Chapman*, T. H. Keho*, Michael S. Bauer*, and M. Dane Picard*

ABSTRACT

The thermal resistance (or Bullard) method is used to judge the utility of petroleum well bottom-hole temperature data in determining surface heat flow and subsurface temperature patterns in a sedimentary basin. Thermal resistance, defined as the quotient of a depth parameter Δz and thermal conductivity k, governs subsurface temperatures as follows:

$$T_B = T_0 + q_0 \sum_{z=0}^{B} \left(\frac{\Delta z}{k}\right),$$

where T_B is the temperature at depth $z = B$, T_0 is the surface temperature, q_0 is surface heat flow, and the thermal resistance ($\Delta z/k$) is summed for all rock units between the surface and depth B. In practice, bottom-hole and surface temperatures are combined with a measured or estimated thermal conductivity profile to determine the surface heat flow q_0 which, in turn, is used for all consequent subsurface temperature computations.

The method has been applied to the Tertiary Uinta Basin, northeastern Utah, a basin of intermediate geologic complexity—simple structure but complex facies relationships—where considerable well data are available. Bottom-hole temperatures were obtained for 97 selected wells where multiple well logs permitted correction of temperatures for drilling effects. Thermal conductivity values, determined for 852 samples from 5 representative wells varying in depth from 670 to 5180 m, together with available geologic data were used to produce conductivity maps for each formation. These maps show intraformational variations across the basin that are associated with lateral facies changes. Formation thicknesses needed for the thermal resistance summation were obtained by utilizing approximately 2000 wells in the WEXPRO Petroleum Information file. Computations were facilitated by describing all formation contacts as fourth-order polynomial surfaces.

Average geothermal gradient and heat flow for the Uinta Basin are 25°C km^{-1} and 57 mW/m^2, respectively. Heat flow appears to decrease systematically from 65 to 40 mWm^{-2} from the Duchesne River northward toward the south flank of the Uinta Mountains. This decrease may be the result of refraction of heat into the highly conductive quartzose Precambrian Uinta Mountain Group. More likely, however, it is related to groundwater recharge in late Paleozoic and Mesozoic sandstone and limestone beds that flank the south side of the Uintas. Heat flow values determined for the southeast portion of the basin show some scatter about a mean value of 64 mWm^{-2} but no systematic variation.

INTRODUCTION

Bottom-hole temperatures (BHT) obtained from routine geophysical logs of petroleum wells comprise, for good reasons, a little used data set in geothermal and heat flow studies. The bottom-hole temperature (and consequently the thermal gradient), and the thermal conductivity profile, both required for heat flow determinations and reasonable interpretation of temperature data, are unobtainable with confidence from routine geophysical logs of the wells taken soon after the completion of drilling. Even if accurate temperature measurements are made (which generally is unnecessary in petroleum well logging), temperatures in and around wells are perturbed by the drilling process, principally by the circulation of mud at a temperature that differs from in-situ conditions. There is seldom sufficient information to make accurate corrections for the perturbation.

Manuscript received by the Editor March, 1983; revised manuscript received September, 1983.
*Department of Geology and Geophysics, University of Utah, 717 W. C. Browning Bldg., Salt Lake City, UT 84112-1183.

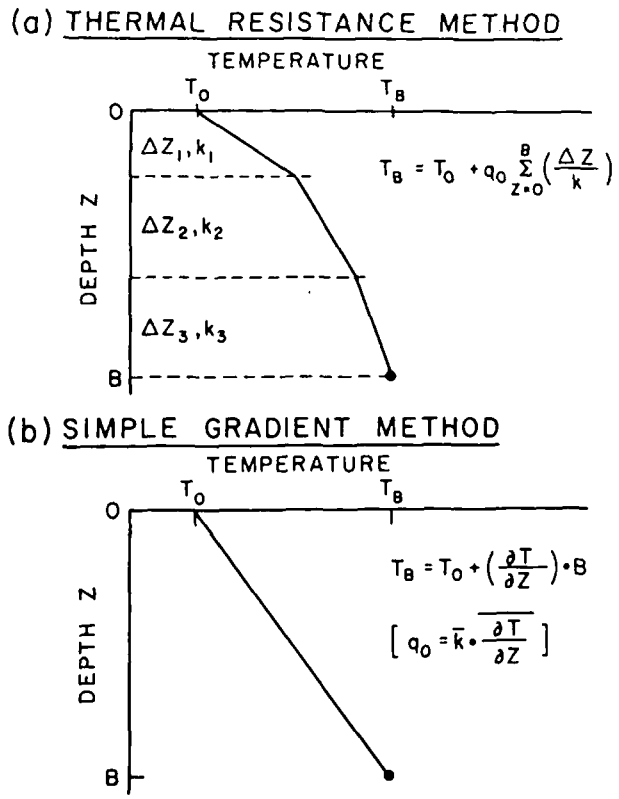

FIG. 1. Schematic representation of two methods for processing BHT data from oil and gas wells: (a) thermal resistance method and (b) simple gradient method. Symbols: T_0 surface temperature, T_B bottom-hole temperature, q_0 surface heat flow, z depth, k thermal conductivity.

Assigning thermal conductivity values for any particular drill hole is more problematic. Thermal conductivities are not routinely measured and general predictive relationships between conductivity and parameters determined in routine geophysical logs are not always reliable (Goss, 1974; Vacquier, 1981). Thus, spatial variations in thermal gradients deduced from BHTs may be either spurious because of errors in the temperature data or, in the case of the gradients being fortuitously correct, the ambiguity in interpreting gradient patterns in terms of tectonic or hydrologic processes rather than conductivity variations will be unresolved.

Despite these difficulties, it is possible, especially upon application of temperature corrections and conductivity measurements, to obtain useful information from BHT data in individual cases. Pertinent studies are Evans and Tammemagi (1974) on the Somalian Horn and Sudan; Evans and Coleman (1974) on North Sea oil fields; Carvalho and Vacquier (1977) on the Reconcavo Basin of Brazil; Carvalho et al (1980) on central Sumatra; Hodge et al (1980) on upper New York State; and Reiter and Tovar (1982) on northern Chihuahua, Mexico. Unfortunately, the most comprehensive study of bottom-hole temperatures in the coterminous USA (AAPG Geothermal Survey of North America, 1976) ignores thermal conductivity effects which makes their thermal gradient maps of limited use.

In this paper we use the thermal resistance method pioneered by Bullard (1939) to determine and evaluate lateral heat flow variations within a single basin and to produce subsurface temperature maps within the basin. Our method does not totally alleviate problems that arise from nonequilibrium temperature logs and incomplete description of thermal conductivity patterns, but it does have as a basis corrected temperature data and measured thermal conductivity values. Further, we do not restrict individual oil and gas fields to a homogenized single gradient and single conductivity function as was done by Carvalho and Vacquier (1977), but instead we allow for lateral changes in several parameters including surface temperature, thermal conductivity, and heat flow. The effects of porosity and temperature on the formation thermal conductivity and hence thermal resistance are also included. The Tertiary Uinta Basin of northeastern Utah is chosen to illustrate our thermal resistance method because of its intermediate geologic complexity, i.e., simple structure but complex facies patterns, and the abundance of petroleum well data.

Thermal resistance method

Thermal resistance is the quotient of a thickness Δz and a characteristic thermal conductivity k. In the case of negligible heat production and fluid movement, subsurface temperatures in horizontally layered, isotropic earth are governed by the thermal resistance of a stratigraphic section in the following way (Bullard, 1939; and Figure 1a):

$$T_B = T_0 + q_0 \sum_{z=0}^{B} \left(\frac{\Delta z}{k}\right), \qquad (1)$$

where T_B is the temperature at depth $z = B$, T_0 is the surface temperature at $z = 0$, q_0 is surface heat flow, and the thermal resistance $(\Delta z/k)$ is summed for all rock units between the surface and depth B. This equation, or the integral form of it, is commonly used in heat flow data reduction, and heat flow (q_0) is calculated as the slope of the plot of consecutive values of T_B versus the summed thermal resistance to the measurement depth. The method is especially suitable when boreholes intersect discrete and horizontal rock units.

The thermal resistance method, as we use it for analysis of heat flow and subsurface temperatures in a sedimentary basin, comprises several steps. First, a set of bottom-hole temperatures (T_B) are compiled and corrected, if possible, for drilling disturbances. The wells from which temperatures are taken should represent a wide geographic distribution throughout the basin. This is not always possible, however, since wells are drilled preferentially in favored localities. Second, thermal conductivity values must be measured for all representative rocks in the basin: drill chips, core samples, and outcrop samples can be used. Laboratory results for conductivities must be modified for effects of temperature, porosity, and possibly anisotropy to simulate in-situ conditions. Temperature-depth profiles and thermal conductivity-depth profiles are allowed to vary with lateral position in the basin. The third step involves summing the thermal resistance at each well from the surface to the depth of the BHT observation and solving for the site heat flow using equation (1).

Ideally, the thermal resistance sum is calculated individually for each well using conductivities and thicknesses for all rock units intersected (Carvalho et al, 1980). This individual well treatment is cumbersome, however, for large numbers of wells. An automatic processing procedure is useful if the basin structure is sufficiently simple and well known so that contacts

between rock units and conductivity variations are describable by simple functions. In the Uinta Basin, formation contact depths are adequately described in terms of low-order polynomial surfaces. The modified form of equation (1) used to calculate individual site heat flow values is

$$q_0(x, y) = [T_{B,\infty}(x, y) - T_0(x, y, h)] \Big/ \sum_{z=0}^{B} \frac{\Delta z(x, y)}{k(x, y, z, \phi, T)}, \tag{2}$$

ϕ being the depth and lithology dependent porosity. For each well the latitude and longitude (equivalently x and y), well collar elevation h, corrected bottom-hole temperature $T_{B,\infty}$, and corresponding depth $z = B$ are stored in a data file. Surface temperature as a function of position, and elevation $T_0(x, y, h)$, rock unit thickness $\Delta z(x, y)$ as a function of position, and thermal conductivity $k(x, y, z, \phi, T)$ as a function of position and depth are calculated from empirical functions. Once surface heat flow values are determined from equation (2) for the wells sampled, and the heat flow field is suitably smoothed, subsurface temperature maps can be calculated by a direct application of the thermal resistance method. Principal features of this procedure as applied to the Unita Basin are given in Table 1; details are discussed later in the text.

The simple gradient method (Klemme, 1975; Chaturvedi and Lory, 1980; Lam et al, 1982) is an alternative approach to analyzing BHT data. Thermal gradients are calculated either as two-point differences using a single BHT and an estimate of the mean annual ground temperature or through regression techniques on multiple bottom-hole temperatures at different depths. This technique for treating BHT data is shown schematically in Figure 1b. The single advantage of the simple gradient method is its convenience: BHT information is commonly stored and available in data files. Scatter in uncorrected temperatures for a common depth in any petroleum field, however, is typically 10° to 20°C (Carvalho and Vacquier, 1977, Figures 3–8) which leads to large uncertainties in the computed gradient. Correction of data for drilling effects reduces scatter but is often not possible from information stored in data files. Also, without thermal conductivity information, the explanation of the scatter is unclear. Our thermal resistance method requires the measurement or estimation of thermal conductivity values but, in return, provides an estimate of actual temperature errors and of lateral heat flow variations.

We now present our application of the thermal resistance method to the problem of heat flow and subsurface temperature variations within the Uinta Basin. The geologic setting of the basin and the basic information available from petroleum exploration are described first. Analyses of temperature and thermal conductivity data and corrections which may be applied to them are then discussed separately. Finally, the heat flow and subsurface temperature maps are presented.

Table 1. Application of thermal resistance method to Uinta Basin study.

Equation (2): $q_0(x, y) = [T_{B,\infty}(x, y) - T_0(x, y, h)] \Big/ \sum_{z=0}^{B} \frac{\Delta z(x, y)}{k(x, y, z, \phi, T)}$

Symbol	Parameter	Procedure/corrections
$T_{B,\infty}$	Bottom-hole temperature at equilibrium (i.e., infinite elapsed time)	Correct for drilling disturbance $T_B(t_e) = T_{B,\infty} + A \log\left(\frac{t_c + t_e}{t_e}\right)$
$T_0(x, y, h)$	Surface ground temperature	Correct for elevation and air lapse rate $T_0(x, y, h) = 22.4 - 0.0067h$ where h is elevation in meters, T_0 in °C
$\Delta z(x, y)$	Unit thickness	Describe formation thicknesses in terms of differences between fourth-order polynominal surfaces $\Delta z_{Fm} = z_j(x, y) - z_i(x, y)$ where z_i, z_j are depths to tops of formations i and j, respectively; z_j may be depth to measurement point.
$k(x, y, z, \phi, T)$	Thermal conductivity	Correct lab measurement of solid component k_s at room temperature to in-situ conditions of variable porosity and temperature $k_r = k_w^{\phi} k_s^{(1-\phi)}$
ϕ	Porosity	$\phi = 0.25 \exp(-z/3.0)$ where z is depth in kilometers
k_w	Thermal conductivity of water	$k_w = 0.56 + 0.003T^{0.827}$; $0 \le T \le 63$°C $k_w = 0.481 + 0.942 \ln T$; $T > 63$°C
k_s	Thermal conductivity of solid matrix	$k_s = k_{s,20}\left(\frac{293}{273 + T}\right)$ where $k_{s,20}$ is laboratory result and T is formation temperature in °C

Geologic setting of Uinta Basin

The Unita Basin is an intraplate sedimentary basin within the northern Colorado Plateau (Figure 2). The geographic basin is bounded on the south by the Book Cliffs, on the west by the southern and central Wasatch Mountains, on the north by the Uinta Mountains, and on the east by the Douglas Creek arch. The basin is roughly elliptical, stretching 210 km along its major east-west axis and 160 km in a north-south direction. It occupies an area of approximately 20,000 km^2 (Picard and High, 1972).

The pre-Tertiary stratigraphic history of the Uinta Basin is one of regularity and stability (Preston, 1957; Untermann and Untermann, 1964). Rock formations range in age from Precambrian through Tertiary, but Mississippian beds uncomformably overlie Cambrian beds. Periods of marine and continental deposition occurred with nonmarine deposition dominant after the Permian (Bruhn et al, 1983). Total thickness of beds ranges

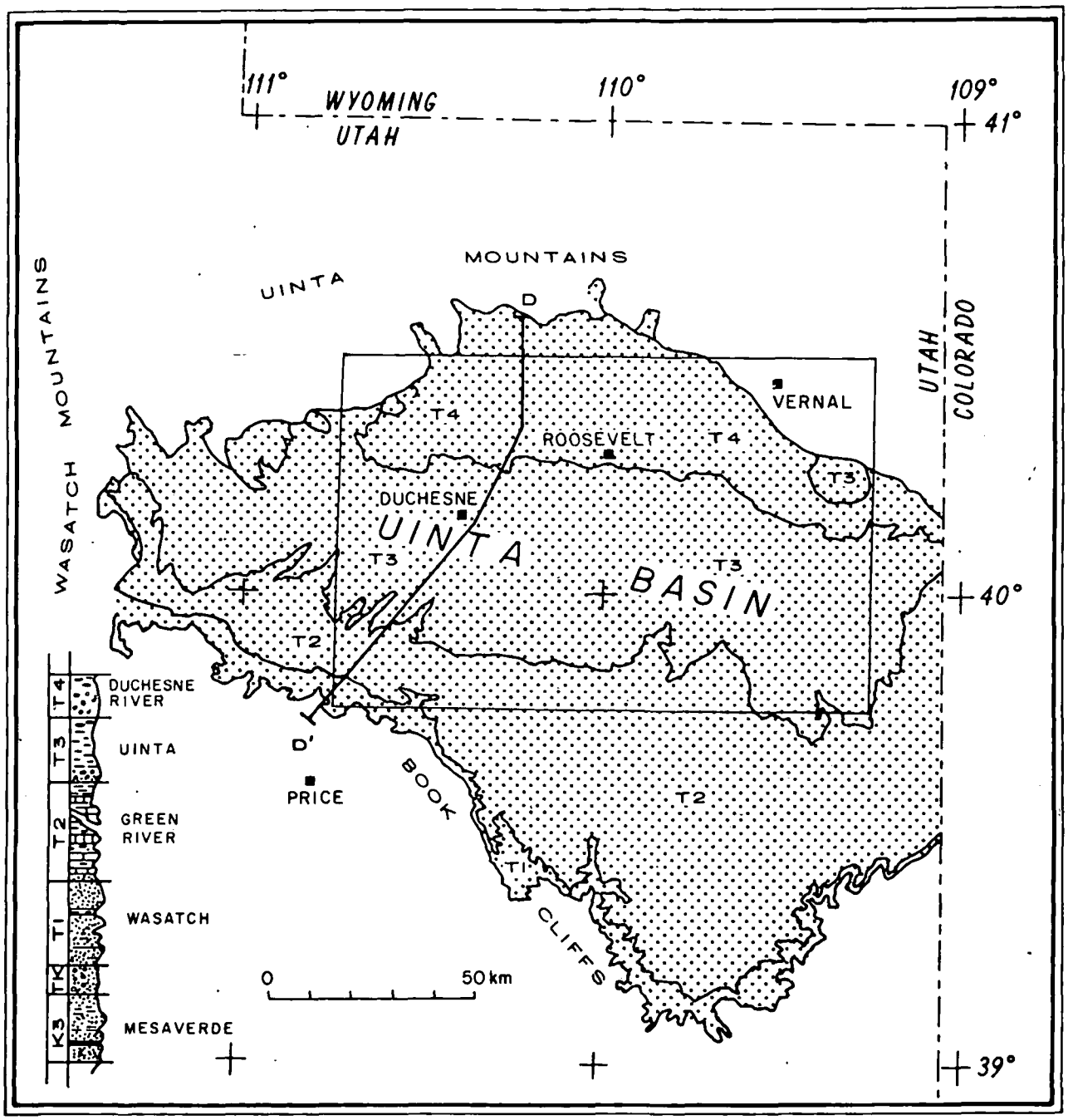

FIG. 2. Location map for the Uinta Basin, northeastern Utah. Shaded area indicates Tertiary outcrops. Rectangle is study area for reference in Figures 7, 10, and 11. Lower left inset shows conventional stratigraphic column for Upper Cretaceous (K3), Cretaceous-Tertiary (TK), and Tertiary (T1 through T4) formations shown on the map and discussed in the text.

from about 13.7 km in the eastern part of the basin to about 19.2 km in the western part. Approximately 4.5 km of the stratigraphic sequence is Tertiary in age.

The Tertiary system of the Uinta Basin (Figure 3) (Bradley, 1931; Picard, 1957; Preston, 1957; Murany, 1964; Untermann and Untermann, 1964; Ryder et al, 1976) began with withdrawal of the Cretaceous sea related to uplift on the west and north. As a result, marine claystone and siltstone grades laterally and is interbedded with nonmarine sandstone, shale, siltstone, and coal seams of channel floodplain and lagoonal character. The final phase of Cretaceous deposition and the first phase of Tertiary deposition are represented by continental facies of clastic rocks. The Cretaceous-Tertiary boundary is difficult to place with certainty.

Coalescing of small freshwater lakes in the western part of the basin brought an end to widespread fluvial deposition (Wasatch formation and equivalents—North Horn, lacustrine Flagstaff, Colton) of the early Tertiary. Two major periods of lacustrine deposition then followed, and the Flagstaff limestone and Green River formation were deposited. Of these, the Green River formation, deposited in Lake Uinta, is more extensive in the Uinta Basin. The complex interfingering of fluvial and deltaic beds with those of lacustrine origin indicates that Lake Uinta, which was probably stable for long periods and is estimated (Picard and High, 1972) to have existed for about 13 million years, underwent many fluctuations as it transgressed across its broad flood plain. In later stages, the lake increased in salinity and gave way to an interfingering of fluvial and lacustrine sediment (Uinta formation of late Eocene age) as it withdrew to the west-central part of the basin.

Deposition of the fluvial Duchesne River formation (probably latest Eocene but perhaps Oligocene for the uppermost member) followed as downwarping ceased and the basin filled with fluvial beds as streams were again the major agents of deposition (Andersen and Picard, 1974).

Along the northern edge of the basin, against the south flank of the Uinta Mountains, Tertiary formations progressively overlap the upturned and eroded edges of pre-Tertiary formations. There, maximum warping has produced the Uinta Basin syncline where dips vary from 10 to 35 degrees on the north limb, but flatten to 2 to 4 degrees on the south limb (Figure 3).

Structure of the basin is relatively simple. Formation contacts form simple concave upward surfaces that can be described by two-dimensional low-order polynomial surfaces with no more than a hundred meters or so misfit to identified contacts across the basin. The interfingering of deltaic, fluvial, and lacustrine deposits from several source areas, in contrast, has resulted in complex lateral facies changes within Tertiary formations with consequent complications for deriving thermal conductivity profiles.

ANALYSIS

Data

The basic data set consists of information from approximately 2000 wells in the area defined by latitudes 39.77°N to 40.50°N and longitudes 109.00°W to 110.75°W which were made available from the WEXPRO Petroleum Information file. The quality and completeness of data in the master file is variable. We required, for instance, knowledge of formation thicknesses for our thermal resistance calculation, and found in the entire data set only 1200 wells with the top of the Green River formation entered, 1000 with the top of the Wasatch formation, and 70 with the top of the Uinta formation. In contrast, surface elevations are included for all wells. Bottomhole temperatures are available for most of the wells, but the correction for drilling disturbances requires multiple BHT measurements at successive times in order to extrapolate to an equilibrium temperature. This requirement eliminates most of the wells and limits the data set of wells with correctable temperatures to approximately 5 percent of all wells in the

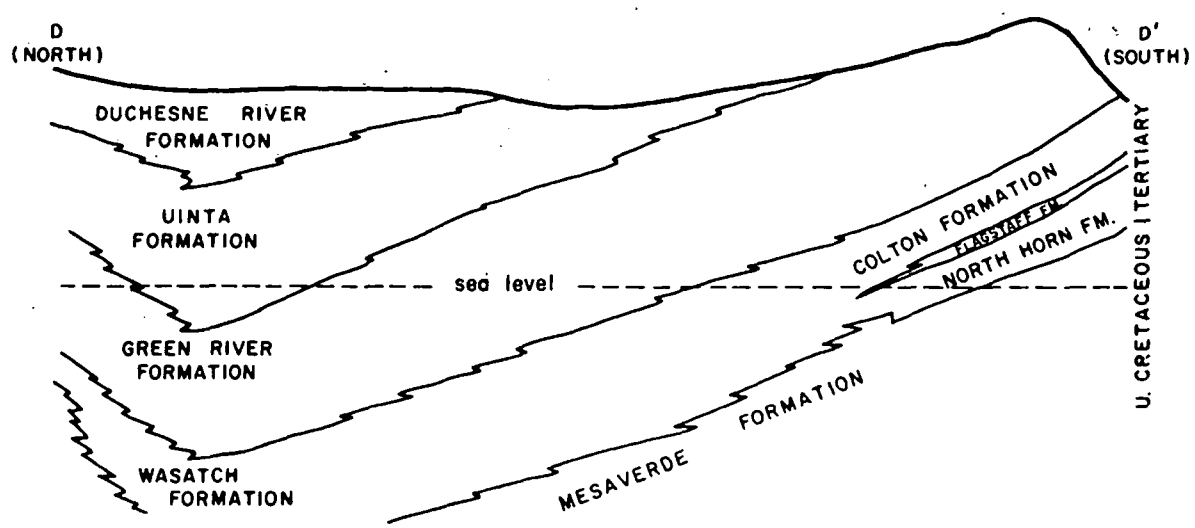

FIG. 3. Schematic north-south cross-section through the Uinta Basin. Section follows profile DD' of Figure 2. Length of the profile is 120 km. Maximum thickness of the Tertiary sequence (Duchesne River through Wasatch Formations) shown is about 4300 m.

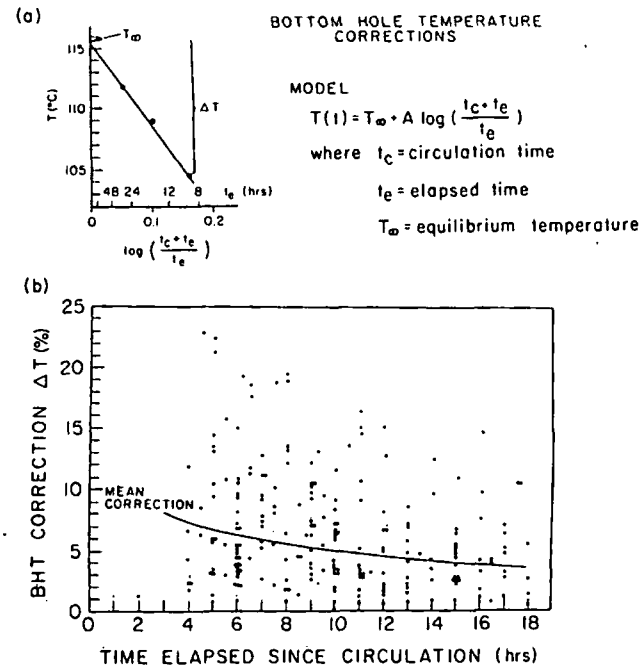

FIG. 4. (a) An example of a BHT correction. Multiple log readings 9; 16, and 32 hours after circulation ceased are used to extrapolate to the equilibrium temperature T_∞. (b) Magnitude of bottom-hole correction, expressed as a percentage of the observed value in °C, as a function of elapsed time after circulation, for 97 wells with multiple BHT values recorded.

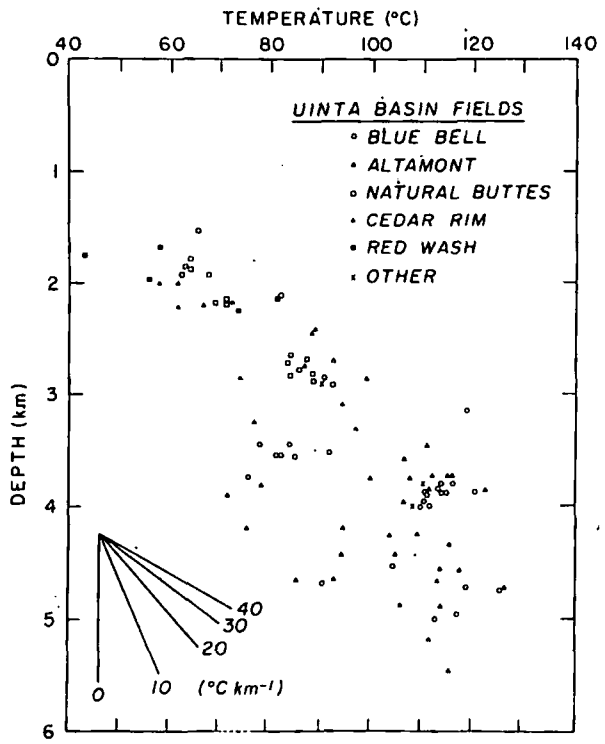

FIG. 5. Corrected bottom-hole temperatures versus depth for 97 wells distributed over the Uinta Basin. Wells are coded with respect to the producing fields.

basin. Few wells drilled prior to 1960 meet this requirement. From the more recent wells with multiple measurements we eliminated those that had identical temperatures recorded for several log runs, believing that a temperature was measured on one log run only and simply recorded on later logs. By carefully searching well logs from the 2000 wells in the Unita Basin, we identified 97 wells for which we could calculate a credible, corrected, bottom-hole temperature.

Five wells were sampled for thermal conductivity measurements. These wells were chosen from those available at the core library of the Utah Geological and Mineral Survey on the basis of having continuous samples from near the surface to below the Wasatch formation. The shallow Cottonwood Springs well was chosen to obtain additional samples from the Duchesne River formation. The wells were also chosen to be as close as possible to areas with concentrations of BHT data while also sampling different areas of the basin. Hindsight suggests that we undersampled the basin in a lateral sense.

Temperatures

Detailed temperature data were taken from well logs. Because of several factors, primarily, fluid circulation before logging, bottom-hole temperatures from well logs are lower than static formation temperatures. The Horner technique (Dowdle and Cobb, 1975; for discussion see Table 1, Lachenbruch and Brewer, 1959) is a method commonly used to correct these temperatures. The technique involves plotting the bottom-hole temperature in a given well versus time according to the equation

$$T_B(t) = T_{B,\infty} + A \log\left(\frac{t_c + t_e}{t_e}\right), \qquad (3)$$

where t_c is the circulation time, t_e is the time elapsed since circulation, and $T_B(t)$ is the time-dependent BHT. By plotting log $[(t_c + t_e)/t_e]$ against T, one can estimate $T_{B,\infty}$, the true formation temperature, as the ordinate intercept as shown in Figure 4a. When the circulation time that corresponds to a BHT measurement was unknown, a standard circulation time of 4 hours was used.

Ninety-seven wells were found in which the bottom-hole temperature was recorded accurately more than once, thus allowing for a determination of the constant A and application of the Horner technique. The determination of A and $T_{B,\infty}$ was done by linear regression. The majority of the wells are located in the Altamont-Bluebell-Cedar Rim trend in Duchesne County north and northeast of Duchesne. Most of the others are in the Natural Buttes field of Uinta County flanking the White River. Bottom-hole temperatures were measured at depths ranging from 1500 m in Natural Buttes to 5500 m in Altamont-Bluebell. These depths correspond to the lower Green River and upper Wasatch formations. Corrected temperatures from the wells are plotted versus depth in Figure 5. The wide scatter indicates that the geothermal gradient is nonuniform throughout the basin. The mean geothermal gradient for the basin from these data is 25°C km^{-1}.

Since the vast majority (about 95 percent) of wells in the Uinta Basin do not have sufficient data for correction by the Horner technique, it is appropriate to investigate the likely error involved if raw uncorrected temperature data were to be used and also the possibility of reducing this error by applying some empirical corrections to the raw temperature data. For this purpose we performed a test using the 97 wells with multi-

ple temperature measurements for which we were able to compute an estimate for the equilibrium temperature (i.e., $T_{B,\infty}$). The difference between this computed equilibrium temperature ($T_{B,\infty}$) and any measured temperature (T_B) can be regarded as the correction necessary for that measurement. The percentage corrections for all measurements are plotted in Figure 4b against time elapsed since circulation when the measurement was made. Three observations can be made. First, all the corrections are positive for this data set, indicating that drilling at these depths produced a cooling effect. Second, errors up to 25 percent may exist in individual measurements made soon after drilling; the correction limit decreases to about 12 percent after 18 hours of elapsed time. Third, a typical correction for this data set (shown as a solid line in Figure 4b) has the form $T_{B,\infty} = T_B(1.11 - 0.026 \ln t_e)$ which amounts to a 7 percent correction for an elapsed time of 4 hours, falling to 3 percent after 20 hours, although there is considerable scatter in the data. The magnitude of this correction agrees with corrections proposed by others. Schoeppel and Gilarranz (1966) suggested that maximum logged temperatures of deep wells are within 5 percent of true static formation temperatures. Carvalho and Vacquier (1977) stated that for elapsed times greater than 10–12 hours the BHTs are accurate to within 8 percent of the true static formation temperatures. For the test data shown in Figure 4b, 80 percent of the data points fall within ± 5 percent of the mean correction based on elapsed time only. This is a tolerable uncertainty for treating new uncorrected temperature data as long as little significance is placed on isolated temperature anomalies which may simply be part of the population outside these limits. Other empirical correction factors based on depth alone (AAPG, 1972) or by depth, circulation time, measurement time, and regional geothermal gradient (Scott, 1982) may provide further improvements in reducing uncertainties in BHT data. Alternative approaches and refinements recently suggested by Middleton (1979, 1982), Leblanc et al (1981), and Lee (1982) for thermal stabilization of a drill hole can also be used where knowledge of thermal properties of drilling mud and wall rock are known. However, in this study we defer further discussion of using uncorrected BHT data and restrict our analysis to the 97 wells where equilibrium temperatures were calculated.

Thermal conductivity

All thermal conductivity values were determined using the modified divided bar designed by Blackwell (Roy et al, 1968) and similar in operation to that described by Sass et al (1971b). The bar was calibrated with standards of fused silica and crystalline quartz using temperature-dependent conductivity given by Ratcliffe (1959) and a procedure given by Chapman (1976) which accounts for lateral heat losses and sample contact resistance. Reproducibility of thermal conductivity determination is typically better than 2 percent and interlaboratory agreement between measurements on identical samples is better than 5 percent (Chapman, 1976). For drill cuttings we used the cell technique of Sass et al (1971a).

Five wells in the Uinta Basin were sampled for detailed thermal conductivity measurements: Rock Creek, Fisher, Cottonwood Springs, Red Wash, and South Ouray. We initially sampled the wells at 30 m intervals, which gave between 10 and 20 samples per formation per well. The sample interval was decreased to 15 m when erratic behavior in the conductivity profile was observed. The increased sample density corresponded to a plan of characterizing basin thermal conductivity in terms of members of formations rather than by entire formations. Subsequent analysis indicates that for the Uinta Basin this is misguided sampling. It would have been preferable to sample a greater number of wells having a broader geographic distribution with fewer samples per formation.

Thermal conductivity results for the five wells are shown in Figure 6. In each figure we have plotted the individual results for all samples measured, together with a histogram representing each formation. Numbers of samples, conductivity, and standard deviation are given in Table 2.

The variety in the thermal conductivity results, both in the formation means between wells and in the distribution of values in a single well, reflects primarily the complex depositional history of the Tertiary Uinta Basin formations. For the South Ouray well (Figure 6) conductivities of all formations are well constrained, as indicated by tight distributions and standard deviations between 0.3 and 0.5 $Wm^{-1}K^{-1}$. In other wells certain formation conductivities are poorly constrained, as for example in the Duchesne River formation in the Fisher well

Table 2. Thermal conductivity results for the Uinta Basin.

	Formations														
	Duchesne River			Uinta			Green River			Wasatch			Mesaverde		
Well	N	k	s.d.	N	k	s.d.	N	k	s.d.	N	k	s.d.	N	k	s.d.
Rock Creek				41	4.37	0.94	135	3.13	0.80						
Fisher	28	4.80	1.65	77	2.78	0.59	106	3.15	0.86	75	2.57	0.30			
Cottonwood Springs	23	4.81	0.35	17	4.37	0.78									
Red Wash				15	2.44	0.41	58	3.70	1.55	37	2.89	0.40	32	2.80	0.79
South Ouray				49	2.12	0.41	53	2.22	0.48	59	2.29	0.38	47	2.79	0.31
(Mean)	51	4.80		199	3.22		352	3.05		171	2.58		79	2.80	

Notes: N is number of samples; k is mean thermal conductivity in $Wm^{-1}K^{-1}$; s.d. is standard deviation in $Wm^{-1}K^{-1}$. Measurements were made on drill chip samples in the laboratory at 20°C and represent the solid matrix conductivity at that temperature. Actual formation thermal conductivity must be corrected for fluid, porosity, and temperature effects as described in text and Table 1.

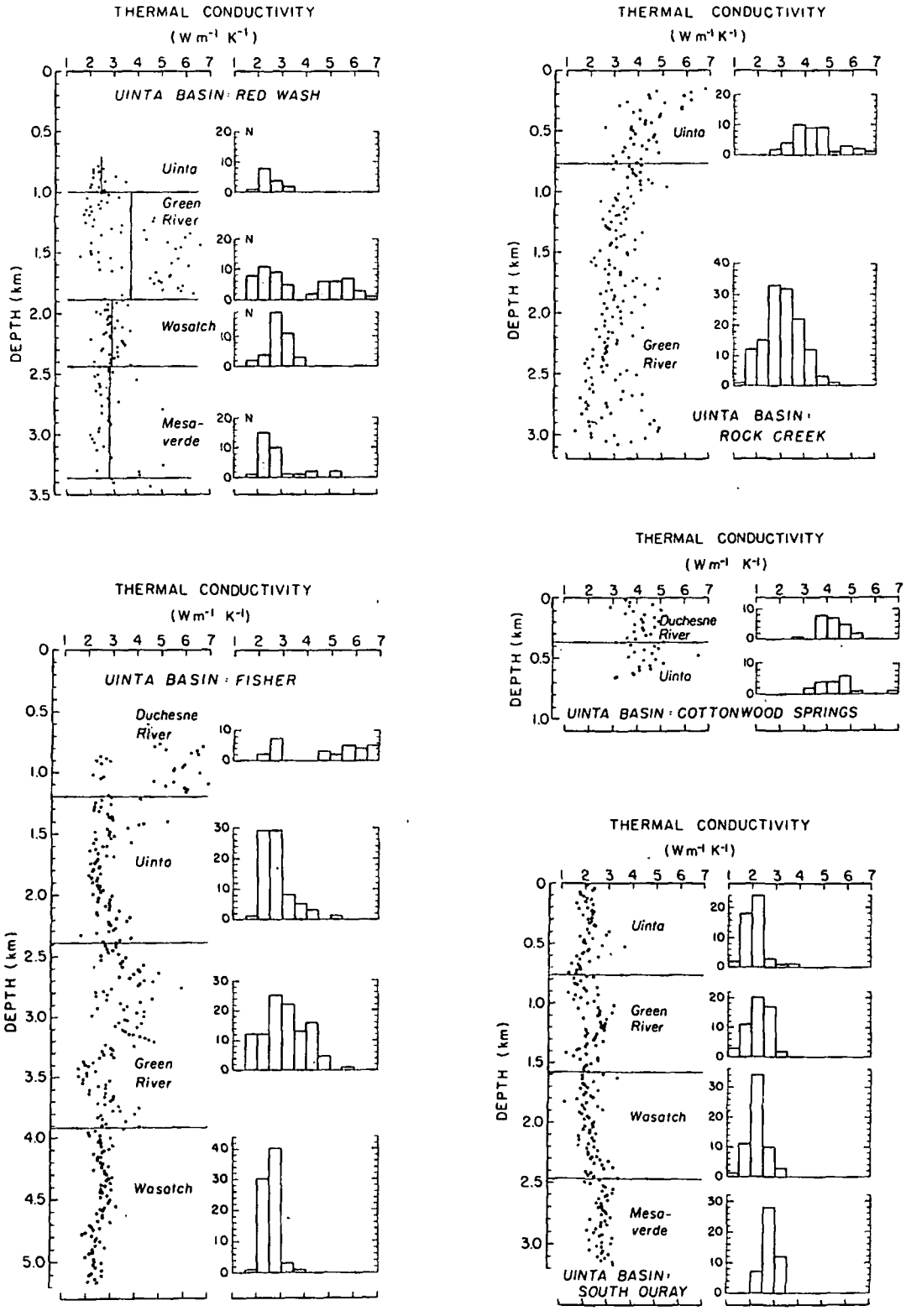

FIG. 6. Thermal conductivity results for five wells in the Uinta Basin. Well locations are shown in Figures 7, 10, and 11. Left side of the figures shows results for individual samples; right side shows histograms of results for each formation in each well. Measurements were made on drill chip samples in the laboratory at 20°C and represent the solid matrix conductivity at that temperature. Actual formation thermal conductivity must be corrected for fluid, porosity, and temperature effects as described in the text and Table 1.

(Figure 6) and in the Green River formation in the Red Wash well (Figure 6) where standard deviations are 1.5 to 1.7 $Wm^{-1}K^{-1}$. In the latter cases the distribution is bimodal because of interbedded sandstone-claystone intervals where the coarser components are characterized by conductivities of 5–7 $Wm^{-1}K^{-1}$, in contrast to claystone-rich beds having conductivities of 1.5–3 $Wm^{-1}K^{-1}$.

Average thermal conductivities given in Table 2 are consistent with values reported in previous studies. Reiter et al (1979) reported a mean conductivity for the Evacuation Creek and upper Parachute Creek members of the Green River formation in the Red Wash field of 2.32 (s.d. 0.25) $Wm^{-1}K^{-1}$. For the same interval in the Red Wash well, the mean for our measurements is 2.50 (s.d. 0.95) $Wm^{-1}K^{-1}$. A second comparison can be made in the South Ouray field. The mean value for the Uinta formation of 2.14 (s.d. 0.45) $Wm^{-1}K^{-1}$ determined in well W-EX-1 by Sass and Munroe (1974) agrees closely with our value of 2.12 (s.d. 0.41) $Wm^{-1}K^{-1}$ (see Table 2).

A less welcome feature of the thermal conductivity results is the variation from well to well in any given formation. The Uinta formation, for example, has a conductivity greater than 4 $Wm^{-1}K^{-1}$ in the Rock Creek and Cottonwood Springs wells, 2.78 $Wm^{-1}K^{-1}$ in the Fisher well, 2.44 $Wm^{-1}K^{-1}$ at Red Wash, and only 2.12 $Wm^{-1}K^{-1}$ at South Ouray. The Green River formation exhibits similar variations. While such patterns are consistent with the facies changes—the high Green River formation conductivity at Red Wash, for example, coincides with an extensive depositional tongue characterized by high sandstone content—the patterns complicate the processing of data on a basin scale.

The common assumption of constant thermal conductivity within a formation, which is reliable for the Mesozoic sedimentary rocks of the central Colorado Plateau on the south (Bodell and Chapman, 1982), is clearly in error in the Uinta Basin. As a consequence, we have developed maps of lateral thermal conductivity variations within the basin.

For each formation we assembled facies maps, cross-sections, available stratigraphic columns, and estimates of sand/clay ratios. By combining this information with the correlation between thermal conductivity and rock type available from our measurements on the 852 samples, we developed the thermal conductivity maps shown in Figure 7 for the Uinta, Green River, Wasatch, and Mesaverde formations. We had insufficient information to discern any systematic variations within the Duchesne River formation other than the decrease in conglomerate clast size eastward across the basin and the decrease in grain size from north to south. The pattern in each formation strongly reflects depositional environment; open lacustrine rocks, for example, generally contain a higher clay fraction and thus a lower conductivity. Although differences of a much

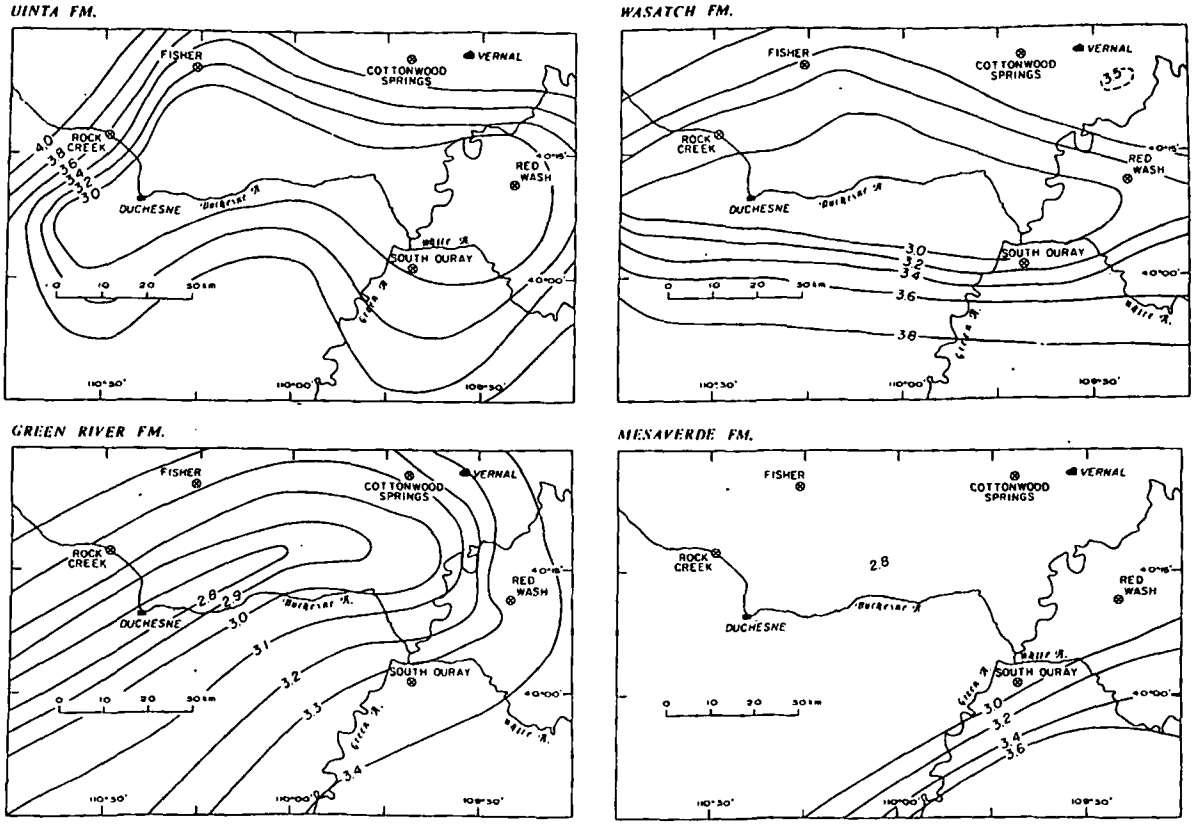

FIG. 7. Thermal conductivity maps of the Uinta, Green River, Wasatch, and Mesaverde formations in the Uinta Basin. Contours represent estimates of the solid component thermal conductivity at 20°C (units $Wm^{-1}K^{-1}$) and are controlled primarily by facies changes. Actual formation conductivity must be corrected for fluid, porosity, and temperature effects.

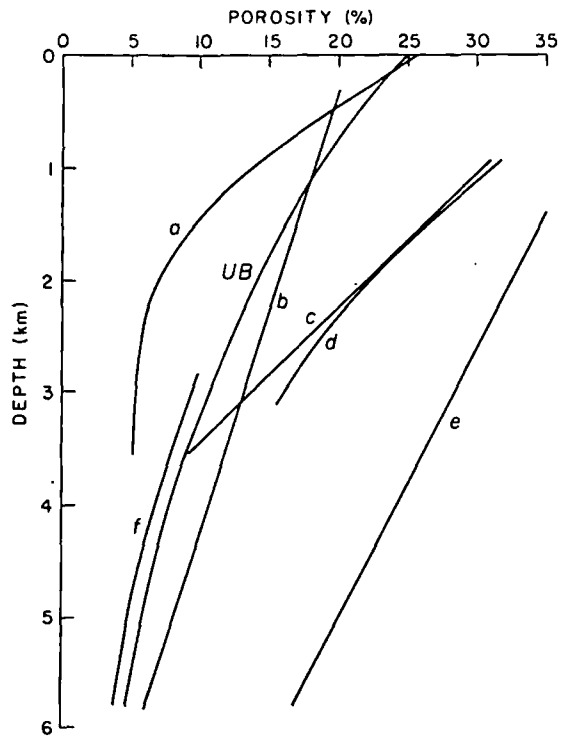

FIG. 8. Porosity depth functions for some typical rock types: (a) Jurassic-Cretaceous shale (Caucasus), (b) Pennsylvanian-Permian sandstone (Texas Okalahoma), (c) Jurassic-Cretaceous sandstone (Caucasus), (d) Jurassic-Cretaceous quartz sandstone, (e) Quaternary sand (Louisiana), (f) Carboniferous silty sandstone. Modified after Jonas and McBride (1977). UB indicates function adopted for the Uinta Basin.

greater magnitude may exist locally, typical conductivity changes across a formation on these smoothed maps are 30 percent. The northwest high-conductivity trend persists through the Uinta and Wasatch formations and may partly explain the lower thermal gradients observed in that part of the basin. For computational purposes, the variations shown in Figure 7 were all expressed in terms of low-order polynomial surfaces by least-squares fitting.

So far the discussion of thermal conductivity values has been based on laboratory measurements of the solid component k_s at room temperature, nominally 20°C. Several corrections must be applied to adjust for in-situ thermal conductivity of porous rocks at elevated temperatures.

For rocks with a porosity ϕ, the water-saturated rock conductivity k_r, appropriate for in-situ conditions, may be calculated as the geometric mean from the pure phase conductivities, weighted according to their fractional volumes

$$k_r = k_w^{\phi} k_s^{(1-\phi)}, \tag{4}$$

where k_w is the conductivity of water. [See Robertson and Peck (1974) for a discussion of this and other possible models for porous rocks and further references.] For a conductivity range of 1.5 to 3.5 $Wm^{-1}K^{-1}$, for example, a 10 percent porosity adjusts the measured conductivity by 9–16 percent and a 20 percent porosity, by 17–30 percent. It was impossible to measure porosities for individual samples, and porosities from well logs are useful only as general indicators. We therefore chose a generalized porosity-depth function to characterize the basin. Figure 8 shows a variety of porosity-depth functions varying from linearly decreasing curves suitable for well-sorted sandstone to exponentially decreasing curves more appropriate for silty and shaly rocks. The distribution chosen for the Uinta Basin based on reports for porosity at specific horizons and concensus of personal communications is

$$\phi = 0.25 \exp(-z/3.0) \tag{5}$$

where z is depth in kilometers. This relation yields a porosity of 25 percent at the surface and 5 percent at 4.8 km depth.

Temperature dependences for water conductivity k_w, assuming that the pores are filled with water, and matrix conductivity k_s are also needed for the conductivity correction. Water has a conductivity of 0.56 $Wm^{-1}K^{-1}$ at 0°C, but it increases to 0.68 $Wm^{-1}K^{-1}$ at 100°C. We have approximated temperature-conductivity data for water given by Kappelmeyer and Haenel (1974) by the following functions:

$$k_w = 0.56 + 0.003T^{0.827}; \qquad 0 \le T \le 63°C \tag{6}$$

$$k_w = 0.481 + 0.942 \ln T; \qquad T > 63°C. \tag{7}$$

These equations were then used to adjust k_w for in-situ conditions in the basin. We have further assumed that the solid matrix conductivity k_s is proportional to the reciprocal of the absolute temperature. Thus

$$k_s = k_{20}[293/(T + 273)], \tag{8}$$

where k_{20} is conductivity determined in the laboratory at 20°C. This correction is significant. For a sample with measured conductivity (20°C) of 3.0 $Wm^{-1}K^{-1}$ the in-situ matrix conductivity varies between 3.1 at the surface (10°C) and 2.2 (135°C) at 5 km depth. No attempt is made to make anisotropy corrections because of the complexity of the problem, considering only drill chips were available for measurement and the relatively small effect it is believed the corrections would have in this situation. However, possible systematic errors introduced by neglecting anisotropy and by making chip measurements on claystones which may have undergone irreversible changes upon drying should not be ignored in the interpretation of results. Blackwell et al (1981) and Sass and Galanis (1983) gave examples of the problem of determining thermal conductivity of shales.

Surface heat flow

This section describes procedures for processing large data sets of BHTs to obtain heat flow patterns and subsurface temperature maps. If, for each well, a corrected BHT is available, and if the rock types are known and can be converted into a thermal conductivity profile, the computation of heat flow is relatively simple. In reality the data set is incomplete and approximate techniques must be adopted.

We approximate in some instances the positions of formation contacts by fourth-order polynomial surfaces. The surfaces were generated from pertinent well information; the top of the Uinta formation was available in 70 well records and the Green River and Wasatch formations in about 1000 records each. The choice of fourth-order polynomials to represent the formations was made on the basis of a plot of rms residual (difference between recorded formation position and calculated position

using the polynomial surface) versus polynomial order. Figure 9 shows that formation contacts are adequately expressed as fourth-order surfaces (second order for Wasatch and Green River) and that little benefit is gained by adding higher orders.

One filtering process required for the Uinta Basin concerned raw data where formation tops identified on well logs departed from the polynomial surfaces by several hundred meters. In such a case the data points were eliminated and the surface coefficients were recalculated. This process led to a reduction of 5 percent in the Wasatch formation records, 10 percent in the Green River formation records, and 10 percent in the Uinta formation records. The discrepancy lies partly in the difficulty of identifying formation boundaries, but also in systematic differences between the stratigraphic conventions adopted by different companies. The average rms misfit for each formation after filtering the data is: Uinta formation, top 81 m; Green River formation, top 70 m; and Wasatch formation, top 70 m.

From these polynomial surfaces, depths to formations were obtained for wells in which any formation top was missing, and formation thickness was calculated for use in the thermal resistance calculation. A subroutine was developed to compute porosity-corrected thermal conductivity for each formation at any location. This subroutine computes the average conductivity of water k_w as a function of temperature, the conductivity of the solid component k_s as function of temperature, the average porosity, and the porosity-corrected thermal conductivity for each formation according to the relations described previously. Because the formations are at different depths in different parts of the basin, the porosity and temperature corrections cause the thermal conductivity of each formation to vary laterally in patterns somewhat different from those governed by facies changes shown in Figure 7. Once the conductivities were calculated, all the information was available for the computation of surface heat flow from the thermal resistance equation.

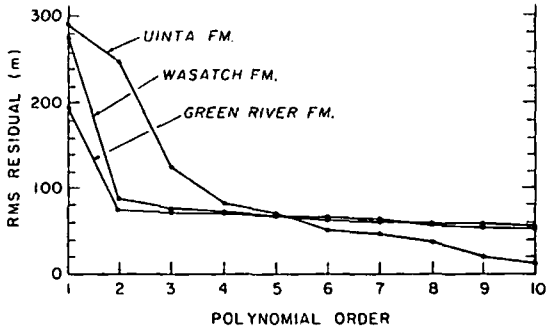

FIG. 9. Root mean square (rms) residuals between position of formation top recorded on well log and position computed from the polynomial surface approximation.

Surface heat flow in the Uinta Basin is shown in Figure 10. After rejecting three anomalous values using the Chauvenet rejection criteria (Beers, 1957, p. 23), the mean heat flow for the 94 wells is 57 mWm^{-2} with a standard deviation of 11 mWm^{-2}. Heat flow varies from 65 to 40 mWm^{-2} on a profile running north from Duchesne. The area to the southeast bordering the White River exhibits no trend in heat flow and illus-

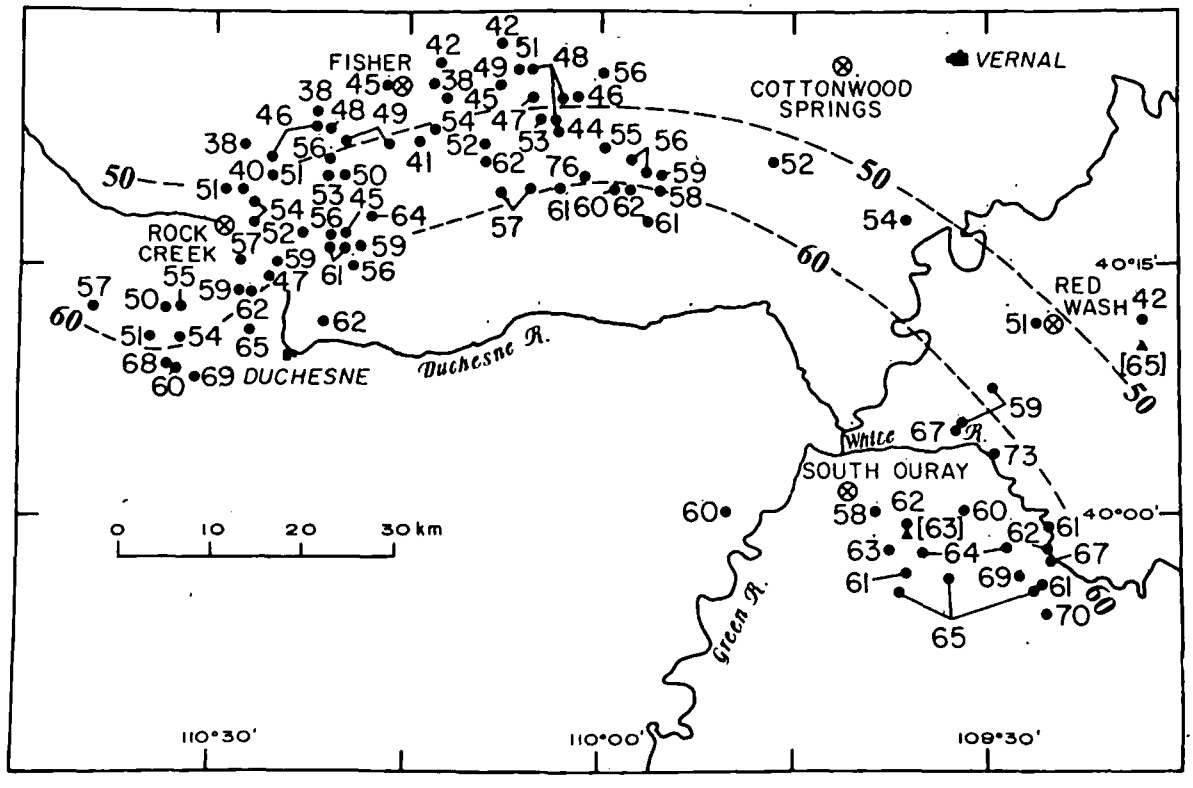

FIG. 10. Surface heat flow for 97 wells (solid dots) in the Uinta Basin computed by the thermal resistance method. Open circles with crosses indicate wells used for thermal conductivity sampling. Triangles give sites of two conventional heat flow determinations with corresponding heat flow values in square brackets.

trates the scatter which can be expected using this method. The range in heat flow computed for 20 wells is 58–73 mWm^{-2}, with a mean and standard deviation of 64 and 4 mWm^{-2}, respectively. We attach no significance to short-range fluctuations of order ± 5 mWm^{-2}, but believe the smooth variations are real.

A test of this treatment of BHT data to produce a heat flow map involves comparing these results with values determined previously in the same area by more conventional heat flow techniques. In this part of the Uinta Basin, only two sites are available for comparison. As shown in Figure 10, the value of 63 mWm^{-2} determined by Sass et al (1971b) at South Ouray over a depth range 61 to 907 m is surrounded by our values of 63, 60, 64, 61, and 63 mWm^{-2}. At the eastern boundary (Figure 10) the value of 65 mWm^{-2} given by Reiter et al (1979) for Red Wash departs considerably from our 42 mWm^{-2} on the north, but is closer to the two nearest values on the west of 51 and 59 mWm^{-2}. The lower value from our method in Red Wash may result from our smoothed conductivity assumption within formations, whereas, in fact, formations undergo rapid facies changes in this region. More likely it is a proper reminder that little significance should be attached to isolated values. A less direct comparison can be made with heat flow determined from conventional heat flow sites to the south of the Uinta Basin. In this sense the Uinta Basin values of 55–65 mWm^{-2} (south of Duschesne and White Rivers, Figure 10) are consistent with the northcentral Colorado plateau values (Table 4 and Figure 8 of Bodell and Chapman, 1982) and in particular with the mean value of 58 mWm^{-2} (31 sites, standard deviation 8 mWm^{-2}) considered representative of the Colorado Plateau interior (Table 5 of Bodell and Chapman, 1982).

Once the surface heat flow pattern is determined, subsurface temperatures at any depth can be calculated by a direct application of the thermal resistance method. An example of temperatures at 1 km depth is shown in Figure 11. The temperature pattern will generally be similar to the heat flow pattern, except where lateral facies variations cause thermal conductivity contrasts. Mean subsurface temperatures in the Uinta Basin are 22 ± 4°C at 500 m depth, 35 ± 7°C at 1000 m, 59 ± 10°C at 2000 m, and 74 ± 12°C at 3000 m.

Error analysis

Throughout the calculation, error propagation was computed using the general formula of Bevington (1969). Since all the errors encountered in formation depths, thermal conductivities, and temperatures were uncorrelated, the covariance terms are all zero. In computations, the average rms errors of the polynomial surfaces were used as the errors of the formation depths whether the depths used were picked formation tops or polynomial computed tops. Accuracy of picked formation tops in the Petroleum Information file is not less than about 50 m (personal communication, J. M. Hummel and C. N. Tripp, 1981). These errors in formation depths result in an

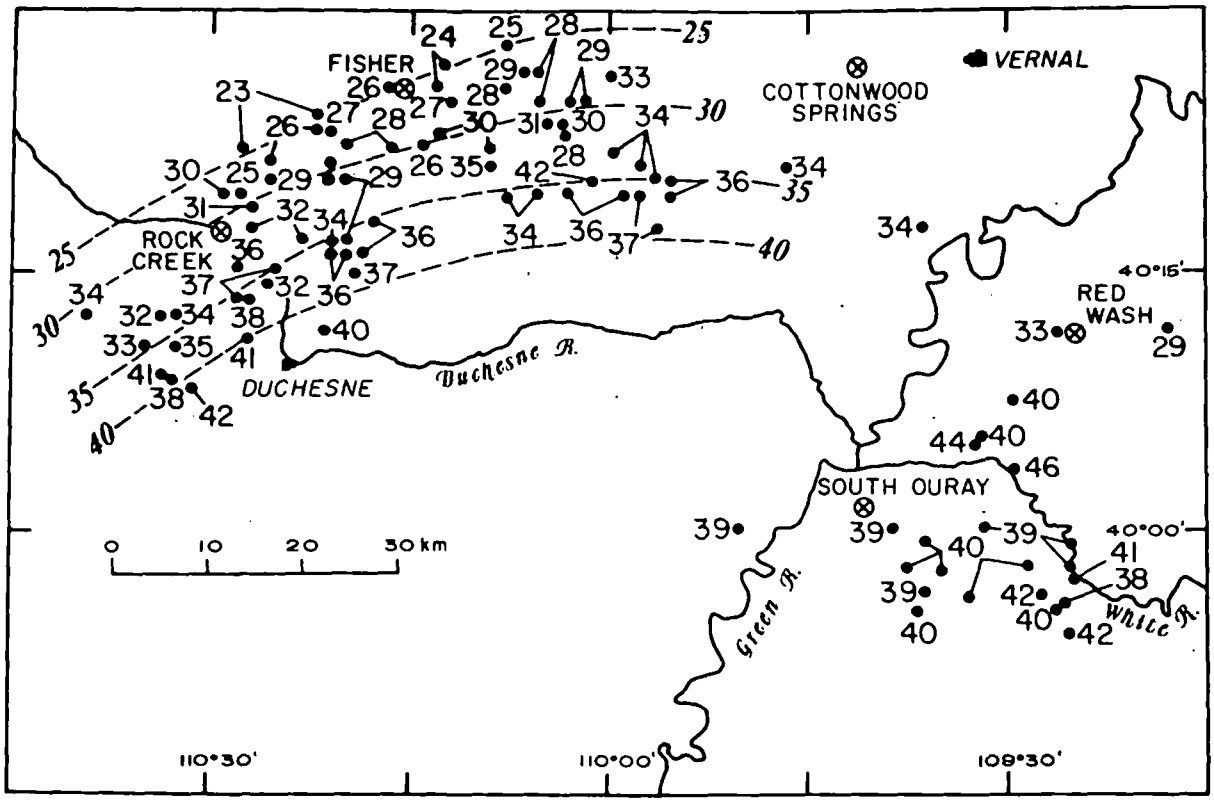

FIG. 11. An example of a subsurface temperature map for the Uinta Basin determined from the heat flow values and application of equation (1) or (2). Temperatures and contours in °C. Such maps are useful for both geothermal utilization and hydrocarbon maturation studies.

average error of 5.6 percent in surface heat flow. An error of 2°C in surface temperature results in an error of about 1 percent in surface heat flow. The standard deviation in formation thermal conductivity, which ranges from 8 to 40 percent, results in a 14 percent error in surface heat flow. The cumulation of these errors results in a total error of about 15 percent in surface heat flow values. Because the errors are uncorrelated, the larger error in thermal conductivity dominates the error propagation. If the error in surface heat flow that is solely the result of conductivity could be reduced from 14 to 10 percent, the cumulative error in surface heat flow would drop to 11 percent. Reducing the error due to conductivity to 5 percent would reduce the cumulation error to 8 percent. These errors may underestimate actual errors if our thermal conductivity measurements on claystones are systematically high, but this effect is difficult to assess.

DISCUSSION

The thermal resistance method described here (see Table 1) ınd applied to the Uinta Basin is generally applicable to well thermal data in sedimentary basins. The method makes few assumptions of uniformity concerning thermal gradients, thermal conductivity, or homogeneity within the basin. Instead, bottom-hole temperature data are treated individually, together with a best estimate of the vertical thermal conductivity profile at the well site, to produce a local heat flow value. Maps of surface heat flow and subsurface temperatures at arbitrary depths are products of the method.

For the Uinta Basin, we restricted our investigation to 97 wells where BHTs could be corrected for drilling effects. These wells comprise only 5 percent of the wells in the Uinta Basin. The magnitude of temperature corrections for these wells suggests that uncorrected BHTs may differ from equilibrium temperatures by as much as 25 percent, and for the Uinta Basin they are systematically low on the average by 7 to 3 percent depending upon time elapsed after circulation. An empirical mean correction for raw BHT data was developed for the 97 wells in the Uinta Basin such that 80 percent of the computed corrections fall within ± 5 percent of the mean correction. Use of this correction would provide access to a much larger data set (the remaining 95 percent of wells in the Uinta Basin) at an acceptable uncertainty level, provided little significance is attached to isolated temperature anomalies.

The heat flow map (Fig. 10) exhibits local coherency between values and yields a mean value of 57 mWm^{-2}, consistent with heat flow determined by conventional heat flow methods in the Uinta Basin and neighboring areas. Discrepancies of ± 5 mWm^{-2} between adjacent wells are considered to be in the noise.

An interesting feature of the heat flow map, if real, is the pronounced decrease of heat flow within the basin from about 65 to 40 mWm^{-2} as the Uinta Mountains are approached (compare Figures 10 and 2). Although we believe this trend to be real, there remains a possibility that the laboratory measurements of thermal conductivity of claystones and mudstones are systematically in error, or that our BHT correction has a systematic depth-dependent error and that these errors have an effect on our heat flow map. The thermal conductivity explanation is suggested, in part, by the spatial similarity in conductivity maps for the Uinta, Green River, and Wasatch formations in the area north of Duchesne (Figure 7) and the heat flow trend as shown in Figure 10. If the conductivity pattern is interpreted to indicate an increasing clay fraction in a southeast direction toward Duchesne, and if our measured conductivities are systematically high, then heat flow values will be correspondingly overestimated across this trend. However, the same argument should hold true for the South Ouray region where similar gradients are seen in the thermal conductivity maps (Figure 7), but no trend is seen in the surface heat flow (Figure 10). The possibility of a depth-dependent bias was checked by plotting surface heat flow against well depth. Whereas heat flow greater than 60 mWm^{-2} is restricted to wells less than 3900 m depth, heat flow less than 50 mWm^{-2} is found for wells varying in depth from 1800 m to 5500 m. Although there is a general trend toward lower heat flow determined in deeper wells, it is difficult to distinguish between systematic error and a physical process controlled by the basin geometry.

There are at least two heat transfer mechanisms that could produce the lateral heat flow gradient seen in Figure 10. The first mechanism is lateral refraction of heat flow into the very conductive quartzite of Precambrian age which comprises much of the Uinta Mountains on the north. The thermal conductivity contrast between younger Uinta Basin sedimentary rocks and the Precambrian Uinta Mountain Group (quartzarenite, subarkose) may attain a ratio of 1 : 2. Such a contrast would produce a similar 1 : 2 discontinuity in surface heat flow across the contact with basinward values being lower. Observed variations in the heat flow field of 40 to greater than 60 mWm^{-2} are consistent with slightly lesser conductivity constrasts. Theoretical considerations of such a conductive heat transfer problem (see, e.g., Carslaw and Jaeger, 1959, sec. 16.4), however, reveal that for the case of an ellipsoid-shaped basin, heat flow is *uniformly* lowered across the basin. Thus, the lateral surface heat flow gradient within the boundaries of the basin can only be produced by refraction if departures from an elliptical shape are large or if the conductivity field has a more complicated structure than we have assumed.

Another explanation of the heat flow field relies on convective heat transport accompanying the circulation of groundwater. The heat flow pattern in the Uinta Basin (Figure 10) is qualitatively consistent with groundwater recharge at the south flank of the Uinta Mountains, probably localized in the steeply dipping sandstone and limestone beds of late Paleozoic and Mesozoic age, and groundwater discharge or updip water flow south of the east-west basin axis. Although each flow regime needs to be modeled in detail, the general modeling results of Smith and Chapman (1983) on thermal effects of regional-scale groundwater flow systems indicate that the heat flow pattern observed in Figure 10 is consistent with a groundwater flow explanation.

Once the surface heat flow field has been established, subsurface temperatures can be readily calculated for any location in the basin. Differences between temperatures computed by the simple gradient method and those computed by the thermal resistance method, for the Uinta Basin on the average, are smaller than we initially expected. There are almost identical porosity corrected thermal conductivities for the Green River and Uinta formations except for thermal conductivities in the fine-grained, carbonate-rich Parachute Creek member of the Green River formation. The Duchesne River and Wasatch formations have significantly different conductivites, but the Duchesne River formation is absent over two-thirds of the study area and is thin compared with the depths of the BHTs where the Duchesne River formation is present. A better test of

this method would be provided by a basin where sharp contrasts exist in the thermal conductivity of different units.

Subsurface temperature maps for the Uinta Basin show similar spatial variations to the surface heat flow map. Such lateral variations may be overlooked unless heat flow values are computed for individual wells and the heat flow field is mapped. The lateral temperature differences predicted for greater depths within the Uinta Basin have important implications for regional differences in hydrocarbon maturation within the basin.

ACKNOWLEDGMENTS

We thank G. W. Hohmann and Diane I. Doser for critically reading the manuscript and offering suggestions for its improvement. J. M. Hummel, Chief Geologist, and C. N. Tripp of WEXPRO gave assistance and advice. We appreciate the generous access to WEXPRO information in the Uinta Basin. M. A. Mabey and W. Pe assisted with thermal conductivity measurements. S. D. Willett assisted with computations. Financial support was provided by DOE/DGE contract no. DEAC0780ID12079.

REFERENCES

American Association of Petroleum Geologists (AAPG), 1976, Basic data file from AAPG Geothermal Survey of North America: Univ. of Oklahoma, Norman.

Andersen, D. W., and Picard, M. D., 1974, Evolution of synorogenic clastic deposits in the intermontane Uinta Basin of Utah, *in* Tectonics and sedimentation: W. R. Dickinson, Ed., Soc. Econ. Paleont. Min., Special Publ. 22, p. 165–189.

Beers, Y., 1957, Introduction to the theory of error: Reading Mass., Addison-Wesley Publ. Co. 66 p.

Bevington, P. R., 1969, Data reduction and error analysis for the physical sciences: New York, McGraw Hill Book Co., Inc. 336 p.

Blackwell, D. D., Steele, J. L., and Steeples, D. W., 1981, Heat flow determinations in Kansas and their implications for midcontinent heat flow patterns (abstract): EOS Trans. Am. Geophys. Union, v. 62, p. 392.

Bodell, J. M., and Chapman, D. S., 1982, Heat flow in the north-central Colorado Plateau: J. Geophys. Res., v. 87, p. 2869–2884.

Bradley, W. H., 1931, Origin and microfossils of the oil shale of the Green River Formation of Colorado and Utah: U.S.G.S. Prof. Paper 168, 58 p.

Bruhn, R. L., Picard, M. D., and Beck, S. L., 1983, Mesozoic and early Tertiary structure and sedimentology of the central Wasatch Mountains, Uinta Mountains and Uinta Basin: Utah Geological and Min. Survey, in press.

Bullard, E. C., 1939, Heat flow in South Africa: Proc. Roy. Soc. London, Ser. A, v. 173, p. 474–502.

Carslaw, H. S., and Jaeger, J. C., 1959, Conduction of heat in solids, 2nd ed.: New York, Oxford Univ. Press, 510 p.

Carvalho, H. da S., and Vacquier, V., 1977, Method for determining terrestrial heat flow in oil fields: Geophysics, v. 42, p. 584–593.

Carvalho, H. da S., Purwoko, S., Thamrin, M., and Vacquier, V., 1980, Terrestrial heat flow in the Tertiary basin of central Sumatra: Tectonophys., v. 69, p. 163–188.

Chapman, D. S., 1976, Heat flow and heat production in Zambia: Ph.D. Thesis, Univ. of Michigan, Ann Arbor, 94 p.

Chaturvedi, L., and Lory, J. K., 1980, A preliminary evaluation of geothermal potential of San Juan Basin, New Mexico, using bottom hole temperatures from oil and gas wells: Geotherm. Res. Council, Trans., v. 4, p. 21–24.

Dowdle, W. L., and Cobb, W. M., 1975, Static formation temperature from well logs—an empirical method: J. Petr. Tech., p. 1326–1330.

Evans, T. R., and Coleman, N. C., 1974, North Sea geothermal gradients: Nature, v. 247, p. 28–30.

Evans, T. R., and Tammemagi, H. Y., 1974, Heat flow and heat production in northeast Africa: Earth Plan. Sci. Lett., v. 23, p. 349–356.

Goss, R. D., 1974, Empirical relationships between thermal conductivity and other physical parameters in rocks: Ph.D. Thesis, Univ. of California, Riverside, 216 p.

Hodge, D. S., Hilfiker, K., De Rito, R., Maxwell, J., Morgan, P., and Swanberg, C., 1980, Relationship of heat flow and temperature gradients to basement lithology, N.Y.: EOS Trans. Am. Geophys. Union, v. 61, p. 363.

Jonas, E. C., and McBride, E. F., 1977, Diagenesis of sandstone and shale: Application to exploration for hydrocarbons: Univ. of Texas at Austin, Continuing. Ed. Program, Publ. 1, 165 p.

Kappelmeyer, O., and Haenel, R., 1974, Geothermics with special reference to application: Geoexploration Monograph Ser. 1, No. 4, Berlin-Stuttgart, Gebr. Borntraeger, 238 p.

Kehle, R. B., 1972, Geothermal survey of North America, 1971, Annual Progress Report: Am. Assoc. Petr. Geol., 31 p.

Klemme, H. D., 1975, Geothermal gradients, heat flow and hydrocarbon recovery, *in* Petroleum and global tectonics: A. G. Fischer and S. Judson, Ed., Princeton, New Jersey, Princeton Univ. Press, p. 251–304.

Lachenbruch, A. H., and Brewer, M. C., 1959, Dissipation of the temperature effect of drilling a well in Arctic Alaska: U.S.G.S. Bull. 1083-C, p. 73–88.

Lam, H. L., Jones, F. W., and Lambert, C., 1982, Geothermal gradients in the Hinton area of west-central Alberta: Can. J. Earth Sci., v. 19, p. 755–766.

Leblanc, Y., Pascoe, L. J., and Jones, F. W., 1981, The temperature stabilization of a borehole: Geophysics, v. 46, p. 1301–1303.

Lee, T. C., 1982, Estimation of formation temperature and thermal property from dissipation of heat generated by drilling: Geophysics, v. 47, p. 1577–1584.

Middleton, M. F., 1979, A model for bottom-hole temperature stabilization: Geophysics, v. 44, p. 1458–1462.

——— 1982, Bottom-hole temperature stabilization with continued circulation of drilling mud: Geophysics, v. 47, p. 1716–1723.

Murany, E. E., 1964, Wasatch formation of the Uinta Basin, *in* Guidebook to the geology and mineral resources of the Uinta Basin: E. F. Sabatka, Ed., Intermountain Assn. of Petroleum Geologists, p. 145–155.

Picard, M. D., 1957, Green River and lower Uinta formations—Subsurface stratigraphic changes in central and eastern Uinta Basin, Utah, *in* Guidebook to the geology of the Uinta Basin: O. G. Seal, Ed., Intermountain Assn. of Petr. Geol., p. 116–130.

Picard, M. D., and High, L. R., Jr., 1972, Criteria for recognizing lacustrine rocks, *in* recognition of ancient sedimentary environments: J. K. Rigby, and W. K. Hamblin, Eds., Soc. of Econ. Palen. and Mineral., Spec. Pub. 16, p. 108–145.

Preston, D. A., 1957, A general discussion of the geologic history of northeastern Utah, *in* Guidebook to the geology of the Uinta Basin: O. G. Seal, Ed., Intermountain Assn. of Petroleum Geologists, p. 21–24.

Ratcliffe, E. H., 1959, Thermal conductivities of fused and crystalline quartz: British J. Appl. Phys., v. 10, p. 22–25.

Reiter, M., and Tovar, J. C., 1982, Estimates of terrestrial heat flow in northern Chihuahua, Mexico, based on petroleum bottom hole temperatures: Geol. Soc. of Am. Bull., v. 93, p. 613–624.

Reiter, M. A., Mansure, A. J., and Shearer, C., 1979, Geothermal characteristics of the Colorado Plateau: Tectonophys., v. 61, p. 183–195.

Robertson, E. C., and Peck, D. L., 1974, Thermal conductivity of vesicular basalt from Hawaii: J. Geophys. Res., v. 79, p. 4875–4888.

Roy, R. F., Decker, E. R., Blackwell, D. D., and Birch, F., 1968, Heat flow in the United States: J. Geophys. Res., v. 73, p. 5207–5221.

Ryder, R. T., Fouch, T. D., and Elison, J. H., 1976, Early Tertiary sedimentation in the western Uinta Basin: Geol. Soc. of Am. Bull., v. 87, p. 496–512.

Sass, J. H. and Galanis, S. P., Jr., 1983, Temperatures, thermal conductivity, and heat flow from a well in Pierre Shale near Hayes, South Dakota: U.S.G.S. open-file Rep. 83–25, 10 p.

Sass, J. H., Lachenbruch, A. H., and Munroe, R. J., 1971a, Thermal conductivity of rocks from measurements on fragments and its application to heat flow determinations: J. Geophys. Res., v. 76, p. 3391–3401.

Sass, J. H., Lachenbruch, A. H., Munroe, R. J., Greene, G. W., and Moses, T. H., Jr., 1971b, Heat flow in the western United States: J. Geophys. Res., v. 76, p. 6376–6413.

Sass, J. H., and Munroe, R. J., 1974, Basic heat-flow data from the United States: U.S.G.S. open-file rep. 74-9, 426 p.

Schoeppel, R. J., and Gilarranz, S., 1966, Use of well log temperatures to evaluate regional geothermal gradients: J. Petr. Tech., v. 18, p. 667–673.

Scott, G. N., 1982, Temperature equilibration in boreholes—A statistical approach: M. S. Thesis, Univ. of Michigan, Ann Arbor, 63 p.

Smith, L., and Chapman, D. S., 1983, On the thermal effects of groundwater flow—1. Regional scale systems: J. Geophys. Res., v. 88, p. 593–608.

Untermann, G. E., and Untermann, B. R., 1964, Geology of Uintah County: Utah Geological and Min. Surv. Bull. 72, 112 p.

Vacquier, V., 1981, Calculation of thermal conductivity from lithologic logs and laboratory measurements on oil well cores, a review: Abstract from Am. Assoc. of Petr. Geol. Research Conf. on the Geothermal Environment of Oil and Gas, Sante Fe, New Mexico.

GEOPHYSICS, VOL. 46, NO. 12 (DECEMBER 1981); P. 1732–1744, 6 FIGS., 2 TABLES.

Continuation of heat flow data: A method to construct isotherms in geothermal areas

Charles A. Brott*, David D. Blackwell‡, and Paul Morgan§

ABSTRACT

A continuation technique for conductive heat flow in a homogeneous isotropic medium is presented which utilizes observed surface heat flow data. The technique uses equivalent point sources and is developed for transient or steady-state conductive heat flow problems for a homogeneous half-space with plane surface and a surface with topographic relief. The technique is demonstrated by comparison with a steady-state fault model and the terrain correction problem; it is also compared to observed heat flow data in two geothermal areas (Marysville, Montana and East Mesa, Imperial Valley, California). Calculated subsurface temperature distributions are compared to analytical models and the results of geophysical studies in deep drillholes in geothermal systems. Even in geothermal systems, where convection is involved in the heat transfer, the boundaries of the "reservoir" associated with the convective system can be treated as a boundary condition and the depth and shape of this boundary can be calculated, since many geothermal systems are controlled by permeability barriers. These barriers may either be due to the natural development of a trap or to self-sealing. Continuation of surface heat flow data is a useful technique in the initial evaluation of geothermal resources as well as an additional tool in the interpretation of regional heat-flow data.

INTRODUCTION

Heat flow anomalies at the earth's surface can be caused by one or more of the following: (1) contrast of thermal conductivity and the resulting refraction of heat; (2) contrast in the sources of heat production; (3) local temperature differences caused by the intrusions of hot (or cold) material; and (4) convection of groundwater. Also, Birch (1950) and most recently Blackwell et al (1980) pointed out that apparent anomalies will arise from topographic features. Numerical models showing the effect of thermal conductivity contrasts were reported by Simmons (1965) and other authors. We develop a simple continuation method for conductive heat flow in a homogeneous isotropic media, which utilizes surface heat-flow data, and use it to put spatial and temporal limits on the sources or temperatures associated with heat flow anomalies. If the source of the anomaly is a distribution of temperature, then the source configuration can be directly calculated. If the source of the anomaly is related to heat generation variations, then the interpretation is more complicated.

The continuation of surface heat flow data to determine subsurface temperature distributions is a useful method for investigating the subsurface in some geothermal areas. Constructed isotherms will converge around the anomaly sources and have a direct relationship to the location of the sources. For example, a geothermal anomaly which is caused by hot circulating fluid in a "simple reservoir" is considered. The term simple reservoir is used to describe a volume consisting of highly permeable rocks with fluid circulation within the volume or reservoir, surrounded by effectively impermeable rocks. The circulating fluid tends to keep the temperature uniform in the reservoir; hence, the boundary of the reservoir is approximately an isotherm. Outside the reservoir, the heat transfer mechanism is only conduction since the rocks are impermeable. Utilizing the surface geothermal gradient in a continuation method, one can construct an isothermal surface which is the same temperature as the reservoir. The isothermal surface can then be used to investigate the relationship of the possible reservoir to geologic or other geophysical information and in resource analysis.

The major problem in the calculation of subsurface temperature distributions is the spatial diffusion of heat. Since the flow of heat is not restricted to the vertical direction, the estimation of subsurface temperatures by extrapolation of surface gradients is erroneous. The correct solution of this problem involves a downward or sourceward continuation which accounts for spreading of heat in all directions. The spatial distribution of heat may be time-dependent, as in the case of a source which has been "turned on" for a short period of time (e.g., a recent emplacement of an intrusive body). For such cases the correct solution must also account for the time dependency of the temperature distribution. Continuation techniques have been described for gravity and magnetics by Grant and West (1965, chapter 8) and many other authors. Although the equations describing steady-state heat flow, gravity, and magnetics are very similar, most gravity and magnetic continuation techniques cannot be applied usefully to

Manuscript received by the Editor December 21, 1979; revised manuscript received May 18, 1981.
*Phillips Petroleum Company, Research and Development, Bartlesville, OK 74004.
‡Department of Geological Sciences, Southern Methodist University, Dallas, TX 75275.
§Lunar and Planetary Institute, 3303 NASA Road One, Houston, TX 77058.

heat-flow data. A problem arises from the basic difference between gravity and magnetic data sets compared to heat flow data sets measured on the surface of the earth. Gravity and magnetic data comprise a set of potential gradient (field strength) values spatially distributed on a plane whose potential also has a lateral variation.

Heat flow data comprise a set of field strength values, but the values are spatially distributed on a plane of essentially uniform potential (the surface temperature). Thus when continuing heat flow data, image sources must be considered. The heat-flow data can be continued by similar techniques as gravity and magnetic fields. However, to compute the subsurface temperatures (an essential parameter in any geothermal investigation), a very complex integration over the continuation path is required (Bodvarsson, 1973).

In the first part of this paper, we present a technique for the sourceward continuation of heat flow data obtained on a plane surface by which subsurface temperatures can be directly estimated for either the steady-state or time-dependent case. The technique consists of constructing equivalent point sources, similar to the method of Dampney (1969) for modeling gravity data.

In a second part, the basic continuation method developed for a plane surface is extended to a form that can be used to obtain terrain corrections. The nature of the terrain correction problem allows it to be identified as the "spaceward" (away from the source) continuation problem where the topographic relief with the nonuniform surface temperature distribution can be represented by a source distribution located on or above the surface (Birch, 1950; Blackwell et al, 1980).

CONTINUATION TECHNIQUE

The continuation method described here is based on a fundamental potential field property: Outside the boundaries of a volume containing sources, the field, once defined, is unique. Even though there is always a family of source solutions which will generate the same field, any source solution which satisfies the surface field strength values can be used to calculate the field parameters at any point outside the volume containing the sources. The source solutions used in this continuation method are an array of line or point sources for the two-dimensional (2-D) or three-dimensional (3-D) case, respectively. By solving simultaneous equations, the source strengths are determined from known surface heat-flow data or geothermal gradients.

The assumptions for obtaining the source strengths are (1) the heat transfer mechanism is by conduction alone; (2) a homogeneous isotropic medium in which no heat is generated occupies the space between the sources and surface; and (3) the sources are continuous in time and have constant heat generation with time. Once the source solution is known, the subsurface temperature can be calculated directly.

The differential equation for the conduction of heat in a homogeneous isotropic medium in which no heat is generated is

$$\nabla^2 T = (1/\kappa)\partial T/\partial t, \tag{1}$$

where T is temperature, κ is diffusivity, t is time, and ∇^2 is the Laplacian ($\nabla^2 = \partial^2/\partial x^2 + \partial^2/\partial y^2 + \partial^2/\partial z^2$). The geothermal gradient g is the negative of the partial derivative of the temperature T along the vertical direction z,

$$g = -\partial T/\partial z. \tag{2}$$

The differential equation for the conduction of heat degenerates into the Laplace equation

$$\nabla^2 T = 0 \tag{3}$$

for the steady-state case.

The infinite-medium solutions for the steady-state and time-dependent temperature and gradient for point and line heat sources of constant heat generation are listed in Table 1 (from Carslaw and Jaeger, 1959, chapters 10 and 14). The solutions are written in two parts: a source term S and a distance term (D for temperatures and G for gradients). Individual solutions for single sources can be superimposed since they are the solutions of second-order linear differential equations. This property is essential because it allows a complex field to be constructed by summing the effects of many simple sources. Also, this property can be exploited through the method of images to obtain a uniform surface temperature. The use of the image sources and the basic ideas of the continuation method are discussed below.

Consider the 2-D model in Figure 1a. The surface geothermal gradients g_i, $i = 1, N$, at the points P_i, $i = 1, N$ (located on the reference plane $z = 0$) are known. Also, the surface temperature of the reference plane is a constant T_s which is known. By using the linear properties of the line source solution for the gradient from Table 1, the contribution to the surface gradient g_{ij} at the point P_i from the source Q_j and its image Q_j' can be expressed by

$$g_{ij}^c = S_j G_{ij} + S_j' G_{ij}', \tag{4a}$$

where S_j and S_j' are source terms which are functions of their respective constant source strengths Q_j and Q_j', and G_{ij} and G_{ij}' are gradient distance terms (see Figure 1a and Table 1). Since S_j' is the image source term of S_j, $S_j' = -S_j$, and since P_i is an equal distance from S_j and S_j' but in a different vertical direction, $G_{ij}' = -G_{ij}$. Therefore equation (4a) may be written as

$$g_{ij}^c = 2S_j G_{ij}. \tag{4b}$$

By superposition of all the N set of sources and images, the total gradient g_i^T at the point P_i is

$$g_i^T = 2\sum_{j=1}^{N} S_j G_{ij}. \tag{5}$$

Similar expressions can be written for the total gradient at each ith point, $i = 1, N$. The parameters defining the distance terms G_{ij} are known, but the individual source strengths Q_j are not known. Since there are N equations and N sets of sources and images, the source terms can be calculated by solving the set of simultaneous equations.

The temperature T_k at any arbitary point P_k below the surface and above the source plane depth can be calculated using the following expression (see Table 1 and Figure 1b)

$$T_k = T_s + \sum_{j=1}^{N} S_j(D_{kj} - D_{ij}), \tag{6}$$

where S_j are the source terms obtained by solving the simultaneous equations, T_s is a known constant surface temperature, and the parameters defining the temperature-distance terms D_{ij} and D_{ij}' are known.

If the time when the sources were emplaced (turned on) is known, the time-dependent form of the source equation may be used and the method of obtaining the solution would be similar.

In three dimensions, point sources are used on a plane $z = a$ and images on a plane $z = -a$. The point source and distance terms are given in Table 1. The only additional complexity is another summation needed to account for the third dimension. For point sources on an $n \times m$ grid, the surface gradient g_{ij} is

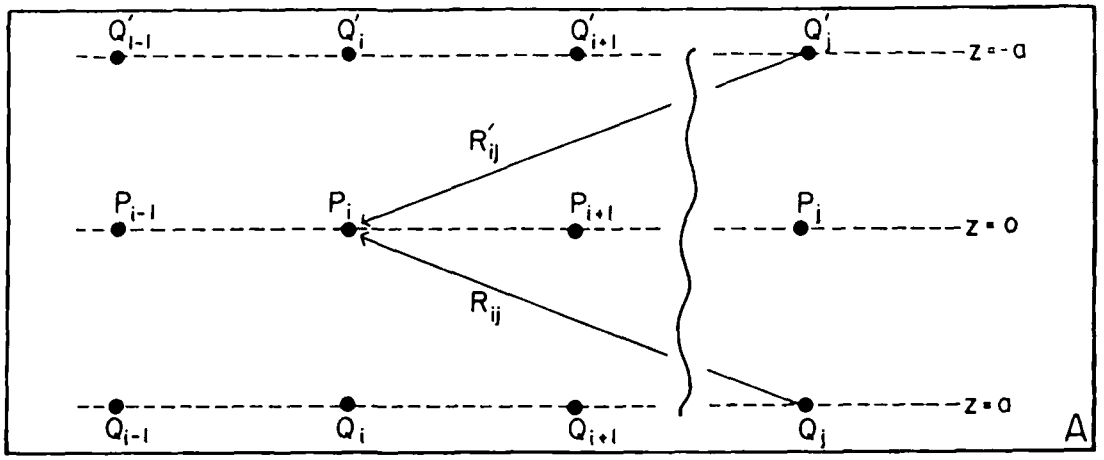

FIG. 1a. Geometry for the continuation model. Sources Q_{i-1}, Q_i, and Q_{i+1} are on the plane $z = a$, with image sources Q'_{i-1}; Q'_i, and Q'_{i+1}, on the plane $z = -a$. The surface gardients are known at points P_{i-1}, P_i, and P_{i+1} on the plane $z = 0$. The distance term between any particular source image point Q_j, or Q'_j, is $R_{ij}(=R'_{ij})$.

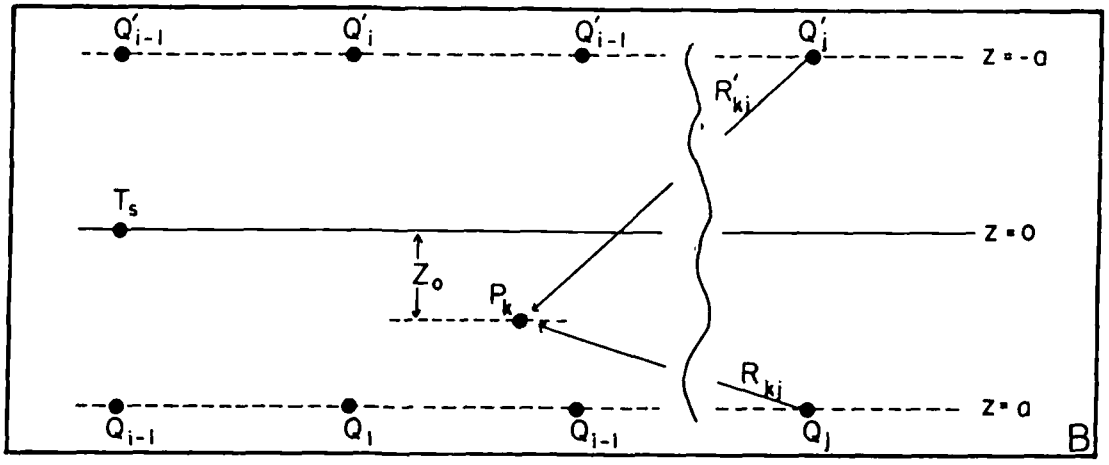

FIG. 1b. Geometry for the continuation model used to compute the subsurface temperature at point P_k which is between the planes $z = 0$ and $z = a$ at depth z_0.

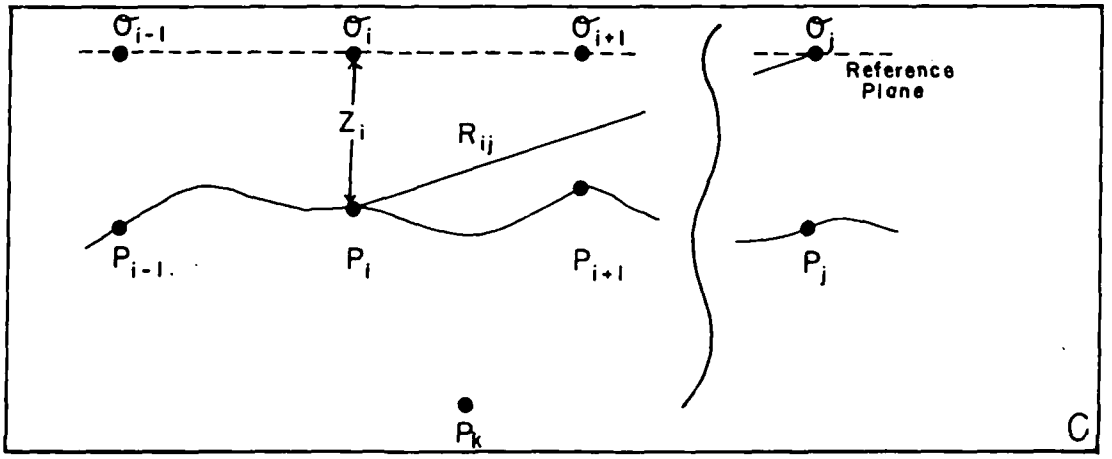

FIG. 1c. Geometry for the terrain correction model. Line doublets σ_{i-1}, σ_i, and σ_{i+1} are on a reference plane. The surface temperatures and the elevation differences of the points P_{i-1}, P_i, and P_{i+1} are known. The vertical distance from the reference plane to point P_k and the gradient at P_k are known.

Table 1. Solutions for constant and continuous point and line sources (Carslaw and Jaeger, 1959).

	Source term	Time-dependent distance term	Steady-state distance term
Temperature (T), $T = S \cdot D$			
Point source	$S = Q/4\pi\kappa$	$D = (1/R)\,\mathrm{erfc}(R/\sqrt{4\kappa t})$	$D = 1/R$
Line source	$S = Q/4\pi\kappa$	$D = -Ei(-R^2/4\kappa t)$ where $-Ei(-x) = \int^{\infty} x(e^{-u}/u)du$	$D = -2\ln(R)$
Geothermal gradient (g), $g = S \cdot G$			
Point source	$S = Q/4\pi\kappa$	$G = [(z - z')/R^3]^*$ $[(2R/\sqrt{\pi\kappa t})\exp(-R^2/4\kappa t) + \mathrm{erfc}(R/\sqrt{4\kappa t})]$	$G = (z - z')/R^3$
Line source	$S = Q/4\pi\kappa$	$G = [2(z - z')/R^2]^*$ $\exp(-R^2/4\kappa t)$	$G = 2(z - z')/R^2$

Q is source strength, t is time, κ is diffusivity, and R is the distance from the source to the field point.
$R^2 = (x - x')^2 + (y - y')^2 + (z - z')^2$ for the point source and
$R^2 = (x - x')^2 + (z - z')^2$ for the line source, where (x, y, z) is the field point and (x', y', z') is the source point.

expressed at a point P_{ij} by

$$g_{ij} = 2 \sum_{k=1}^{n} \cdot \sum_{l=1}^{m} S_{kl} G_{ijkl}, \qquad (7)$$

and temperature T_{ij} is expressed at a point P_{ij} by

$$T_{ij} = \sum_{k=1}^{n} \sum_{l=1}^{m} S_{kl} \cdot (D_{ijkl} - D_{ijkl\cdot}) + T_s. \qquad (8)$$

If the models have a known uniform-background geothermal gradient g_0, it can be introduced in the gradient equations [equations (5) and (7)] by adding it to the right-hand side of the equations, and to the temperature equations [equations (6) and (8)] by adding the product $(g_0 z)$ of a uniform background gradient and the vertical distance to the reference plane to the right side of the equations.

TERRAIN CORRECTION TECHNIQUE

The terrain correction involves a spaceward (away from the source) continuation. Since the surface temperature is a boundary, the topographic relief and nonuniform surface temperatures are modeled by the use of vertical line or point doublets (temperature dipoles). The use of dipoles to model variable surface potential is a well-known technique (see Grant and West 1965; Carslaw and Jaeger, 1959). The same fundamental potential field properties, assumptions, and restrictions which apply to the continuation method discussed above also apply to this terrain correction technique.

The solutions for the vertical line and point doublets are listed in Table 2 (from Carslaw and Jaeger, 1959, chapters 10 and 14). The solutions are written in two parts, a source term σ and a distance term (Δ for temperature and Γ for gradients). Again, individual doublets can be superimposed since they are also solutions for a second-order linear differential equation (1) or equation (3). This superposition property is essential because it allows a complex temperature distribution on an irregular surface to be represented by the sum of the effects of many doublets. The use of the doublets and the basics of the terrain correction method are discussed below.

Consider the 2-D model in Figure 1c. The topographic relief is shown by a line and surface temperatures T_i, $i = 1, N$ are known at points P_i, $i = 1, N$, respectively. The observed gradient g is known at point P_{N+1}. Using the line doublet solutions for the temperature from Table 2, a general equation for the

Table 2. Solutions for constant and continuous point and line doublets (Carslaw and Jaegar, 1959).

	Source term	Steady-state distance term
Temperature (T), $T = \sigma \cdot \Delta$		
Point doublet	$\sigma = Q/4\pi\kappa$	$\Delta = (z - z')/R^3$
Line doublet	$\sigma = Q/4\pi\kappa$	$\Delta = 2(z - z')/R^2$
Gradient (g), $g = \sigma \cdot \Gamma$		
Point doublet	$\sigma = Q/4\pi\kappa$	$\Gamma = [1 - 3(z - z')^2/R^2]/R^3$
Line doublet	$\sigma = Q/4\pi\kappa$	$\Gamma = 2[1 - 2(z - z')^2/R^2]/R^2$

Q is the source strength, κ is diffusivity, and R is the distance from the source to the field point.
$R^2 = (x - x')^2 + (y - y')^2 + (z - z')^2$ for point doublets and
$R^2 = (x - x')^2 + (z - z')^2$ for line doublets, where (x, y, z) is the field point and (x', y', z') is the source point.

temperature T_i at P_i can be written as

$$T_i = \sum_{j=1}^{n} (\sigma_j \Delta_{ij}) + z_i \alpha, \quad (9)$$

where the dipole source terms σ_j are a function of their respective source strengths, the temperature distance terms Δ_{ij} are functions of the distance from their respective sources to the point P_i, z_i is the distance from the reference plane to the point P_i, and α is the undisturbed regional gradient (Figure 1c and Table 2). Using the doublet solutions for the gradient from Table 2, the gradient g at P_{N+1} can be written as

$$g = \sum_{j=1}^{N} (\sigma_j \Gamma_{N+1,j}) + \alpha, \quad (10)$$

where the source terms are the same as above, the gradient distance terms $\Gamma_{N+1,j}$ are a function of the distance from their respective source to the point P_{N+1}, and α is the same undisturbed gradient as above.

Since the parameters defining the temperature and gradient distance terms Δ_{ij} and $\Gamma_{N+1,j}$ are known, these terms can be cal-

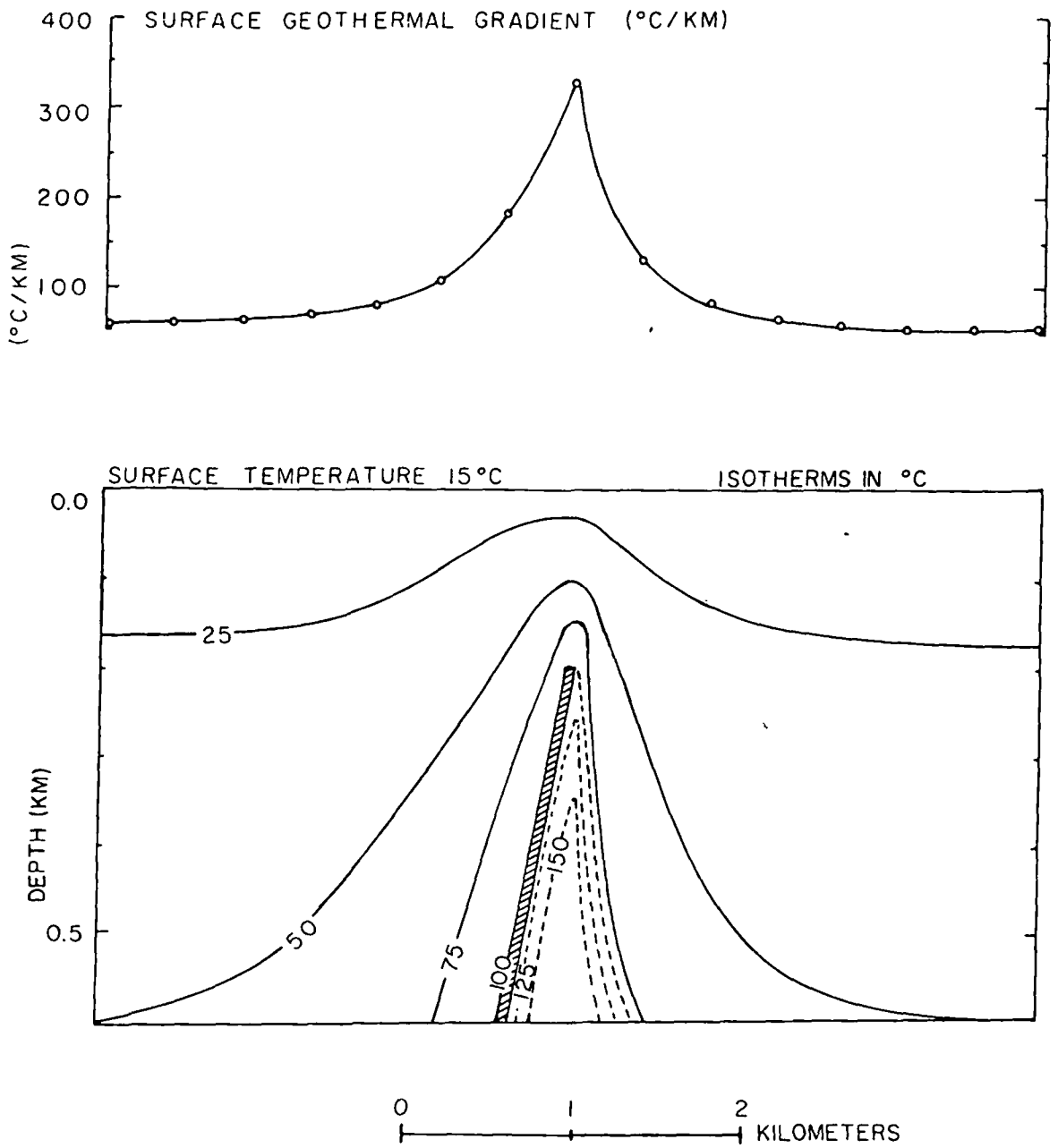

FIG. 2. A steady-state 2-D fault model with surface geothermal gradient shown above the model. The fault has a constant temperature of 100°C which is interpreted as circulation of hot fluid along and in the fault zone dipping 45 degrees to the left. The numerical model isotherms are shown by solid lines and the continued isotherms are shown by dashed lines where they diverge from the numerical model isotherms. A constant background gradient of 54°C/km and a uniform surface temperature of 15°C are used in this model.

culated (Table 2). Since there are $N + 1$ equations, the N source terms σ_j and the undisturbed gradient α can be found by solving the equations simultaneously.

The purpose of a terrain correction is usually to find the undisturbed gradient α, but if the subsurface temperatures are needed, they can be calculated by using the source terms σ_1 and the undisturbed gradient as shown in equation (11). By using the linear properties of the solutions in Table 2, the temperature T_k at point P_k in Figure 1c can be calculated by

$$T_k = \sum_{j=1}^{N} \sigma_j \Delta_{kj} + z_k \alpha, \tag{11}$$

where the temperature distance terms Δ_{kj} are a function of distance from their respective source to the point P_k. The source terms σ_j and the undisturbed gradient α are obtained from the simultaneous solution of equations (10). The parameters defining the temperature distance terms Δ_{kj} and z_k, and the distance from the reference plane $z = 0$ to P_k, are known. Equation (11) can now be solved directly.

In three dimensions, the point doublet solutions for the temperature and gradient from Table 1 are used, and the only additional complexity is the summation of the third dimension. The temperature T_{ij} at a point P_{ij} due to point doublets on an $n \times m$ grid is expressed by

$$T_{ij} = z_{ij}\alpha + \sum_{k=1}^{n} \cdot \sum_{l=1}^{m} \sigma_{ij} \Delta_{ijkl}, \tag{12}$$

and the gradient g_{ij} at a point P_{ij} is expressed by

$$g_{ij} = \alpha + \sum_{k=1}^{n} \sum_{l=1}^{m} \sigma_{ij} \Gamma_{ijkl}. \tag{13}$$

The source and dipole solutions discussed in this and the previous section can be combined and a modified equation derived to find subsurface temperatures when a gradient distribution (due to subsurface lateral variations in heat flow) is known on a surface with topographic relief. The equations are easily derived from the equations presented for the separate solutions; they are not included here.

Dipoles are chosen to match the surface temperature, which varies as a function of position on the boundary surface (also is a function of position) because they can be used to define a specific temperature more readily than sources. Birch (1950) similarly used a dipole distribution to derive his time-dependent terrain correction.

UTILIZATION OF THE CONTINUATION METHOD

The continuation method discussed here requires that the surface heat flow data be digitized on a grid. It is convenient to use equal grid spacing. An interpolation polynomial can be used to obtain the data values at other than measured points (Carnahan et al, 1969, chapter 1; and many other authors). Alternatively, a least-square polynomial or a Fourier series may be fitted to the data and the value at each data point obtained from evaluation of the resulting polynomial or series (Claerbout, 1976, chapter 6; Henderson and Cordell, 1971).

Sharp irregularities or variations in the surface heat flow data which may be due to shallow anomalies (Simmons, 1967) or erroneous data can cause serious problems when applying the continuation method. Ku et al (1971) pointed out, with reference to sourceward continuation of gravity data, that the Gibbs phenomenon, or high-amplitude oscillations, occur at places of sharp variation in surface data and that a low-pass filter could be used to reduce or eliminate these oscillations. Thus smoothing of the surface data, which reduces these sharp variations, can be used as a low-pass filter, allowing continuation of the temperature to greater depths than would be possible with the unsmoothed data. A very simple way of applying a low-pass filter to discrete data is to increase the grid spacing, since the wavelength of the anomaly is directly related to the depth of the source (Ku et al, 1971). The sampling rate of the surface data is critical because, for large grid spacing, aliasing of short-wavelength anomalies can occur. Since short-wavelength anomalies are the result of shallow sources, increased grid spacing or low-pass filtering allows continuation to greater depths without oscillations; however, detailed information contained in the data is lost.

The depth of the plane of point or line sources below the surface can be estimated in a manner similar to finding the depths to the center of bodies producing gravitational anomalies. Simmons (1967) developed methods for estimating the depth of theoretical surface heat flow anomalies, and these methods can be used to approximate the depth of the source plane. The height of the image source plane above the surface is equal to the depth of the source plane below the surface.

The solution of the large number of simultaneous equations needed to determine the source terms can be performed using matrix methods. The size of the matrix becomes very large for the 3-D case and requires a large amount of computer storage. Future work is planned to use the continuation method to determine filter coefficients so that sourceward continuation can be done by use of the Fourier transform. Sourceward continuation of gravity data using the Fourier transform, coupled with filter coefficients, is described by Odegard and Berg (1965), Kanasewich and Agarwal (1970), and others. By using the Fourier transform, less computer storage would be needed and an analog for fast Fourier transformation (Cooley and Tukey, 1965) could be used to reduce the computing time. Because of the sparse data sets usually available for geothermal interpretation, use of the more formal data analysis techniques may not be justified.

STEADY-STATE FAULT MODEL

Figure 2 shows a 2-D steady-state model of 100°C water circulating along a fault dipping at 45 degrees (crosshatch pattern). The model has a constant background gradient of 54°C/km and a uniform surface temperature of 15°C. The subsurface model isotherms (solid lines) were computed by a finite-difference numerical technique. The calculated surface geothermal gradient profile is shown above the model.

Subsurface isotherms were calculated using the continuation method discussed above, given the surface gradient from the finite-difference solution and using steady-state line sources. The terms, constants, and equations used in the continuation method are as follows: The source S and the distance (G, D) terms for the gradient and temperatures used for steady-state line sources were of the form shown in Table 1. The depth to the line sources and height to the image sources were chosen to be 0.8 km, and the gradient profile was first sampled at horizontal intervals of 0.4 km (open circles in Figure 2). The depth of 0.8 km was chosen to show that constructed isotherms will converge around the fault.

The simultaneous equations used to evaluate the source terms were derived using the 2-D surface gradient equation [equation (5)]. The subsurface temperatures were calculated using the 2-D temperature equation [equation (6)]. Isotherms were constructed from these temperatures. At depths greater than 0.3 km, the isotherms showed oscillations below the sharp peak of

the surface gradient. In order to calculate temperatures below 0.3 km, the surface gradient data were smoothed by increasing the interval (grid spacing) of the surface gradient to 0.8 km (effectively applying a low-pass filter to the surface data). The oscillations below the surface gradient peak were reduced, and continuated temperatures were computed to a depth of 0.6 km. The calculated temperatures below 0.3 km are the average of first dropping the even numbered sample grid spaces, then the odd numbered grid spaces.

The constructed 25°, 50°, and 75°C isotherms calculated by the continuation technique closely follow the isotherms calculated by the finite-difference technique (Figure 2). On the left side of the model the 100°C isotherm corresponds to the left side of the fault, but the right side (dashed line) diverges from the fault, as do calculated isotherms greater than 100°C. By continuation of the potential field (surface gradient) below the circulating 100°C water at the tip of the fault (0.2 km), one of the basic continuation premises was violated.

The circulating 100°C water along the fault is the actual source which causes the observed surface gradient; therefore, solutions obtained by continuation below the actual source depth are not valid. By smoothing the surface field data, the depth to the source in the real case appeared deeper, and continuation below the actual source depth was accomplished. Isotherms that fold under themselves as shown in the model only occur below the circulating 100°C water (the actual source). Similarly shaped isotherms cannot be obtained by a continuation technique using a generalized source distribution.

The above 2-D model demonstrates that continuation of the surface data is useful in defining spatial limits to a simple reservoir which is a combined problem of convection and conduction. The shape and size of the upper part of the simple reservoir (circulating 100°C water along the fault) is delineated by the 100°C isotherm. The source solution obtained is not unique because any of the constructed isotherms could be used to define the upper part of a corresponding simple reservoir with that temperature. In order to determine reliably which isotherm defines the actual reservoir, knowledge of the temperature or depth of the reservoir is essential.

The maximum possible depth to the reservoir can be estimated by applying the half-width rule to the surface gradient profile. Using the depth obtained from the half-width rule (0.25 km), the corresponding temperature would be 100°–125°C.

TERRAIN MODEL

Figure 3 shows a 2-D terrain model from Birch (1967). The temperature T at any point can be calculated by

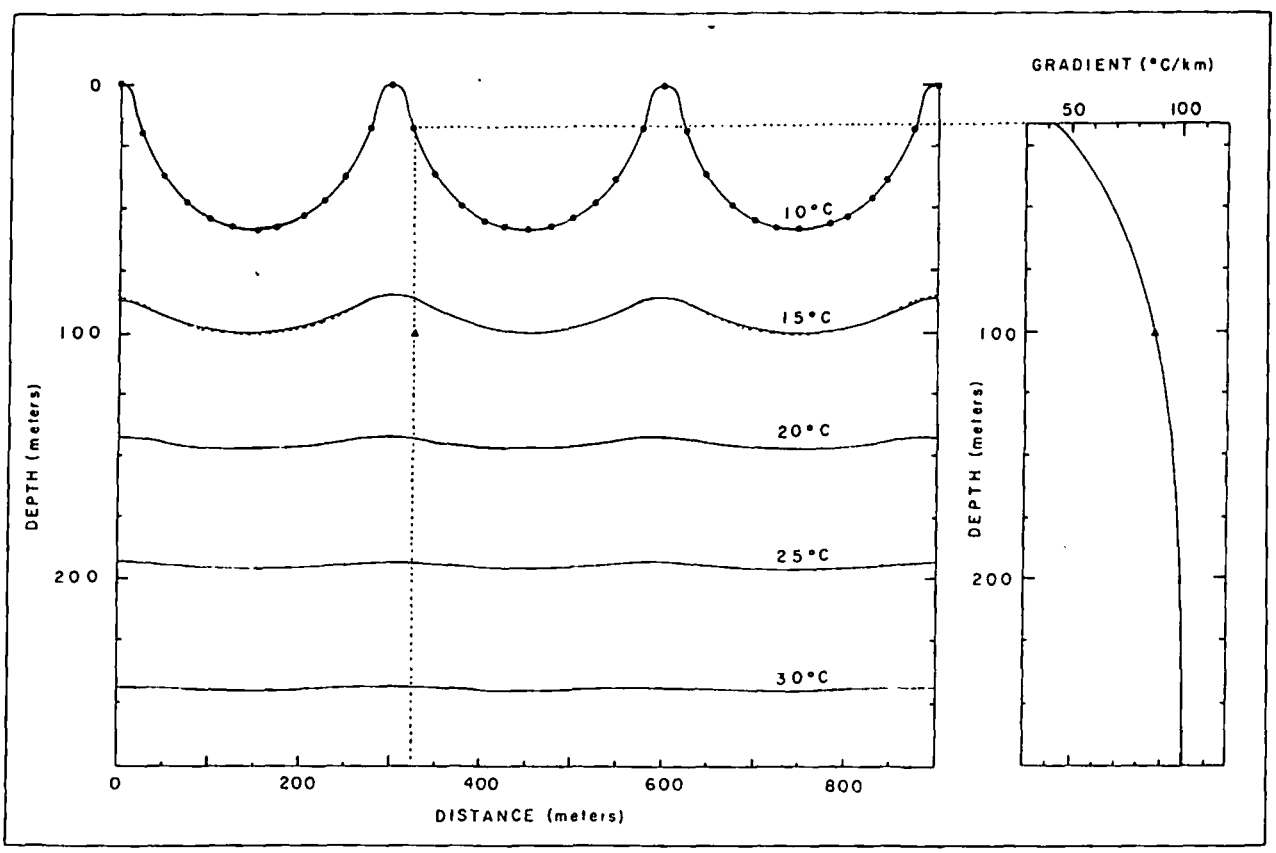

FIG. 3. 2-D terrain model from Birch (1967). The model has a uniform surface temperature of 10°C, and the undisturbed gradient at depth is 100°C/km. Dots on the surface of the model show the sampling locations of surface temperature. Model isotherms are shown as solid lines. The dashed lines show locations where the isotherms constructed by the continuation technique deviated from the model isotherms. The dotted vertical line shows the location of the gradient-depth curve to the right of the model. The solid triangles on the model and on the gradient-depth curve show the location of the known gradient used in the illustration of the terrain correction technique.

$$T(x, z) = T_0 + \alpha(z - ae^{-kz} \cos kx), \quad (14)$$

where z is the depth, positive downward; x distance, T_0 surface temperature, k wavelength, and α the undisturbed vertical gradient. The surface (z) varies nearly sinusoidally with x and is defined by

$$z = ae^{-kz} \cos kx, \quad (15)$$

where ae^{-kz} is the amplitude. The vertical gradient anywhere in the model can be calculated by

$$\frac{\partial T}{\partial z} = \alpha(1 + kae^{-kz} \cos kx). \quad (16)$$

The values of the parameters used in the model shown in Figure 3 are $a = 17.5$ m, $k = 2\pi/300$ m^{-1}, $T_0 = 10$°C, and $\alpha = 100$°C/km. Model isotherms are shown as solid lines, and a model gradient-depth curve at a horizontal position of 325 m (dashed line) is shown to the left of the model.

The terrain correction method developed above was applied to the model to find the undisturbed gradient and to construct subsurface isotherms. The terms, constants, and equations used are as follows: The doublet sources σ and the distance Γ and Δ for the gradients and temperatures are of the form shown in Table 2. The reference plane for the source is 25 m above the actual surface. The surface temperature was sampled every 25 m horizontally (shown as solid circles in Figure 3). The gradient was sampled at a depth of approximately 82 m below the surface and at a horizontal displacement of 325 m as shown by the solid triangle. The simultaneous equations used to evaluate the source terms were derived from the 2-D temperature and gradient equations [equations (9) and (10)]. The subsurface temperatures and gradients are calculated at intervals of 25 m for several depths.

The isotherms constructed from the terrain correction method closely follow the model isotherms (Figure 3). The calculated undisturbed gradient is 100.6°C/km, whereas the undisturbed model gradient is 100°C/km (0.6 percent error). The vertical gradient-depth curve for 325-m horizontal displacement is also shown in Figure 3. The constructed gradient-depth curve very closely follows the model gradient-depth curve. The model used to test the terrain correction technique is very simple but illustrates that the technique can be used to calculate corrected geothermal gradients from wells located in areas of topographic relief. The terrain correction problem is very complex, and this

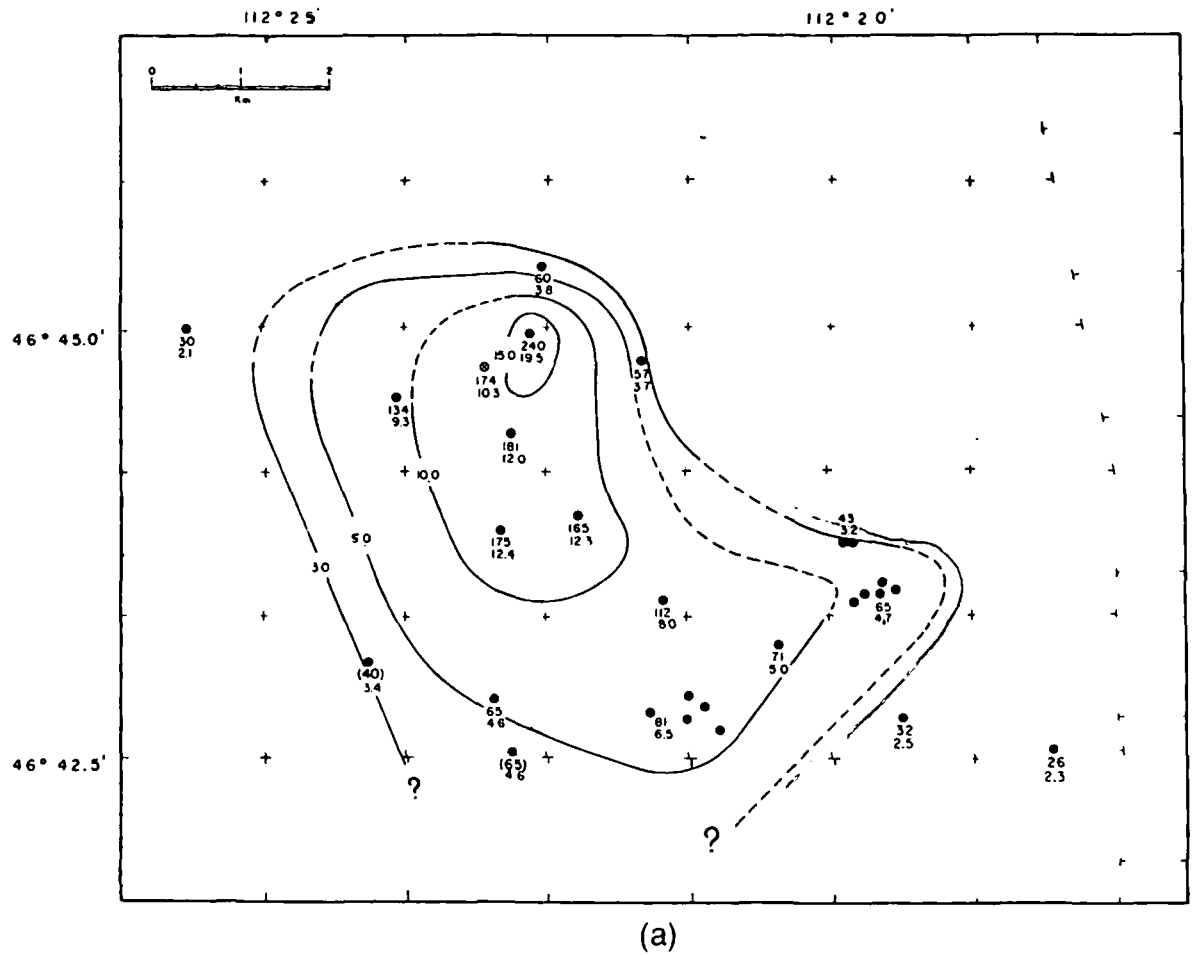

(a)

FIG. 4a. Marysville surface heat flow and geothermal gradient map (Blackwell et al, 1975). The location of the deep geothermal well (MGE #1) is shown as the circle with the cross, and the locations of other wells available for gradient and heat flow studies are shown as solid circles. The upper number of each pair is the terrain corrected geothermal gradient in °C/km. The lower figure is the terrain corrected surface heat flow value in μcal/cm^2 sec. Gradient values which are shown in parentheses have been adjusted for thermal conductivity variation (see Blackwell et al, 1975). The crosses are section corners.

discussion is not intended as a complete discussion of the problem (see Blackwell et al, 1980).

A difficulty with fitting the surface temperatures often occurs in the valleys because the surface there is relatively far from the plane of dipoles, yet it has very abrupt changes in temperature due to microclimatic effects. The technique described above can be modified so that the dipoles are spaced a fixed distance above the topography (say 100 m), and the surface of dipoles thus mimics the topography. As long as the location of each dipole is specified so that the distance term is known, the solution proceeds exactly as discussed above. We have used this feature to calculate detailed terrain corrections involving very complicated surface temperature variations.

THE APPLICATION OF THE HEAT FLOW CONTINUATION METHOD TO GEOTHERMAL AREAS

Marysville, Montana

The Marysville geothermal area in Montana is characterized by high heat flow (up to 19.5 μcal/cm^2 sec; 81.5 mW/m^2; Figure 4a), a negative gravity anomaly, high electrical resistivity, nearby microseismic activity, and low seismic ground noise (see Blackwell et al, 1975; Blackwell and Morgan, 1976). The geothermal anomaly appears to be bounded to the northeast by the subcrop of a Mesozoic granodiorite body, the Marysville stock, as shown in Figure 4b; and a fault has been mapped along the south side of the Marysville stock. Results from a 2.1-km test well drilled close to the peak of the geothermal anomaly (Figure 4a) indicate that the anomaly is caused by hydrothermal convection along distributed fracture zones in a Cenozoic granite porphyry. Maximum temperatures of 100°C were measured in the test well, and the modeled system is assumed to act as a simple reservoir with a temperature of about 95°C at its upper surface.

Heat flow data from the Marysville anomaly were continued sourceward using steady-state point sources. The heat flow map was digitized on a 15 × 15 square grid with spacing of 500 m, and the data were assumed to be on a datum plane located at the mean level of the actual topography. The heat flow values Q were used to determine surface vertical geothermal gradients using the one-dimensional (1-D) steady-state heat conduction equation

$$Q = gK, \tag{17}$$

where K is the rock thermal conductivity. A value for K of

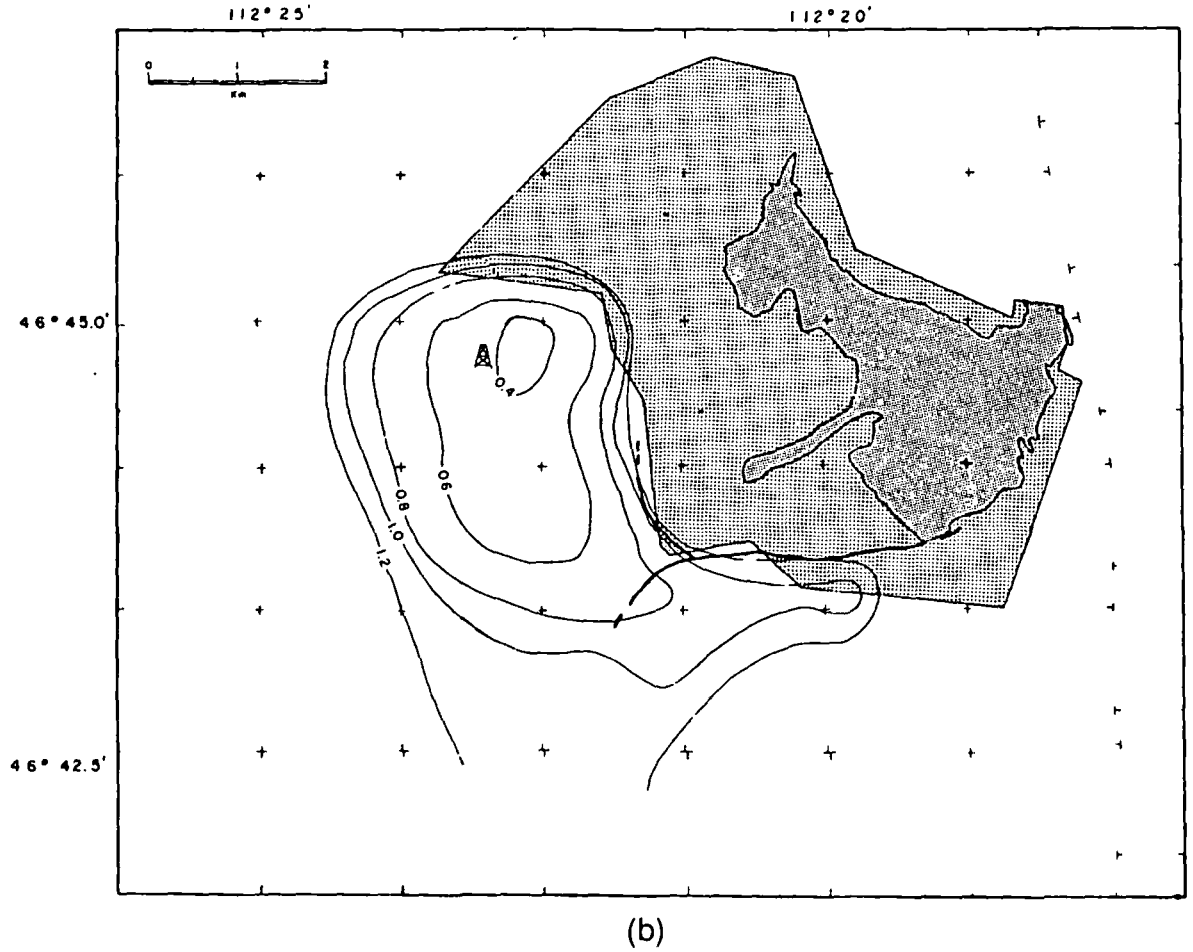

(b)

FIG. 4b. Marysville stock and geothermal reservoir (Blackwell et al, 1975). The outcrop and maximum subcrop of the stock are shown as dark and light shaded regions, respectively. The subcrop extent of the stock is based on the interpretation of magnetic data. The dark line shows the location of a major fault along the south edge of the stock. The depth to the contours of the geothermal reservoir is based on the continuation of surface heat flow data and is the same as 95°C isotherm, assumed to be the reservoir temperature. The location of the deep geothermal well (MGE #1) is shown by the derrick symbol. The crosses are section corners.

7.5 mcal/cm-sec-°C (3.1 W/m°K) was used based upon the mean thermal conductivity of core samples from the heat flow boreholes. The source term S and the distance terms (G and D) for the steady-state point sources used for the surface gradient and temperatures are given in Table 1. The sources and image sources were located 2.5 km below and above the datum plane, respectively, and the simultaneous equations used to calculate the source terms were derived from the 3-D gradient equation [equation (4)]. Using the 3-D temperature equation [equation (8)], subsurface temperatures were calculated on several planes below the datum plane and the 95°C isotherm was contoured on each of the planes.

Figure 4b shows the contours of the 95°C isotherm in the depth range of 0.4 km to 1.2 km at 0.2 km intervals, superimposed on the outline of the Marysville stock. The 95°C isothermal surface is interpreted to have approximately the same configuration as the geothermal reservoir. Very steep sides to the reservoir are indicated on the north and northeast, with relatively steep sides on the west and southwest. A complex shape is indicated in the south and southeast. The northern and eastern part of the reservoir is apparently bounded to the north and northeast by the Marysville stock. A narrow east-west salient of the 95°C isotherm is observed south of the stock. The narrowness of this salient suggests that its origin may be geothermal fluid moving along a narrow zone, such as a fault, either flowing east away from or west into the main reservoir. A fault has been mapped on the south side of the Marysville stock (Figure 4b) which could be the structure controlling this narrow zone of subsurface fluid flow.

The source of the Marysville geothermal anomaly was already known before the heat flow continuation method was applied, and it was from the deep test well data that the 95°C isothermal surface was chosen to represent the upper surface of the reservoir. Even without the deep well data, the subsurface temperatures from the continuation of the shallow heat flow data give an indication of the source of the anomaly. Since the distance between the 3 to 15 HFU contours in Figure 4a in the northeast is approximately 1 km, application of the half-width rule indicates the maximum source depth to be 0.5 km where the calculated temperature is approximately 100°C.

Simple extrapolation of the surface heat flow data using equation (17) to map the 95°C isothermal surface results in a set of contours similar to the heat flow contours shown in Figure 4a. The fine detail of the reservoir shape is not delineated and the narrow east-west salient is not defined, so the anomaly cannot be as directly related to the mapped fault. This example illustrates the power of the continuation technique in the geologic interpretation of surface geothermal anomalies.

East Mesa, Imperial Valley, California

The East Mesa geothermal anomaly is in the Imperial Valley, California, on the eastern flank of the Salton trough, the sediment-filled structural depression that forms the northern extension of the Gulf of California and East Pacific Rise. A range of geophysical and geochemical surveys all outline the same general target area covering an area of 40 km^2 where the heat flow is in excess of 5 μcal/cm^2 sec (210 mW/m^2) as shown in Figure 5a. Five deep wells have been drilled into the anomaly, the locations of which are also indicated on Figure 5a. The re-

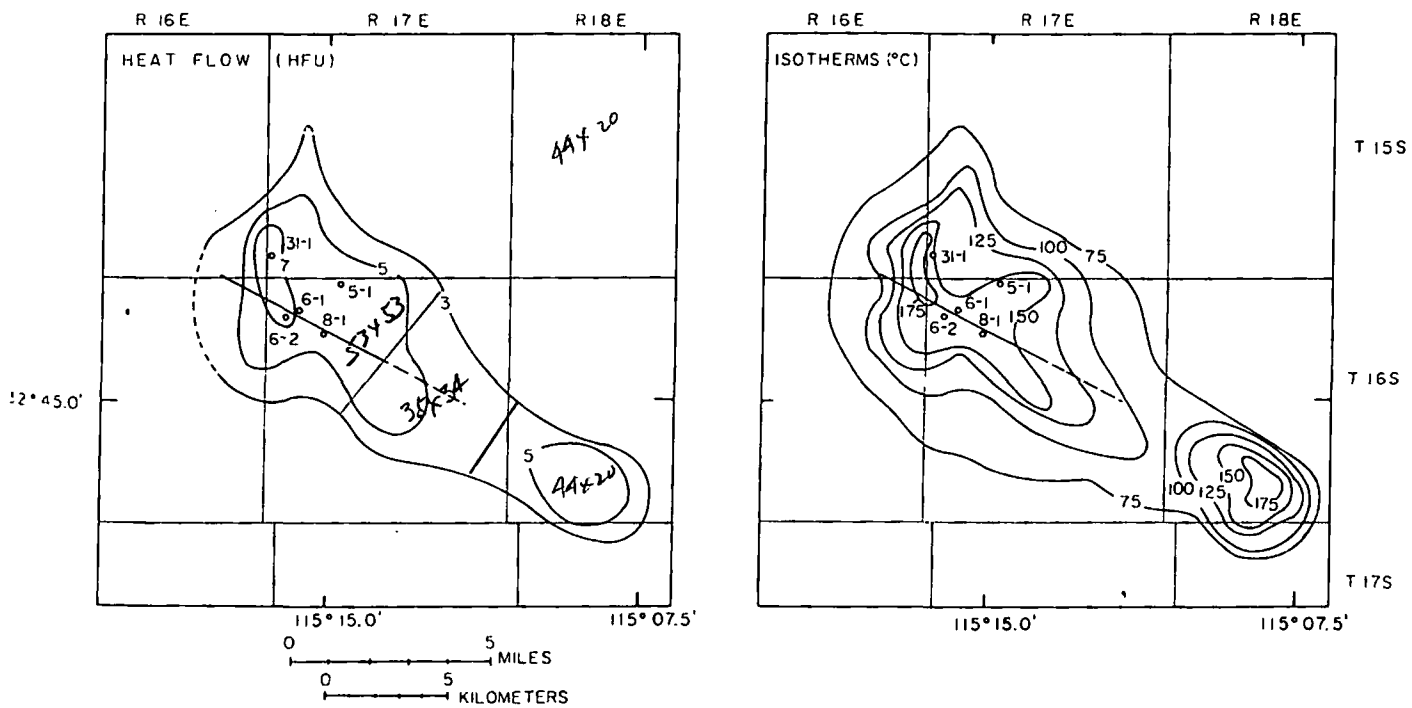

FIG. 5. (a) Generalized heat flow map of the East Mesa geothermal anomaly (after Swanberg, 1975). Heat flow contours of 3.0, 5.0, and 7.0 μcal/m^2 sec (125, 210, and 295 mW/m^2) are shown, together with the locations of the five deep wells (open circles 31-1, 5-1, 6-1, 6-2 and 8-1) and the fault mapped by Combs and Hadley (1977). (b) Computed isotherms between 75 and 175°C at 25°C intervals on a plane 0.8 km below the surface. The deep wells and fault are as shown in Figure 5a.

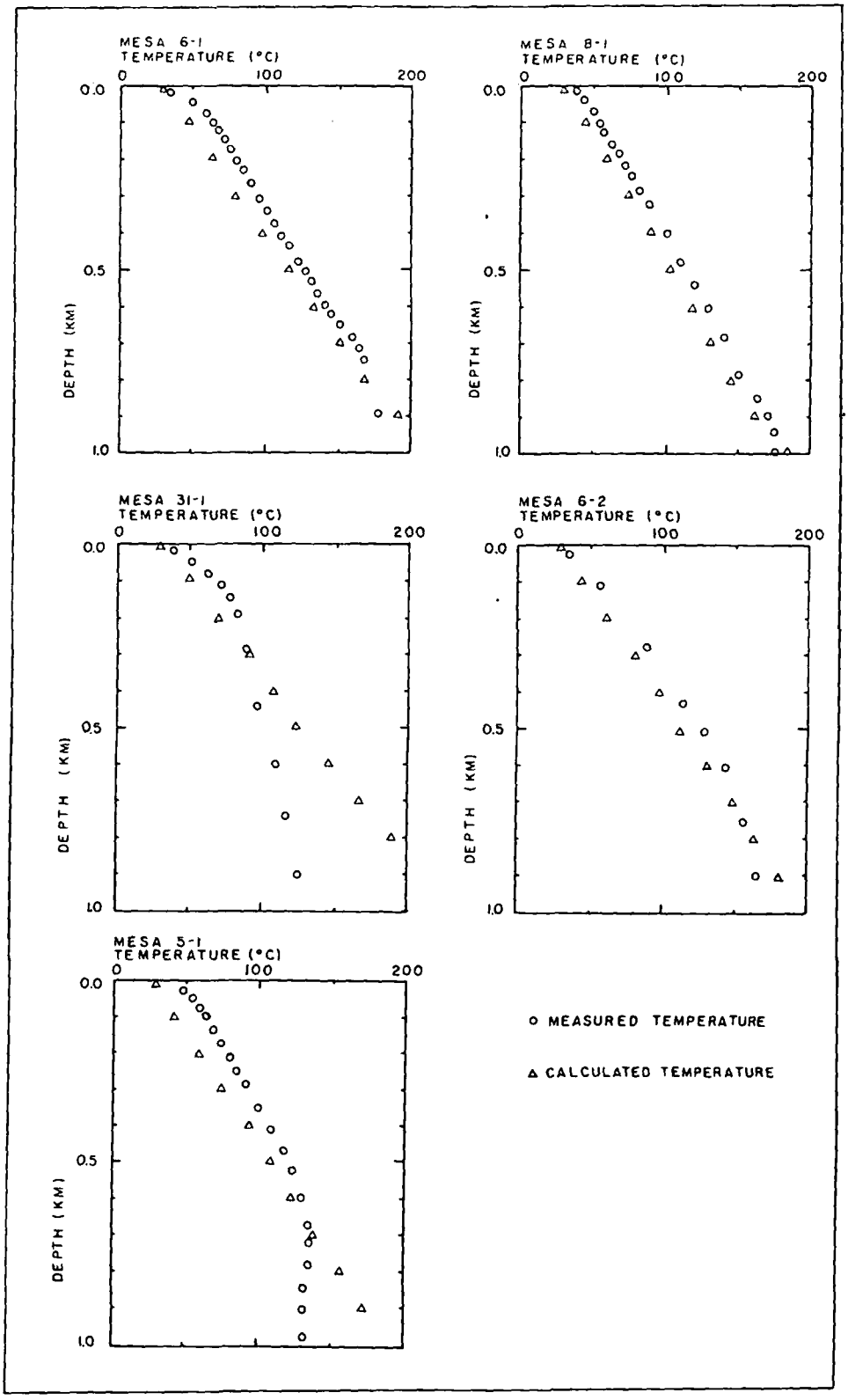

FIG. 6. Temperature-depth data from deep Mesa wells (6-1, 8-1, 31-1, 6-2, and 5-1). The measured temperatures are open circles and the calculated temperatures are triangles. The calculated temperatures as offset by 10°C for clarity.

sults from the deep drilling and surface geophysics were summarized by Swanberg (1974).

Heat flow data from the East Mesa anomaly were digitized on a 15 × 15 grid with a grid spacing of 1.6 km. Subsurface temperatures were calculated using the sourceward continuation method following exactly the same procedure used for the Marysville data described above, except that a thermal conductivity appropriate to the Mesa sediments, 3.8 mcal/cm-sec-°C (1.5 W/m°K), was used in equation (17). The sources and image sources were located on a plane 3 km below and above the datum plane, respectively. Isotherms are constructed from the calculated subsurface temperatures on a plane 0.8 km below the datum plane.

The geothermal anomaly appears to be caused by a complex reservoir as indicated by the temperature-depth curves from the deep test wells shown in Figure 6. Three of the curves for wells 6-1, 6-2, and 8-1 become isothermal at temperatures in the range of 175°–200°C, whereas the curves for wells 31-1 and 5-1 become isothermal in the range of 100°–150°C. Therefore, the temperatures at the top of the reservoir are not constant, and it cannot be assumed to be a single isothermal surface as in the case of the simple reservoir.

Figure 5b shows contours of the 75° to 175°C isotherms at 25°C intervals at a depth of 0.8 km. The 100°C and above contours delineate two possible shallow reservoirs probably interconnected at depth. The isotherms at 0.8-km depth in the northwestern portion of the anomaly have a complex shape. A salient from this portion of the anomaly projects approximately southeast and strongly suggests fluid flow along a narrow zone, probably along a fault.

A fault has been mapped by Combs and Hadley (1977) close to this salient which could be the surface expression of this narrow high-temperature zone. The 150°C isotherm has a very complex shape with two additional salients pointing to the north and northeast. These two lobes suggest other zones of fluid flow approximately perpendicular to the southeast salient. The smaller southeast portion of the anomaly has greater horizontal temperature gradients than the main anomaly, especially to the northeast. A small lobe in the 175°C contour projects toward the main anomaly and is aligned with the mapped fault, suggesting an origin related to the main anomaly.

The calculated subsurface temperatures are compared to the temperature-depth data from the five deep test wells in Figure 6. Above the reservoir the calculated temperatures are slightly lower than the observed temperatures, indicating that too low a value was assumed for the mean surface temperature. There is basically very good agreement between the calculated and observed shape of the temperature-depth curves in the area of applicability of the continuation technique, i.e., outside the reservoir. The observed and computed curves diverge inside the reservoir.

Simple extrapolation of the surface heat flow data would have revealed none of the complexities in the subsurface isotherms which were obtained from the continuation method. The extrapolated isotherms would simply reflect the surface heat flow pattern in Figure 5a. The results of the continuation clearly show the anomaly to be caused by fluid flow along the narrow zones and indicate a complex relationship between the zones. The origin of the anomaly as flow along a fault intersection and the radiating fault zones is suggested by the resulting temperature model.

DISCUSSION

The simple continuation method described here is a useful technique to estimate subsurface isotherms in a geothermal area. As demonstrated in the 2-D model and the Marysville and East Mesa geothermal areas, this method can be applied where thermal convection occurs at depth if the zone of fluid convection can be treated as a boundary condition for a conductive solution. This method is useful in defining spatial limits of such geothermal reservoirs. By application of the half-width rule to the surface gradient profile, the temperature range of the reservoir may be indicated, but better resolution and reservoir delineation are obtained if the depth or temperature is known. The use of the present continuation method is limited to cases where the heat flow anomaly is not related to contrasting thermal conductivity and resulting refraction of heat.

An advantage of this approach to interpretation of heat flow is that it is not model dependent, and complicated heat flow anomaly patterns can be interpreted more easily. The solution can be used for time dependent as well as steady-state thermal conditions, although no examples have been discussed. The solution technique is identical, except the time of initiation of the continuous sources and sinks must be independently known because a different solution exists for each different time. The time-dependent technique was used by Blackwell et al (1978) to interpret a regional heat flow anomaly in the Cascade range in the Pacific Northwest.

The method used for continuation assumes that the source distribution can be represented by a large number of line or point sources on a plane and requires a large amount of computer storage to solve the large number of simultaneous equations used to determine the source terms. Even though the use of the point or line sources is a crude approximation of the actual heat source, the method does give accurate subsurface temperatures. A similar method using different types of source distributions can easily be developed. However, the amount of known heat flow data in geothermal areas is limited and the use of more sophisticated types of source distributions is not justified.

The terrain correction discussed here can be used as an alternative mathematical solution to the terrain correction solution discussed by Blackwell et al (1980). With inclusion of the microclimatic effects discussed by Blackwell et al (1980), an alternative terrain correction technique can be developed. The continuation and terrain correction techniques can be combined to solve more complex problems. The mathematical formalization is not presented, but the development of the combined technique is very similar to the derivation of the continuation or terrain correction techniques presented.

ACKNOWLEDGMENTS

We wish to extend our thanks to M. J. Holdaway, E. Herrin, J. Combs, W. J. Peeples, and G. Salaita for critically reviewing this manuscript and making helpful suggestions. John Steele of Southern Methodist University supplied several of the finite-difference models which were used. Jacqueline Landon did the typing. The work was supported by National Science Foundation grant no. HES 74-19550A01 and U.S.G.S. grant no. 1408-001-G-425 to Southern Mehodist University.

REFERENCES

Birch, F., 1950, Flow of heat in the Front Range, Colorado: GSA Bull., v. 61, p. 567–630.

——— 1967, Low values of oceanic heat flow: J. Geophys. Res., v. 72, p. 2261–2262.

Blackwell, D. D., Brott, C. A., Goforth, T. T., Holdaway, M. J., Morgan, P., Petefish, D., Rape, T., Steele, J. L., Spafford, R. E., and Waibel, A. F., 1975, Geological and geophysical exploration at Marysville geothermal area: NSF-RANN tech. rep. NSF-RA-N-74031b, 104 p.

Blackwell, D. D., Hull, D. A., Bowen, R. G., and Steele, J. L., 1978,

Heat flow of Oregon: Oregon Dept. of Geol. and Mineral Ind. spec. paper 4, 42 p.
Blackwell, D. D., and Morgan, P., 1976, Geological and geophysical exploration of the Marysville geothermal area, Montana, USA: Proc. 2nd U.N. Symp. Dev. of Geothermal Potential, Washington, D.C., U.S. Govt. Printing Office, p. 895–902.
Blackwell, D. D., Steele, J. L., and Brott, C. A., 1980, The terrain effect on terrestrial heat flow: J. Geophys. Res., v. 85, p. 4757–4772.
Bodvarsson, G., 1973, Downward continuation of constrained potential fields: J. Geophys. Res., v. 78, p. 1288–1292.
Carnahan, B., Luther, H. A., and Willers, J. D., 1969, Applied numerical methods: New York, John Wiley and Sons, Inc., 604 p.
Carslaw, H. S., and Jaeger, J. C., 1959, Conduction of heat in solids, 2nd ed.: Oxford, Clarendon Press, 510 p.
Claerbout, J. F., 1976, Fundamentals of geophysical data processing with applications to petroleum prospecting: New York, McGraw-Hill, Inc., 274 p.
Combs, J., and Hadley, D. M., 1977, Microeathquake investigation of the Mesa geothermal anomaly, Imperial Valley, California: Geophysics, v. 42, p. 17–33.
Cooley, J. W., and Tukey, J. W., 1965, An algorithm for the machine calculation of complete Fourier series: Math. Comp., v. 19, p. 2970–2871.
Dampney, C. N. G., 1969, The equivalent source technique: Geophysics, v. 34, p. 39–53.
Grant, F. S., and West, G. F., 1965, Interpretation theory in applied geophysics: New York, McGraw-Hill, Inc., 584 p.
Henderson, R. G., and Cordell, L., 1971, Reduction of unevenly spaced potential field data to a horizontal plane by means of finite harmonic series: Geophysics, v. 36, p. 856–866.
Kanasewich, E. R., and Agarwal, R. G., 1970, Analysis of combined gravity and magnetic fields in wave number domain: J. Geophys. Res., v. 75, p. 5702–5712.
Ku, C. C., Telford, W. M., and Lin, S. H., 1971, The use of linear filtering in gravity problems: Geophysics, v. 36, p. 1174–1203.
Odegard, M. E., and Berg, J. W., Jr., 1965, Gravity interpretation using the Fourier integral: Geophysics, v. 30, p. 424–438.
Simmons, G., 1965, Effect of thermal conductivity contrasts on measured heat flow (abst.): AGU Trans. v. 46, p. 176.
———1967, Interpretation of heat flow anomalies: Rev. Geophys., v. 5, p. 41–52.
Swanberg, C. A., 1974, Heat flow and geothermal potential of the East Mesa KGRA, Imperial Valley, California: Proc. Conf. on Res. for Dev. of Geothermal Energy Resources, National Science Foundation NSF-R4-N-74-159., p. 85–98.

GEOPHYSICS, VOL. 46, NO. 12 (DECEMBER 1981); P. 1732–1744, 6 FIGS., 2 TABLES.

Continuation of heat flow data: A method to construct isotherms in geothermal areas

Charles A. Brott*, David D. Blackwell‡, and Paul Morgan§

ABSTRACT

A continuation technique for conductive heat flow in a homogeneous isotropic medium is presented which utilizes observed surface heat flow data. The technique uses equivalent point sources and is developed for transient or steady-state conductive heat flow problems for a homogeneous half-space with plane surface and a surface with topographic relief. The technique is demonstrated by comparison with a steady-state fault model and the terrain correction problem; it is also compared to observed heat flow data in two geothermal areas (Marysville, Montana and East Mesa, Imperial Valley, California). Calculated subsurface temperature distributions are compared to analytical models and the results of geophysical studies in deep drillholes in geothermal systems. Even in geothermal systems, where convection is involved in the heat transfer, the boundaries of the "reservoir" associated with the convective system can be treated as a boundary condition and the depth and shape of this boundary can be calculated, since many geothermal systems are controlled by permeability barriers. These barriers may either be due to the natural development of a trap or to self-sealing. Continuation of surface heat flow data is a useful technique in the initial evaluation of geothermal resources as well as an additional tool in the interpretation of regional heat-flow data.

INTRODUCTION

Heat flow anomalies at the earth's surface can be caused by one or more of the following: (1) contrast of thermal conductivity and the resulting refraction of heat; (2) contrast in the sources of heat production; (3) local temperature differences caused by the intrusions of hot (or cold) material; and (4) convection of groundwater. Also, Birch (1950) and most recently Blackwell et al (1980) pointed out that apparent anomalies will arise from topographic features. Numerical models showing the effect of thermal conductivity contrasts were reported by Simmons (1965) and other authors. We develop a simple continuation method for conductive heat flow in a homogeneous isotropic media, which utilizes surface heat-flow data, and use it to put spatial and temporal limits on the sources or temperatures associated with heat flow anomalies. If the source of the anomaly is a distribution of temperature, then the source configuration can be directly calculated. If the source of the anomaly is related to heat generation variations, then the interpretation is more complicated.

The continuation of surface heat flow data to determine subsurface temperature distributions is a useful method for investigating the subsurface in some geothermal areas. Constructed isotherms will converge around the anomaly sources and have a direct relationship to the location of the sources. For example, a geothermal anomaly which is caused by hot circulating fluid in a "simple reservoir" is considered. The term simple reservoir is used to describe a volume consisting of highly permeable rocks with fluid circulation within the volume or reservoir, surrounded by effectively impermeable rocks. The circulating fluid tends to keep the temperature uniform in the reservoir; hence, the boundary of the reservoir is approximately an isotherm. Outside the reservoir, the heat transfer mechanism is only conduction since the rocks are impermeable. Utilizing the surface geothermal gradient in a continuation method, one can construct an isothermal surface which is the same temperature as the reservoir. The isothermal surface can then be used to investigate the relationship of the possible reservoir to geologic or other geophysical information and in resource analysis.

The major problem in the calculation of subsurface temperature distributions is the spatial diffusion of heat. Since the flow of heat is not restricted to the vertical direction, the estimation of subsurface temperatures by extrapolation of surface gradients is erroneous. The correct solution of this problem involves a downward or sourceward continuation which accounts for spreading of heat in all directions. The spatial distribution of heat may be time-dependent, as in the case of a source which has been "turned on" for a short period of time (e.g., a recent emplacement of an intrusive body). For such cases the correct solution must also account for the time dependency of the temperature distribution. Continuation techniques have been described for gravity and magnetics by Grant and West (1965, chapter 8) and many other authors. Although the equations describing steady-state heat flow, gravity, and magnetics are very similar, most gravity and magnetic continuation techniques cannot be applied usefully to

Manuscript received by the Editor December 21, 1979; revised manuscript received May 18, 1981.
*Phillips Petroleum Company, Research and Development, Bartlesville, OK 74004.
‡Department of Geological Sciences, Southern Methodist University, Dallas, TX 75275.
§Lunar and Planetary Institute, 3303 NASA Road One, Houston, TX 77058.

heat-flow data. A problem arises from the basic difference between gravity and magnetic data sets compared to heat flow data sets measured on the surface of the earth. Gravity and magnetic data comprise a set of potential gradient (field strength) values spatially distributed on a plane whose potential also has a lateral variation.

Heat flow data comprise a set of field strength values, but the values are spatially distributed on a plane of essentially uniform potential (the surface temperature). Thus when continuing heat flow data, image sources must be considered. The heat-flow data can be continued by similar techniques as gravity and magnetic fields. However, to compute the subsurface temperatures (an essential parameter in any geothermal investigation), a very complex integration over the continuation path is required (Bodvarsson, 1973).

In the first part of this paper, we present a technique for the sourceward continuation of heat flow data obtained on a plane surface by which subsurface temperatures can be directly estimated for either the steady-state or time-dependent case. The technique consists of constructing equivalent point sources, similar to the method of Dampney (1969) for modeling gravity data.

In a second part, the basic continuation method developed for a plane surface is extended to a form that can be used to obtain terrain corrections. The nature of the terrain correction problem allows it to be identified as the "spaceward" (away from the source) continuation problem where the topographic relief with the nonuniform surface temperature distribution can be represented by a source distribution located on or above the surface (Birch, 1950; Blackwell et al, 1980).

CONTINUATION TECHNIQUE

The continuation method described here is based on a fundamental potential field property: Outside the boundaries of a volume containing sources, the field, once defined, is unique. Even though there is always a family of source solutions which will generate the same field, any source solution which satisfies the surface field strength values can be used to calculate the field parameters at any point outside the volume containing the sources. The source solutions used in this continuation method are an array of line or point sources for the two-dimensional (2-D) or three-dimensional (3-D) case, respectively. By solving simultaneous equations, the source strengths are determined from known surface heat-flow data or geothermal gradients.

The assumptions for obtaining the source strengths are (1) the heat transfer mechanism is by conduction alone; (2) a homogeneous isotropic medium in which no heat is generated occupies the space between the sources and surface; and (3) the sources are continuous in time and have constant heat generation with time. Once the source solution is known, the subsurface temperature can be calculated directly.

The differential equation for the conduction of heat in a homogeneous isotropic medium in which no heat is generated is

$$\nabla^2 T = (1/\kappa)\partial T/\partial t, \tag{1}$$

where T is temperature, κ is diffusivity, t is time, and ∇^2 is the Laplacian ($\nabla^2 = \partial^2/\partial x^2 + \partial^2/\partial y^2 + \partial^2/\partial z^2$). The geothermal gradient g is the negative of the partial derivative of the temperature T along the vertical direction z,

$$g = -\partial T/\partial z. \tag{2}$$

The differential equation for the conduction of heat degenerates into the Laplace equation

$$\nabla^2 T = 0 \tag{3}$$

for the steady-state case.

The infinite-medium solutions for the steady-state and time-dependent temperature and gradient for point and line heat sources of constant heat generation are listed in Table 1 (from Carslaw and Jaeger, 1959, chapters 10 and 14). The solutions are written in two parts: a source term S and a distance term (D for temperatures and G for gradients). Individual solutions for single sources can be superimposed since they are the solutions of second-order linear differential equations. This property is essential because it allows a complex field to be constructed by summing the effects of many simple sources. Also, this property can be exploited through the method of images to obtain a uniform surface temperature. The use of the image sources and the basic ideas of the continuation method are discussed below.

Consider the 2-D model in Figure 1a. The surface geothermal gradients g_i, $i = 1, N$, at the points P_i, $i = 1, N$ (located on the reference plane $z = 0$) are known. Also, the surface temperature of the reference plane is a constant T_s which is known. By using the linear properties of the line source solution for the gradient from Table 1, the contribution to the surface gradient g_{ij} at the point P_i from the source Q_j and its image Q_j' can be expressed by

$$g_{ij}^c = S_j G_{ij} + S_j' G_{ij}', \tag{4a}$$

where S_j and S_j' are source terms which are functions of their respective constant source strengths Q_j and Q_j', and G_{ij} and G_{ij}' are gradient distance terms (see Figure 1a and Table 1). Since S_j' is the image source term of S_j, $S_j' = -S_j$, and since P_i is an equal distance from S_j and S_j' but in a different vertical direction, $G_{ij}' = -G_{ij}$. Therefore equation (4a) may be written as

$$g_{ij}^c = 2S_j G_{ij}. \tag{4b}$$

By superposition of all the N set of sources and images, the total gradient g_i^T at the point P_i is

$$g_i^T = 2\sum_{j=1}^{N} S_j G_{ij}. \tag{5}$$

Similar expressions can be written for the total gradient at each ith point, $i = 1, N$. The parameters defining the distance terms G_{ij} are known, but the individual source strengths Q_j are not known. Since there are N equations and N sets of sources and images, the source terms can be calculated by solving the set of simultaneous equations.

The temperature T_k at any arbitary point P_k below the surface and above the source plane depth can be calculated using the following expression (see Table 1 and Figure 1b)

$$T_k = T_s + \sum_{j=1}^{N} S_j(D_{kj} - D_{ij}), \tag{6}$$

where S_j are the source terms obtained by solving the simultaneous equations, T_s is a known constant surface temperature, and the parameters defining the temperature-distance terms D_{ij} and D_{ij}' are known.

If the time when the sources were emplaced (turned on) is known, the time-dependent form of the source equation may be used and the method of obtaining the solution would be similar.

In three dimensions, point sources are used on a plane $z = a$ and images on a plane $z = -a$. The point source and distance terms are given in Table 1. The only additional complexity is another summation needed to account for the third dimension. For point sources on an $n \times m$ grid, the surface gradient g_{ij} is

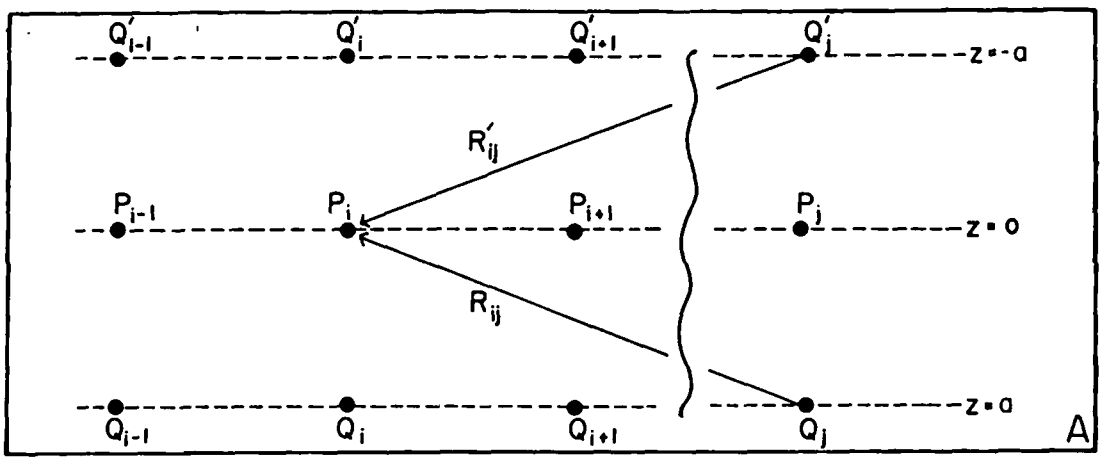

FIG. 1a. Geometry for the continuation model. Sources Q_{i-1}, Q_i, and Q_{i+1} are on the plane $z = a$, with image sources Q'_{i-1}, Q'_i, and Q'_{i+1}, on the plane $z = -a$. The surface gardients are known at points P_{i-1}, P_i, and P_{i+1} on the plane $z = 0$. The distance term between any particular source image point Q_j, or Q'_j, is $R_{ij}(=R'_{ij})$.

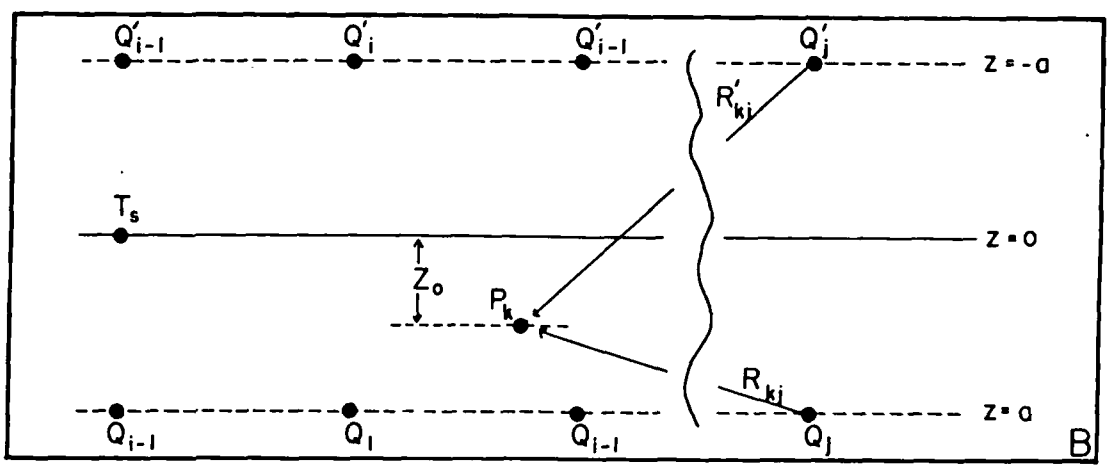

FIG. 1b. Geometry for the continuation model used to compute the subsurface temperature at point P_k which is between the planes $z = 0$ and $z = a$ at depth z_0.

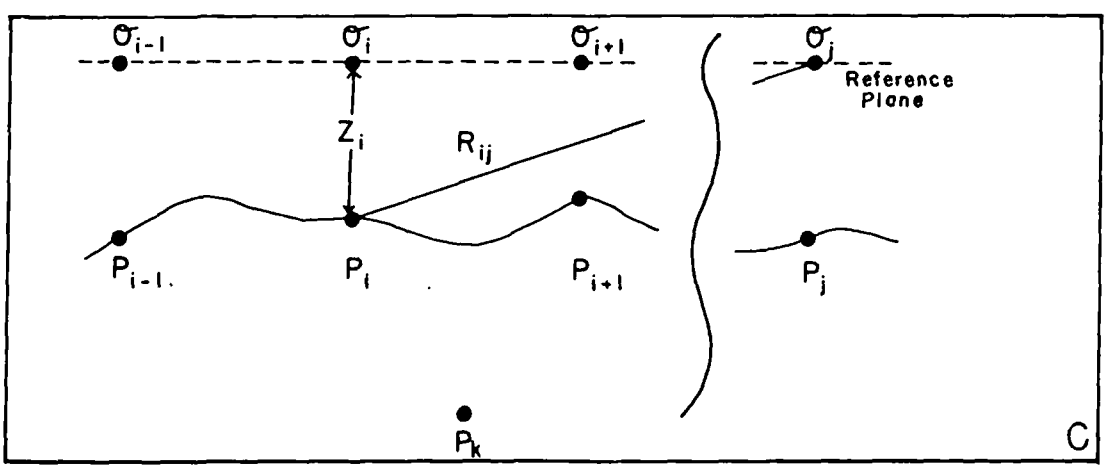

FIG. 1c. Geometry for the terrain correction model. Line doublets σ_{i-1}, σ_i, and σ_{i+1} are on a reference plane. The surface temperatures and the elevation differences of the points P_{i-1}, P_i, and P_{i+1} are known. The vertical distance from the reference plane to point P_k and the gradient at P_k are known.

Table 1. Solutions for constant and continuous point and line sources (Carslaw and Jaeger, 1959).

	Source term	Time-dependent distance term	Steady-state distance term
Temperature (T), $T = S \cdot D$			
Point source	$S = Q/4\pi\kappa$	$D = (1/R)\,\mathrm{erfc}(R/\sqrt{4\kappa t})$	$D = 1/R$
Line source	$S = Q/4\pi\kappa$	$D = -Ei(-R^2/4\kappa t)$ where $-Ei(-x) = \int^{\infty} x(e^{-u}/u)du$	$D = -2\ln(R)$
Geothermal gradient (g), $g = S \cdot G$			
Point source	$S = Q/4\pi\kappa$	$G = [(z - z')/R^3]^* [(2R/\sqrt{\pi\kappa t})\exp(-R^2/4\kappa t) + \mathrm{erfc}(R/\sqrt{4\kappa t})]$	$G = (z - z')/R^3$
Line source	$S = Q/4\pi\kappa$	$G = [2(z - z')/R^2]^* \exp(-R^2/4\kappa t)$	$G = 2(z - z')/R^2$

Q is source strength, t is time, κ is diffusivity, and R is the distance from the source to the field point.
$R^2 = (x - x')^2 + (y - y')^2 + (z - z')^2$ for the point source and
$R^2 = (x - x')^2 + (z - z')^2$ for the line source, where (x, y, z) is the field point and (x', y', z') is the source point.

expressed at a point P_{ij} by

$$g_{ij} = 2 \sum_{k=1}^{n} \cdot \sum_{l=1}^{m} S_{kl} G_{ijkl}, \qquad (7)$$

and temperature T_{ij} is expressed at a point P_{ij} by

$$T_{ij} = \sum_{k=1}^{n} \sum_{l=1}^{m} S_{kl} \cdot (D_{ijkl} - D_{ijkl'}) + T_s. \qquad (8)$$

If the models have a known uniform-background geothermal gradient g_0, it can be introduced in the gradient equations [equations (5) and (7)] by adding it to the right-hand side of the equations, and to the temperature equations [equations (6) and (8)] by adding the product $(g_0 z)$ of a uniform background gradient and the vertical distance to the reference plane to the right side of the equations.

TERRAIN CORRECTION TECHNIQUE

The terrain correction involves a spaceward (away from the source) continuation. Since the surface temperature is a boundary, the topographic relief and nonuniform surface temperatures are modeled by the use of vertical line or point doublets (temperature dipoles). The use of dipoles to model variable surface potential is a well-known technique (see Grant and West 1965; Carslaw and Jaeger, 1959). The same fundamental potential field properties, assumptions, and restrictions which apply to the continuation method discussed above also apply to this terrain correction technique.

The solutions for the vertical line and point doublets are listed in Table 2 (from Carslaw and Jaeger, 1959, chapters 10 and 14). The solutions are written in two parts, a source term σ and a distance term (Δ for temperature and Γ for gradients). Again, individual doublets can be superimposed since they are also solutions for a second-order linear differential equation (1) or equation (3). This superposition property is essential because it allows a complex temperature distribution on an irregular surface to be represented by the sum of the effects of many doublets. The use of the doublets and the basics of the terrain correction method are discussed below.

Consider the 2-D model in Figure 1c. The topographic relief is shown by a line and surface temperatures T_i, $i = 1, N$ are known at points P_i, $i = 1, N$, respectively. The observed gradient g is known at point P_{N+1}. Using the line doublet solutions for the temperature from Table 2, a general equation for the

Table 2. Solutions for constant and continuous point and line doublets (Carslaw and Jaegar, 1959).

	Source term	Steady-state distance term
Temperature (T), $T = \sigma \cdot \Delta$		
Point doublet	$\sigma = Q/4\pi\kappa$	$\Delta = (z - z')/R^3$
Line doublet	$\sigma = Q/4\pi\kappa$	$\Delta = 2(z - z')/R^2$
Gradient (g), $g = \sigma \cdot \Gamma$		
Point doublet	$\sigma = Q/4\pi\kappa$	$\Gamma = [1 - 3(z - z')^2/R^2]/R^3$
Line doublet	$\sigma = Q/4\pi\kappa$	$\Gamma = 2[1 - 2(z - z')^2/R^2]/R^2$

Q is the source strength, κ is diffusivity, and R is the distance from the source to the field point.
$R^2 = (x - x')^2 + (y - y')^2 + (z - z')^2$ for point doublets and
$R^2 = (x - x')^2 + (z - z')^2$ for line doublets, where (x, y, z) is the field point and (x', y', z') is the source point.

temperature T_i at P_i can be written as

$$T_i = \sum_{j=1}^{n} (\sigma_j \Delta_{ij}) + z_i \alpha, \quad (9)$$

where the dipole source terms σ_j are a function of their respective source strengths, the temperature distance terms Δ_{ij} are functions of the distance from their respective sources to the point P_i, z_i is the distance from the reference plane to the point P_i, and α is the undisturbed regional gradient (Figure 1c and Table 2). Using the doublet solutions for the gradient from Table 2, the gradient g at P_{N+1} can be written as

$$g = \sum_{j=1}^{N} (\sigma_j \Gamma_{N+1,j}) + \alpha, \quad (10)$$

where the source terms are the same as above, the gradient distance terms $\Gamma_{N+1,j}$ are a function of the distance from their respective source to the point P_{N+1}, and α is the same undisturbed gradient as above.

Since the parameters defining the temperature and gradient distance terms Δ_{ij} and $\Gamma_{N+1,j}$ are known, these terms can be cal-

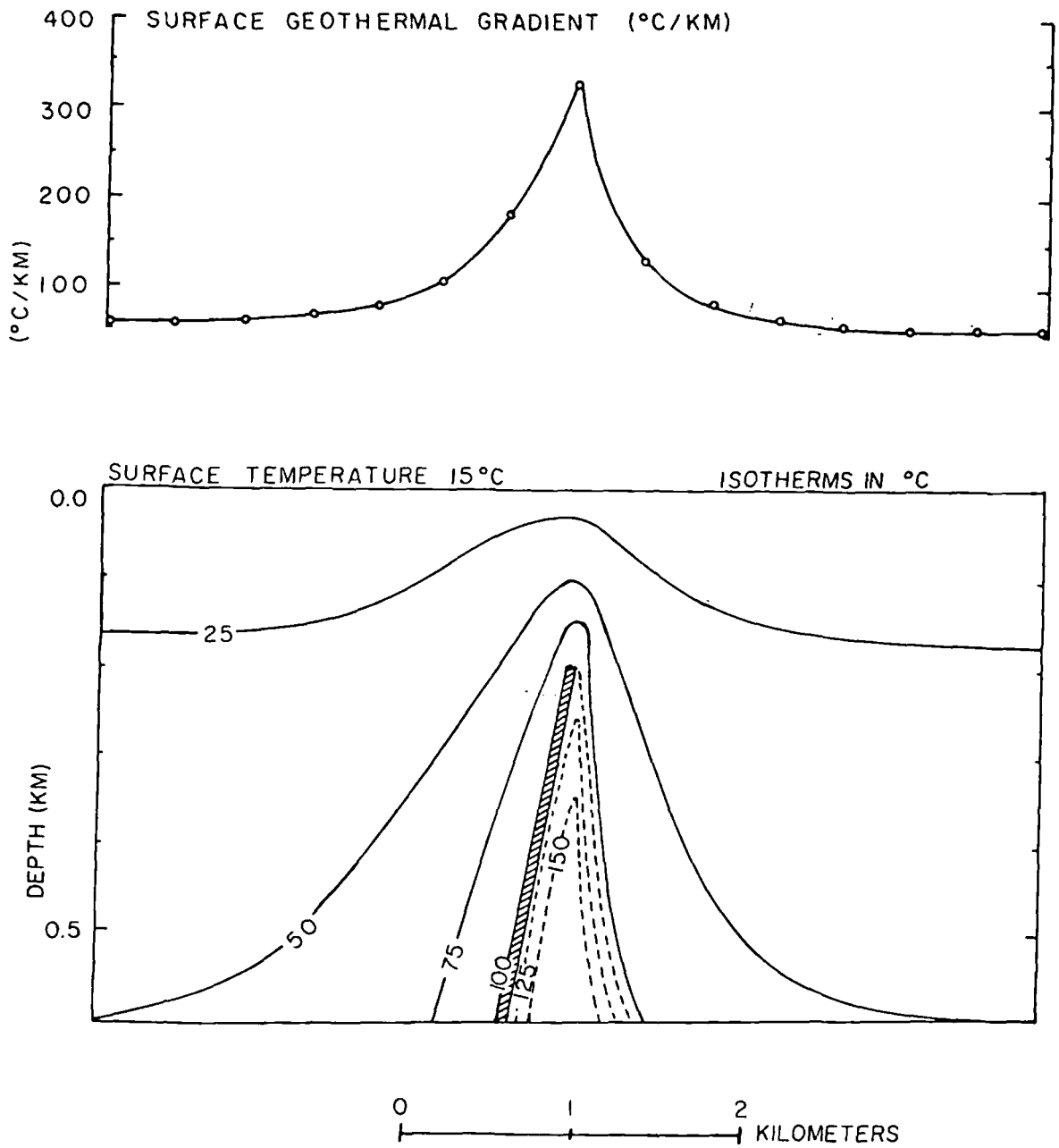

FIG. 2. A steady-state 2-D fault model with surface geothermal gradient shown above the model. The fault has a constant temperature of 100°C which is interpreted as circulation of hot fluid along and in the fault zone dipping 45 degrees to the left. The numerical model isotherms are shown by solid lines and the continued isotherms are shown by dashed lines where they diverge from the numerical model isotherms. A constant background gradient of 54°C/km and a uniform surface temperature of 15°C are used in this model.

culated (Table 2). Since there are $N + 1$ equations, the N source terms σ_j and the undisturbed gradient α can be found by solving the equations simultaneously.

The purpose of a terrain correction is usually to find the undisturbed gradient α, but if the subsurface temperatures are needed, they can be calculated by using the source terms σ_1 and the undisturbed gradient as shown in equation (11). By using the linear properties of the solutions in Table 2, the temperature T_k at point P_k in Figure 1c can be calculated by

$$T_k = \sum_{j=1}^{N} \sigma_j \Delta_{kj} + z_k \alpha, \tag{11}$$

where the temperature distance terms Δ_{kj} are a function of distance from their respective source to the point P_k. The source terms σ_j and the undisturbed gradient α are obtained from the simultaneous solution of equations (10). The parameters defining the temperature distance terms Δ_{kj} and z_k, and the distance from the reference plane $z = 0$ to P_k, are known. Equation (11) can now be solved directly.

In three dimensions, the point doublet solutions for the temperature and gradient from Table 1 are used, and the only additional complexity is the summation of the third dimension. The temperature T_{ij} at a point P_{ij} due to point doublets on an $n \times m$ grid is expressed by

$$T_{ij} = z_{ij}\alpha + \sum_{k=1}^{n} \cdot \sum_{l=1}^{m} \sigma_{ij} \Delta_{ijkl}, \tag{12}$$

and the gradient g_{ij} at a point P_{ij} is expressed by

$$g_{ij} = \alpha + \sum_{k=1}^{n} \sum_{l=1}^{m} \sigma_{ij} \Gamma_{ijkl}. \tag{13}$$

The source and dipole solutions discussed in this and the previous section can be combined and a modified equation derived to find subsurface temperatures when a gradient distribution (due to subsurface lateral variations in heat flow) is known on a surface with topographic relief. The equations are easily derived from the equations presented for the separate solutions; they are not included here.

Dipoles are chosen to match the surface temperature, which varies as a function of position on the boundary surface (also is a function of position) because they can be used to define a specific temperature more readily than sources. Birch (1950) similarly used a dipole distribution to derive his time-dependent terrain correction.

UTILIZATION OF THE CONTINUATION METHOD

The continuation method discussed here requires that the surface heat flow data be digitized on a grid. It is convenient to use equal grid spacing. An interpolation polynomial can be used to obtain the data values at other than measured points (Carnahan et al, 1969, chapter 1; and many other authors). Alternatively, a least-square polynomial or a Fourier series may be fitted to the data and the value at each data point obtained from evaluation of the resulting polynomial or series (Claerbout, 1976, chapter 6; Henderson and Cordell, 1971).

Sharp irregularities or variations in the surface heat flow data which may be due to shallow anomalies (Simmons, 1967) or erroneous data can cause serious problems when applying the continuation method. Ku et al (1971) pointed out, with reference to sourceward continuation of gravity data, that the Gibbs phenomenon, or high-amplitude oscillations, occur at places of sharp variation in surface data and that a low-pass filter could be used to reduce or eliminate these oscillations. Thus smoothing of the surface data, which reduces these sharp variations, can be used as a low-pass filter, allowing continuation of the temperature to greater depths than would be possible with the unsmoothed data. A very simple way of applying a low-pass filter to discrete data is to increase the grid spacing, since the wavelength of the anomaly is directly related to the depth of the source (Ku et al, 1971). The sampling rate of the surface data is critical because, for large grid spacing, aliasing of short-wavelength anomalies can occur. Since short-wavelength anomalies are the result of shallow sources, increased grid spacing or low-pass filtering allows continuation to greater depths without oscillations; however, detailed information contained in the data is lost.

The depth of the plane of point or line sources below the surface can be estimated in a manner similar to finding the depths to the center of bodies producing gravitational anomalies. Simmons (1967) developed methods for estimating the depth of theoretical surface heat flow anomalies, and these methods can be used to approximate the depth of the source plane. The height of the image source plane above the surface is equal to the depth of the source plane below the surface.

The solution of the large number of simultaneous equations needed to determine the source terms can be performed using matrix methods. The size of the matrix becomes very large for the 3-D case and requires a large amount of computer storage. Future work is planned to use the continuation method to determine filter coefficients so that sourceward continuation can be done by use of the Fourier transform. Sourceward continuation of gravity data using the Fourier transform, coupled with filter coefficients, is described by Odegard and Berg (1965), Kanasewich and Agarwal (1970), and others. By using the Fourier transform, less computer storage would be needed and an analog for fast Fourier transformation (Cooley and Tukey, 1965) could be used to reduce the computing time. Because of the sparse data sets usually available for geothermal interpretation, use of the more formal data analysis techniques may not be justified.

STEADY-STATE FAULT MODEL

Figure 2 shows a 2-D steady-state model of 100°C water circulating along a fault dipping at 45 degrees (crosshatch pattern). The model has a constant background gradient of 54°C/km and a uniform surface temperature of 15°C. The subsurface model isotherms (solid lines) were computed by a finite-difference numerical technique. The calculated surface geothermal gradient profile is shown above the model.

Subsurface isotherms were calculated using the continuation method discussed above, given the surface gradient from the finite-difference solution and using steady-state line sources. The terms, constants, and equations used in the continuation method are as follows: The source S and the distance (G, D) terms for the gradient and temperatures used for steady-state line sources were of the form shown in Table 1. The depth to the line sources and height to the image sources were chosen to be 0.8 km, and the gradient profile was first sampled at horizontal intervals of 0.4 km (open circles in Figure 2). The depth of 0.8 km was chosen to show that constructed isotherms will converge around the fault.

The simultaneous equations used to evaluate the source terms were derived using the 2-D surface gradient equation [equation (5)]. The subsurface temperatures were calculated using the 2-D temperature equation [equation (6)]. Isotherms were constructed from these temperatures. At depths greater than 0.3 km, the isotherms showed oscillations below the sharp peak of

the surface gradient. In order to calculate temperatures below 0.3 km, the surface gradient data were smoothed by increasing the interval (grid spacing) of the surface gradient to 0.8 km (effectively applying a low-pass filter to the surface data). The oscillations below the surface gradient peak were reduced, and continuated temperatures were computed to a depth of 0.6 km. The calculated temperatures below 0.3 km are the average of first dropping the even numbered sample grid spaces, then the odd numbered grid spaces.

The constructed 25°, 50°, and 75°C isotherms calculated by the continuation technique closely follow the isotherms calculated by the finite-difference technique (Figure 2). On the left side of the model the 100°C isotherm corresponds to the left side of the fault, but the right side (dashed line) diverges from the fault, as do calculated isotherms greater than 100°C. By continuation of the potential field (surface gradient) below the circulating 100°C water at the tip of the fault (0.2 km), one of the basic continuation premises was violated.

The circulating 100°C water along the fault is the actual source which causes the observed surface gradient; therefore, solutions obtained by continuation below the actual source depth are not valid. By smoothing the surface field data, the depth to the source in the real case appeared deeper, and continuation below the actual source depth was accomplished. Isotherms that fold under themselves as shown in the model only occur below the circulating 100°C water (the actual source). Similarly shaped isotherms cannot be obtained by a continuation technique using a generalized source distribution.

The above 2-D model demonstrates that continuation of the surface data is useful in defining spatial limits to a simple reservoir which is a combined problem of convection and conduction. The shape and size of the upper part of the simple reservoir (circulating 100°C water along the fault) is delineated by the 100°C isotherm. The source solution obtained is not unique because any of the constructed isotherms could be used to define the upper part of a corresponding simple reservoir with that temperature. In order to determine reliably which isotherm defines the actual reservoir, knowledge of the temperature or depth of the reservoir is essential.

The maximum possible depth to the reservoir can be estimated by applying the half-width rule to the surface gradient profile. Using the depth obtained from the half-width rule (0.25 km), the corresponding temperature would be 100°–125°C.

TERRAIN MODEL

Figure 3 shows a 2-D terrain model from Birch (1967). The temperature T at any point can be calculated by

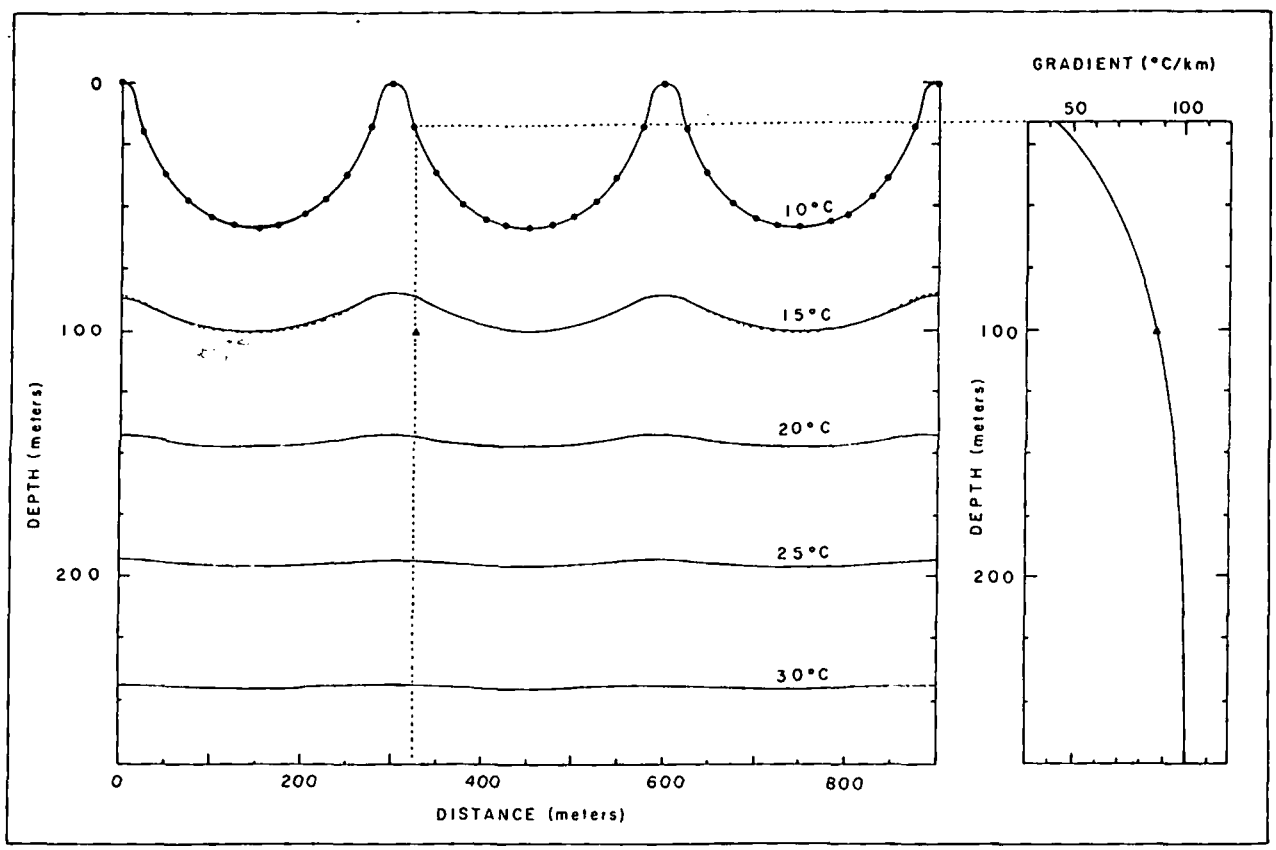

FIG. 3. 2-D terrain model from Birch (1967). The model has a uniform surface temperature of 10°C, and the undisturbed gradient at depth is 100°C/km. Dots on the surface of the model show the sampling locations of surface temperature. Model isotherms are shown as solid lines. The dashed lines show locations where the isotherms constructed by the continuation technique deviated from the model isotherms. The dotted vertical line shows the location of the gradient-depth curve to the right of the model. The solid triangles on the model and on the gradient-depth curve show the location of the known gradient used in the illustration of the terrain correction technique.

$$T(x, z) = T_0 + \alpha(z - ae^{-kz} \cos kx), \quad (14)$$

where z is the depth, positive downward; x distance, T_0 surface temperature, k wavelength, and α the undisturbed vertical gradient. The surface (z) varies nearly sinusoidally with x and is defined by

$$z = ae^{-kz} \cos kx, \quad (15)$$

where ae^{-kz} is the amplitude. The vertical gradient anywhere in the model can be calculated by

$$\frac{\partial T}{\partial z} = \alpha(1 + kae^{-kz} \cos kx). \quad (16)$$

The values of the parameters used in the model shown in Figure 3 are a = 17.5 m, $k = 2\pi/300$ m^{-1}, T_0 = 10°C, and α = 100°C/km. Model isotherms are shown as solid lines, and a model gradient-depth curve at a horizontal position of 325 m (dashed line) is shown to the left of the model.

The terrain correction method developed above was applied to the model to find the undisturbed gradient and to construct subsurface isotherms. The terms, constants, and equations used are as follows: The doublet sources σ and the distance Γ and Δ for the gradients and temperatures are of the form shown in Table 2. The reference plane for the source is 25 m above the actual surface. The surface temperature was sampled every 25 m horizontally (shown as solid circles in Figure 3). The gradient was sampled at a depth of approximately 82 m below the surface and at a horizontal displacement of 325 m as shown by the solid triangle. The simultaneous equations used to evaluate the source terms were derived from the 2-D temperature and gradient equations [equations (9) and (10)]. The subsurface temperatures and gradients are calculated at intervals of 25 m for several depths.

The isotherms constructed from the terrain correction method closely follow the model isotherms (Figure 3). The calculated undisturbed gradient is 100.6°C/km, whereas the undisturbed model gradient is 100°C/km (0.6 percent error). The vertical gradient-depth curve for 325-m horizontal displacement is also shown in Figure 3. The constructed gradient-depth curve very closely follows the model gradient-depth curve. The model used to test the terrain correction technique is very simple but illustrates that the technique can be used to calculate corrected geothermal gradients from wells located in areas of topographic relief. The terrain correction problem is very complex, and this

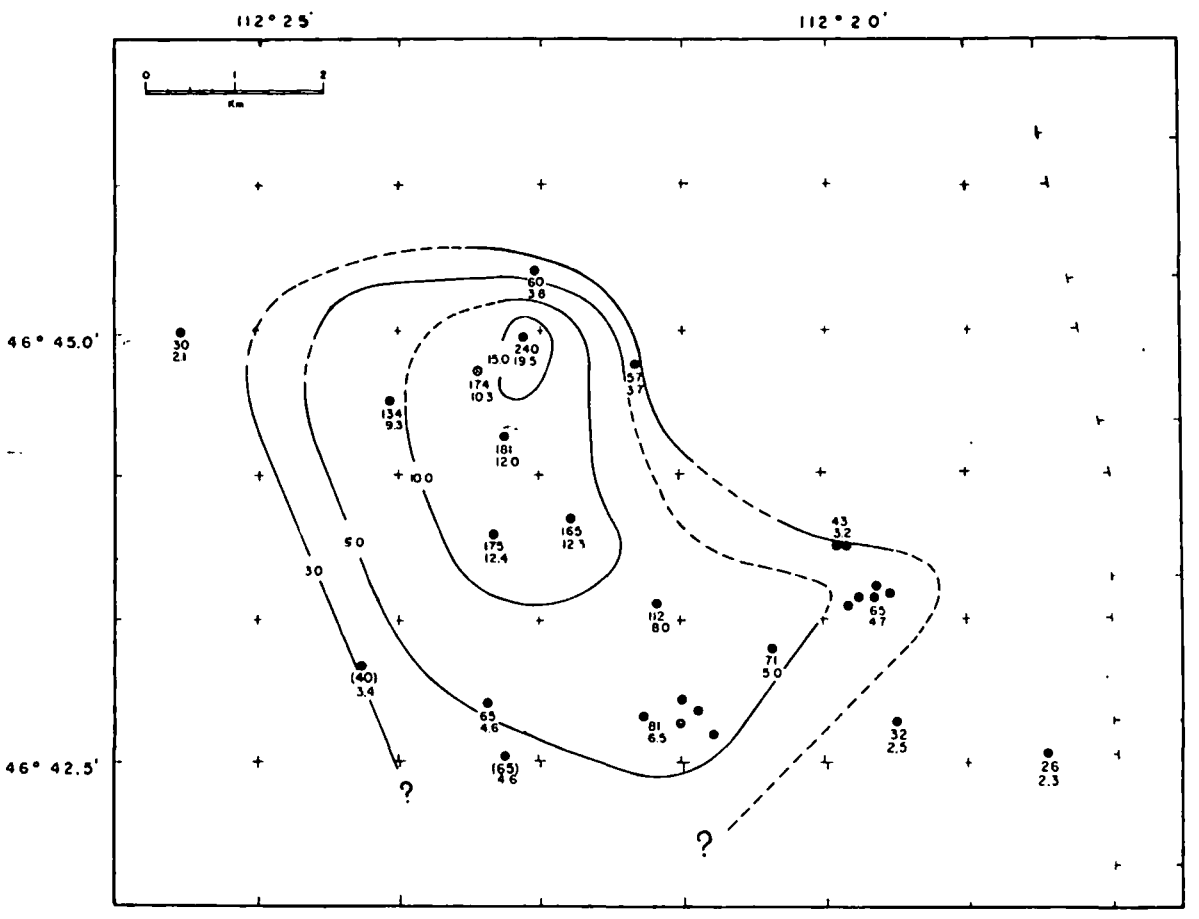

(a)

FIG. 4a. Marysville surface heat flow and geothermal gradient map (Blackwell et al, 1975). The location of the deep geothermal well (MGE #1) is shown as the circle with the cross, and the locations of other wells available for gradient and heat flow studies are shown as solid circles. The upper number of each pair is the terrain corrected geothermal gradient in °C/km. The lower figure is the terrain corrected surface heat flow value in μcal/cm^2 sec. Gradient values which are shown in parentheses have been adjusted for thermal conductivity variation (see Blackwell et al, 1975). The crosses are section corners.

discussion is not intended as a complete discussion of the problem (see Blackwell et al, 1980).

A difficulty with fitting the surface temperatures often occurs in the valleys because the surface there is relatively far from the plane of dipoles, yet it has very abrupt changes in temperature due to microclimatic effects. The technique described above can be modified so that the dipoles are spaced a fixed distance above the topography (say 100 m), and the surface of dipoles thus mimics the topography. As long as the location of each dipole is specified so that the distance term is known, the solution proceeds exactly as discussed above. We have used this feature to calculate detailed terrain corrections involving very complicated surface temperature variations.

THE APPLICATION OF THE HEAT FLOW CONTINUATION METHOD TO GEOTHERMAL AREAS

Marysville, Montana

The Marysville geothermal area in Montana is characterized by high heat flow (up to 19.5 μcal/cm^2 sec; 81.5 mW/m^2; Figure 4a), a negative gravity anomaly, high electrical resistivity, nearby microseismic activity, and low seismic ground noise (see Blackwell et al, 1975; Blackwell and Morgan, 1976). The geothermal anomaly appears to be bounded to the northeast by the subcrop of a Mesozoic granodiorite body, the Marysville stock, as shown in Figure 4b; and a fault has been mapped along the south side of the Marysville stock. Results from a 2.1-km test well drilled close to the peak of the geothermal anomaly (Figure 4a) indicate that the anomaly is caused by hydrothermal convection along distributed fracture zones in a Cenozoic granite porphyry. Maximum temperatures of 100°C were measured in the test well, and the modeled system is assumed to act as a simple reservoir with a temperature of about 95°C at its upper surface.

Heat flow data from the Marysville anomaly were continued sourceward using steady-state point sources. The heat flow map was digitized on a 15 × 15 square grid with spacing of 500 m, and the data were assumed to be on a datum plane located at the mean level of the actual topography. The heat flow values Q were used to determine surface vertical geothermal gradients using the one-dimensional (1-D) steady-state heat conduction equation

$$Q = gK, \tag{17}$$

where K is the rock thermal conductivity. A value for K of

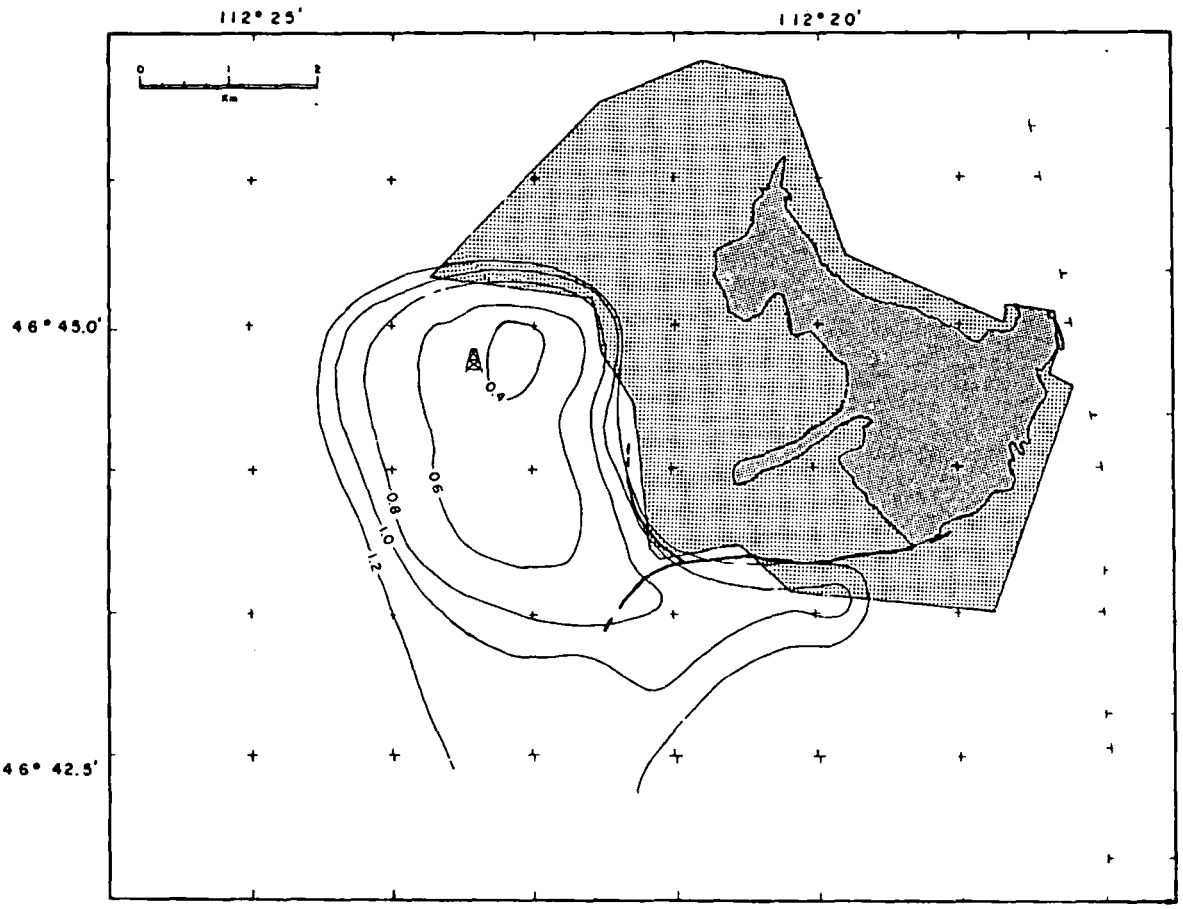

(b)

FIG. 4b. Marysville stock and geothermal reservoir (Blackwell et al, 1975). The outcrop and maximum subcrop of the stock are shown as dark and light shaded regions, respectively. The subcrop extent of the stock is based on the interpretation of magnetic data. The dark line shows the location of a major fault along the south edge of the stock. The depth to the contours of the geothermal reservoir is based on the continuation of surface heat flow data and is the same as 95°C isotherm, assumed to be the reservoir temperature. The location of the deep geothermal well (MGE #1) is shown by the derrick symbol. The crosses are section corners.

7.5 mcal/cm-sec-°C (3.1 W/m°K) was used based upon the mean thermal conductivity of core samples from the heat flow boreholes. The source term S and the distance terms (G and D) for the steady-state point sources used for the surface gradient and temperatures are given in Table 1. The sources and image sources were located 2.5 km below and above the datum plane, respectively, and the simultaneous equations used to calculate the source terms were derived from the 3-D gradient equation [equation (4)]. Using the 3-D temperature equation [equation (8)], subsurface temperatures were calculated on several planes below the datum plane and the 95°C isotherm was contoured on each of the planes.

Figure 4b shows the contours of the 95°C isotherm in the depth range of 0.4 km to 1.2 km at 0.2 km intervals, superimposed on the outline of the Marysville stock. The 95°C isothermal surface is interpreted to have approximately the same configuration as the geothermal reservoir. Very steep sides to the reservoir are indicated on the north and northeast, with relatively steep sides on the west and southwest. A complex shape is indicated in the south and southeast. The northern and eastern part of the reservoir is apparently bounded to the north and northeast by the Marysville stock. A narrow east-west salient of the 95°C isotherm is observed south of the stock. The narrowness of this salient suggests that its origin may be geothermal fluid moving along a narrow zone, such as a fault, either flowing east away from or west into the main reservoir. A fault has been mapped on the south side of the Marysville stock (Figure 4b) which could be the structure controlling this narrow zone of subsurface fluid flow.

The source of the Marysville geothermal anomaly was already known before the heat flow continuation method was applied, and it was from the deep test well data that the 95°C isothermal surface was chosen to represent the upper surface of the reservoir. Even without the deep well data, the subsurface temperatures from the continuation of the shallow heat flow data give an indication of the source of the anomaly. Since the distance between the 3 to 15 HFU contours in Figure 4a in the northeast is approximately 1 km, application of the half-width rule indicates the maximum source depth to be 0.5 km where the calculated temperature is approximately 100°C.

Simple extrapolation of the surface heat flow data using equation (17) to map the 95°C isothermal surface results in a set of contours similar to the heat flow contours shown in Figure 4a. The fine detail of the reservoir shape is not delineated and the narrow east-west salient is not defined, so the anomaly cannot be as directly related to the mapped fault. This example illustrates the power of the continuation technique in the geologic interpretation of surface geothermal anomalies.

East Mesa, Imperial Valley, California

The East Mesa geothermal anomaly is in the Imperial Valley, California, on the eastern flank of the Salton trough, the sediment-filled structural depression that forms the northern extension of the Gulf of California and East Pacific Rise. A range of geophysical and geochemical surveys all outline the same general target area covering an area of 40 km^2 where the heat flow is in excess of 5 μcal/cm^2 sec (210 mW/m^2) as shown in Figure 5a. Five deep wells have been drilled into the anomaly, the locations of which are also indicated on Figure 5a. The re-

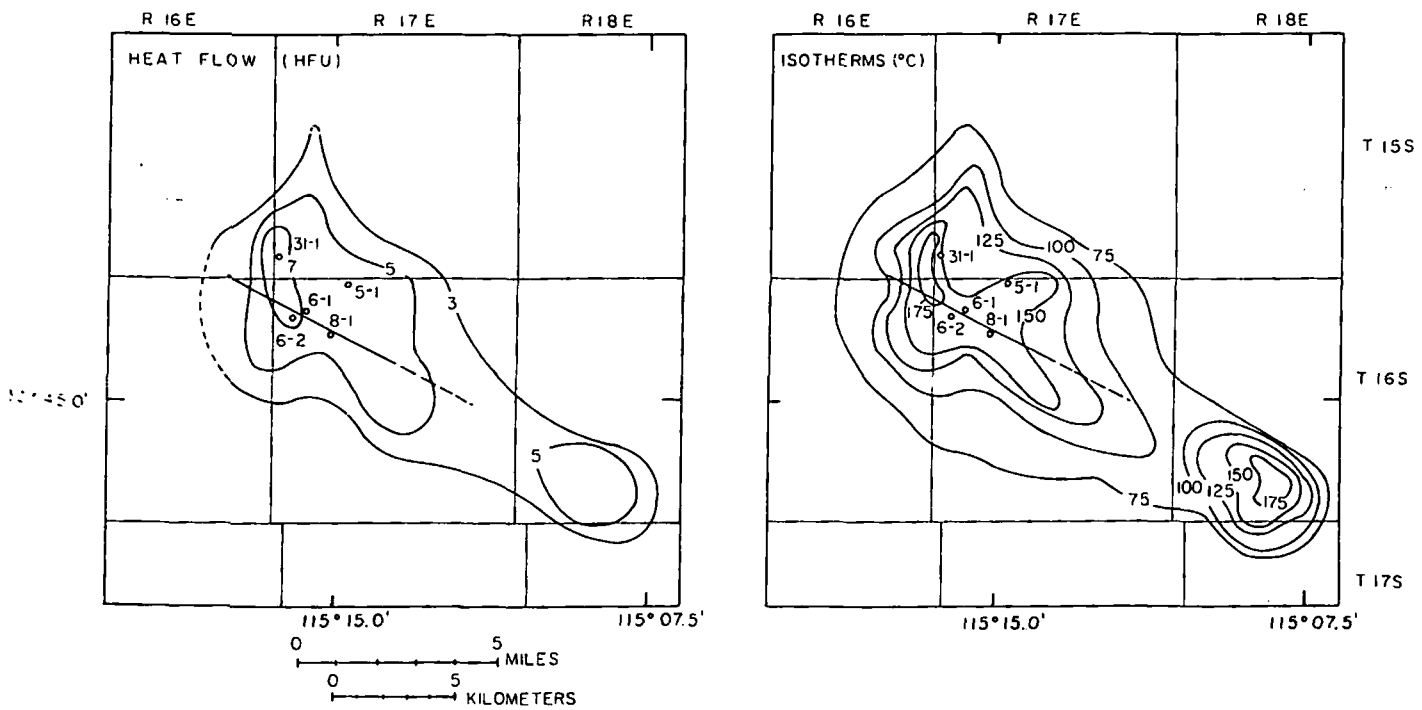

FIG. 5. (a) Generalized heat flow map of the East Mesa geothermal anomaly (after Swanberg, 1975). Heat flow contours of 3.0, 5.0, and 7.0 μcal/m^2 sec (125, 210, and 295 mW/m^2) are shown, together with the locations of the five deep wells (open circles 31-1, 5-1, 6-1, 6-2 and 8-1) and the fault mapped by Combs and Hadley (1977). (b) Computed isotherms between 75 and 175°C at 25°C intervals on a plane 0.8 km below the surface. The deep wells and fault are as shown in Figure 5a.

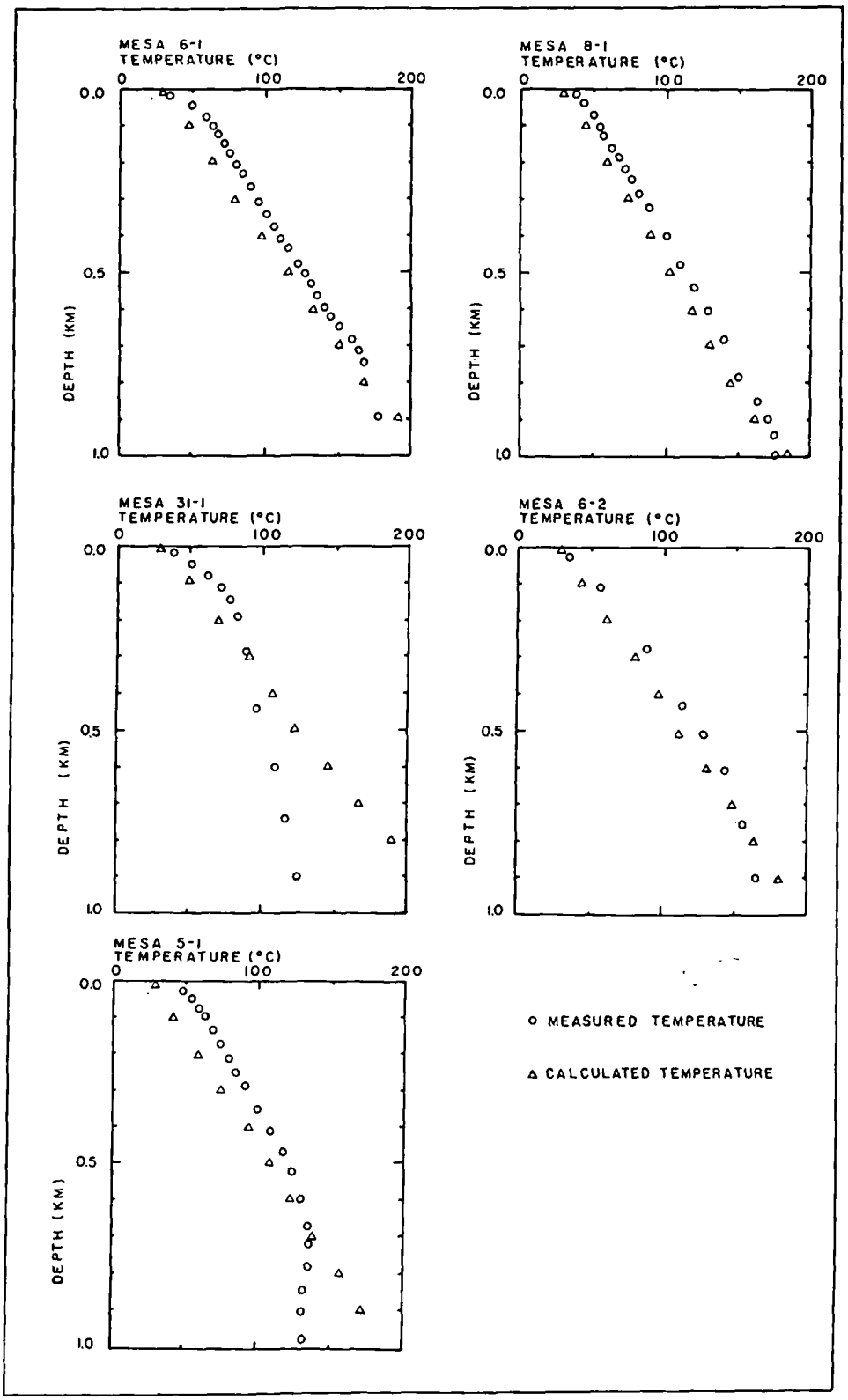

FIG. 6. Temperature-depth data from deep Mesa wells (6-1, 8-1, 31-1, 6-2, and 5-1). The measured temperatures are open circles and the calculated temperatures are triangles. The calculated temperatures as offset by 10°C for clarity.

sults from the deep drilling and surface geophysics were summarized by Swanberg (1974).

Heat flow data from the East Mesa anomaly were digitized on a 15 × 15 grid with a grid spacing of 1.6 km. Subsurface temperatures were calculated using the sourceward continuation method following exactly the same procedure used for the Marysville data described above, except that a thermal conductivity appropriate to the Mesa sediments, 3.8 mcal/cm-sec-°C (1.5 W/m°K), was used in equation (17). The sources and image sources were located on a plane 3 km below and above the datum plane, respectively. Isotherms are constructed from the calculated subsurface temperatures on a plane 0.8 km below the datum plane.

The geothermal anomaly appears to be caused by a complex reservoir as indicated by the temperature-depth curves from the deep test wells shown in Figure 6. Three of the curves for wells 6-1, 6-2, and 8-1 become isothermal at temperatures in the range of 175°–200°C, whereas the curves for wells 31-1 and 5-1 become isothermal in the range of 100°–150°C. Therefore, the temperatures at the top of the reservoir are not constant, and it cannot be assumed to be a single isothermal surface as in the case of the simple reservoir.

Figure 5b shows contours of the 75° to 175°C isotherms at 25°C intervals at a depth of 0.8 km. The 100°C and above contours delineate two possible shallow reservoirs probably interconnected at depth. The isotherms at 0.8-km depth in the northwestern portion of the anomaly have a complex shape. A salient from this portion of the anomaly projects approximately southeast and strongly suggests fluid flow along a narrow zone, probably along a fault.

A fault has been mapped by Combs and Hadley (1977) close to this salient which could be the surface expression of this narrow high-temperature zone. The 150°C isotherm has a very complex shape with two additional salients pointing to the north and northeast. These two lobes suggest other zones of fluid flow approximately perpendicular to the southeast salient. The smaller southeast portion of the anomaly has greater horizontal temperature gradients than the main anomaly, especially to the northeast. A small lobe in the 175°C contour projects toward the main anomaly and is aligned with the mapped fault, suggesting an origin related to the main anomaly.

The calculated subsurface temperatures are compared to the temperature-depth data from the five deep test wells in Figure 6. Above the reservoir the calculated temperatures are slightly lower than the observed temperatures, indicating that too low a value was assumed for the mean surface temperature. There is basically very good agreement between the calculated and observed shape of the temperature-depth curves in the area of applicability of the continuation technique, i.e., outside the reservoir. The observed and computed curves diverge inside the reservoir.

Simple extrapolation of the surface heat flow data would have revealed none of the complexities in the subsurface isotherms which were obtained from the continuation method. The extrapolated isotherms would simply reflect the surface heat flow pattern in Figure 5a. The results of the continuation clearly show the anomaly to be caused by fluid flow along the narrow zones and indicate a complex relationship between the zones. The origin of the anomaly as flow along a fault intersection and the radiating fault zones is suggested by the resulting temperature model.

DISCUSSION

The simple continuation method described here is a useful technique to estimate subsurface isotherms in a geothermal area. As demonstrated in the 2-D model and the Marysville and East Mesa geothermal areas, this method can be applied where thermal convection occurs at depth if the zone of fluid convection can be treated as a boundary condition for a conductive solution. This method is useful in defining spatial limits of such geothermal reservoirs. By application of the half-width rule to the surface gradient profile, the temperature range of the reservoir may be indicated, but better resolution and reservoir delineation are obtained if the depth or temperature is known. The use of the present continuation method is limited to cases where the heat flow anomaly is not related to contrasting thermal conductivity and resulting refraction of heat.

An advantage of this approach to interpretation of heat flow is that it is not model dependent, and complicated heat flow anomaly patterns can be interpreted more easily. The solution can be used for time dependent as well as steady-state thermal conditions, although no examples have been discussed. The solution technique is identical, except the time of initiation of the continuous sources and sinks must be independently known because a different solution exists for each different time. The time-dependent technique was used by Blackwell et al (1978) to interpret a regional heat flow anomaly in the Cascade range in the Pacific Northwest.

The method used for continuation assumes that the source distribution can be represented by a large number of line or point sources on a plane and requires a large amount of computer storage to solve the large number of simultaneous equations used to determine the source terms. Even though the use of the point or line sources is a crude approximation of the actual heat source, the method does give accurate subsurface temperatures. A similar method using different types of source distributions can easily be developed. However, the amount of known heat flow data in geothermal areas is limited and the use of more sophisticated types of source distributions is not justified.

The terrain correction discussed here can be used as an alternative mathematical solution to the terrain correction solution discussed by Blackwell et al (1980). With inclusion of the microclimatic effects discussed by Blackwell et al (1980), an alternative terrain correction technique can be developed. The continuation and terrain correction techniques can be combined to solve more complex problems. The mathematical formalization is not presented, but the development of the combined technique is very similar to the derivation of the continuation or terrain correction techniques presented.

ACKNOWLEDGMENTS

We wish to extend our thanks to M. J. Holdaway, E. Herrin, J. Combs, W. J. Peeples, and G. Salaita for critically reviewing this manuscript and making helpful suggestions. John Steele of Southern Methodist University supplied several of the finite-difference models which were used. Jacqueline Landon did the typing. The work was supported by National Science Foundation grant no. HES 74-19550A01 and U.S.G.S. grant no. 1408-001-G-425 to Southern Mehodist University.

REFERENCES

Birch, F., 1950, Flow of heat in the Front Range, Colorado: GSA Bull., v. 61, p. 567–630.

——— 1967, Low values of oceanic heat flow: J. Geophys. Res., v. 72, p. 2261–2262.

Blackwell, D. D., Brott, C. A., Goforth, T. T., Holdaway, M. J., Morgan, P., Petefish, D., Rape, T., Steele, J. L., Spafford, R. E., and Waibel, A. F., 1975, Geological and geophysical exploration at Marysville geothermal area: NSF-RANN tech. rep. NSF-RA-N-74031b, 104 p.

Blackwell, D. D., Hull, D. A., Bowen, R. G., and Steele, J. L., 1978,

Heat flow of Oregon: Oregon Dept. of Geol. and Mineral Ind. spec. paper 4, 42 p.
Blackwell, D. D., and Morgan, P., 1976, Geological and geophysical exploration of the Marysville geothermal area, Montana, USA: Proc. 2nd U.N. Symp. Dev. of Geothermal Potential, Washington, D.C., U.S. Govt. Printing Office, p. 895–902.
Blackwell, D. D., Steele, J. L., and Brott, C. A., 1980, The terrain effect on terrestrial heat flow: J. Geophys. Res., v. 85, p. 4757–4772.
Bodvarsson, G., 1973, Downward continuation of constrained potential fields: J. Geophys. Res., v. 78, p. 1288–1292.
Carnahan, B., Luther, H. A., and Willers, J. D., 1969, Applied numerical methods: New York, John Wiley and Sons, Inc., 604 p.
Carslaw, H. S., and Jaeger, J. C., 1959, Conduction of heat in solids, 2nd ed.: Oxford, Clarendon Press, 510 p.
Claerbout, J. F., 1976, Fundamentals of geophysical data processing with applications to petroleum prospecting: New York, McGraw-Hill, Inc., 274 p.
Combs, J., and Hadley, D. M., 1977, Microeathquake investigation of the Mesa geothermal anomaly, Imperial Valley, California: Geophysics, v. 42, p. 17–33.
Cooley, J. W., and Tukey, J. W., 1965, An algorithm for the machine calculation of complete Fourier series: Math. Comp., v. 19, p. 2970–2871.
Dampney, C. N. G., 1969, The equivalent source technique: Geophysics, v. 34, p. 39–53.
Grant, F. S., and West, G. F., 1965, Interpretation theory in applied geophysics: New York, McGraw-Hill, Inc., 584 p.
Henderson, R. G., and Cordell, L., 1971, Reduction of unevenly spaced potential field data to a horizontal plane by means of finite harmonic series: Geophysics, v. 36, p. 856–866.
Kanasewich, E. R., and Agarwal, R. G., 1970, Analysis of combined gravity and magnetic fields in wave number domain: J. Geophys. Res., v. 75, p. 5702–5712.
Ku, C. C., Telford, W. M., and Lin, S. H., 1971, The use of linear filtering in gravity problems: Geophysics, v. 36, p. 1174–1203.
Odegard, M. E., and Berg, J. W., Jr., 1965, Gravity interpretation using the Fourier integral: Geophysics, v. 30, p. 424–438.
Simmons, G., 1965, Effect of thermal conductivity contrasts on measured heat flow (abst.): AGU Trans. v. 46, p. 176.
———1967, Interpretation of heat flow anomalies: Rev. Geophys., v. 5, p. 41–52.
Swanberg, C. A., 1974, Heat flow and geothermal potential of the East Mesa KGRA, Imperial Valley, California: Proc. Conf. on Res. for Dev. of Geothermal Energy Resources, National Science Foundation NSF-R4-N-74-159., p. 85–98.

GEOPHYSICS, VOL. 48, NO. 9 (SEPTEMBER 1983); P. 1212–1218. 7 FIGS., 1 TABLE

Localized heat flow and Tertiary mineralization in southern New Mexico

Gary W. Zielinski* and Gail Moritz DeCoursey‡

ABSTRACT

Eight shallow (< 100 m deep) relative heat flow determinations from southern New Mexico reveal a systematic 3 HFU (125 mW/m²) increase occurring within a distance of 2 km. The maximum surface heat flow appears roughly to overlie a Tertiary granitic body at a depth of about 600 m within an area of known hydrothermal mineralization. The presence of the anomaly, believed to be of subsurface origin, implies an active heat source centered at a depth of 1140 m, perhaps associated with hydrothermal circulation. Higher radioactive heat production in granites may contribute to convective instability and explain the apparent lateral coincidence between the anomaly and the body. This situation appears, on a local scale, analogous to coinciding zones of high present-day heat flow and mineralization in England and Wales (Brown et al, 1980). In both cases, mineralization is associated with granitic intrusion that has occurred at a previous time which is much greater than the thermal time constant for cooling bodies. Shallow heat flow determinations may be useful in locating other similar areas and investigating possible associations of mineralization and thermal history.

INTRODUCTION

Cenozoic volcanism and concomitant mineralization is a well-established and widespread feature of the geology of New Mexico (Lindgren et al, 1910; Lasky and Wooton, 1933; Talmage and Wooton, 1937; Callaghan, 1953; Northrop, 1959). Our study area, encompassing roughly 30 km² in southern New Mexico, comprises a local example of this occurrence. The area consists of a group of east-west trending ridges of sedimentary and volcanic rock rising more than 200 m above a broad plain of Tertiary and Quaternary alluvium. From information provided by Gulf Mineral Resources Company, the sedimentary sequence in the area consists predominately of Paleozoic carbonates reaching a thickness of over 500 m. Extrusive volcanic activity began in the Early Cretaceous and culminated in the Middle Tertiary with the emplacement of a granitic pluton, an apophysis of which is exposed nearby. Hydrothermal mineral deposits, including varying concentrations of gold, silver, copper, lead, and zinc, recognized prior to 1880, exist in small but commercial quantities.

Compilations of terrestrial heat flow data from New Mexico (Reiter et al, 1975; Edwards et al, 1978; Shearer and Reiter, 1981) indicate generally above average and variable heat flow. This is largely attributed to varying amounts of Cenozoic magmatism, hydrothermal circulation, and radioactive heat production in the crust. In order to investigate the present-day thermal regime in our study area in relation to local volcanism and mineralization, a suite of 8 shallow (~35 m) relative heat flow determinations was attempted in November, 1980. The particular location of the measurements was based on the availability of subsurface data from previous deep drilling. It was hoped that these determinations might reveal some additional information on the area's thermal history; at the same time, the uncertainties as well as the potential of shallow land-based heat flow measurements could be explored.

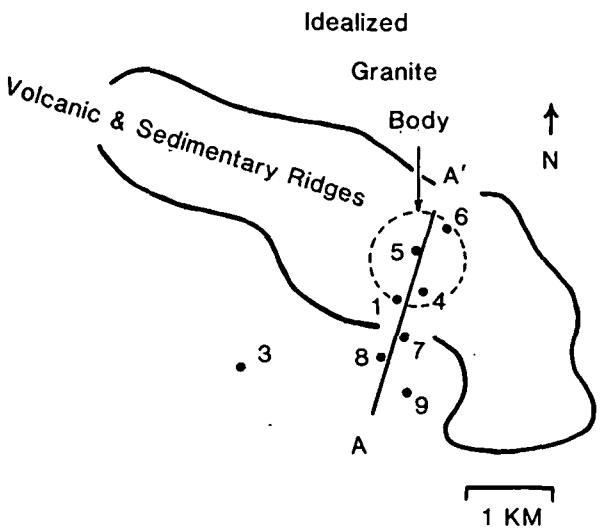

FIG. 1. Relative position of heat flow stations (numbered dots), the local zone of volcanic and sedimentary topographic relief and an idealized granite body (dashed circle) for the study area in southern New Mexico.

Manuscript received by the Editor August 19, 1982; revised manuscript received December 29, 1982.
*Dept. of Geochemistry and Minerals, Gulf Research and Development Company, P.O. Drawer 2038, Pittsburgh, PA 15230.
‡Formerly Dept. of Geological Sciences, University of Rochester, Rochester, NY 14627; presently Marathon Oil Company, P.O. Box 3128, Houston, TX 77001.

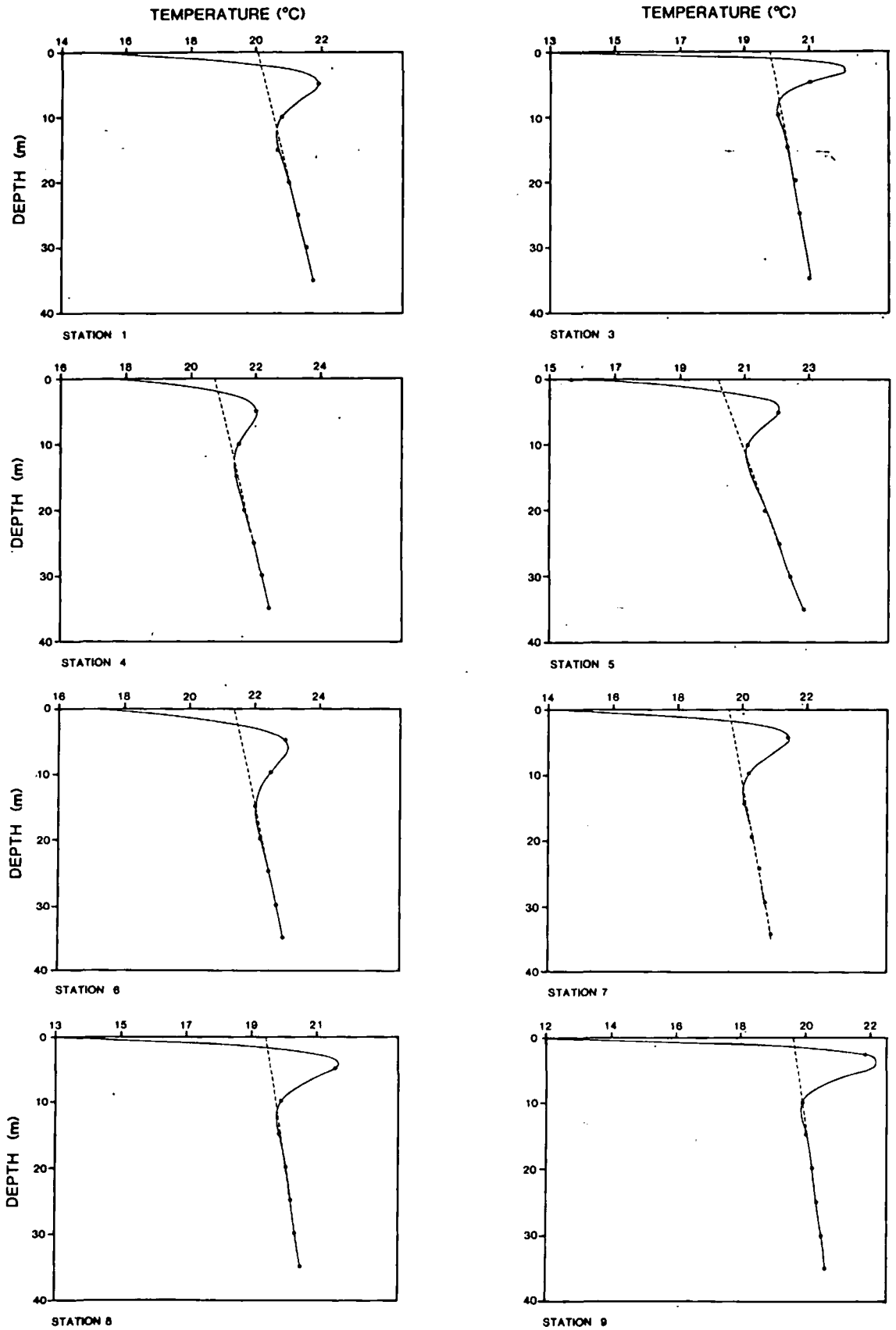

FIG. 2. Observed temperatures (dots) and calculated temperatures (solid curves) for the heat flow stations versus depth. Dashed lines represent estimated geothermal gradients from regression.

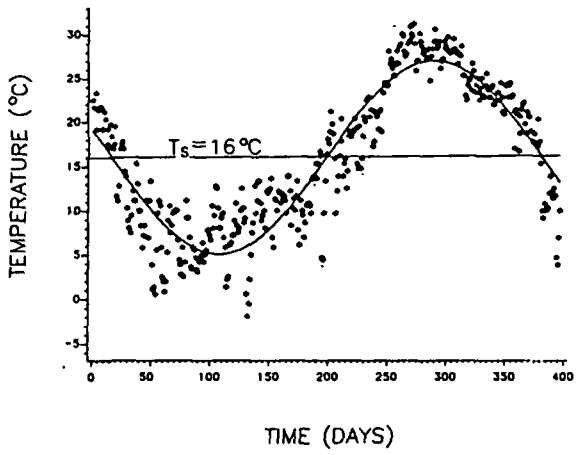

FIG. 3. Observed surface air temperatures for the study area in southern New Mexico, from October 1, 1979 (day 0) to October 31, 1980 (day 396). The solid curve is the best fit sinusoid.

MEASUREMENTS

The orientation of the heat flow stations, given in Figure 1, is roughly perpendicular to the principal topographic trend. Measurements were made in the upper 35 m of thermally equilibrated boreholes. These were accomplished by lowering a thermistor probe into each borehole and obtaining equilibrated readings from 5 to 35 m in 5 m increments. The thermistor output was monitored with a digital ohm-meter operating in the 4-wire mode and converted to temperature by a previously determined calibration function (Steinhart and Hart, 1968). Considerable laboratory testing of the measurement system against a platinum resistance thermometer and resistance bridge allows estimates of absolute accuracy at about 0.02°C and relative error at <0.002°C. Because of the long equilibration time of the thermistor probe, only 2 sites could be completed per day resulting in a total 4 day sampling period. The results of these measurements are shown in Figure 2 (black dots).

The temperature values shown in Figure 2 were obtained in a depth interval where it is likely that the dominant transient component of the temperature field results from the seasonal fluctuation of surface temperature. The indirect method of Lee (1977) was used to remove this transient component from the temperature profiles and to obtain an estimate of the mean equilibrium geothermal gradient and a value of the average thermal diffusivity over the depth interval for each station. More specifically, the procedure uses a linearized form of the solution for heat conduction in a homogeneous half-space with sinusoidally varying surface temperature (period = 1 year),

$$T_{ji} = T_s + gz_i + \delta_j x_i + \varepsilon_j y_i \qquad (1)$$

where

$$\delta_j = A \sin \omega(t_j - t_0),$$

$$\varepsilon_j = -A \cos \omega(t_j - t_0),$$

and

$$x_i = \exp(-z_i\sqrt{\omega/2\mu}) \cos(z_i\sqrt{\omega/2\mu}),$$

$$y_i = \exp(-z_i\sqrt{\omega/2\mu}) \sin(z_i\sqrt{\omega/2\mu}).$$

T_{ji} are the temperatures measured at depth z_i at time t_j, T_s is the mean surface temperature, A is the amplitude of the annual surface temperature variation, g is the geothermal gradient, ω is the angular velocity of the annual temperature variation (2×10^{-7} sec^{-1}), t_0 is the time when $T(z = 0) = T_s$, and μ is thermal diffusivity. A minimum root-mean-square (rms) error solution to equation (1) is sought after assigning discrete values of μ ranging from 0.001 to 0.020 cm^2/sec in increments of 10^{-4} cm^2/sec, which covers the range of values normally observed for most soils and rock (Kappelmeyer and Haenel, 1974). Corresponding best-fit values of μ and g are assumed to be the correct values. The data in Figure 2, however, were not adequate to obtain a best-fit solution to equation (1) by the indirect method of Lee (1977) without imposing one additional constraint. This was obtained from daily surface air temperature measurements (recorded at a U.S. Weather Service station located 55 km away) for a period of 1 year prior to our field measurements (Figure 3). The solid curve in Figure 3 is the best-fit sinusoid (period = 1 year) to the data. This allows an estimate of t_0 and hence $t_j - t_0$ could be specified in equation (1) for each station assuming there is no difference in phase between the annual air temperature and ground temperature fluctuations at the surface.

The results of reduction of the temperature data in Figure 2 are summarized in Table 1. The theoretical temperature profiles corresponding to the parameters in Table 1 are plotted along with the data in Figure 2 (solid curves). The dashed lines in Figure 2 indicate the computed geothermal gradient for each station resulting from removal of the periodic component from the temperature data. Based on the values of the coefficient of determination R^2 obtained (Table 1), there is in general a good fit ($R^2 = 1$ would indicate a perfect fit) of the data to the assumed conductive theory [equation (1)]. The values of T_s in Table 1 average about 4°C higher than the mean annual air temperature (Figure 3). This is no doubt the result of direct radiative heating of the ground. (The air temperatures were recorded in a covered shed.) Because of this effect, Kappelmeyer and Haenel (1974) stated that workers often recommend the

Table 1. Summary of thermal results.

Station	μ	g	T_s	A	R^2	K	q
1	10.5	5.10	20.01	9.31	.9996	5.71	2.91
3	4.1	3.59	19.82	12.51	.9924	3.02	1.08
4	12.9	4.91	20.72	5.86	.9996	6.72	3.30
5	10.1	7.72	20.18	8.60	.9992	5.54	4.28
6	16.7	4.38	21.39	7.82	.9995	8.31	3.64
7	10.0	3.81	19.57	9.32	.9999	5.50	2.09
8	8.7	3.07	19.43	11.52	.9998	4.95	1.52
9	6.7	2.94	19.54	14.33	.9993	4.11	1.21

μ = Thermal diffusivity ($\times 10^{-3}$ cm^2 sec^{-1})
g = Geothermal gradient ($\times 10^{-4}$ °C cm^{-1})
T_s = Mean surface temperature (°C)
A = Amplitude of the surface temperature change (°C)
R^2 = Coefficient of determination
K = Thermal conductivity ($\times 10^{-3}$ cal °C^{-1} cm^{-1} sec^{-1})
q = Heat flow ($\times 10^{-6}$ cal cm^{-2} sec^{-1})

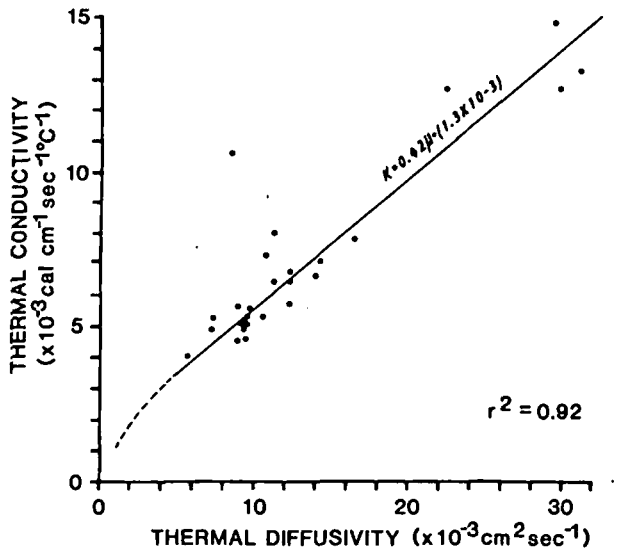

FIG. 4. Relationship between thermal diffusivity and thermal conductivity. Dots are data for solid rock taken from Kappelmeyer and Haenel (1974) and the straight line is the least-squares fit to the data. The dashed line is an empirical representation of thermal diffusivity versus thermal conductivity for unconsolidated ocean bottom sediment derived from Bullard (1963).

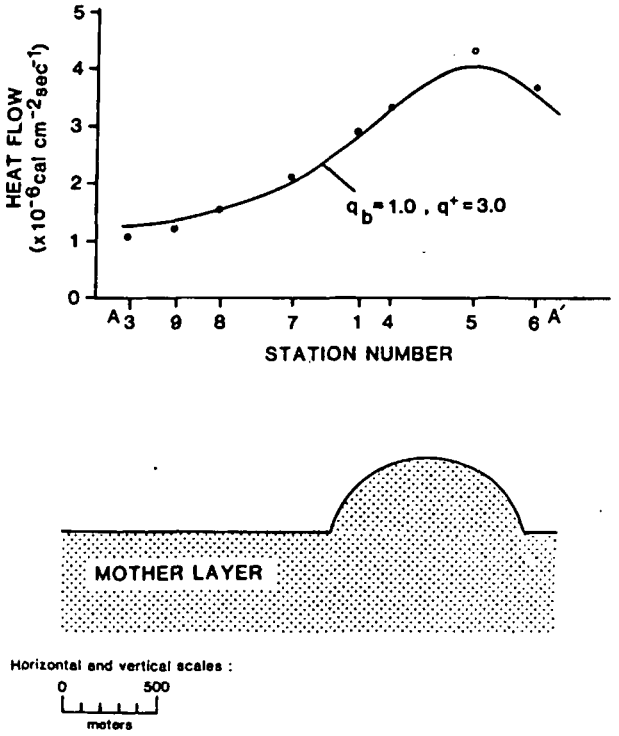

FIG. 5. Observed (dots) and theoretical heat flow (curve) along section A-A' in Figure 1. q_b is background heat flow and q^+ is the additional heat flow from a spherical source. Below is the simplified geometry of a subsurface granitic body. Depth and lateral extent are based on information from deep boreholes.

rule of thumb addition of 1°C to the mean annual air temperature to estimate mean ground temperature. Clearly, from Table 1, this difference can be significantly larger. The site-to-site variation in T_s (Table 1) is most likely due to differences in the exposure of the ground to incident solar radiation since differences in albedo caused by variations in ground cover over the area are probably insignificant.

For most of the stations the lithology corresponding to the temperature measurement interval comprised undifferentiated Quaternary gravel, soil, and alluvium. The values of μ obtained from the data reduction (Table 1) are therefore highly variable, as might be expected; however, for station 1 and possibly station 7 measurements were obtained in dolomite. These are in excellent agreement with measured values reported in the literature (Kappelmeyer and Haenel, 1974). The values of μ in Table 1 were used to obtain a rough estimate of thermal conductivity K for each station. This was done by plotting average values of thermal conductivity versus average thermal diffusivity for a wide range of lithologies (Figure 4). The data are from the compilation of Kappelmeyer and Haenel (1974). Included also is a theoretical relation (dashed curve) for unconsolidated sediments (Bullard, 1963). A least-squares line fit to the data over the range appropriate for consolidated rocks leads to the relation $K = 1.3 \times 10^{-3} + 0.42\ \mu$ which was used to compute the thermal conductivity given in Table 1. Implicit in this procedure is the assumption that, over the range appropriate to consolidated rocks, variations in the density and heat capacity of rocks are small compared with variations in thermal conductivity. The data in Figure 4 sufficiently support this assumption for the present purposes. This estimate of K in turn allows an estimate of relative heat flow $q = Kg$ for each site, which is also given in Table 1.

Transient temperature disturbances caused by thermal convection within the boreholes (Diment, 1967; Gretener, 1967) cannot be ruled out a priori for the temperature data in Figure 2. This effect does not, however, appear to present a problem to the data set in general. The level of agreement of the data set to conductive theory (Figure 2 and Table 1) and the uniformity of computed parameters (Table 1) do not suggest the presence of serious random temperature perturbations, particularly in view of the sizeable and remarkably systematic trend observed in the heat flow values, which will be seen in the next section.

RESULTS

The results of the heat flow estimates for each station (Table 1) are plotted in Figure 5 as a function of relative position projected on line A-A' (Figure 1). The lower section of Figure 5 shows the suggested position of a subsurface granitic body (Figure 1) approximated by a hemisphere. The approximate depth and lateral extent of the granite as well as its approximate location with respect to the heat flow measurements are based on information from deep boreholes provided by Gulf Mineral Resources Company. The continuity of the body and the existence of the mother layer are somewhat speculative and largely for the purpose of the heat flow interpretation.

The relative heat flow values in Figure 5 exhibit a large and systematic increase as the ridge province (Figure 1) is approached from the south-southwest. The maximum observed increase in relative heat flow of 3 HFU (1 HFU = 10^{-6} cal cm^{-2} sec = 41.8 mW/m^2) appears to be centered around station 5. Since the magnitude of the observed increase is too large to be accounted for by heat conduction effects of

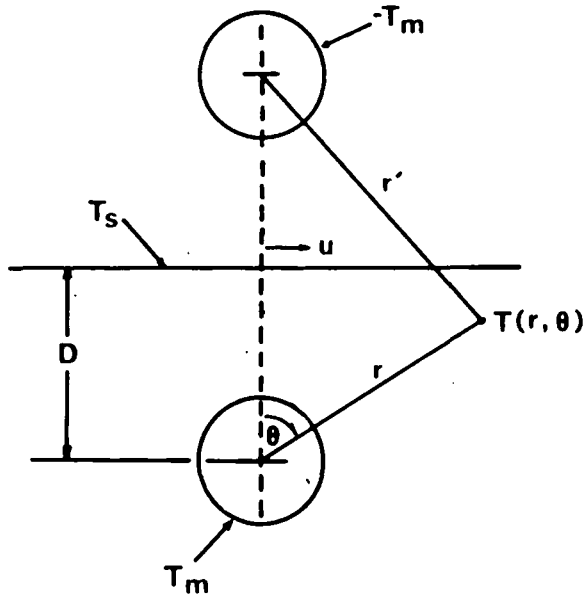

FIG. 6. Geometry for applying the method of images to a buried sphere.

surface topography, nor does it relate to individual station elevation or slope orientation, a subsurface cause must be responsible.

Hardee and Larson (1980) arrived at a relation for the steady state surface heat flow as a function of horizontal position u for a sphere of radius a at constant temperature T_m, buried at depth D in a medium initially at zero temperature, with a horizontal surface held at constant temperature T_s (see Figure 6). Their result was that

$$\frac{q}{q^+} = \left[1 + \left(\frac{u}{D}\right)^2\right]^{-2}, \tag{2}$$

where

$$q^+ = -\frac{2aK(T_m - T_s)}{D^2}, \tag{3}$$

is the maximum heat flow (at $r = D$, $\theta = 0$). The solid curve in Figure 5 is the result of applying equations (2) and (3) to the heat flow data. Equation (2) was used to estimate from the data the depth D to the center of a spherical source capable of creating the observed anomaly ($D = 1140$ m). The heat flow values at stations 3 and 9 suggest a background heat flow $q_b(u \to \infty)$ of about 1 HFU so that a value of $q^+ \cong 3$ HFU is then required to fit the observations near the crest of the anomaly. From equation (3), for example, a temperature excess of 50°C (for $K = 7$ mcal °C^{-1} cm^{-1} sec^{-1}), its position and depth coinciding with the surface of the granitic body illustrated in Figure 5, would produce the theoretical heat flow profile (solid curve) in Figure 5, which is in excellent agreement with the measurements. This result suggests a possible association between the granite body and the observed relative heat flow. Furthermore, it is clear from the magnitude of the required temperature excess that heat conduction effects resulting from possible contrasts in thermal properties and radioactive heat production (between the granite and surrounding rock) alone are incapable of accounting for the observed anomaly.

In order to test the possibility that the suggested temperature excess is the result of transient cooling of the body from an originally molten state, we have applied the method of images to a sphere cooling from some initial temperature T_m. From the solution for an infinite region,

$$T(r, t) = \frac{T_m}{2}\left(\operatorname{erf}\frac{r+a}{2\sqrt{\mu t}} - \operatorname{erf}\frac{r-a}{2\sqrt{\mu t}} - \frac{2\sqrt{\mu t}}{r\sqrt{\pi}} \cdot \{\exp[-(r-a)^2/4\mu t] - \exp[-(r+a)^2/4\mu t]\}\right) \tag{4}$$

(Carslaw and Jaeger, 1959), the solution for a semi-infinite medium (Figure 6) becomes

$$T(r, t) = \frac{T_m}{2}\left\{\operatorname{erf}\frac{r+a}{2\sqrt{\mu t}} - \operatorname{erf}\frac{r-a}{2\sqrt{\mu t}} - \frac{2\sqrt{\mu t}}{r\sqrt{\pi}} \cdot \{\exp[-(r-a)^2/4\mu t] - \exp -(r+a)^2/4\mu t\}\right\} - \frac{T_m}{2}\left\{\operatorname{erf}\frac{r'+a}{2\sqrt{\mu t}} - \operatorname{erf}\frac{r'-a}{2\sqrt{\mu t}} - \frac{2\sqrt{\mu t}}{r'\sqrt{\pi}} \cdot \{\exp[-(r'-a)^2/4\mu t] - \exp[-(r'+a)^2/4\mu t]\}\right\}, \tag{5}$$

where

$$r' = [r^2 + 4D^2 - 4rD\cos\theta]^{1/2}.$$

The solution for heat flow q is

$$q = -K\left.\frac{dT}{dr}\right|_{\theta=0} = -KT_m \exp\left(-\frac{(D+a)^2}{4\mu t}\right)\left[\frac{1}{\sqrt{\pi\mu t}} - \frac{a+D}{D\sqrt{\pi\mu t}} - \frac{2\sqrt{\mu t}}{D^2\sqrt{\pi}}\right] + T_m \exp\left(-\frac{(D-a)^2}{4\mu t}\right)\left[\frac{-1}{\sqrt{\pi\mu t}} - \frac{a+D}{D\sqrt{\pi\mu t}} + \frac{2\sqrt{\mu t}}{D^2\sqrt{\pi}}\right]. \tag{6}$$

In Figure 7 we have plotted heat flow versus time from equation (6) for a cooling sphere with $T_m = 1000$°C, $K = 7$ mcal °C^{-1} cm^{-1} sec^{-1}, $\mu = 0.01$ cm^2 sec^{-1}, and the approximate observed dimensions (inset) which correspond to Figure 5. First seen (Figure 7) is a buildup of heat flow as heat from the buried sphere reaches the surface and then a decrease as that heat is eventually lost. The important result, however, is that all this occurs within 100,000 years. Thus, if the granite body, approximated by a sphere, is of Tertiary age, no residual heat flow would be expected to remain at present time. Our theoretical treatment of the cooling granite body neglects possible cooling by convective heat transfer. However, incorporating convection in our model would decrease the estimated cooling time and, therefore, would not alter our conclusion.

It is also possible to speculate on the existence of a somewhat deeper mother layer (Figure 5) of considerable lateral extent as a source of residual transient heat flow. The heat flow solution for a cooling, buried half-space (used to represent a cooling granitic batholith in Goguel, 1976), given by

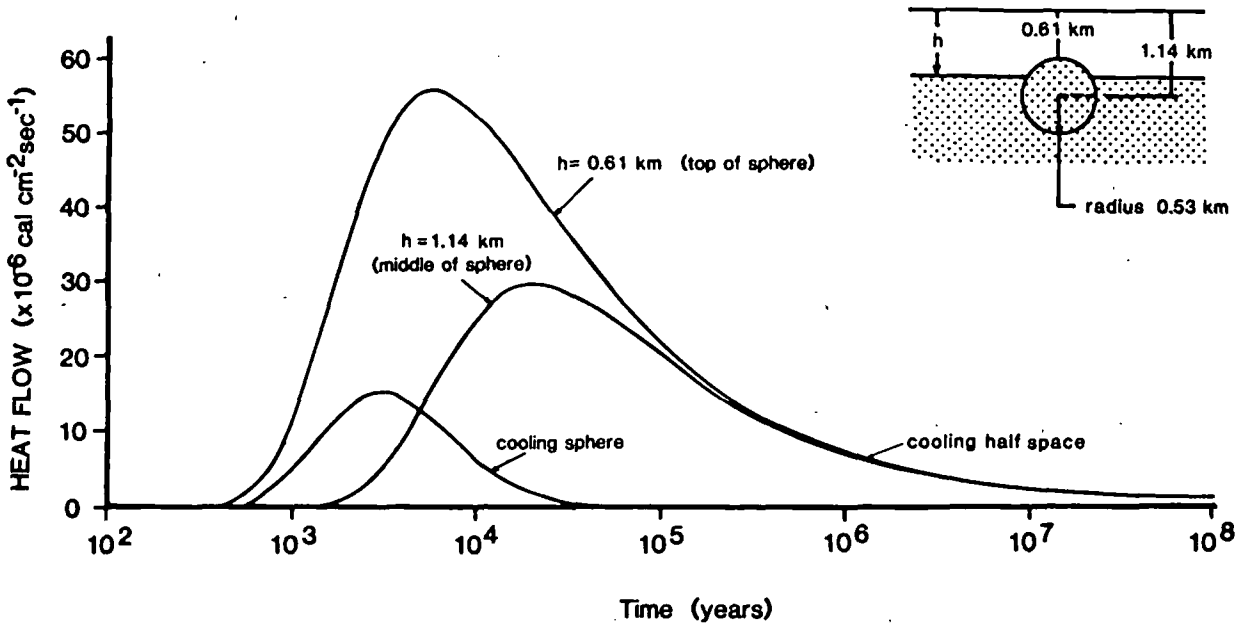

FIG. 7. Theoretical cooling of a buried half-space (at depth h) and cooling sphere. Dimensions and geometry are inset.

$$q = \frac{-2KT_m}{2\sqrt{\pi\mu t}} \exp(-h^2/4\mu t), \quad (7)$$

was used to explore this possibility. These results are also plotted in Figure 7 for the same parameters as the cooling sphere but for depths $h = 610$ m (corresponding to the top of the sphere) and $h = D = 1140$ m. In both cases (Figure 7) significant residual heat flow remains after 10^7 years. Thus a mother layer cooling from mid-Tertiary time is capable of supplying enough heat to account for the observed q^+ of 3 HFU. Still, transient cooling of a smaller wavelength granite body as a mechanism is insufficient to account for the shape of the observed heat flow anomaly even if heat is supplied by the mother layer. The effect of the thermal conductivity contrast between granite and limestone or dolomite is far too small (Lovering, 1935) to offset the rapid cooling time of a sphere or hemisphere of an appropriate size (Figures 5 and 7).

Based on these results, it must be concluded that the heat flow anomaly observed in the study area is not the direct result of transient cooling of a granite body, but must be indicative of an active (or recently active) process such as hydrothermal circulation. The heat flow estimated for stations 3 and 9, 1.08 and 1.21 HFU, is less than most published values from the surrounding area, ~2.0 HFU (Reiter et al, 1975; Edwards et al, 1978; Shearer and Reiter, 1981). Although the absolute accuracy of the shallow heat flow determinations in Table 1 is not well established, the range of values does not significantly depart from that observed via deep borehole observations in areas of extensive volcanic activity in northeastern New Mexico and southeastern Colorado (Edwards et al, 1978). The low background heat flow ($q_b = 1$ HFU) suggested earlier could imply low reduced heat flow as well as a low contribution from crustal radioactive heat production. Leaching of radioactive elements by moving groundwater has been suggested to explain locally nonrepresentative crustal radioactivity in Arizona (Shearer and Reiter, 1981). In that same study, forced and free convection by moving groundwater was called upon to explain some of the variability of heat flow measurements taken shallower than 650 m. The heat flow pattern shown in Figure 5 also might be the result of a local redistribution of heat by hydrothermal convection occurring at depth. In this case the low values at stations 3 and 9 could be indicative of removal of heat as in the case of a downgoing limb of a convection cell. Higher concentrations of heat-producing elements in the granite body, while incapable of producing 3 HFU to cause the observed anomaly, may contribute to the convective instability. Such a mechanism might focus the convection and explain the location of the heat flow high over the granite body.

CONCLUSIONS

There appears to be spatial coincidence between a present-day heat flow anomaly, a Tertiary granitic body, and hydrothermal mineralization within a localized area in southern New Mexico. Based on the heat flow values obtained, hydrothermal circulation is believed to be the most likely explanation for the heat flow anomaly. Higher radioactive heat production in the granite body may explain the spatial coincidence between the anomaly and the body. The situation appears analogous to the regional association between zones of high heat flow, metalliferous mineralization, and intrusive bodies in England and Wales (Brown et al, 1980). There it was postulated that Caledonian age intrusive bodies focused the development of hydrothermal systems responsible for post-Carboniferous mineralization, and that these systems have persisted through time to create the present-day high heat flow.

Our results suggest the possibility of such occurrences on a local scale and the potential of shallow thermal measurements as an aid in locating and understanding them.

ACKNOWLEDGMENTS

The authors wish to thank Tom Heidrick, Jerzy Maciolek, Ian Lerche and two anonymous reviewers for helpful comments which led to improvements in the original manuscript. We also thank Gulf Oil Corporation for permission to publish the heat flow data and Tom Heidrick for encouraging us to make the measurements.

REFERENCES

Brown, G. C., Cassidy, J., Oxburgh, E. R., Plant, J., Sabine, P. A., and Watson, J. V., 1980, Basement heat flow and metalliferous mineralization in England and Wales: Nature, v. 288, p. 657–659.

Bullard, E. C., 1963, The flow of heat through the floor of the ocean, *in* The Sea: M. Hill, Ed., v. 3, p. 218–232.

Callaghan, E., 1953, Volcanic rocks of southwestern New Mexico: N. Mex. Geol. Soc., 4th Field Conference.

Carslaw, H. S., and Jaeger, J. C., 1959, Conduction of heat in solids: Oxford University Press, Oxford.

Diment, W. H., 1967, Thermal regime of a large diameter borehole: Instability of the water column and comparison of air- and water-filled conditions: Geophysics, v. 32, p. 720–726.

Edwards, C. L., Reiter, M., Shearer, C., and Young, W., 1978, Terrestrial heat flow and crustal radioactivity in northeastern New Mexico and southeastern Colorado: GSA Bull., v. 89, p. 1341–1350.

Goguel, J., 1976, Geothermics: New York, McGraw-Hill Book Co.

Gretener, P. E., 1967, On the thermal instability of large diameter wells—An observational report: Geophysics, v. 32, p. 727–738.

Hardee, H. C., and Larson, D. W., 1980, Thermal techniques for characterizing magma body geometrics: Geothermics, v. 9, p. 237–249.

Kappelmeyer, O., and Haenel, R., 1974, Geothermics with special reference to application: Geoexploration Monographs, series 1, no. 4, Gebrüder Borntraeger, Berlin.

Lasky, S. G., and Wooton, T. P., 1933, The metal resources of New Mexico and their economic features: N. Mex. School of Mines, State Bur. Mines and Mineral Res. Bull. 7.

Lee, T-C., 1977, On shallow-hole temperature measurements—A test study in the Salton Sea geothermal field: Geophysics, v. 42, p. 572–583.

Lindgren, W., Graton, L. C., and Gordon, C. H., 1910, The ore deposits of New Mexico: U.S.G.S. Prof. Paper 68.

Lovering, T. S., 1935, Theory of heat conduction applied to geological problems: GSA Bull., v. 46, p. 69–94.

Northrop, S. A., 1959, Minerals of New Mexico: Albuquerque, Univ. of N. Mex. Press, revised edition.

Reiter, M., Edwards, C. L., Hartman, H., and Weidman, C., 1975, Terrestrial heat flow along the Rio Grande rift, New Mexico and southern Colorado: GSA Bull., v. 86, p. 811–818.

Shearer, C., and Reiter, M., 1981, Terrestrial heat flow in Arizona: J. Geophys. Res., v. 86, p. 6249–6260.

Steinhart, J. S., and Hart, S. R., 1968, Calibration curves for thermistors: Deep-Sea Res., v. 15, p. 497–503.

Talmage, S. B., and Wooton, T. P., 1937, The non-metallic mineral resources of New Mexico and their economic features; N. Mex. School of Mines, State Bur. Mines and Mineral Res. Bull. 12.

GEOPHYSICS, VOL. 48, NO. 9 (SEPTEMBER 1983); P. 1212–1218, 7 FIGS., 1 TABLE

Localized heat flow and Tertiary mineralization in southern New Mexico

Gary W. Zielinski* and Gail Moritz DeCoursey‡

ABSTRACT

Eight shallow (< 100 m deep) relative heat flow determinations from southern New Mexico reveal a systematic 3 HFU (125 mW/m^2) increase occurring within a distance of 2 km. The maximum surface heat flow appears roughly to overlie a Tertiary granitic body at a depth of about 600 m within an area of known hydrothermal mineralization. The presence of the anomaly, believed to be of subsurface origin, implies an active heat source centered at a depth of 1140 m, perhaps associated with hydrothermal circulation. Higher radioactive heat production in granites may contribute to convective instability and explain the apparent lateral coincidence between the anomaly and the body. This situation appears, on a local scale, analogous to coinciding zones of high present-day heat flow and mineralization in England and Wales (Brown et al, 1980). In both cases, mineralization is associated with granitic intrusion that has occurred at a previous time which is much greater than the thermal time constant for cooling bodies. Shallow heat flow determinations may be useful in locating other similar areas and investigating possible associations of mineralization and thermal history.

INTRODUCTION

Cenozoic volcanism and concomitant mineralization is a well-established and widespread feature of the geology of New Mexico (Lindgren et al, 1910; Lasky and Wooton, 1933; Talmage and Wooton, 1937; Callaghan, 1953; Northrop, 1959). Our study area, encompassing roughly 30 km^2 in southern New Mexico, comprises a local example of this occurrence. The area consists of a group of east-west trending ridges of sedimentary and volcanic rock rising more than 200 m above a broad plain of Tertiary and Quaternary alluvium. From information provided by Gulf Mineral Resources Company, the sedimentary sequence in the area consists predominately of Paleozoic carbonates reaching a thickness of over 500 m. Extrusive volcanic activity began in the Early Cretaceous and culminated in the Middle Tertiary with the emplacement of a granitic pluton, an apophysis of which is exposed nearby. Hydrothermal mineral deposits, including varying concentrations of gold, silver, copper, lead, and zinc, recognized prior to 1880, exist in small but commercial quantities.

Compilations of terrestrial heat flow data from New Mexico (Reiter et al, 1975; Edwards et al, 1978; Shearer and Reiter, 1981) indicate generally above average and variable heat flow. This is largely attributed to varying amounts of Cenozoic magmatism, hydrothermal circulation, and radioactive heat production in the crust. In order to investigate the present-day thermal regime in our study area in relation to local volcanism and mineralization, a suite of 8 shallow (~35 m) relative heat flow determinations was attempted in November, 1980. The particular location of the measurements was based on the availability of subsurface data from previous deep drilling. It was hoped that these determinations might reveal some additional information on the area's thermal history; at the same time, the uncertainties as well as the potential of shallow land-based heat flow measurements could be explored.

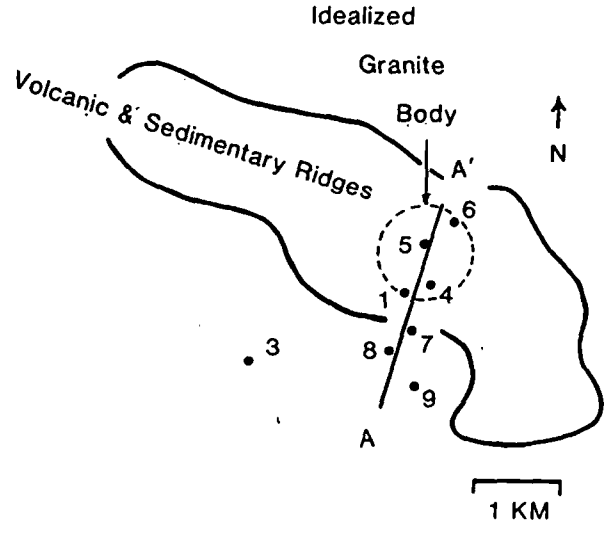

FIG. 1. Relative position of heat flow stations (numbered dots), the local zone of volcanic and sedimentary topographic relief and an idealized granite body (dashed circle) for the study area in southern New Mexico.

Manuscript received by the Editor August 19, 1982; revised manuscript received December 29, 1982.
*Dept. of Geochemistry and Minerals, Gulf Research and Development Company, P.O. Drawer 2038, Pittsburgh, PA 15230.
‡Formerly Dept. of Geological Sciences, University of Rochester, Rochester, NY 14627; presently Marathon Oil Company, P.O. Box 3128, Houston, TX 77001.

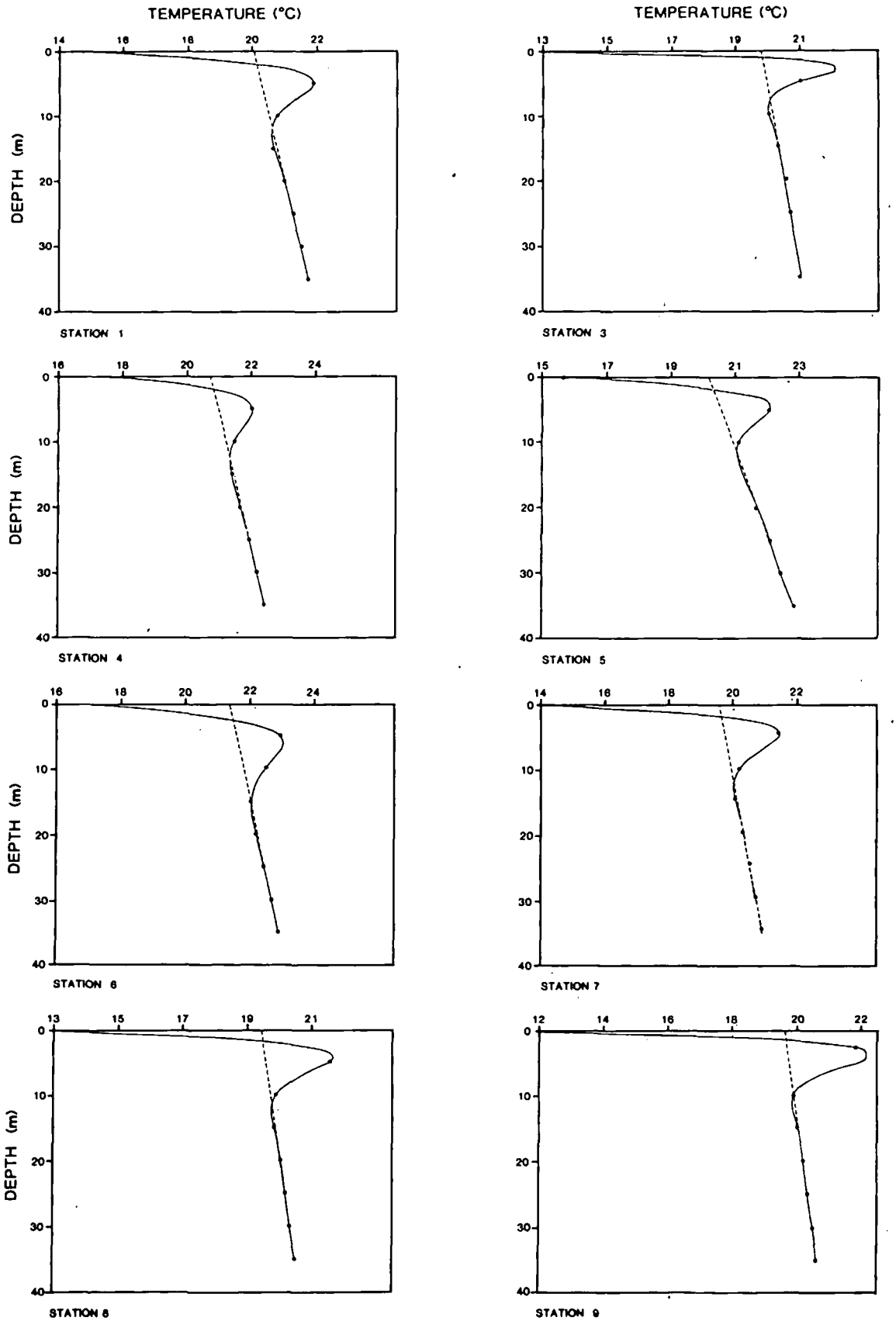

FIG. 2. Observed temperatures (dots) and calculated temperatures (solid curves) for the heat flow stations versus depth. Dashed lines represent estimated geothermal gradients from regression.

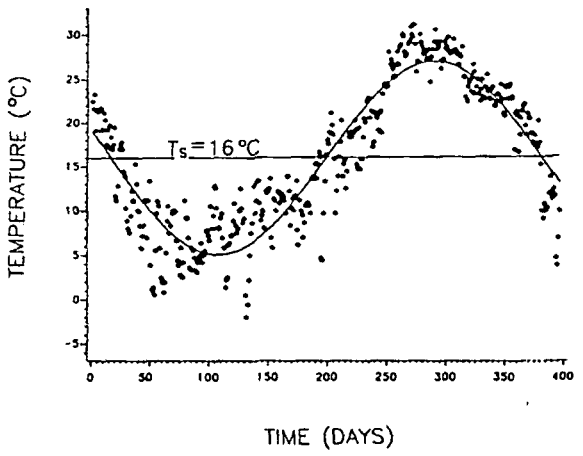

FIG. 3. Observed surface air temperatures for the study area in southern New Mexico, from October 1, 1979 (day 0) to October 31, 1980 (day 396). The solid curve is the best fit sinusoid.

MEASUREMENTS

The orientation of the heat flow stations, given in Figure 1, is roughly perpendicular to the principal topographic trend. Measurements were made in the upper 35 m of thermally equilibrated boreholes. These were accomplished by lowering a thermistor probe into each borehole and obtaining equilibrated readings from 5 to 35 m in 5 m increments. The thermistor output was monitored with a digital ohm-meter operating in the 4-wire mode and converted to temperature by a previously determined calibration function (Steinhart and Hart, 1968). Considerable laboratory testing of the measurement system against a platinum resistance thermometer and resistance bridge allows estimates of absolute accuracy at about 0.02°C and relative error at <0.002°C. Because of the long equilibration time of the thermistor probe, only 2 sites could be completed per day resulting in a total 4 day sampling period. The results of these measurements are shown in Figure 2 (black dots).

The temperature values shown in Figure 2 were obtained in a depth interval where it is likely that the dominant transient component of the temperature field results from the seasonal fluctuation of surface temperature. The indirect method of Lee (1977) was used to remove this transient component from the temperature profiles and to obtain an estimate of the mean equilibrium geothermal gradient and a value of the average thermal diffusivity over the depth interval for each station. More specifically, the procedure uses a linearized form of the solution for heat conduction in a homogeneous half-space with sinusoidally varying surface temperature (period = 1 year),

$$T_{ji} = T_s + gz_i + \delta_j x_i + \varepsilon_j y_i \qquad (1)$$

where

$$\delta_j = A \sin \omega(t_j - t_0),$$

$$\varepsilon_j = -A \cos \omega(t_j - t_0),$$

and

$$x_i = \exp(-z_i\sqrt{\omega/2\mu}) \cos(z_i\sqrt{\omega/2\mu}),$$

$$y_i = \exp(-z_i\sqrt{\omega/2\mu}) \sin(z_i\sqrt{\omega/2\mu}).$$

T_{ji} are the temperatures measured at depth z_i at time t_j, T_s is the mean surface temperature, A is the amplitude of the annual surface temperature variation, g is the geothermal gradient, ω is the angular velocity of the annual temperature variation (2×10^{-7} sec^{-1}), t_0 is the time when $T(z = 0) = T_s$, and μ is thermal diffusivity. A minimum root-mean-square (rms) error solution to equation (1) is sought after assigning discrete values of μ ranging from 0.001 to 0.020 cm^2/sec in increments of 10^{-4} cm^2/sec, which covers the range of values normally observed for most soils and rock (Kappelmeyer and Haenel, 1974). Corresponding best-fit values of μ and g are assumed to be the correct values. The data in Figure 2, however, were not adequate to obtain a best-fit solution to equation (1) by the indirect method of Lee (1977) without imposing one additional constraint. This was obtained from daily surface air temperature measurements (recorded at a U.S. Weather Service station located 55 km away) for a period of 1 year prior to our field measurements (Figure 3). The solid curve in Figure 3 is the best-fit sinusoid (period = 1 year) to the data. This allows an estimate of t_0 and hence $t_j - t_0$ could be specified in equation (1) for each station assuming there is no difference in phase between the annual air temperature and ground temperature fluctuations at the surface.

The results of reduction of the temperature data in Figure 2 are summarized in Table 1. The theoretical temperature profiles corresponding to the parameters in Table 1 are plotted along with the data in Figure 2 (solid curves). The dashed lines in Figure 2 indicate the computed geothermal gradient for each station resulting from removal of the periodic component from the temperature data. Based on the values of the coefficient of determination R^2 obtained (Table 1), there is in general a good fit ($R^2 = 1$ would indicate a perfect fit) of the data to the assumed conductive theory [equation (1)]. The values of T_s in Table 1 average about 4°C higher than the mean annual air temperature (Figure 3). This is no doubt the result of direct radiative heating of the ground. (The air temperatures were recorded in a covered shed.) Because of this effect, Kappelmeyer and Haenel (1974) stated that workers often recommend the

Table 1. Summary of thermal results.

Station	μ	g	T_s	A	R^2	K	q
1	10.5	5.10	20.01	9.31	.9996	5.71	2.91
3	4.1	3.59	19.82	12.51	.9924	3.02	1.08
4	12.9	4.91	20.72	5.86	.9996	6.72	3.30
5	10.1	7.72	20.18	8.60	.9992	5.54	4.28
6	16.7	4.38	21.39	7.82	.9995	8.31	3.64
7	10.0	3.81	19.57	9.32	.9999	5.50	2.09
8	8.7	3.07	19.43	11.52	.9998	4.95	1.52
9	6.7	2.94	19.54	14.33	.9993	4.11	1.21

μ = Thermal diffusivity ($\times 10^{-3}$ cm^2 sec^{-1})
g = Geothermal gradient ($\times 10^{-4}$ °C cm^{-1})
T_s = Mean surface temperature (°C)
A = Amplitude of the surface temperature change (°C)
R^2 = Coefficient of determination
K = Thermal conductivity ($\times 10^{-3}$ cal °C^{-1} cm^{-1} sec^{-1})
q = Heat flow ($\times 10^{-6}$ cal cm^{-2} sec^{-1})

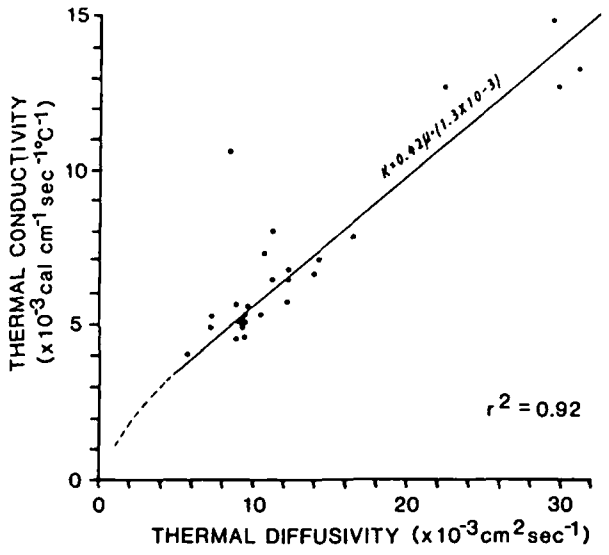

FIG. 4. Relationship between thermal diffusivity and thermal conductivity. Dots are data for solid rock taken from Kappelmeyer and Haenel (1974) and the straight line is the least-squares fit to the data. The dashed line is an empirical representation of thermal diffusivity versus thermal conductivity for unconsolidated ocean bottom sediment derived from Bullard (1963).

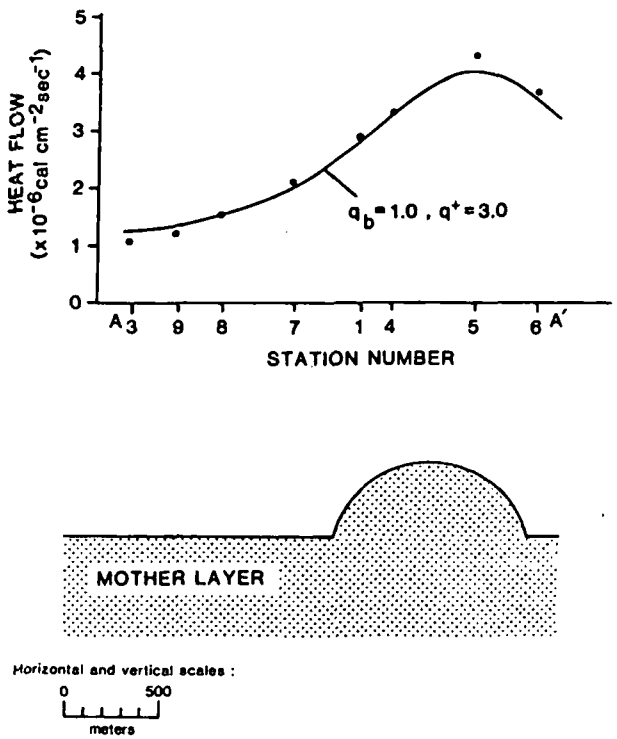

FIG. 5. Observed (dots) and theoretical heat flow (curve) along section A-A' in Figure 1. q_b is background heat flow and q^+ is the additional heat flow from a spherical source. Below is the simplified geometry of a subsurface granitic body. Depth and lateral extent are based on information from deep boreholes.

rule of thumb addition of 1°C to the mean annual air temperature to estimate mean ground temperature. Clearly, from Table 1, this difference can be significantly larger. The site-to-site variation in T_s (Table 1) is most likely due to differences in the exposure of the ground to incident solar radiation since differences in albedo caused by variations in ground cover over the area are probably insignificant.

For most of the stations the lithology corresponding to the temperature measurement interval comprised undifferentiated Quaternary gravel, soil, and alluvium. The values of μ obtained from the data reduction (Table 1) are therefore highly variable, as might be expected; however, for station 1 and possibly station 7 measurements were obtained in dolomite. These are in excellent agreement with measured values reported in the literature (Kappelmeyer and Haenel, 1974). The values of μ in Table 1 were used to obtain a rough estimate of thermal conductivity K for each station. This was done by plotting average values of thermal conductivity versus average thermal diffusivity for a wide range of lithologies (Figure 4). The data are from the compilation of Kappelmeyer and Haenel (1974). Included also is a theoretical relation (dashed curve) for unconsolidated sediments (Bullard, 1963). A least-squares line fit to the data over the range appropriate for consolidated rocks leads to the relation $K = 1.3 \times 10^{-3} + 0.42\ \mu$ which was used to compute the thermal conductivity given in Table 1. Implicit in this procedure is the assumption that, over the range appropriate to consolidated rocks, variations in the density and heat capacity of rocks are small compared with variations in thermal conductivity. The data in Figure 4 sufficiently support this assumption for the present purposes. This estimate of K in turn allows an estimate of relative heat flow $q = Kg$ for each site, which is also given in Table 1.

Transient temperature disturbances caused by thermal convection within the boreholes (Diment, 1967; Gretener, 1967) cannot be ruled out a priori for the temperature data in Figure 2. This effect does not, however, appear to present a problem to the data set in general. The level of agreement of the data set to conductive theory (Figure 2 and Table 1) and the uniformity of computed parameters (Table 1) do not suggest the presence of serious random temperature perturbations, particularly in view of the sizeable and remarkably systematic trend observed in the heat flow values, which will be seen in the next section.

RESULTS

The results of the heat flow estimates for each station (Table 1) are plotted in Figure 5 as a function of relative position projected on line A-A' (Figure 1). The lower section of Figure 5 shows the suggested position of a subsurface granitic body (Figure 1) approximated by a hemisphere. The approximate depth and lateral extent of the granite as well as its approximate location with respect to the heat flow measurements are based on information from deep boreholes provided by Gulf Mineral Resources Company. The continuity of the body and the existence of the mother layer are somewhat speculative and largely for the purpose of the heat flow interpretation.

The relative heat flow values in Figure 5 exhibit a large and systematic increase as the ridge province (Figure 1) is approached from the south-southwest. The maximum observed increase in relative heat flow of 3 HFU (1 HFU = 10^{-6} cal cm^{-2} sec = 41.8 mW/m^2) appears to be centered around station 5. Since the magnitude of the observed increase is too large to be accounted for by heat conduction effects of

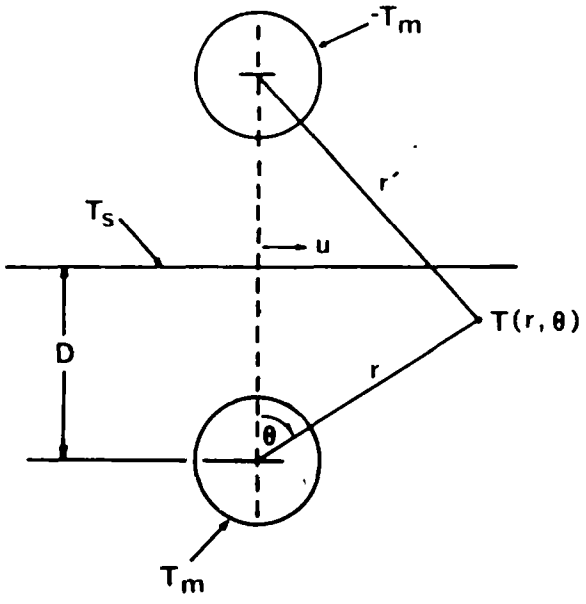

FIG. 6. Geometry for applying the method of images to a buried sphere.

surface topography, nor does it relate to individual station elevation or slope orientation, a subsurface cause must be responsible.

Hardee and Larson (1980) arrived at a relation for the steady state surface heat flow as a function of horizontal position u for a sphere of radius a at constant temperature T_m, buried at depth D in a medium initially at zero temperature, with a horizontal surface held at constant temperature T_s (see Figure 6). Their result was that

$$\frac{q}{q^+} = \left[1 + \left(\frac{u}{D}\right)^2\right]^{-2}, \tag{2}$$

where

$$q^+ = -\frac{2aK(T_m - T_s)}{D^2}, \tag{3}$$

is the maximum heat flow (at $r = D$, $\theta = 0$). The solid curve in Figure 5 is the result of applying equations (2) and (3) to the heat flow data. Equation (2) was used to estimate from the data the depth D to the center of a spherical source capable of creating the observed anomaly ($D = 1140$ m). The heat flow values at stations 3 and 9 suggest a background heat flow $q_b(u \to \infty)$ of about 1 HFU so that a value of $q^+ \cong 3$ HFU is then required to fit the observations near the crest of the anomaly. From equation (3), for example, a temperature excess of 50°C (for $K = 7$ mcal °C^{-1} cm^{-1} sec^{-1}), its position and depth coinciding with the surface of the granitic body illustrated in Figure 5, would produce the theoretical heat flow profile (solid curve) in Figure 5, which is in excellent agreement with the measurements. This result suggests a possible association between the granite body and the observed relative heat flow. Furthermore, it is clear from the magnitude of the required temperature excess that heat conduction effects resulting from possible contrasts in thermal properties and radioactive heat production (between the granite and surrounding rock) alone are incapable of accounting for the observed anomaly.

In order to test the possibility that the suggested temperature excess is the result of transient cooling of the body from an originally molten state, we have applied the method of images to a sphere cooling from some initial temperature T_m. From the solution for an infinite region,

$$T(r, t) = \frac{T_m}{2}\left(\operatorname{erf}\frac{r+a}{2\sqrt{\mu t}} - \operatorname{erf}\frac{r-a}{2\sqrt{\mu t}} - \frac{2\sqrt{\mu t}}{r\sqrt{\pi}} \cdot \{\exp[-(r-a)^2/4\mu t] - \exp[-(r+a)^2/4\mu t]\}\right) \tag{4}$$

(Carslaw and Jaeger, 1959), the solution for a semi-infinite medium (Figure 6) becomes

$$T(r, t) = \frac{T_m}{2}\left\{\operatorname{erf}\frac{r+a}{2\sqrt{\mu t}} - \operatorname{erf}\frac{r-a}{2\sqrt{\mu t}} - \frac{2\sqrt{\mu t}}{r\sqrt{\pi}} \cdot \{\exp[-(r-a)^2/4\mu t] - \exp -(r+a)^2/4\mu t\}\right\} - \frac{T_m}{2}\left\{\operatorname{erf}\frac{r'+a}{2\sqrt{\mu t}} - \operatorname{erf}\frac{r'-a}{2\sqrt{\mu t}} - \frac{2\sqrt{\mu t}}{r'\sqrt{\pi}} \cdot \{\exp[-(r'-a)^2/4\mu t] - \exp[-(r'+a)^2/4\mu t]\}\right\}, \tag{5}$$

where

$$r' = [r^2 + 4D^2 - 4rD\cos\theta]^{1/2}.$$

The solution for heat flow q is

$$q = -K\left.\frac{dT}{dr}\right|_{\theta=0} = -KT_m \exp\left(-\frac{(D+a)^2}{4\mu t}\right)\left[\frac{1}{\sqrt{\pi\mu t}} - \frac{a+D}{D\sqrt{\pi\mu t}} - \frac{2\sqrt{\mu t}}{D^2\sqrt{\pi}}\right] + T_m \exp\left(-\frac{(D-a)^2}{4\mu t}\right)\left[\frac{-1}{\sqrt{\pi\mu t}} - \frac{a+D}{D\sqrt{\pi\mu t}} + \frac{2\sqrt{\mu t}}{D^2\sqrt{\pi}}\right]. \tag{6}$$

In Figure 7 we have plotted heat flow versus time from equation (6) for a cooling sphere with $T_m = 1000$°C, $K = 7$ mcal °C^{-1} cm^{-1} sec^{-1}, $\mu = 0.01$ cm^2 sec^{-1}, and the approximate observed dimensions (inset) which correspond to Figure 5. First seen (Figure 7) is a buildup of heat flow as heat from the buried sphere reaches the surface and then a decrease as that heat is eventually lost. The important result, however, is that all this occurs within 100,000 years. Thus, if the granite body, approximated by a sphere, is of Tertiary age, no residual heat flow would be expected to remain at present time. Our theoretical treatment of the cooling granite body neglects possible cooling by convective heat transfer. However, incorporating convection in our model would decrease the estimated cooling time and, therefore, would not alter our conclusion.

It is also possible to speculate on the existence of a somewhat deeper mother layer (Figure 5) of considerable lateral extent as a source of residual transient heat flow. The heat flow solution for a cooling, buried half-space (used to represent a cooling granitic batholith in Goguel, 1976), given by

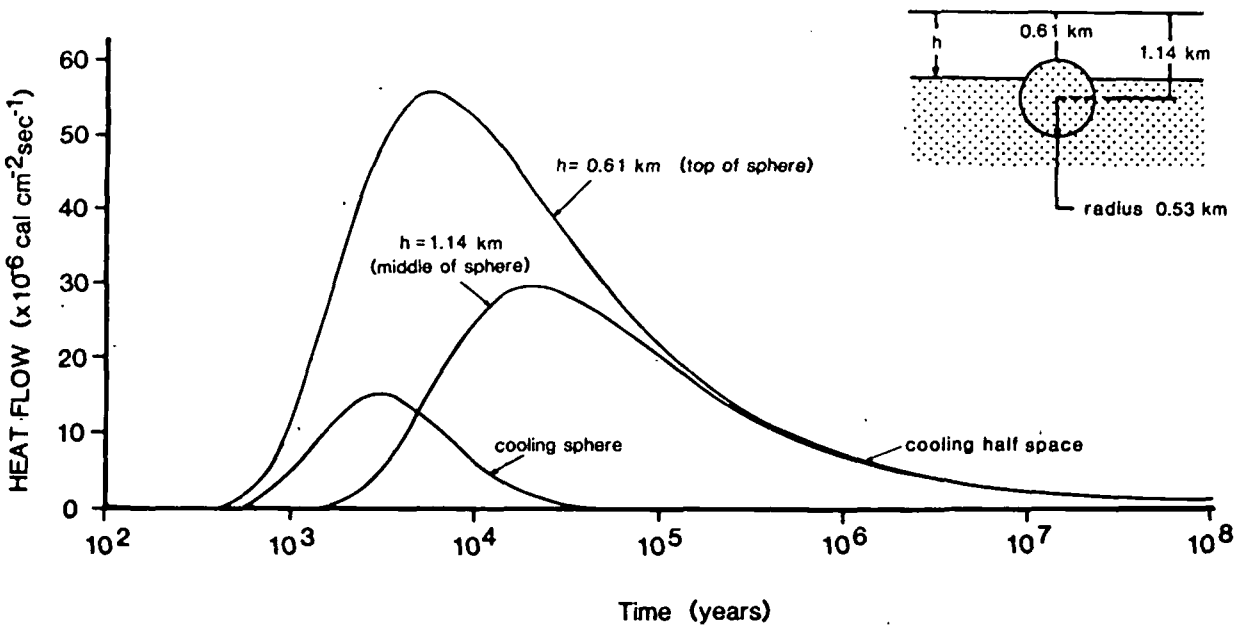

FIG. 7. Theoretical cooling of a buried half-space (at depth h) and cooling sphere. Dimensions and geometry are inset.

$$q = \frac{-2KT_m}{2\sqrt{\pi\mu t}} \exp(-h^2/4\mu t), \quad (7)$$

was used to explore this possibility. These results are also plotted in Figure 7 for the same parameters as the cooling sphere but for depths $h = 610$ m (corresponding to the top of the sphere) and $h = D = 1140$ m. In both cases (Figure 7) significant residual heat flow remains after 10^7 years. Thus a mother layer cooling from mid-Tertiary time is capable of supplying enough heat to account for the observed q^+ of 3 HFU. Still, transient cooling of a smaller wavelength granite body as a mechanism is insufficient to account for the shape of the observed heat flow anomaly even if heat is supplied by the mother layer. The effect of the thermal conductivity contrast between granite and limestone or dolomite is far too small (Lovering, 1935) to offset the rapid cooling time of a sphere or hemisphere of an appropriate size (Figures 5 and 7).

Based on these results, it must be concluded that the heat flow anomaly observed in the study area is not the direct result of transient cooling of a granite body, but must be indicative of an active (or recently active) process such as hydrothermal circulation. The heat flow estimated for stations 3 and 9, 1.08 and 1.21 HFU, is less than most published values from the surrounding area, ~2.0 HFU (Reiter et al, 1975; Edwards et al, 1978; Shearer and Reiter, 1981). Although the absolute accuracy of the shallow heat flow determinations in Table 1 is not well established, the range of values does not significantly depart from that observed via deep borehole observations in areas of extensive volcanic activity in northeastern New Mexico and southeastern Colorado (Edwards et al, 1978). The low background heat flow ($q_b = 1$ HFU) suggested earlier could imply low reduced heat flow as well as a low contribution from crustal radioactive heat production. Leaching of radioactive elements by moving groundwater has been suggested to explain locally nonrepresentative crustal radioactivity in Arizona (Shearer and Reiter, 1981). In that same study, forced and free convection by moving groundwater was called upon to explain some of the variability of heat flow measurements taken shallower than 650 m. The heat flow pattern shown in Figure 5 also might be the result of a local redistribution of heat by hydrothermal convection occurring at depth. In this case the low values at stations 3 and 9 could be indicative of removal of heat as in the case of a downgoing limb of a convection cell. Higher concentrations of heat-producing elements in the granite body, while incapable of producing 3 HFU to cause the observed anomaly, may contribute to the convective instability. Such a mechanism might focus the convection and explain the location of the heat flow high over the granite body.

CONCLUSIONS

There appears to be spatial coincidence between a present-day heat flow anomaly, a Tertiary granitic body, and hydrothermal mineralization within a localized area in southern New Mexico. Based on the heat flow values obtained, hydrothermal circulation is believed to be the most likely explanation for the heat flow anomaly. Higher radioactive heat production in the granite body may explain the spatial coincidence between the anomaly and the body. The situation appears analogous to the regional association between zones of high heat flow, metalliferous mineralization, and intrusive bodies in England and Wales (Brown et al, 1980). There it was postulated that Caledonian age intrusive bodies focused the development of hydrothermal systems responsible for post-Carboniferous mineralization, and that these systems have persisted through time to create the present-day high heat flow.

Our results suggest the possibility of such occurrences on a local scale and the potential of shallow thermal measurements as an aid in locating and understanding them.

ACKNOWLEDGMENTS

The authors wish to thank Tom Heidrick, Jerzy Maciolek, Ian Lerche and two anonymous reviewers for helpful comments which led to improvements in the original manuscript. We also thank Gulf Oil Corporation for permission to publish the heat flow data and Tom Heidrick for encouraging us to make the measurements.

REFERENCES

Brown, G. C., Cassidy, J., Oxburgh, E. R., Plant, J., Sabine, P. A., and Watson, J. V., 1980, Basement heat flow and metalliferous mineralization in England and Wales: Nature, v. 288, p. 657–659.

Bullard, E. C., 1963, The flow of heat through the floor of the ocean, *in* The Sea: M. Hill, Ed., v. 3, p. 218–232.

Callaghan, E., 1953, Volcanic rocks of southwestern New Mexico: N. Mex. Geol. Soc., 4th Field Conference.

Carslaw, H. S., and Jaeger, J. C., 1959, Conduction of heat in solids: Oxford University Press, Oxford.

Diment, W. H., 1967, Thermal regime of a large diameter borehole: Instability of the water column and comparison of air- and water-filled conditions: Geophysics, v. 32, p. 720–726.

Edwards, C. L., Reiter, M., Shearer, C., and Young, W., 1978, Terrestrial heat flow and crustal radioactivity in northeastern New Mexico and southeastern Colorado: GSA Bull., v. 89, p. 1341–1350.

Goguel, J., 1976, Geothermics: New York, McGraw-Hill Book Co.

Gretener, P. E., 1967, On the thermal instability of large diameter wells—An observational report: Geophysics, v. 32, p. 727–738.

Hardee, H. C., and Larson, D. W., 1980, Thermal techniques for characterizing magma body geometrics: Geothermics, v. 9, p. 237–249.

Kappelmeyer, O., and Haenel, R., 1974, Geothermics with special reference to application: Geoexploration Monographs, series 1, no. 4, Gebrüder Borntraeger, Berlin.

Lasky, S. G., and Wooton, T. P., 1933, The metal resources of New Mexico and their economic features: N. Mex. School of Mines, State Bur. Mines and Mineral Res. Bull. 7.

Lee, T-C., 1977, On shallow-hole temperature measurements—A test study in the Salton Sea geothermal field: Geophysics, v. 42, p. 572–583.

Lindgren, W., Graton, L. C., and Gordon, C. H., 1910, The ore deposits of New Mexico: U.S.G.S. Prof. Paper 68.

Lovering, T. S., 1935, Theory of heat conduction applied to geological problems: GSA Bull., v. 46, p. 69–94.

Northrop, S. A., 1959, Minerals of New Mexico: Albuquerque, Univ. of N. Mex. Press, revised edition.

Reiter, M., Edwards, C. L., Hartman, H., and Weidman, C., 1975, Terrestrial heat flow along the Rio Grande rift, New Mexico and southern Colorado: GSA Bull., v. 86, p. 811–818.

Shearer, C., and Reiter, M., 1981, Terrestrial heat flow in Arizona: J. Geophys. Res., v. 86, p. 6249–6260.

Steinhart, J. S., and Hart, S. R., 1968, Calibration curves for thermistors: Deep-Sea Res., v. 15, p. 497–503.

Talmage, S. B., and Wooton, T. P., 1937, The non-metallic mineral resources of New Mexico and their economic features; N. Mex. School of Mines, State Bur. Mines and Mineral Res. Bull. 12.

GEOPHYSICS, VOL. 48, NO. 7 (JULY 1983); P. 975–996, 14 FIGS., 5 TABLES.

Geothermal prospecting with Shallo-Temp surveys

L. A. LeSchack* and J. E. Lewis‡

ABSTRACT

The Shallo-Temp® survey is an inexpensive and rapid "first look" geophysical technique that is useful in planning the more traditional and costly reconnaissance drilling geothermal exploration programs. The technique is based on making many soil temperature measurements at 2-m depths over a given exploration area and correcting these measurements for the effects of elevation and surface geologic and meteorologic conditions. Corrections for surface conditions are made with an "annual wave correction model." The output from the model is the normally expected 2-m temperature for the given site at the date for which input data were provided. The difference between the measured and computed 2-m temperature data represents effects of geothermal heat flow. A Shallo-Temp residual map is compared both to a 2-m temperature map for a specific date (September, 1977) and to a mean annual 2-m temperature map for the Coso known geothermal resource area producing the same anomaly pattern in each case. Additional case history studies at Upsal Hogback in Nevada, and Animus Valley in New Mexico provide evidence to support the applicability of the Shallo-Temp technique throughout the Basin and Range Province. The technique developed is not designed to replace reconnaissance drilling but rather help focus standard reconnaissance programs. The two potentially most reliable applications of the technique are in extending trends where standard reconnaissance holes have been drilled or filling in detail between widely spaced holes, and in surveying for near-surface anomalies that might be developed for direct heating applications.

®Registered trademark of LeSchack Associates, Ltd.

INTRODUCTION

Background

Shallow temperature measurements (2–5 m) have been made by a number of investigators in the geologic sciences for the past several decades, but the potential of shallow reconnaissance surveys for geophysical exploration has not been extensively developed. This paper presents three case histories where the shallow temperature survey method was used in eastern California, Nevada, and New Mexico, and the results can be compared with existing relatively deep reconnaissance temperature gradient and heat flow measurements.

An early example of shallow temperature surveying at a geothermal area was presented by Kintzinger (1956) in his survey of hot ground near Lordsburg in New Mexico. Using thermistors emplaced at a depth of 1 m, he observed a temperature anomaly of some 10°C surrounding a hydrothermal area. Cartwright (1968) showed that thermistors emplaced at a depth of 50 cm could closely approximate theoretical temperature anomalies at the surface owing to shallow lying aquifers. Birman (1969), emplacing thermistors at a depth of 3 m, measured temperature variations caused by groundwater flow in southern California and began actively using shallow temperature geothermal surveying as one of a combination of geophysical and geologic techniques for locating groundwater on a commercial basis. O'Brien (1970) also conducted studies of a groundwater flow using shallow temperature survey techniques.

A detailed study of the application of this technique to locating salt domes and shallow faults in the Netherlands was provided by Poley and Van Steveninck (1970). Their technique was used most satisfactorily in southern California by Sabins (1976). Noble and Ojiambo (1975), emplacing thermistors at 1-m depth, helped delineate a geothermal area in Kenya. Lee (1977a), using data obtained at depths greater than we consider shallow (up to 15 m), showed the potential of extrapolating near-surface temperature gradients to much greater depths in known geothermal areas. Lee and Cohen (1979) measured, at 2-m depth, geothermal gradients at various sites at the Salton Sea, California, where thermal gradients ranged from 0.02°C/m to 4.3°C/m. Lachenbruch et al (1976) provided a temperature map of the Long Valley area at a depth of 10 m. They concluded that as long as synoptic observations are used at these sites, essentially the same temperature pattern emerges for contours at the 6-m depth, and much of it persists at 3 m. This observation provided strong motivation for us to commence our shallow temperature studies at Long Valley, Coso known geothermal resource area (KGRA), California, and discussed in LeSchack et al (1977).

Despite the previous research cited, little attempt has been made to use the shallow temperature survey technique as an operational geophysical exploration tool, especially for geothermal reconnaissance surveys. This, we suspect, is because adequate case histories of known geothermal areas where this technique has been used have not been presented in the literature,

Manuscript received by the Editor March 5, 1982; revised manuscript received October 8, 1982.
*LeSchack Associates, Ltd., P.O. Box 646, Long Key, Florida 33001.
‡McGill University, Department of Geography, 805 Sherbooke Street West, Montreal, PQ, Canada H3A 2K6.

and potential perturbing effects on the shallow temperature data, real or imagined, have not been subjected to adequate scrutiny.

The advantages and disadvantages of shallow temperature surveys

The obvious advantage of a shallow temperature survey is that it is rapid and inexpensive. Whelan (1977) determined that an overall average cost in 1975 for drilling relatively deep thermal gradient or heat flow holes was approximately $60/m. We estimate an approximate cost of $50 per hole for such drilling when 100 or more 2-m holes are to be emplaced at a given survey site.

The economic advantages of shallow temperature surveying are clear. The overall disadvantages are clear also, and have long been known. The major purpose of our study has been to compensate for various perturbing effects (discussed below) which impinge on temperature measurements at 2-m depths to permit cost-effective use of shallow temperature reconnaissance surveys for geothermal exploration.

Lovering and Goode (1963), Poley and Van Steveninck (1970), and Kappelmeyer and Haenel (1974) very adequately covered the perturbing effects which are of concern to us, and which have in fact encouraged deep reconnaissance drilling almost to the exclusion of shallow measurements. These effects are due to (1) diurnal solar heating variation, (2) annual solar heating variations, (3) aperiodic solar heating variations, (4) variations in surface albedo, which affects amount of energy absorbed, (5) variations in surface roughness, which affect amount of heat convected away due to turbulent flow of the wind, (6) variations of soil thermal diffusivity, (7) slope and exposure of the terrain, (8) variations in elevation, and (9) variations in level of groundwater and groundwater movement.

Temperature variations from these effects are generally negligible below a depth of 20–30 m, with the exception of groundwater movement. Hence, the great majority of reconnaissance surveying has been conducted below this level to avoid these effects; and to obtain a relatively long vertical section along which temperature gradients can be measured. In the interests of developing a rapid, cost-effective thermal reconnaissance surveying technique, however, we have developed along the lines shown by Birman (1969) and Poley and Van Steveninck (1970) a methodology for evaluating the perturbing effects (with the exception of groundwater movement) and correcting for them at a depth of 2 m. These perturbing effects are, in fact, what physically produces the annual temperature wave at 2 m. If the annual temperature wave can be simulated from a simple set of observations, then these perturbing effects (which are considered noise) can be subtracted thus obtaining the geothermal signal. As a result, we believe that at least for certain areas, the many perturbing effects often held up as disadvantages to shallow temperature surveying can be eliminated or shown to have little effect, leaving for the shallow temperature surveying technique the advantages of speed and low cost.

FIELD PROCEDURES

Three case histories studied

In the past few years data from relatively deep reconnaissance heat flow holes and complementary geologic and geophysical data have become available for the Coso Geothermal areas of eastern California, the Upsal Hogback area of Nevada, and the Animus Valley of New Mexico. As a result, it was possible to examine the efficacy of shallow temperature measurement as a reconnaissance mapping tool at these three areas. Direct comparisons with deeper temperature and heat flow measurements were made and are discussed.

Our basic field procedure involves augering a 2-m deep hole for each measurement location, inserting a thermistor probe, backfilling the hole, waiting until the thermistor equilibrates, and finally making a measurement of the temperature at that site. Generally, drilling was accomplished using a two-operator General Hole Digger (Model 21) powered by a 3-hp Tecumseh 2-cycle gasoline engine with a 5-cm (2-in) auger (LeSchack et al, 1977).

The thermistor probes were constructed by taping a Yellow Springs Instrument Company (YSI) no. 401 thermistor to the end of a 2.1-m long, 1.3-cm (0.5 inch) diameter PVC pipe. Both single and multielement thermistor probes were used at the Coso site. The thermistors are guaranteed by the manufacturer to be interchangeable to a tolerance of ±0.1°C within the temperature range of 0°–80°C, the range in which we worked. They were read, after equilibrium was reached, with a YSI model 46 TUC Tele-thermometer, a Wheatstone bridge that has an accuracy of ±0.15°C.

DATA COLLECTION

The data discussed here were collected at Coso by the authors, at Upsal Hogback in Nevada by the U.S. Geological Survey, and at Animus Valley in New Mexico (the site of Kintzinger's work in 1956) by the authors for New Mexico State University. The Coso case history study is more detailed than at the other sites and, therefore, we have chosen to discuss this first to illustrate the various elements of the Shallo-Temp® technique.

During the 1977 summer, 102 1-element probes were emplaced at Coso as shown in Figure 1. The criteria for emplacement were easy accessibility, i.e., along roads or trails, and knowledge that a geothermal anomaly, already identified with deep reconnaissance drilling (Combs, 1975; Combs, 1976), would be covered.

Albedo, surface roughness, and soil samples from a depth of 30–40 cm were collected at each of 24 selected sites. Four 6-element probes, emplaced at representative locations around the anomaly, were read approximately every six hours between noon of September 24 to noon of September 25, 1977.

EXAMINING THE DATA

As expected from Birman (1969), Poley and Van Steveninck (1970), and Sabins (1976), emplacement of probes at 2-m depth avoided completely the effect of diurnal variations of solar input. Figure 2 shows the soil temperature variations over one diurnal cycle for four representative sites at Coso. It can be seen, therefore, that at these sites diurnal variation is negligible below a depth of 1 m.

At a depth of 2 m, however, our probes are well within the range of the annual temperature cycle which can usually be observed to a depth of some 20 m. Corrections must be made for the effects of this annual wave. The effect of aperiodic solar variations of any period have been deemed negligible as far as our data are concerned because they can be assumed to cause temperature changes during a typical survey less than those caused by the annual variation.

Elevation and topographic corrections to 2-m temperature data

It would be expected that the temperature at 2-m depth would be affected by the mean annual temperature at the surface. Assuming an adiabatic lapse rate of −1.0°C/100 m of elevation, it is clear that a noticeable mean annual surface temperature differ-

®Registered trademark of LeSchack Associates, Ltd.

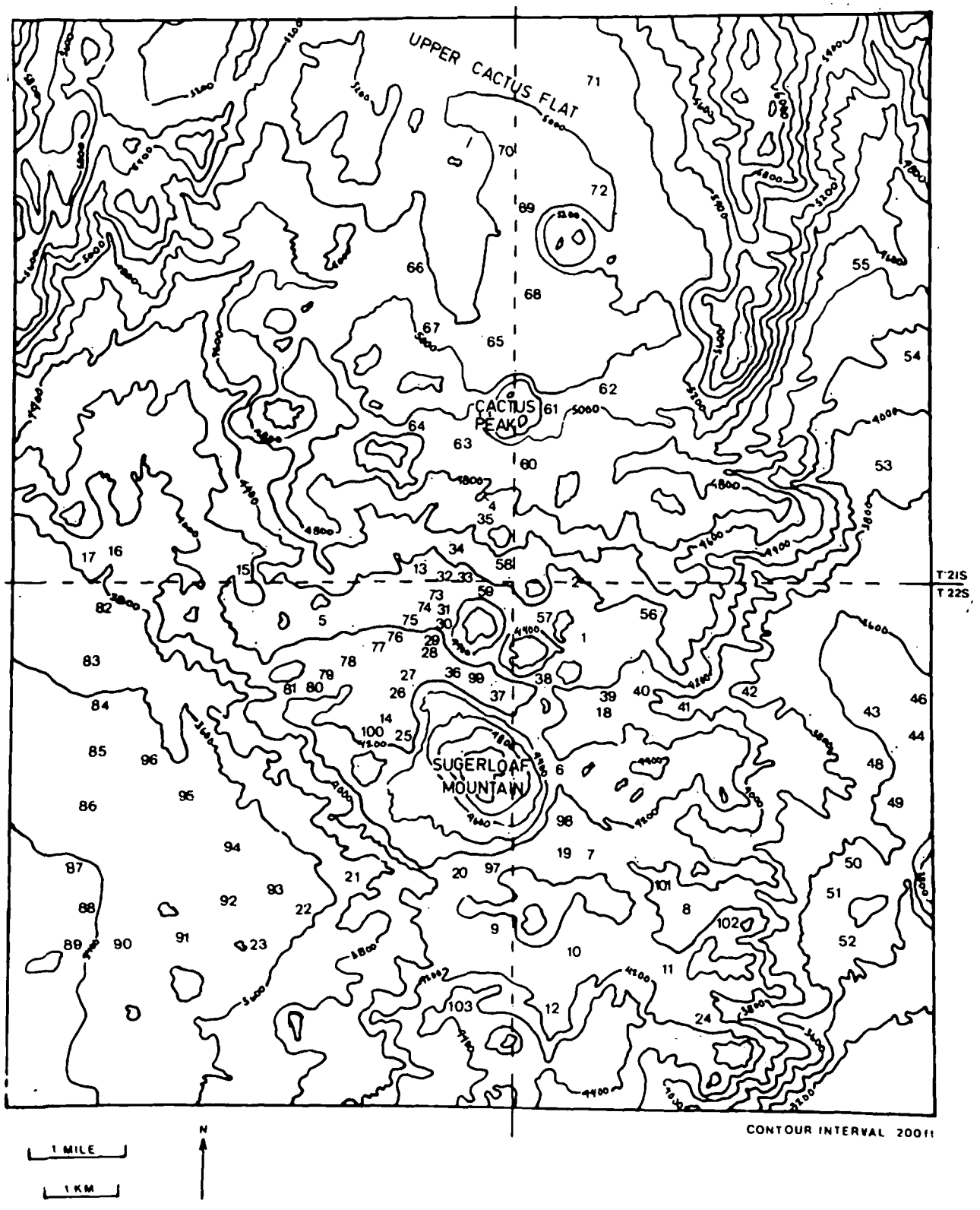

FIG. 1. Locations of 2-m temperature stations at Coso. The first 24 were emplaced in July 1977, the rest in September 1977. (Haiwee Reservoir and Little Lake quadrangles).

ence would be experienced between the highest and lowest sites at the Coso area. We tested this by computing the correlation coefficient for the 2-m temperature-elevation sets at Coso. We chose two relatively flat areas, one to the west of the anomaly and the other to the north, where there was a large difference in mean elevation but relatively little temperature or elevation variation within each of the areas. The correlation coefficient among all these data is −0.87, indicating a significant negative correlation between temperature and elevation. This negative correlation would be expected if the temperatures were affected by temperature change due to elevation.

The mean elevation difference between the northern data set and the western data set is 434 m (1424 ft). With an adiabatic lapse rate of −1.0°C/100 m elevation change, the calculated mean temperature difference should be 4.34°C. The measured mean temperature difference is 3.81°C. The 2-m temperatures have been corrected to an arbitrarily picked datum of 1036.3 m (3400 ft), using the adiabatic lapse rate of −1.0°C/100 m.

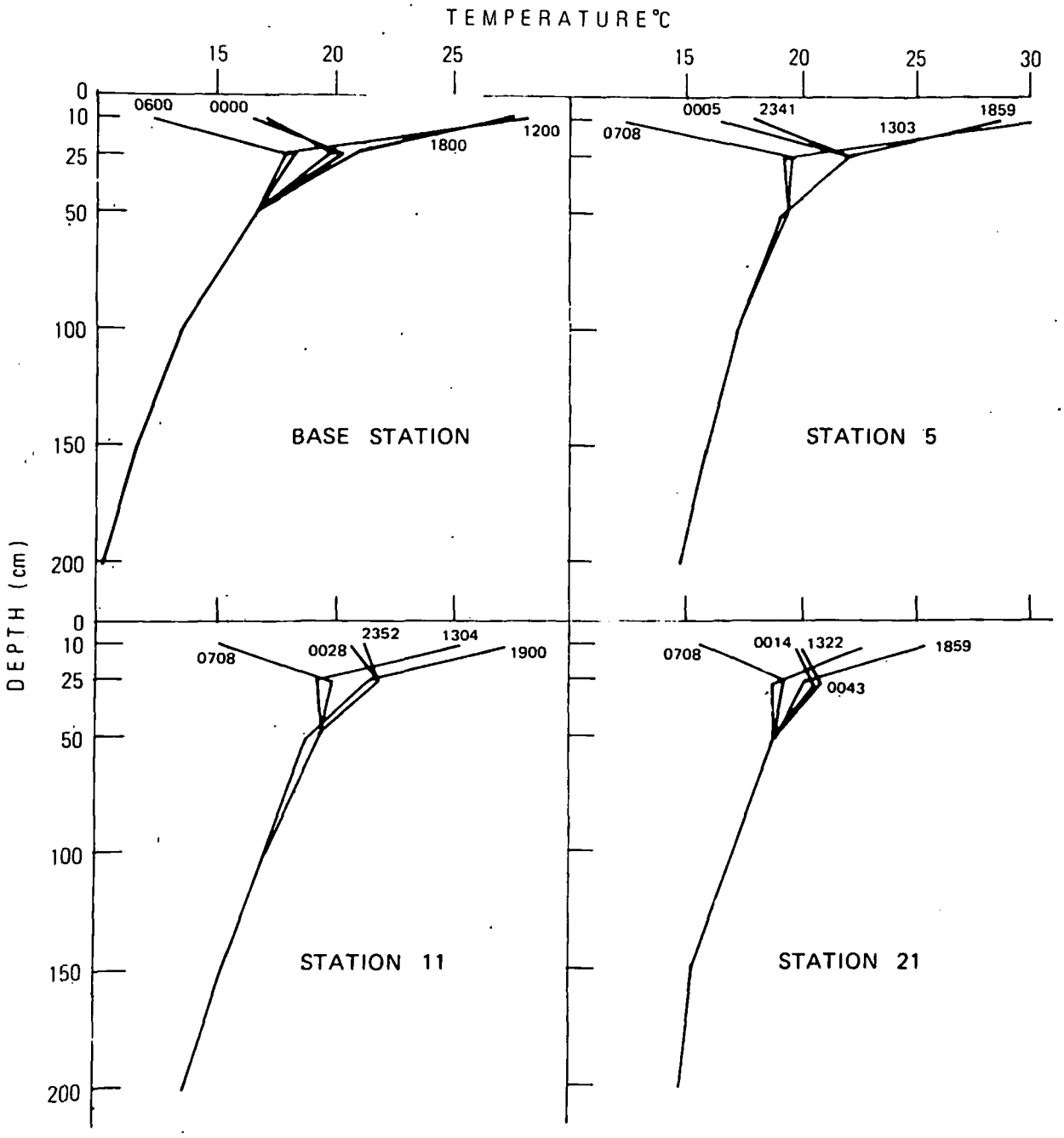

FIG. 2. Typical diurnal soil temperature variations at Coso, September 24–25, 1977. Mean times indicated on profiles.

At Coso we took care to see that topographic disturbances were kept to a minimum. We made every attempt to gather our data where the slope of the terrain was close to zero and therefore the exposure of this surface to the sun would vary little from place to place.

With one exception we kept our sites far enough away from large topographic features, i.e., hills, gorges, etc., so that topographic effects as estimated according to the techniques described by Lachenbruch (1968) would be minimal. In the one exception, site 16 at Coso was deliberately chosen close to a sharp drop-off. Site 17, its neighbor 15 m away, was sufficiently removed to be unaffected. The measured temperature difference between the sites, 0.5°C, was consistent with the value estimated according to Lachenbruch's technique. Therefore, the corrections caused by topographic effects are negligible at this case history site. We have substantiated this theoretically at Coso using the Lee FINITEG model (Lee, 1977b) in a separate analysis (LeSchack, et al, 1980).

Seasonal variations of the 2-m temperatures at Coso

Figure 3 is a contour map[1] of the 2-m temperature values recorded at Coso in September 1977, corrected for elevation. An area of higher temperature coincided well with the electrical resistivity and aeromagnetic anomalies independently obtained by Fox (1978a, b). Two-meter temperatures were also measured at three additional times, February in 1978, May in 1978, and

[1]All of the contour maps were generated by SYMAP computer program and the contours redrawn from the computer output. The contour intervals were objectively determined by the SYMAP program.

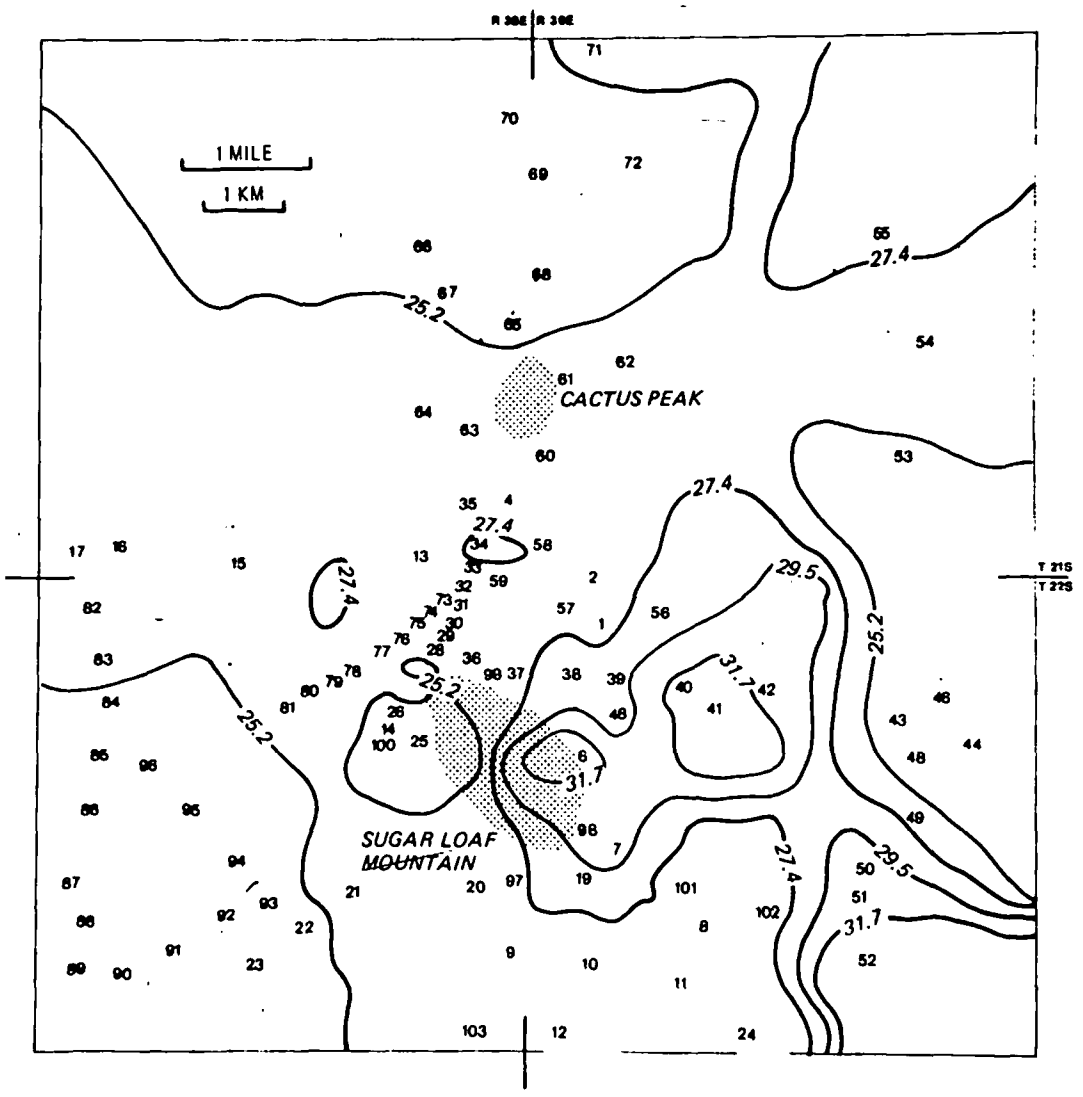

FIG. 3. 2-m temperature contour map for Coso, September 1977, corrected for elevation. Temperature in °C.

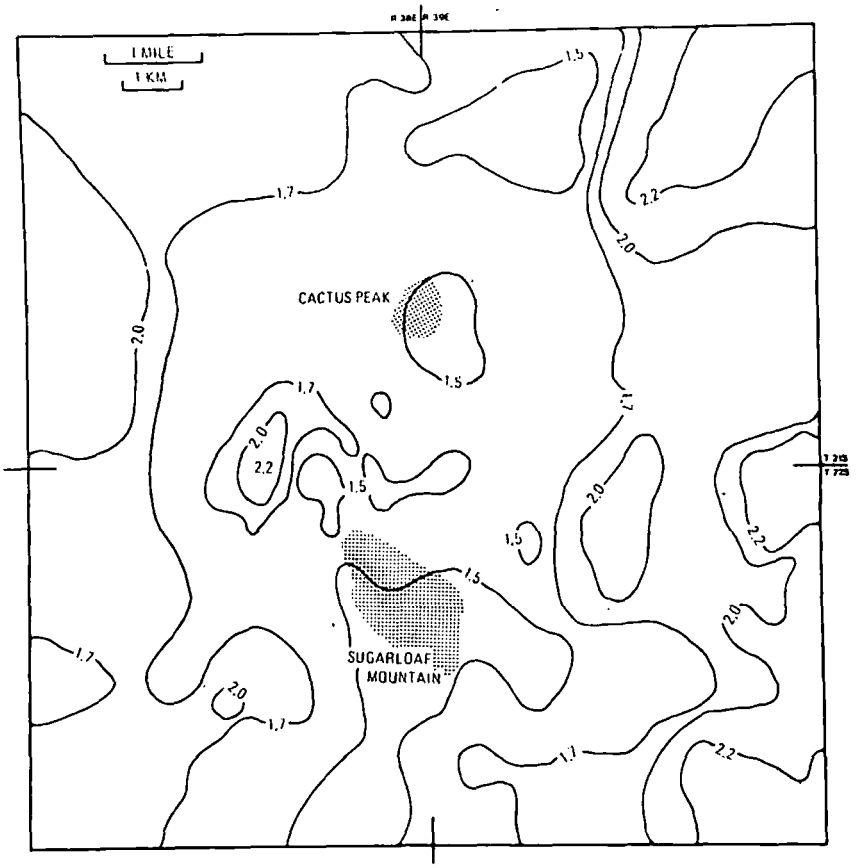

FIG. 4. Thermal diffusivity ($cm^2/sec \times 10^{-3}$) contour map for Coso, integrated from the surface to 2m.

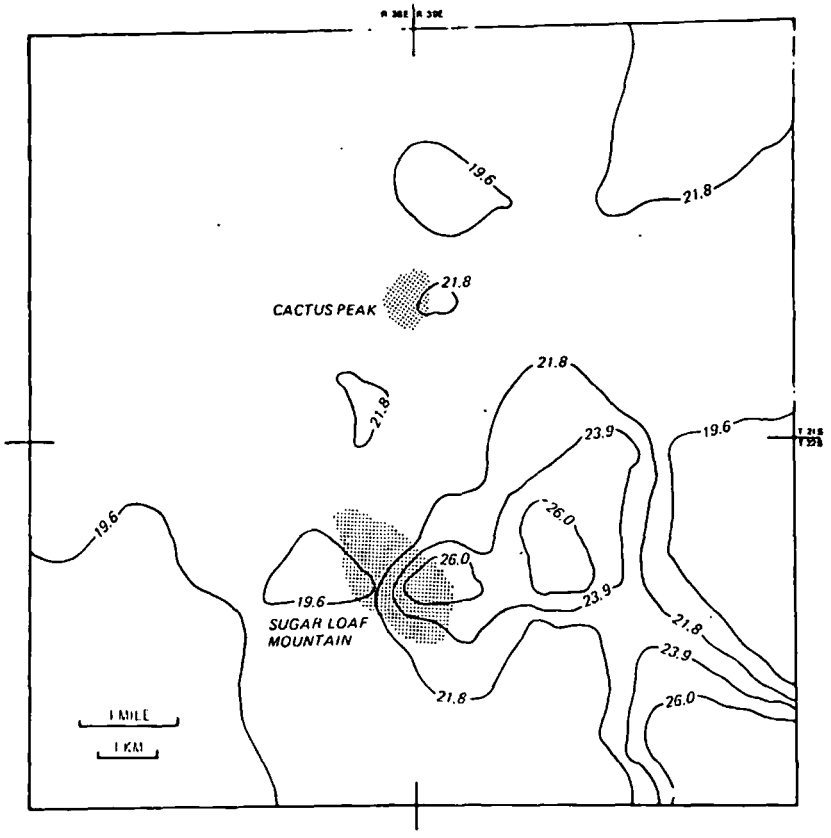

FIG. 5. Mean annual temperature contour map for Coso, corrected for elevation. Temperature in °C.

August in 1978, permitting a 1-year temperature cycle to be observed (LeSchack et al, 1979).

Examination of the four temperature contour maps shows only minor temperature pattern differences. Overall temperatures vary with the season, but the character of the pattern remains much the same. A decision to proceed with further exploration could undoubtedly have been made based on any one of the contour maps independently.

It is important to investigate the cause of these temperature pattern differences over time. The differences do not significantly alter the shape of the temperature pattern at Coso because of the high signal-to-noise (S/N) ratio at this prospect. However, this would not be the case with a weaker anomaly elsewhere. From sensitivity tests conducted with our annual temperature model (to be discussed later), it is clear that variations in soil thermal diffusivity play the most significant role in affecting temperature variation at 2-m depth. We have computed a value of thermal diffusivity at each of the 102 sites at Coso using the phase lag method.[2]

From data collected in September in 1977, and February, May, and August in 1978, we plotted an annual temperature curve at 2-m depth. We assumed at 2 m the curve would be sinusoidal [following the procedures outlined in Van Wijk (1966)] and therefore fitted a sine curve to the data points. The annual minimum at the surface was assumed to be December 21. From the curves constructed for each site, the time lag in weeks between the minimum at the surface and the minimum at 2 m was computed. A value of thermal diffusivity integrated between the surface and 2 m, and integrated over time, was calculated using the following relationship:

$$K_x = \frac{x^2 P}{4\pi(t_x - t_0)}, \qquad (1)$$

where x is the thickness of layer (cm), K_x is the thermal diffusivity of layer (cm^2/sec), P is the period of the annual temperature wave (sec), and $t_x - t_0$ is the time lag between temperature waves at the ground surface and at the base of layer (sec).

Lag times $t_x - t_0$ are due to the thermal diffusivity and varied from 10–15 weeks. The values of thermal diffusivity K_x for each site were then computed. From those values a contour map of thermal diffusivity was prepared (Figure 4). From each annual curve we also computed the annual mean temperature at 2-m depth. These values corrected for elevation are contoured in Figure 5.

The mean annual temperature map is the ideal map to be obtained from 2-m temperature data. It is not practical for exploration purposes, since a year's data must be collected; however, it is useful in the present study. When the mean temperature map is compared with the thermal diffusivity map, little correspondence can be seen because thermal diffusivity variations are purely a function of the near surface (0–2 m) soil conditions. On the other hand, the thermal diffusivity values produce broad, smooth contours which strengthen our assumption that thermal diffusivity values have physical significance.

Although the range of thermal diffusivities at Coso is relatively small, they do affect temperature variations at a depth of 2 m. It is instructive to examine these time variations in temperatures from place to place, especially between September and February when the greatest differences occur. The intra-annual range of temperature differences is from 5.4°C to 12.7°C. This range provides a measure of temperature differences that are likely to occur in other locations with similar soil and surface meteorological conditions.

[2]This method for estimating thermal diffusivity is not the procedure used when conducting an operational Shallo-Temp® survey. The operational method is discussed in a later section of the paper.

THE ANNUAL WAVE CORRECTION MODEL

Introduction

As can be seen from the above, the use of 2-m temperatures for geothermal exploration at a specified date is predicated on removal of the annual temperature wave which masks the geothermal signal. This annual effect must be mathematically specified and filtered from observed data before assessing the geothermal potential of a target region.

The partitioning of energy flux (radiant, sensible, evaporative, and soil) at the earth's interface is a function of meteorological and surface conditions. Meteorological parameters such as solar radiation and wind velocity, and surface conditions such as albedo and surface roughness, will determine the amount of energy propagated into the soil. Once the energy is conducted into the soil matrix, the physical properties of the soil will determine the magnitude and speed of propagation of the soil heat flux. Therefore, the soil's thermal diffusivity and conductivity properties, which are conditioned by mineral, water, and air content, influence the amplitude and phase of the annual temperature wave at 2 m.

We developed an annual wave correction model (AWCM) to account for the annual soil temperature wave, based on the work of Goodwin (1972). Given local monthly climatic parameters and surface-soil conditions, the model can reconstruct surface energy exchanges (sensible, latent, and soil heat fluxes) and soil temperatures to a depth of 10 m.

Appendix A describes the theoretical form of the AWCM and presents some of the model's underlying assumptions. The numerical schemes are outlined with emphasis on methods of constructing the soil's temperature profile.

Inputs and output of the AWCM

Input.—The AWCM requires six data parameters and 15 mean monthly values for each of the eight data variables.

The parameters include (fixed values once specified): soil properties, climatological properties, and numerical node constants for the model. Data variables are climatological variables, and surface characteristics.

The soil properties needed as input are thermal conductivity and diffusivity. Thermal diffusivity (cm^2/sec) is obtained by measuring the temperature amplitude decrease with depth or temperature phase change with time, or in conjunction with in-situ soil thermal conductivity measurements with a probe (LeSchack et al, 1979).

The two climatological parameters are the mean temperature (°C) for the 15 monthly average temperature values and a cloud-type correction factor which modifies effective outgoing radiation values, as specified in Sellers (1965). The node spacing for the soil was tested for numerical stability, and a value of 100 cm was found satisfactory. The instrument shelter (standard Stevenson screen) height of 150 cm was used as the atmosphere's upper boundary condition. These latter parameters remain constant for the 15 month test period and for each site location.

The two sets of data variables consist of five climatological and four surface variables. These variables are submitted to a Fourier mathematical smoothing routine which computes a value for each

variable at 91 time steps, producing output data spaced every five days over the 15-month period. The input climatological variables are: mean monthly dew point (°C), mean monthly percent clear skies (percent), mean monthly atmospheric pressure (corrected to mean elevation of 1258 m) (mbar), mean monthly air temperature (°C), and mean monthly wind speed (cm/sec). These variables were obtained between January 1977 and March 1978 from the weather facility at the Naval Weapons Center, China Lake, California, located 25 miles south of Coso. The values are considered uniform over an extensive area, justifying their extrapolation to the Coso region.

The surface characteristics values are: surface aerodynamic roughness (cm), thermal diffusivity, surface reflectivity-albedo (percent), and surface relative humidity (percent). The aerodynamic roughness is calculated from measured geometric properties of the surface following techniques outlined in Lettau (1969). The surface relative humidity is defined as the percent of wet fraction which is determined by the soil moisture content in the upper horizon. The third variable, albedo, is the ratio of reflected solar radiation to the total incoming solar (global)[3] radiation. Albedo and surface roughness were measured at 24 individual field sites. Surface relative humidity was calculated from soil samples taken at these same locations. The soil samples were sealed in double plastic bags and sent to a laboratory for analysis. Once a surface characteristic was determined, it was assumed constant for a given site over the 15-month period for which meteorological data were gathered. Given the arid to semiarid nature of the test location, we feel this assumption is correct. These surface values were handled as follows:

[3]Global radiation is the sum of direct beam and diffuse radiation on a horizontal surface.

Surface roughness.—This was measured at Coso sites 1–24. Photographs were taken at all 102 sites. The 24 measured sites had surface roughness values Z_0 ranging from 0.1 to 16.1 cm. From the photographs, the range of these values appeared to be roughly representative of the remainder of the area. For the purpose of evaluating our correction model and reducing the number of individual computations, we divided surface roughness into four categories A—D: A had a mean value of 3 cm; B a mean value of 8 cm; C a mean value of 12 cm; and D a mean value of 18 cm. From examination of the photographs of the measured sites, i.e., 1–24, we subjectively assigned the remaining sites into appropriate surface roughness categories.

Thermal diffusivity.—Thermal diffusivity was computed at Coso using the phase lag method as described by equation (1). The values ranged from 0.0012 to 0.0025 cm^2/sec. In exploration practice, thermal diffusivity can be obtained rapidly in conjunction with a thermal conductivity

Table 1. Temperature, thermal diffusivity, roughness/diffusivity group, computed normal temperatures, and residuals for Coso KGRA.

Station[a]	Temp. °C[b] (Sept. 1977)	Thermal[c] diffusivity	Thermal diffusivity/ surface-roughness class[d]	Computed temp. (°C)	Residual (°C)
1	27.0	1.62	2B	23.7	3.3
2	25.5	1.51	2B	23.7	1.8
3	26.0	1.31	1B	22.6	3.4
4	27.0	1.62	2A	24.8	2.2
5	27.7	2.27	5B	25.8	1.9
6	33.2	1.22	1B	22.6	10.6
7	30.1	1.51	2B	23.7	6.4
8	26.2	1.62	2B	23.7	2.5
9	27.3	1.51	2C	23.3	4.0
10	25.7	1.75	3A	25.6	0.0
11	26.7	1.75	3B	24.4	2.2
12	25.3	1.62	3D	23.0	2.3
13	25.8	1.75	3B	24.4	1.4
14	23.5	1.62	2A	24.8	−1.3
15	25.6	1.62	2C	23.3	2.3
16	26.3	1.91	3A	25.6	0.7
17	26.7	2.27	5A	27.0	−0.3
18	28.6	1.75	3B	24.4	4.2
19	29.4	1.51	2B	23.7	6.7
20	26.1	1.40	1B	22.6	3.5
21	26.3	1.75	3B	24.4	1.9
22	25.0	1.62	2C	23.3	1.7
23	25.1	1.62	2B	23.7	1.4
24	25.7	1.91	3B	24.4	1.3
25	23.5	1.22	1C	22.2	1.3
26	26.0	1.62	2A	24.8	1.2
27	25.0	1.40	1B	22.6	2.4
28	25.7	1.91	3C	24.1	1.6
29	25.9	1.62	2B	23.7	2.2

[a]No data were taken at station 47.
[b]Temperature values in °C have all been corrected for elevation differences. Corrections based on an adiabatic lapse rate of −1.0°C/100 m. Corrections are keyed to an arbitrarily picked datum of 1036 m elevation.
[c]Thermal diffusivity is expressed in $cm^2/sec \times 10^{-3}$.
[d]Surface roughness (A–D) and thermal diffusivity classes (1–5) were determined according to procedures discussed in the section input variables.

Table 1. (cont.) Temperature, thermal diffusivity, roughness/diffusivity group, computed normal temperatures, and residuals for Coso KGRA.

Station[a]	Temp. °C[b] (Sept. 1977)	Thermal[c] diffusivity	Thermal diffusivity/ surface-roughness class[d]	Computed temp. (°C)	Residual (°C)
30	26.7	1.40	1A	23.6	3.1
31	26.5	1.40	1B	22.6	3.9
32	26.7	1.40	1D	21.9	4.8
33	28.8	1.91	3C	24.1	4.7
34	26.5	1.40	1B	22.6	3.9
35	26.0	1.51	2B	23.7	2.3
36	25.4	1.91	3D	23.7	1.7
37	26.9	1.62	2D	23.0	3.9
38	28.0	1.62	2D	23.0	5.0
39	29.1	1.51	2B	23.7	5.4
40	31.7	1.31	1B	22.6	9.1
41	33.3	1.91	3C	24.1	9.2
42	31.2	2.07	4C	24.7	6.5
43	25.0	1.75	3B	24.4	0.6
44	23.1	1.62	2C	23.3	−0.2
45	23.6	2.07	4B	25.1	−1.6
46	24.7	2.48	5B	25.8	−1.1
48	24.8	1.91	3B	24.4	0.4
49	25.3	2.07	4B	25.1	0.2
50	29.9	1.62	2A	24.8	5.1
51	30.8	1.62	2B	23.7	7.1
52	33.8	2.27	5A	27.0	6.8
53	25.1	1.75	3B	24.4	0.7
54	26.2	1.91	3B	24.4	1.8
55	28.0	2.27	5A	27.0	1.0
56	28.3	1.62	2A	24.8	3.5
57	26.9	1.40	1C	22.2	4.7
58	27.6	1.62	2B	23.7	3.9
59	26.7	1.62	2C	23.3	3.4
60	26.7	1.40	1B	22.6	4.1
61	27.0	1.40	1A	23.6	3.4
62	26.1	1.62	2C	23.3	2.6
63	26.7	1.51	2A	24.8	1.9
64	26.3	1.62	2A	24.8	1.5
65	24.7	1.62	2A	24.8	−0.1
66	25.0	1.75	3A	25.6	−0.6
67	25.2	1.62	2A	24.8	0.4
68	23.8	1.62	2A	24.8	−1.0
69	23.1	1.40	1A	23.6	−0.5
70	24.3	1.75	3B	24.4	−0.1
71	25.7	1.62	2B	23.7	2.0
72	24.9	1.40	1A	23.6	1.3
73	26.9	1.62	2A	24.8	2.1
74	26.6	1.75	3A	25.6	1.0
75	24.9	1.40	1C	22.2	2.7
76	25.6	1.22	1B	22.6	3.0
77	25.7	1.51	2B	23.7	1.9
78	25.6	1.62	2B	23.7	1.9
79	26.6	1.75	3B	24.4	2.2
80	26.6	1.75	3A	25.6	1.0
81	25.4	1.51	2A	24.8	0.6
82	26.8	1.91	3A	25.6	1.2
83	25.7	1.75	3C	24.1	1.6
84	25.2	1.90	3B	24.4	0.8
85	24.7	1.75	3A	25.6	−0.9
86	24.5	1.75	3A	25.6	1.1
87	24.3	1.62	2B	23.7	0.6
88	23.2	1.75	3A	25.6	−2.4
89	23.5	1.75	3B	24.4	−0.9
90	23.7	1.91	3B	24.4	−0.7
91	24.1	1.91	3B	24.4	−0.3
92	24.1	1.91	3B	24.4	−0.3
93	25.1	2.07	4A	26.3	−1.2
94	23.8	1.51	2B	23.7	0.1
95	24.7	1.91	3B	24.4	0.3
96	24.8	1.91	3A	25.6	−0.8
97	27.2	1.31	1B	22.6	4.6
98	30.2	1.22	1A	23.6	6.6
99	25.6	1.51	2D	23.0	2.6
100	25.3	1.62	2D	23.0	2.3
101	26.7	1.40	1A	23.6	3.1
102	26.0	1.51	2B	23.7	2.3
103	26.3	1.40	1B	22.6	3.7

Table 2. Surface roughness/thermal diffusivity combinations and other model input values.

Surface roughness class (cm)	Thermal Diffusivity Class (cm^2/sec)				
	1	2	3	4	5
A	0.0013	0.0016	0.00185	0.0021	0.0024
	3	3	3	3	3
B	0.0013	0.0016	0.00185	0.0021	0.0024
	8	8	8	8	8
C	0.0013	0.0016	0.00185	0.0021	
	12	12	12	12	
D	0.0013	0.0016	0.00185		
	18	18	18		

Other input variables:
(1) mean albedo, 0.33; (2) mean percentage moisture, 0.05; (3) volumetric heat capacity (ρc), 0.4.

probe (LeSchack et al, 1979). As above, to reduce the number of computations, we divided the thermal diffusivity values into five categories as follows:

Category	Mean thermal diffusivity (cm^2/sec)
1	0.0013
2	0.0016
3	0.00185
4	0.0021
5	0.0024

Surface albedo.—During preliminary evaluation of the annual wave correction model, variation of surface albedo from 25–40 percent had little noticeable effect on 2-m temperatures. We used the mean value of 33 percent derived from 24 site measurements, which we felt were representative of the remainder of the Coso area.

The AWCM has an attached solar radiation generator[4], which calculates mean 5-day global radiation values corrected for changing sky cover conditions.

Output.—The model output consists of 5-day interval values for sensible, latent, soil heat flux, and net radiation. At each time step, a soil temperature profile is printed consisting of temperatures at a 1-m node spacing down to a depth of 10 meters.

EVALUATING THE ANNUAL WAVE CORRECTION MODEL

To evaluate the AWCM and obtain a residual geothermal anomaly map, we would be required to make 102 computations of normal temperatures at 2-m depths. However, since the main input variables for each site, i.e., surface roughness and thermal diffusivity, appeared repetitive in various combinations, we divided both variables into four surface roughness categories and five thermal diffusivity categories, as discussed above. Each site was given a surface roughness-thermal diffusivity classification; they are listed along with the September, 1977, temperatures corrected for elevation in Table 1. Table 2 shows the various combinations. Using this technique, we reduced the number of computations from 102 to 17. In view of the uncertainties in the model and the input data, a larger range of classifications with an increase in the number of computations was not considered justifiable.

Using the 17 sets of input variables shown in Table 2, we chose to evaluate the model for data gathered during September 22–24, 1977, because at that time of year the 2-m temperatures are close to their peak annual value. This results in maximum temperature contrast between areas of low and high thermal diffusivity. The computed normal temperatures are shown in matrix form in Table 3.

Table 3. Computed "normal" temperatures for 17 sets of model input data based on surface roughness/thermal diffusivity classes. Temperatures in °C.

Surface roughness class (cm)	Thermal diffusivity class				
	1	2	3	4	5
A	23.6	24.8	25.6	26.3	27.0
B	22.6	23.7	24.4	25.1	25.8
C	22.2	23.3	24.1	24.7	
D	21.9	23.0	23.7		

PREPARING A RESIDUAL MAP

In theory, if there is no anomalous geothermal heat flux, evaluation of the AWCM at each site for a given date should produce a 2-m temperature value equal to that actually measured for the same date. Any measured temperature greater than that computed by the model could be assumed to be caused by higher than normal heat flow. Values for the site, the roughness-diffusivity group, the measured temperature for September, 1977, corrected for elevation, and the computed temperatures are listed in Table 1. The differences between the measured values minus the computed values, i.e., the residuals, are tabulated. Residual temperatures were calculated by subtracting "normal" 2-m temperatures computed from AWCM for September 22–24, 1977, from 2-m temperatures during this same period. Note the close similarity between Figure 3 and the residual anomaly patterns in Figure 6. When these residuals are compared in the same fashion to the mean annual temperature map for Coso, as in Figures 5 and 6, the close association can also be seen. In short, the same map that was developed using a year's temperature data can be duplicated in much less time using temperatures recorded at a specific time (September 22–24) along with appropriate corrections through the use of AWCM.

[4]John Davies of McMaster University provided the algorithm for this solar radiation routine.

A TEST OF THE MODEL'S RELIABILITY

Because the model has not yet been fully refined, and because there is uncertainty in the accuracy of our input data, we have evaluated on a statistical basis the reliability of our simulated normal temperatures. Using the residual map as a guide, we chose two areas: the southwest and the north where there are a number of data points and geothermal heat flow appears to be normal. At each site we compared the observed temperatures with their respective computed temperatures using the Student-*t* test, a statistical test for comparing data populations. The values are listed in Table 4. At both areas we can accept the null hypothesis that there is no significant difference between the means at the 5 percent level, i.e., there is a 95 percent probability that the computed and measured values come from the same population. If this is so, it suggests that the residual values for the entire Coso area are probably accurate to ±1.4°C, based on the root-mean-square (rms) of the standard deviation of ±0.96°C for the observed temperatures corrected for elevation and a standard deviation of ±0.94°C for the associated computed values, in the nonanomalous areas.

COMPARISON OF OUR 2-m TEMPERATURE DATA AT COSO WITH OTHER GEOLOGIC AND GEOPHYSICAL DATA

Other researchers have independently gathered geologic and geophysical data at Coso that appear wholly consistent with our data. Electrical resistivity surveys (Fox, 1978a) and low-altitude aeromagnetic surveys (Fox, 1978b) show anomalies coincident

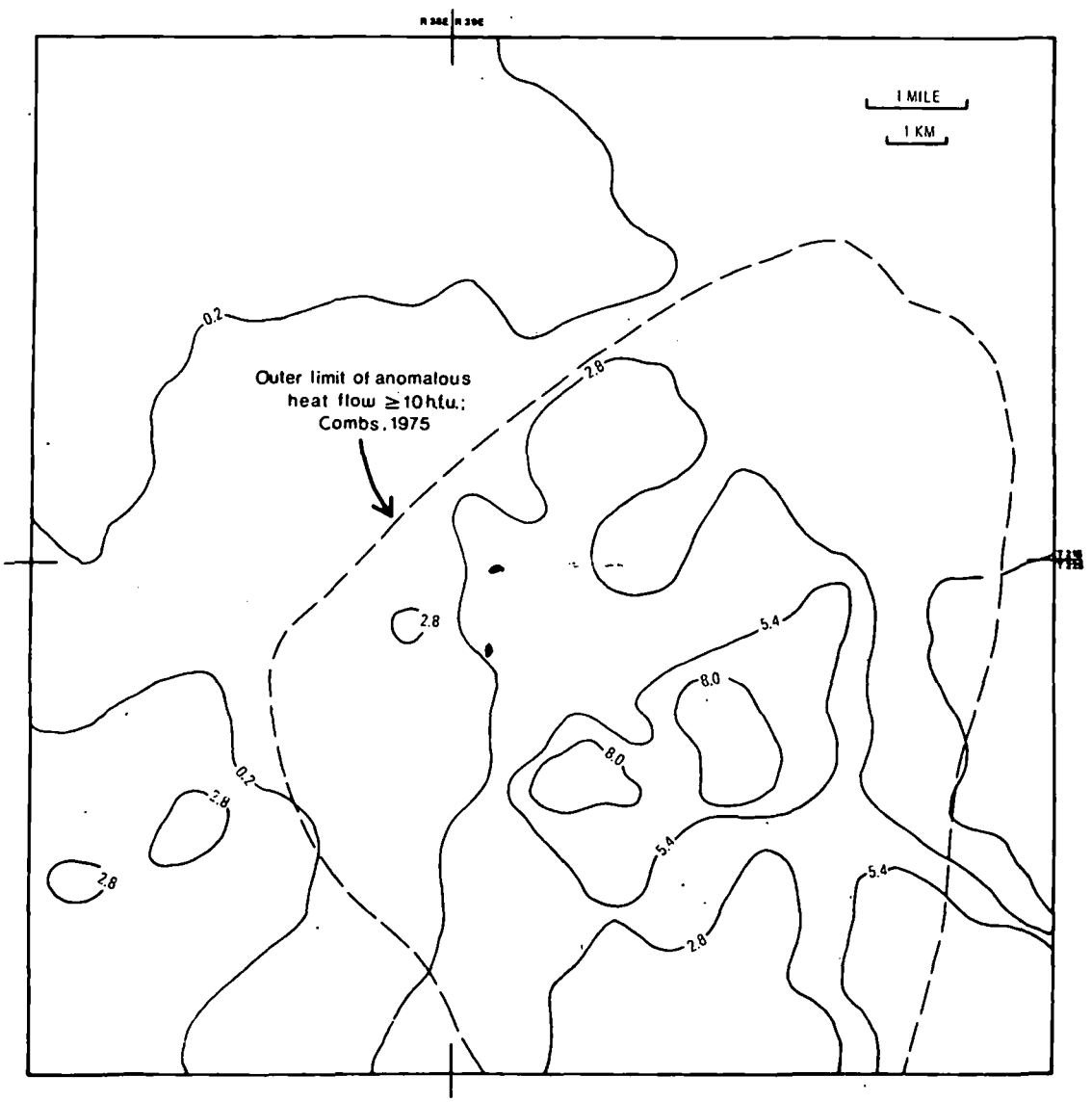

FIG. 6. Residual temperature contour map for Coso in °C.

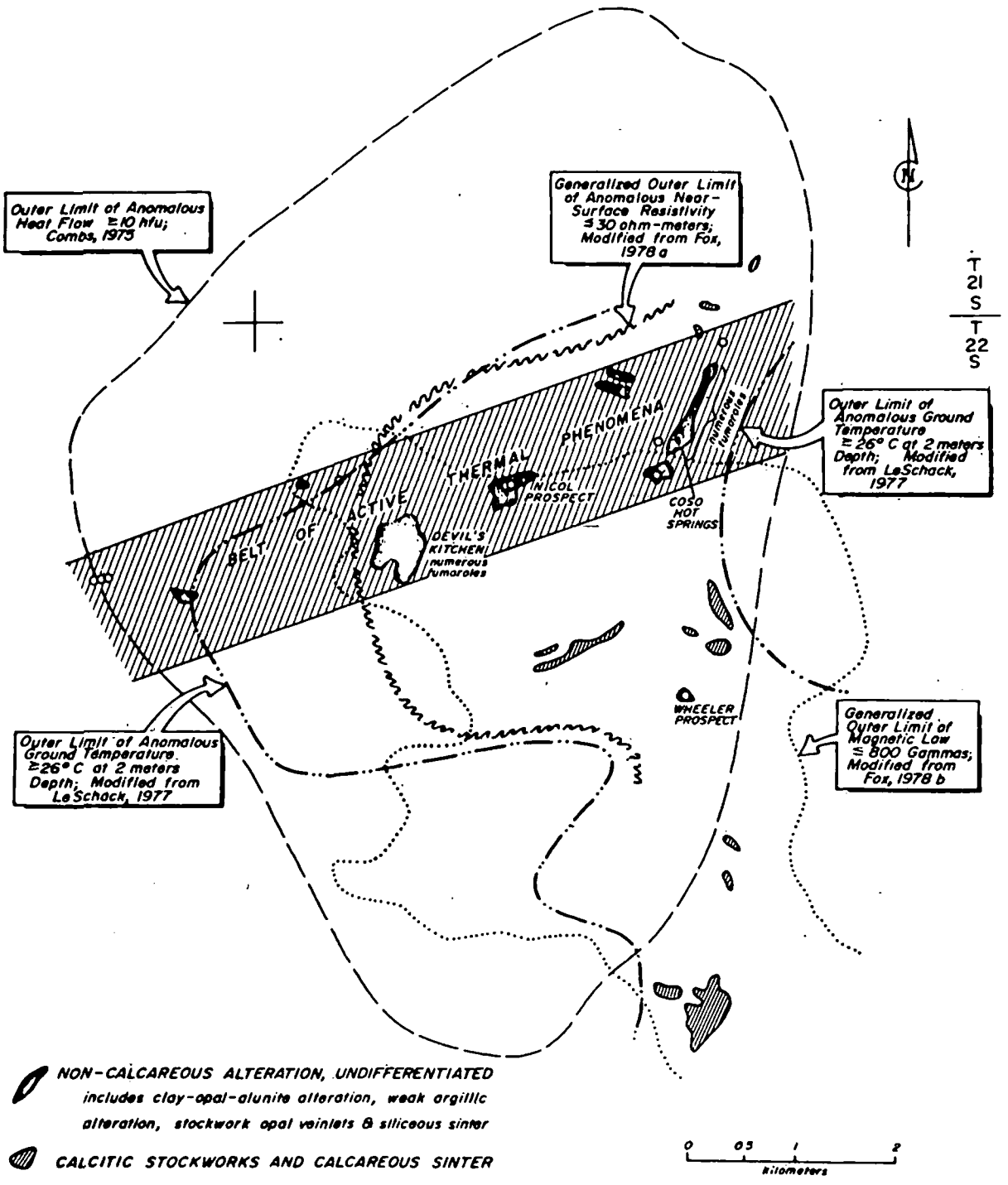

FIG. 7. Generalized alteration and geophysical map of Coso (after Hulen, 1978).

Table 4. A comparison of September, 1977 temperatures, recorded at two nonanomalous areas at Coso and corrected for elevation, with temperatures computed for the same site and time with the annual wave correction model.

West

Station	Temperature °C observed	computed
16	26.3	25.6
17	26.7	27.0
22	25.0	23.3
23	25.1	23.7
82	26.8	25.6
83	25.7	24.1
84	25.2	24.1
85	24.7	25.6
86	24.5	25.6
87	24.3	23.7
88	23.2	25.6
89	23.5	24.4
90	23.7	24.4
91	24.1	24.4
92	24.1	24.4
93	25.1	26.3
94	23.8	23.7
95	24.7	24.4
96	24.8	25.6

Computed t value = 0.03187

North

Station	Temperature °C observed	computed
65	24.7	24.8
66	25.0	25.6
67	25.2	24.8
68	23.8	24.8
69	23.1	23.6
70	24.3	24.4
71	25.7	23.7
72	24.9	23.6

Computed t value = 0.44926

STD of computed values = ±0.94
STD of observed values = ±0.96

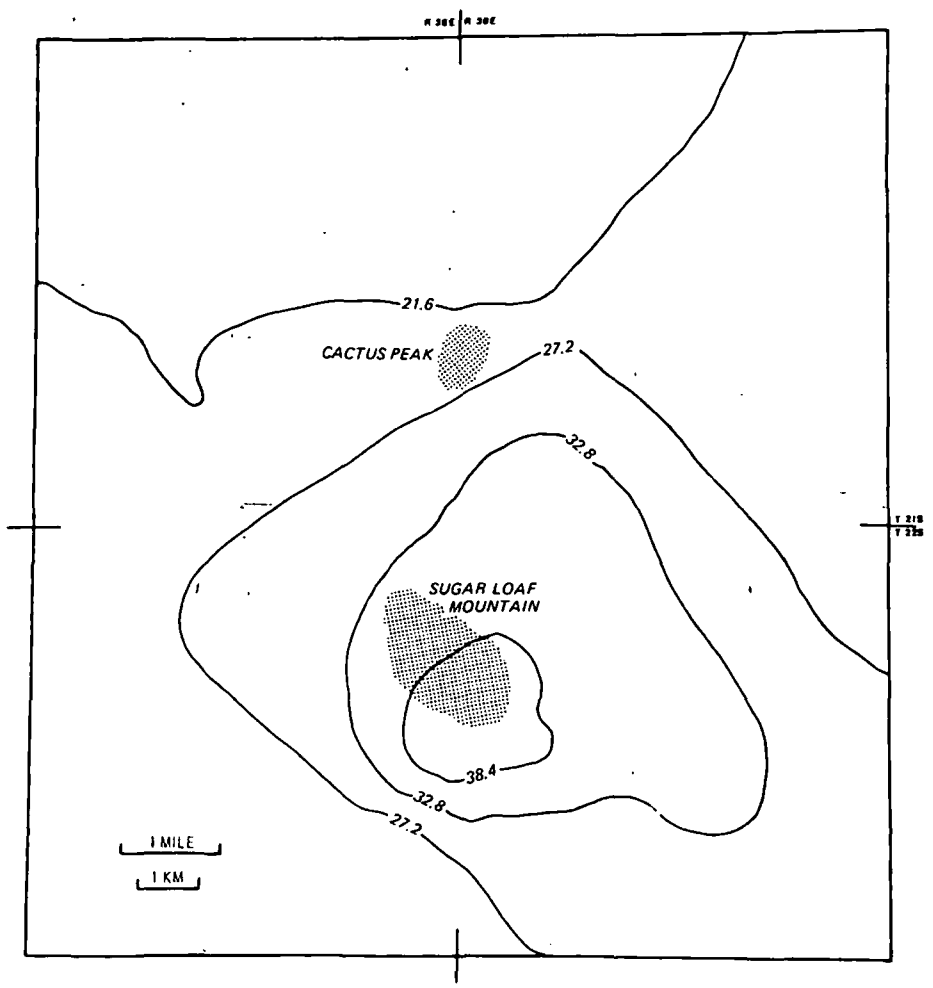

FIG. 8. A computer-generated 30-m temperature contour map at Coso based on the 21 drill sites of Combs (1975, 1976) is compared with a similarly constructed residual anomaly map using our 102 2-m temperatures recorded on September 22–23, 1977 (Figure 6). Our data were corrected as described in the text. A clear similarity of the anomaly patterns can be seen.

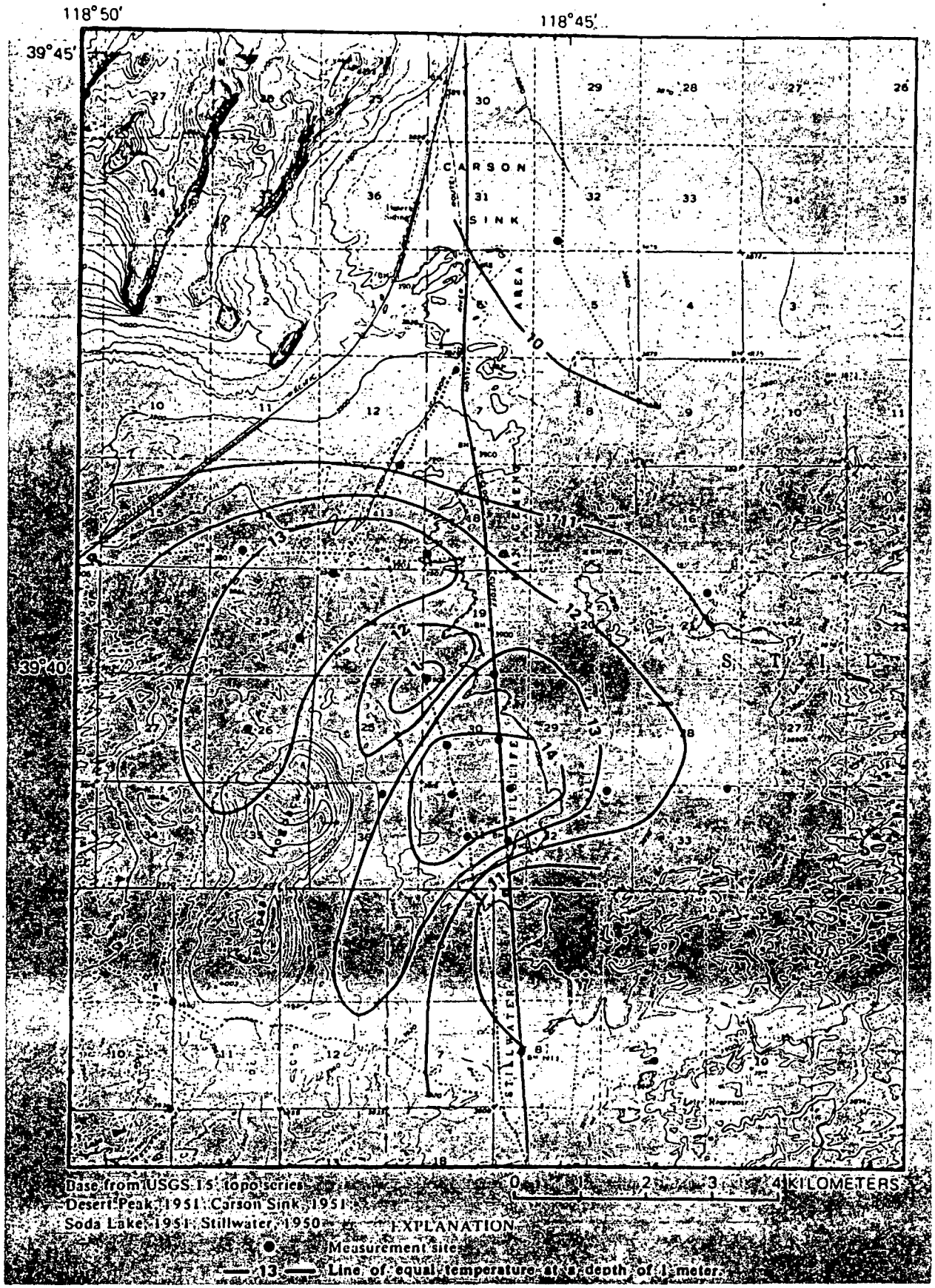

FIG. 9. Upsal Hogback area showing temperature at a depth of 1 m, December 2, 1975 (after Olmsted, 1977).

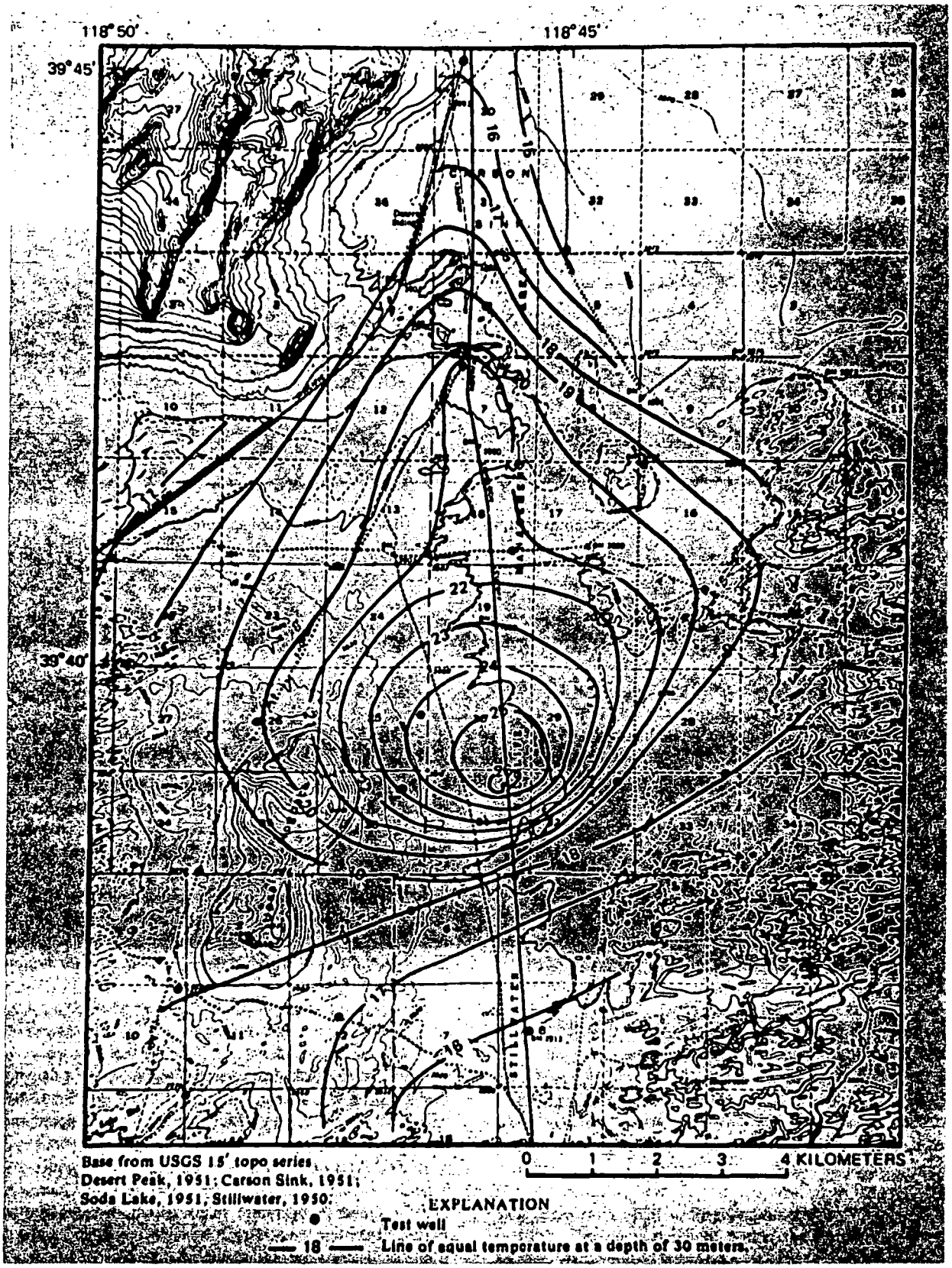

FIG. 10. Upsal Hogback area showing temperature in test wells at a depth of 30 m, September 1975 (after Olmsted, 1977).

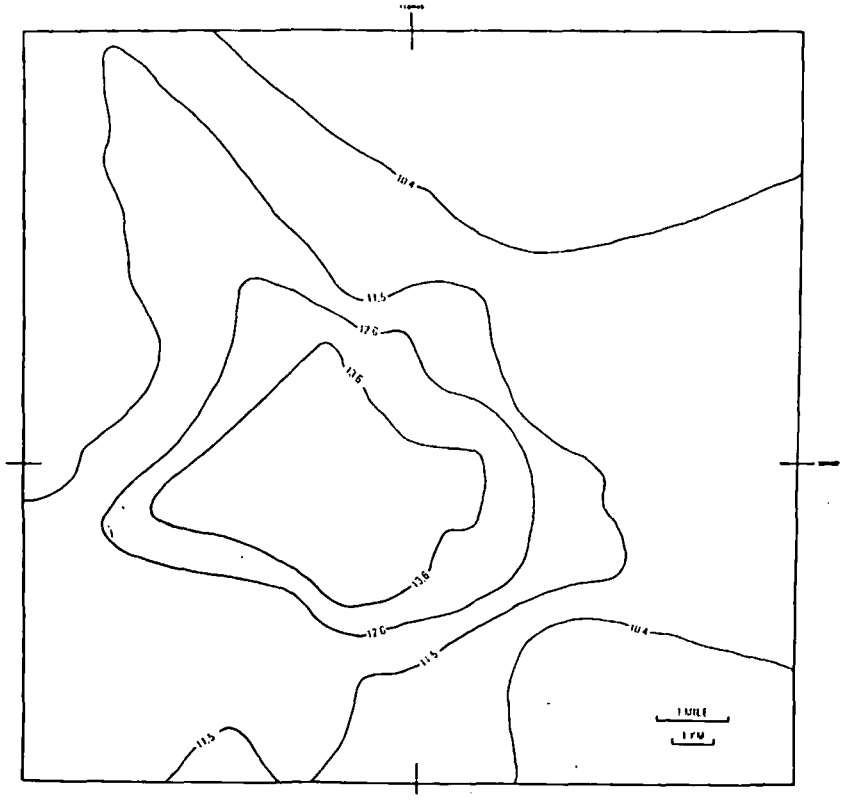

FIG. 11. Corrected 1-m temperature contour map for Upsal Hogback. Temperature in °C.

with our shallow temperature anomaly. A mapping of surface hydrothermal alteration products coincides with our temperature anomaly. These coincident anomalies are shown in Figure 7, prepared by Hulen (1978).

From the point of view of exploration strategy, however, it is valuable to compare the temperature patterns obtained by Combs (1975, 1976) using standard reconnaissance drilling to 30 m with our corrected 2-m anomaly (Figure 8). Exploration decisions that could have been made from the standard 30-m temperature map could probably have been made using our technique.

Table 5. Temperatures at 8 common points at Upsal Hogback.

Point Location (Section)[a]	Temperatures °C			ΔT (June-Dec)
	June	October	December	
30	20.8	17.8	10.8	10.0
8	18.9	15.9	10.9	8.0
36	22.3	18.4	13.0	9.3
33	18.0	15.8	11.5	6.5
18	18.8	17.3	11.9	6.9
32	19.2	18.1	12.8	6.4
19/30	19.2	18.2	13.2	6.0
31	20.4	19.3	14.4	6.0

[a] See Olmsted (1977), Figure 13.

CORRECTING 1-M TEMPERATURE DATA AT UPSAL HOGBACK FOR THERMAL DIFFUSIVITY VARIATIONS

Olmsted (1977) reported 1-m temperature data taken at Upsal Hogback in Nevada (near Carson Sink) in June, October, and December, 1975. These data were recorded at a site where temperature data for a number of 30-m holes were available. He compared the uncorrected 1-m temperature data for December with the 30-m data and concluded that without making proper corrections for the shallow temperature data there is no meaningful correlation that would be useful for predicting the observed anomaly at 30 m. The compared 1-m and 30-m data are shown in Figures 9 and 10.

Having examined the effects of thermal diffusivity at Long Valley and Coso, respectively, 150 and 240 miles south of Upsal Hogback, and recognizing some similarities in the geologic settings, we then asked if corrections to Olmsted's data could be derived from the information he presented (Olmsted, 1977). If so, would the corrected data be more useful in targeting the 30-m anomaly than the uncorrected data?

Examination of the 1-m temperature data presented by Olmsted shows that eight points are common to the June, October, and December temperature maps. From these maps we have estimated the temperatures for the eight points and listed them in Table 5. There were not sufficient data during the year to calculate the thermal diffusivities at these points, but it appears from Table 5 that the first three data points with a mean T of 9.1° may

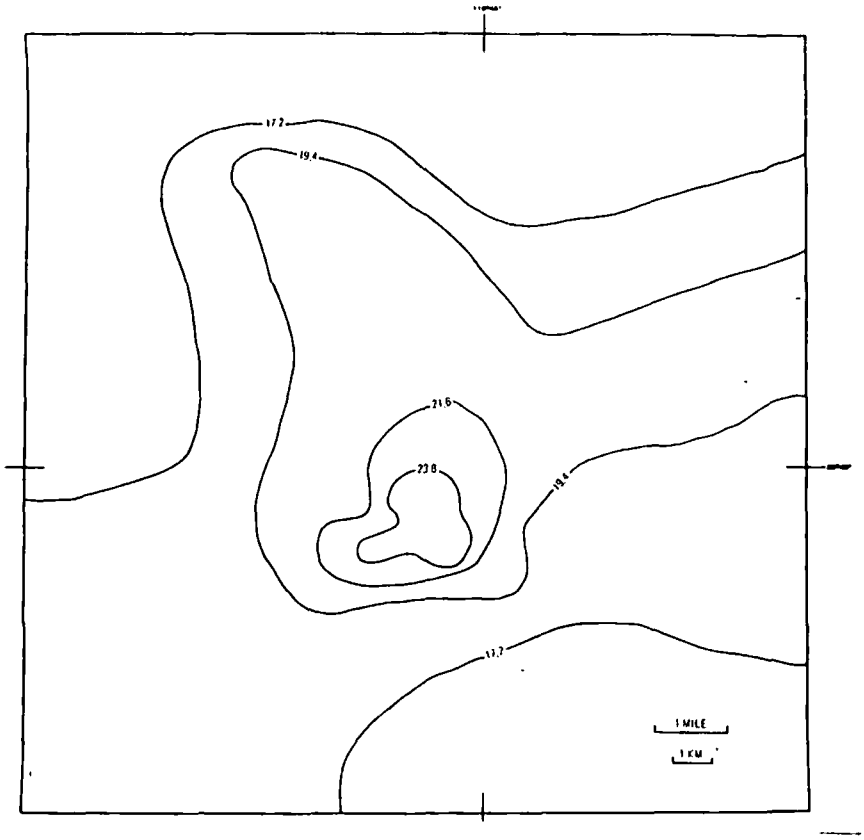

FIG. 12. 30-m temperature contour map. Data values derived from contour map shown in Figure 10. Temperature in °C.

have a significantly higher thermal diffusivity than the remaining five points with a mean T of 6.4°C. We have assumed the five points with the lower Ts represent the thermal diffusivities of the majority of the data points used to prepare Olmsted's December map (Figure 9), i.e., the majority of the data points have essentially the same thermal diffusivity.

Accordingly, because it is clear that the first three data points have significantly higher thermal diffusivities than the majority, we eliminated them from Olmsted's December data set and recontoured the December 1-m temperature map. Figure 11 shows the new contour map with elevation corrections (although these were relatively small). The SYMAP program was used to contour these data and avoid personal bias. For comparison, we recontoured Olmsted's 30-m data by the same program (Figure 12). Comparing the two maps with corrections for surface effects, Olmsted's 1-m temperature data correlate well with the 30-m temperature anomaly and would have been useful for targeting the deeper anomaly. Olmsted (1978) later confirmed our interpretation, indicating that he had taken additional data (unpublished) at his site for a complete annual cycle. His mean annual 1-m temperature contours were consistent with our interpretation shown in Figure 11.

In summary, Olmsted correctly points out that his uncorrected 1-m temperatures do not correlate well with 30-m temperatures at the same location. However, when we correct the data set by removing key data points that do not have the same thermal diffusivity, we get better targeting of the 30-m anomaly. This is additional strong evidence for gathering thermal diffusivity data when making a shallow temperature survey.

A SHALLOW ANOMALY AT ANIMUS VALLEY, NEW MEXICO

Two-m temperature data were collected at Animus Valley in New Mexico at a site studied by Kintzinger (1956). The survey areas are shown in Figures 13 and 14.

The size and strength of the anomaly might provide some indication of its value as a predictor of resources at depth. A conductive, steady-state thermal source at depth behaves like other potential fields and can be expressed by the Laplace equation. Accordingly, depth estimation by the half-width method (Nettleton, 1940) will provide a likely maximum depth at which the anomaly may occur. The caveat, of course, is that although our technique does indeed remove time variations of the thermal anomaly so that we are effectively measuring steady state temperature, it is never clear how much of the anomaly is the result of conductive heat transfer and how much the result of convective flow. The half-width method does provide a guide to the probable maximum depth at which the measured anomaly is located.

Using a horizontal cylinder as a model at Animus Valley, the maximum predicted depth at which a purely conductive source

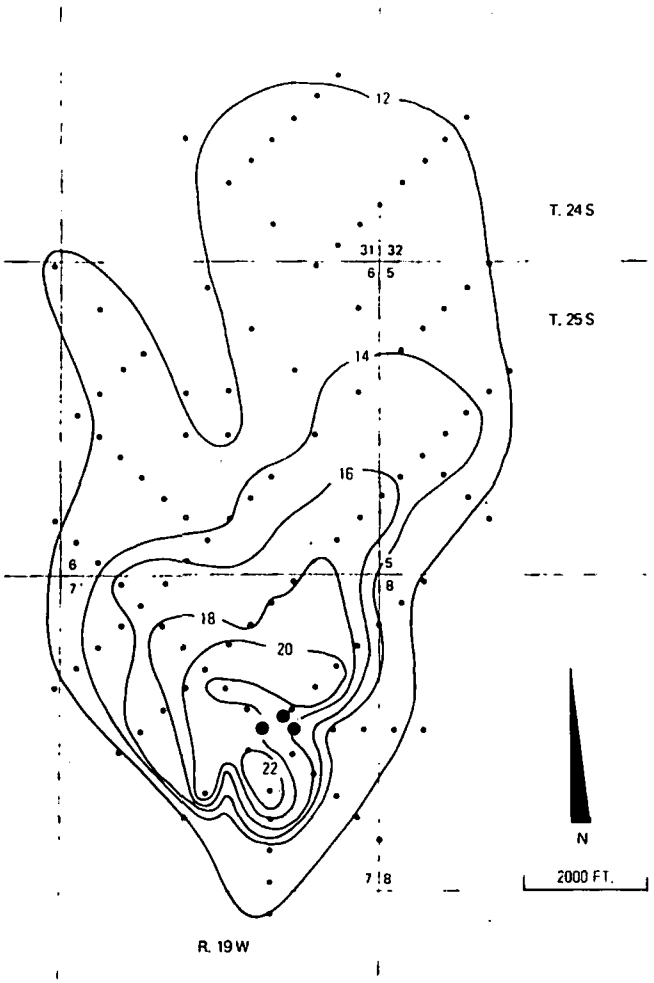

FIG. 13. Geothermal map. Temperature 1 m below surface; contour interval 2°C (redrawn from Kintzinger, 1956).

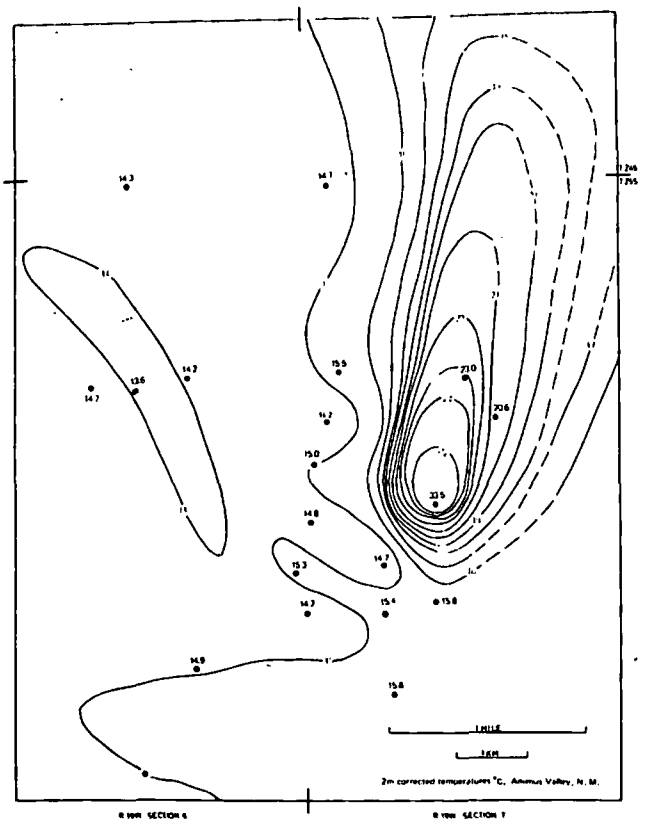

FIG. 14. Corrected temperatures 2 m below the surface, Animus Valley, south of Lordsburg, NM, March 1980; contour interval 1°C. The anomaly is centered in section 7, R.19W, T.25S, on the Swallow Fork Peak quadrangle.

could be found is 200 m (Figure 14). This is not indicative of a substantial source, but we should point out that at this site hot water at a temperature of 96°C is pumped from wells at a depth of 27 m and is used commercially to heat greenhouses. Using hindsight, shallow temperature measurements might have predicted this. For comparison, the Coso anomaly has a computed maximum depth of 1500 m. Ongoing commercial exploration there has brought in six wells that are producing an abundant supply of high-quality geothermal fluids and dry steam from a steam zone at a depth of 450 m (Evans, 1982).

CONDUCTING A SHALLO-TEMP SURVEY

The luxury of recording sufficient data for computing the mean annual 2-m temperatures at a prospect, as we did at Coso, is not likely to occur in examining a commercial prospect where speed and low cost are important. However, we have seen from the foregoing work that a procedure exists for rapidly acquiring not only the 2-m temperatures but also the associated soil, surface, and meteorological data needed to develop the equivalent of a "normal" soil temperature map at a depth of 2 m. We call this procedure the Shallo-Temp survey. The generalized steps for conducting this survey are as follows:

(1) At each site, drill two adjacent 2-m holes.
(2) Insert thermistor probe in one, thermal conductivity probe in the other.
(3) Take soil sample for type determination.
(4) Measure surface roughness, surface albedo, and thermal conductivity.
(5) After equilibration read thermistor probe.
(6) Using annual wave correction program, input 18–24 months of weather data from nearest Weather Bureau station, thermal diffusivity (calculated from thermal conductivity), surface roughness and albedo. Output is normal 2-m temperature for given location and time.
(7) Subtract normal 2-m temperatures from observed 2-m temperatures corrected for elevation to obtain residual geothermal anomaly.

With experience, the ancillary data can be obtained and processed rapidly and a corrected 2-m temperature map can be constructed that reflects only geothermal heat flux at 2 m.

We are constantly confronted with horror stories of explorationists who, obtaining an exciting anomaly at 30, 50, or 100 m depth, embark upon an expensive deeper drilling program only to

find that their anomaly has disappeared at some greater depth. Clearly, in those cases a 2-m survey can, at best, mirror the anomalies developed at these 30, 50, or 100 m levels. It cannot predict the disappearance of the anomaly below some depth. On the other hand, the Shallo-Temp survey is relatively quick and inexpensive, and it can be a useful tool for developing exploration strategy and focusing the standard reconnaissance effort in the examination of a prospect. Of great significance is the fact that governmental permits are relatively easy to obtain. Because most of our drilling has been conducted with a hand-held auger, implying little potential for damage to the environment, Bureau of Land Management officers have been quick to provide the appropriate permits when we have requested them.

The size and shape of the 2-m temperature anomalies are, in themselves, indicative of the potential value of the survey. High temperature anomalies of limited areal extent such as the one at Animus Valley strongly suggest a very shallow heat source. In this case, such a survey could have predicted the possibility of a shallow source of heat for space heating. Indeed, this may become the most important application of the Shallo-Temp survey because its cost is within the acceptable range for small landowners and developers.[5]

CONCLUSIONS

The Shallo-Temp survey, when used in an appropriate geologic setting such as exists in the Basin and Range Province and when applied as a first-look geophysical tool, with an understanding of its physical limitations, can be a cost-effective geothermal reconnaissance technique to help develop exploration strategy. It is inherently quicker and less expensive than other techniques that require drilling, because the holes are so shallow and federal permits are relatively easy to obtain. It is not designed to replace reconnaissance drilling but rather help focus standard reconnaissance programs. The two potentially most reliable applications of Shallo-Temp surveys are in extending trends in prospects where standard reconnaissance holes have been drilled or filling in detail between widely spaced holes, and in surveying for near-surface anomalies that might be developed for direct heating applications.

ACKNOWLEDGMENTS

We wish to acknowledge the many persons who assisted us in gathering field data and who provided guidance in our research.

At the U.S. Naval Weapons Center, the site of the Coso KGRA, we could continually count on the assistance and good will of Dr. Carl Austin, Carl Halsey, Charles Rodgers, and Dr. James Whelan. These gentlemen assisted in many ways in expediting and supporting our efforts at the Naval Weapons Center.

Dr. Roy A. Bailey, USGS, Reston, Virginia, gave us much guidance at the Long Valley site where he has conducted extensive research. David C. Chang, for several years staff geologist for LeSchack Associates, Ltd., assisted in much of the field work. Dr. Lokesh Chaturvedi of New Mexico State Univ. at Las Cruces assisted us in gathering the data at Animus Valley, New Mexico, not only personally but through a consulting contract between the University and LeSchack Associates, Ltd.

The major portion of this work was supported under Dept. of Energy contract EG-77-C-01-4021. Other support came from the Earth Physics Program of the Office of Naval Research under contract N00014-78-C-0535. We wish to acknowledge also the assistance and guidance provided by Larry Ball and Dr. Robert Andrews, who were then our program managers at DOE and ONR, respectively. The Geography Dept. at McGill University kindly provided support in the preparation of this manuscript.

[5]The Coso area is a case in point. LeSchack Associates, Ltd. conducted a proprietory Shallo-Temp survey in 1979 that extended several miles to the west for the Coso survey discussed in this paper. A developer who had leases in this western area, and was known to be planning to drill standard reconnaissance holes on his leases, was offered the opportunity to obtain the Shallo-Temp survey of this area for $5,000. He declined, and shortly thereafter embarked upon his reconnaissance drilling program at many times the cost of the Shallo-Temp survey. Since our Shallo-Temp survey replicated so well the standard reconnaissance drilling data (Combs, 1975, 1976) as well as agreeing with the other geophysical data obtained just a few miles to the east, we could have felt confident in telling the developer in question what he discovered on his own at considerably greater expense: the Coso anomaly did not extend anywhere near his leases.

REFERENCES

Birman, J. H., 1969, Geothermal Exploration for Ground Water: G.S.A. Bull. v. 80, p. 617–630.

——— 1977, Pers. Comm., Dept. of Geology, Occidental College, Los Angeles.

Businger, J. A., Wyngaard, J. C., Izumi, Y., and Bradley, E. F., 1971, Flux profile relationship in the atmospheric surface layer: J. Atmos. Sci., v. 28, p. 181–189.

Cartwright, K., 1968, Thermal prospecting for ground water: Water Resources Res., v. 4, p. 395–401.

Combs, J., 1975, Heat flow and microearthquake studies, Coso Geothermal Area, China Lake, California: Final rep., July 1965, Inst. for Geosciences, Univ. of Texas at Dallas, under contract N00023-74-C-2099, sponsored by the Advanced Research Projects Agency, ARPA order no. 2800.

——— 1976, Heat flow determinations in the Coso Geothermal Area, California: The Coso Geothermal Project, Tech. rept. no. 3, December, Battelle Northwest Laboratories, Richland. WA and Center for Energy Studies, Univ. of Texas at Dallas, Richardson, under contract E(45-1)-1830, ERDA.

Dyer, A. J., 1967, The turbulent transport of heat and water vapor in an unstable atmosphere: Quart. J. Roy. Meteor. Soc., v. 93, p. 501–508.

Evans, T., 1982, China Lake geothermal is a major success: BLM Newsbeat, U.S. Dept. of Interior, Calif. State Office.

Fox, R. C., 1978a, Dipole-dipole resistivity survey of a portion of the Coso Hot Springs KGRA, Inyo County, California: Univ. of Utah Research Inst. Earth Sci. Lab., Salt Lake City, under contract EY-76-S-07-1601 for Dept. of Energy.

——— 1978b, Low altitude aeromagnetic survey of a portion of the Coso Hot Springs KGRA, Inyo County, California: Univ. of Utah Research Inst. Earth Sci. Lab., Salt Lake City, under contract no. EY-76-S-07-1601 for Dept. of Energy.

Goodwin, C., 1972, Annual active layer simulator for permafrost regions: M.S. thesis, Univ. of Michigan, Ann Arbor (unpublished).

Hulen, J. B., 1978, Geology and alteration of the Coso Geothermal Area, Inyo County, California: Univ. of Utah Research Inst. Earth Sci. Lab., Salt Lake City, under contract EG-78-C-07-1701 for Dept. of Energy.

Kappelmeyer, O., and Haenel, R., 1974, Geothermics—with special reference to application: Berlin-Stuttgart, Gebruder Borntraeger.

Kintzinger, P. R., 1956, Geothermal survey of hot ground near Lordsburg, New Mexico: Science, v. 124, p. 629–630.

Lachenbruch, A. H., 1968, Rapid estimation of the topographic disturbance to superficial thermal gradients: Rev. of Geophys., v. 6, p. 365–400.

Lachenbruch, A. H., Sorey, M. L., Lewis, R. E., and Sass, J. H., 1976, The near-surface hydrothermal regime of Long Valley Caldera: J. Geophys. Res., v. 81, p. 763–768.

Lee, T.-C., 1977a, On Shallow-hole temperature measurements—A test study in the Salton Sea Geothermal Field: Geophysics, v. 42, p. 572–583.

——— 1977b, Application of finite element analysis to terrestrial heat flow: UCR/IGPP-77/15, Inst. of Geophs. and Plan. Phys., Univ. of Cal, Riverside.

Lee, T.-C., and Cohen, L. H., 1979, Onshore and offshore measurements of temperature gradients in the Salton Sea Geothermal Area, California: Geophysics, v. 44, p. 206–215.

LeSchack, L. A., Lewis, J. E., and Chang, D. C., 1977, Rapid reconnaissance of geothermal prospects using shallow temperature surveys: Semi-annual tech. rep. by LeSchack Associates Ltd., under U.S. Dept. of Energy contract EG-77-C-01-4021.

——— 1980, Rapid reconnaissance of geothermal prospects using shallow temperature surveys: Third tech. rep. by LeSchack Associates Ltd., under U.S. Dept. of Energy contract EG-77-C-01-4021 and Office of Naval Research contract N00014-78-C-0535.

LeSchack, L. A., Lewis, J. E., Chang, D. C., Lewellen, R. I., and

O'Hara, N. W., 1979, Rapid reconnaissance of geothermal prospects using shallow temperature surveys: Second tech. rep. by LeSchack Associates, Ltd. under U.S. Dept. of Energy contract EG-77-C-01-4021 and Office of Naval Research contract N00014-78-C-0535.
Lettau, H. H., 1969, Note on aerodynamic roughness—Parameter estimation on the basis of roughness element description: J. Appl. Meteor., v. 8, p. 828–832.
Lovering, T. S., and Goode, H. D., 1963, Measuring geothermal gradients in drill holes less than 60 feet deep East Tintic District, Utah: U.S.G.S. Bull., 1172, Wash. D.C.
Montieth, J. L., 1973, Principle of environmental physics: London, Edward Arnold.
Nettleton, L. L., 1940, Geophysical prospecting for oil: New York, McGraw-Hill.
Noble, J. W., and Ojiambo, S. B., 1975, Geothermal exploration in Kenya: Proc. 2nd U.N. Symp. on use of geothermal resources, San Francisco, May 20–29 1975, p. 189–204.
O'Brien, P. J., 1970, Aquifer transmissivity distribution as reflected by overlying soil temperature patterns: Ph.D. thesis, The Pennsylvania State Univ.
Oke, T. R., 1978, Boundary layer climates: London, Methuen Co.
Olmsted, F. H., 1977, Use of temperature surveys at a depth of 1 meter in geothermal exploration in Nevada: U.S.G.S. prof. paper 1044-B, Washington, D.C.
——— 1978, Personal Communication, USGS, Menlo Park, Calif.
Outcalt, S. I., 1972, The development and application of a simple digital surface climate simulator: J. Appl. Meteor., v. 11, p. 629–636.
Paulson, C. A., 1970, The mathematical representative of wind speed and temperature in the unstable atmospheric surface layer: J. Appl. Meteor, v. 9, p. 857–861.
Pease, R., Lewis, J. E. and Outcalt, S. I., 1976, Urban terrain climatology and remote sensing: Annals of Assoc. Amer. Geog., v. 66, p. 557–569.
Poley, J. Ph., and Van Steveninck, J., 1970, Geothermal prospecting—Delineation of shallow salt domes and surface faults by temperature measurements at a depth of approximately 2 meters: Geophys. Prosp., v. 18, p. 666–700.
Sabins, F., 1976, Pers. Comm., Chevron Oil Field Research, La Habra, Calif.
Sellers, W. D., 1965, Physical climatology: Chicago, Univ. of Chicago Press.
Van Wijk, W. R., Ed., 1966, The physics of plant environment: Amsterdam, North Holland Publ. Co., 2nd ed.
Whelan, J. A., 1977, Thermal gradient and heat flow drilling: Final rep., v. 5, under Nat'l Sci. Foundation contract GI-43741, Univ. of Utah, Salt Lake City.

APPENDIX

Model structure

Theoretical basis of model.—The radiation balance for a particular surface (SFC) is expressed for clear sky conditions as

$$Q^* = (1 - \alpha)(Q + q) + \varepsilon\sigma T_{SKY}^4 - \varepsilon\sigma T_{SFC}^4, \quad (A-1)$$

where Q^* is net radiation, α is albedo, $Q + q$ is beam plus diffuse solar radiation, σ is the Stefan-Boltzmann constant, and ε is emissivity. For a complete description of this formulation, the reader should consult Sellers (1965), Oke (1978), and Montieth (1973). The sky radiation is estimated using the empirical equation

$$\varepsilon\sigma T_{SKY}^4 = T_{AIR}^4(a + b\sqrt{e}), \quad (A-2)$$

where a and b are empirical constants and e is vapor pressure of the air.

Using the assumption that the soil surface radiates essentially as a black body, equation (A–1) can be written as

$$Q^* = (1 - \alpha)(Q + q) + \sigma T_{AIR}^4(a + b\sqrt{e}) - \sigma T_{SFC}^4. \quad (A-3)$$

Since α, $(Q + q)$, T_{AIR}, and e are assigned as data, Q^* can be calculated explicitly as a function of surface temperature T_{SFC}.

Equation (A–3) is for clear sky conditions. Variations in radiation input induced by changing cloud cover are corrected by using percent clear sky and a correction factor for the cloud type following Sellers (1965). Equation (A–3) is rewritten as

$$Q^* = (1 - \alpha)(Q + q) + [\sigma T_{AIR}^4(a + b\sqrt{e}) - \sigma T_{SFC}^4] \cdot [P_c + (1 - P_c)C_T], \quad (A-4)$$

where P_c is percent clear sky and C_T is cloud correction factor.

The nonradiative components of the energy balance need to be specified to complete the total energy exchange at the earth's interface. The nonradiative transfers are

$$Q^* = Q_H + Q_L + Q_s, \quad (A-5)$$

where Q_H = sensible energy flux, Q_L = latent energy flux, and Q_s = soil energy flux.

The first two transfers of energy occur in the surface layer (a layer of the atmosphere up to approximately 10 m) by turbulent transfer, whereas soil heat flux occurs through a conductive process.

Sensible energy flux.—Sensible heat is transported by turbulent eddies which are a function of the stability regime of the lower atmosphere. Therefore, any expression describing sensible energy transfer must incorporate a stability-dependent function. The annual simulation model uses the Businger-Dyer (Businger, 1971; Dyer, 1967) formulation for calculation of sensible energy flux in the surface layer. An assumption characteristic of all surface layer calculations is that the energy flux is constant throughout this layer.

The stability of the surface layer is determined by the Richardson number:

$$\mathrm{Ri} = g\,\frac{\overline{\partial\theta}}{\partial z}\Big/\,\theta\left(\frac{\overline{\partial U}}{\partial z}\right)^2, \quad (A-6)$$

where g is acceleration due to gravity, θ is the potential temperature, z is the vertical coordinate, and U is the magnitude of the mean horizontal wind vector.

The Ri number is a dimensionless quantity which varies from <-0.025 for a free convective regime, to >-0.025 and <0 for forced convection, where zero defines the neutral condition; from >0 to <0.4 is a stable state. Finally, values for the Ri number $>.4$ define a laminar condition where essentially all turbulent motion is suppressed.

Under neutral atmosphere conditions the mean wind flow is logarithmic with height

$$\frac{\overline{\partial U}}{\partial z} = \frac{u^*}{k\,z}, \quad (A-7)$$

where u^* is friction velocity and k is the von Karman constant. If equation (A–7) is integrated from some reference height Z_0 (Z_0 = surface roughness), one obtains

$$\bar{U} = (\mu^*/k)\ln\left(\frac{z}{z_0}\right). \quad (A-8)$$

If Z_u is the instrument height and $\bar{U}$ is the mean wind speed

from $Z_0(U = 0)$ to Z_a, then

$$u^* = k\,\bar{U}/\ln\left(\frac{z_a}{z_0}\right). \quad \text{(A-9)}$$

where u^* is a scaling parameter for the wind.

Similarly, from

$$\frac{\overline{\partial\theta}}{\partial z} = \theta^*/z, \quad \text{(A-10)}$$

where θ^* scales temperature, one obtains

$$\theta^* = (\theta_{z_a} - \theta_0)/\ln\left(\frac{z_a}{z_0}\right). \quad \text{(A-11)}$$

Now the sensible heat flux can be calculated by

$$Q_H = \rho c\, k\, u^* \theta^*, \quad \text{(A-12)}$$

where ρc = volumetric heat capacity of air, ρ = air density, and c = specific heat.

Under nonneutral conditions equations (A-9) and (A-11) are modified by subtracting ψ_1 and ψ_2 which are functions of atmospheric stability (Paulson, 1970).

From the original work of Businger (1971) and Dyer (1967), Paulson showed that ψ_1 is given for unstable conditions by

$$\psi_1 = 2\ln[(1 + X)/2] + \ln[(1 + X^2)/2] - 2\tan^{-1}X + \frac{\pi}{2}, \quad \text{(A-13)}$$

where

$$X = \left(1 - \gamma\frac{z}{L}\right)^{1/4}, \quad \text{(A-14)}$$

γ is an empirical constant, and z/L is a stability function such that

$$\mathrm{Ri} = Zm/L,$$

where Zm is geometric mean height of the layer and L is the Obukov length given by

$$L = -u^{*3}\rho\, c\, T/k\, g\, Q_H.$$

For stable temperatures the following expression is used

$$\psi_2 = 2\ln[(1 + X^2)/2]. \quad \text{(A-15)}$$

Under stable conditions,

$$L = Z_M(1 - 7\,\mathrm{Ri})/\mathrm{Ri}, \quad \text{(A-16)}$$

and

$$\psi_2 = \psi_1 = 7\left(\frac{z}{L}\right). \quad \text{(A-17)}$$

When Ri = 0 (neutral conditions), the stability parameters ψ_1 and ψ_2 are equal to zero.

Latent energy flux.—The transfer of latent energy is obtained by using the Bowen ratio in conjunction with equation (A-12). The Bowen ratio is an expression of energy partition between sensible and latent energy flux

$$B = \frac{Q_H}{Q_L}. \quad \text{(A-18)}$$

Q_H and Q_L can be written in terms of a gradient relationship as follows:

$$Q_H = -\rho\, c\, K_H\frac{\partial\theta}{\partial z} \quad \text{(A-19)}$$

and

$$Q_L = -\rho\, c\, K_L\frac{\partial q}{\partial z}, \quad \text{(A-20)}$$

where ρ is air density, L is latent heat of vaporization, q is specific humidity, and K_H and K_L are the eddy diffusivity coefficients for heat and moisture, respectively.

Dividing equations (A-19) and (A-20), one obtains the Bowen ratio; if $K_H = K_L$, which is the general assumption, then

$$Q_L = \frac{Q_H L(q_2 - q_1)}{c(\theta_2 - \theta_1)}. \quad \text{(A-21)}$$

Serious questions exist as to the legitimacy of long term arithmetric mean values in the computation of average Richardson numbers and energy fluxes at time scales considered in this model. The physical reality of these assumptions remains to be tested.

Soil energy flux.—Soil heat flux is related to the time-rate-of-change of the soil heat content by

$$Q_s = \frac{\partial h}{\partial t}. \quad \text{(A-22)}$$

The heat content for a column of soil at depth z and unit area is

$$h = \rho\, c\, z\, \overline{T}, \quad \text{(A-23)}$$

where $\overline{T}$ is mean temperature of the soil. Setting equation (A-23) equal to the time rate change of temperature produces

$$Q_s = \frac{\partial h}{\partial t} = \rho\, c\, z\frac{\overline{\partial T}}{\partial t}. \quad \text{(A-24)}$$

The flow of heat into the soil can also be given by

$$Q_s = k\frac{\partial T}{\partial z}, \quad \text{(A-25)}$$

where k is thermal conductivity of the soil. Then

$$\frac{\partial Q_s}{\partial z} = \rho c\,\frac{\partial T}{\partial t} = \frac{\partial}{\partial z}\left(k\frac{\partial T}{\partial z}\right). \quad \text{(A-26)}$$

When k is constant with depth, the Fickian diffusion equation is obtained by rewriting equation (A-26) to produce

$$\frac{\partial T}{\partial t} = \frac{k}{\rho c}\left(\frac{\partial^2 T}{\partial z^2}\right) = K_s\left(\frac{\partial^2 T}{\partial z^2}\right), \quad \text{(A-27)}$$

where K_s is the soil thermal diffusivity.

The solution of equation (A-27) for equally spaced nodes is the method for obtaining the time history of soil temperatures given a periodic surface forcing function. Q_s is calculated from equation (A-26) after the temperature distribution is computed.

In a desert region such as Coso, it is assumed that convection of heat by percolating water in the soil is small, especially averaged over 5 days, and that no freeze-thaw phase changes occur. In addition, a major assumption of the model at the specified time scale is that mean temperature profiles in the soil over a five-day period are linear.

Numerical scheme

The finite-difference equations are developed for the Richardson number, sensible energy, and latent energy fluxes (Goodwin, 1972; Outcalt, 1972). The Fickian diffusion equation (A-28) is

developed in the finite form utilizing a back-differencing method. The temperature at depth Z_N in the soil at time increment I is given by

$$T_N(I) = T_N(I-1) + K_x \frac{\Delta t}{(\Delta z^2)} [T_{N-1}(I-1) - 2T_N(I-1) + T_{N+1}(I-1)], \quad \text{(A-28)}$$

where T_{N+1} is the temperature at some depth $Z_{N+1} > Z$, K_x is soil thermal diffusivity, and t and z are the time increment and depth increment, respectively. This equation is solved for 10 nodal points with Δz equal to 1 m and Δt equal to 4.32×10^5 sec (or 5 days). The quantity $K_x(\Delta t/\Delta z^2)$ has very interesting properties and is referred to as the Fourier modulus. This modulus can be used to determine the computational stability of equation (A-28). The stability criterion is

$$0 < K_x \frac{\Delta t}{\Delta z^2} < \frac{1}{2}.$$

The numerical solution of equation (A-28) for equally spaced nodes is stable (real) only if the above condition is satisfied. Inserting the range of values for soil thermal diffusivity and the time-depth increments, the stability criterion is always satisfied within the context of the Coso simulation. The finite-difference equation for soil heat flux at time I is then

$$Q_s(I) = k(T_N - T_{SFC})/\Delta z. \quad \text{(A-29)}$$

The complete numerical solution for the model at a particular time step hinges on the specification of all the variables needed to calculate the components of surface energy transfer on the meteorological (M) and surface (G) based data. The four components of surface energy transfer are net radiation Q^*, and the soil Q_s, sensible Q_H, and latent Q_L heat fluxes. These can be specified as transcendental in surface temperature T in the familiar energy conservation equation

$$Q^*(G, M, T) \pm Q_s(G, T) \pm Q_H(G, M, T) \pm Q_L(G, M, T) = 0. \quad \text{(A-30)}$$

An interval-halving algorithm is selected to carry out a search for that temperature which will drive the above equation to a zero sum condition. Thus, at each iteration, the surface temperature and all of the components of surface energy transfer are output in addition to the substrate (soil) temperature profile (Pease et al, 1976).

GEOPHYSICS, VOL. 48, NO. 5 (MAY 1983); P. 618-626, 11 FIGS.

Thermal hydrology and heat flow of Beowawe geothermal area, Nevada

Christian Smith*

ABSTRACT

Inflections in temperature-depth profiles from forty 150 m thermal gradient holes define a shallow thermal flow system in the Whirlwind Valley near the Beowawe Geysers. U.S. Geological Survey hydrologic data reveal the vertical and west-to-east components of cold water flow at the water table above the thermal flow system. The temperature inflections break most abruptly in areas with a downward component of flow at the water table. The inflections are thought to indicate the level where the buoyant thermal water maintains a dynamic equilibrium with the overlying cold water. Combining these geophysical and hydrologic data suggests areas away from The Geysers where thermal water may rise from the deep reservoir into the alluvium. These leakage areas may be viable geothermal exploration targets. Even if the temperatures of the leakage were subeconomic, knowledge of where upwelling occurs could be helpful in assessing the potential for energy production. The systematic acquisition of hydrologic data is recommended as a standard component of hydrothermal resource exploration programs.

Measurements of thermal conductivity from chip samples from the shallow holes and from Chevron Resources Company's Ginn 1-13 geothermal exploration hole (2917 m T.D.) enable inferences based on heat flow. The average heat flow east of the Dunphy Pass fault zone, 110 mW/m^2, may be representative of background in this portion of the Battle Mountain high heat flow province. Thermal gradient and conductivity data from the deep well have a wide range of values (65–144°C/km, 1.59–5.95 $Wm^{-1}K^{-1}$) but produce a relatively constant heat flow of 235 mW/m^2 above a depth of 1600 m. The shallow data indicate that the area with similarly high surficial heat flow extends as far east as the Dunphy Pass fault zone, suggesting that this Miocene rift boundary may form the eastern margin of the Beowawe hydrothermal system.

INTRODUCTION

The geysering action of vandalized wells drilled in the late 1950s for geothermal exploration at Beowawe, Nevada, may have been the most spectacular hydrothermal phenomenon created artificially in the United States. The location of the blowing wells, known as The Geysers, is shown in Figure 1. They were spudded in a 1 km long opaline sinter terrace on the south flank of the Whirlwind Valley in Eureka and Lander Counties, Nevada, approximately 50 km east of the town of Battle Mountain. At this time (spring 1981), The Geysers play intermittently.

Struhsacker (1980) gave the most thorough description of the stratigraphic and structural framework of the Beowawe area. Other recent geologic summaries were given in Zoback (1979) and Garside and Schilling (1979). As shown in Figure 1, The Geysers lie along the Malpais fault zone at the base of the Malpais Rim. The steep fault-scarp slope faces north-northwest towards the Whirlwind Valley. Tertiary lava flows and tuffaceous sediments crop out on the Malpais dip slope. The Malpais scarp exposes an older normal fault system, the Dunphy Pass fault zone, that has a northwest trend. This Oligocene to Miocene fault zone forms the eastern margin of a major northwest-trending graben that is part of the southern extension of a 750 km long linear aeromagnetic and structural feature called the Oregon-Nevada lineament (Stewart et al, 1975).

The Tertiary volcanic section within the graben is approximately 1400 m thick; east of the Dunphy Pass fault zone, it is only 100 m thick. The detailed volcanic stratigraphy of Struhsacker (1980) is included in Figure 2. The underlying Ordovician Valmy formation is a shattered sequence of siliceous eugeosynclinal sediments that are part of the Roberts Mountains thrust sheet. Carbonaceous siltstone, chert, and quartzite of the Valmy formation crop out along the Malpais east of the Dunphy Pass fault zone and are encountered by the deep geothermal test wells in the Whirlwind Valley. Tertiary diabase dikes that intrude both the Valmy and the volcanic rocks are thought to be the source for the pronounced aeromagnetic anomaly associated with the Oregon-Nevada Lineament and

Presented at the 50th Annual International SEG Meeting, November 18, 1980, in Houston. Manuscript received by the Editor April 29, 1981; revised manuscript received June 24, 1982.
*Formerly Earth Science Laboratory, University of Utah Research Institute, Salt Lake City; presently Chevron Resources Co., P.O. Box 7147, San Francisco, CA 94107-7147.

alluvium along the buried extension of the Malpais fault zone to the west of The Geysers (Smith, 1979). Since water level and vertical hydraulic gradient data are not available there, it is not possible to decipher the hydrologic system that sustains the high thermal water levels. One plausible flow system would limit the source of thermal water to The Geysers and suggest that it preferentially flows laterally along the fault zone. If this were the case, vertical hydraulic gradient data would probably show only a small vertical component of groundwater flow.

An alternative flow system that would account for the high thermal water levels in the alluvium suggests that the western extension of the Malpais fault zone may be a channel for rising thermal water. If this buried structure were a local source of thermal water, vertical hydraulic gradients along its trace would indicate an upward flow of water.

A few strategically placed piezometers could determine whether the western extension of the Malpais fault zone allows water to rise from depth. If it does, it may prove to be a viable geothermal exploration target or the key to the location of a deep permeable reservoir.

HEAT FLOW

Figure 2 summarizes the mean and standard deviations of the measured thermal conductivities for each of the major rock units in the Beowawe area. All thermal conductivity values were determined using a modified divided bar apparatus at the University of Utah (Chapman et al, 1981). Computations of the thermal conductivities of the 61 drill-chip samples were made using the cell technique of Sass et al (1971b) but were not corrected for in-situ porosity. Uncertainty about the in-situ porosity is the major source of error in the computation of surface heat flow. The porosity of the alluvial and tuffaceous materials may exceed 30 percent; if so, the conductivities mea-

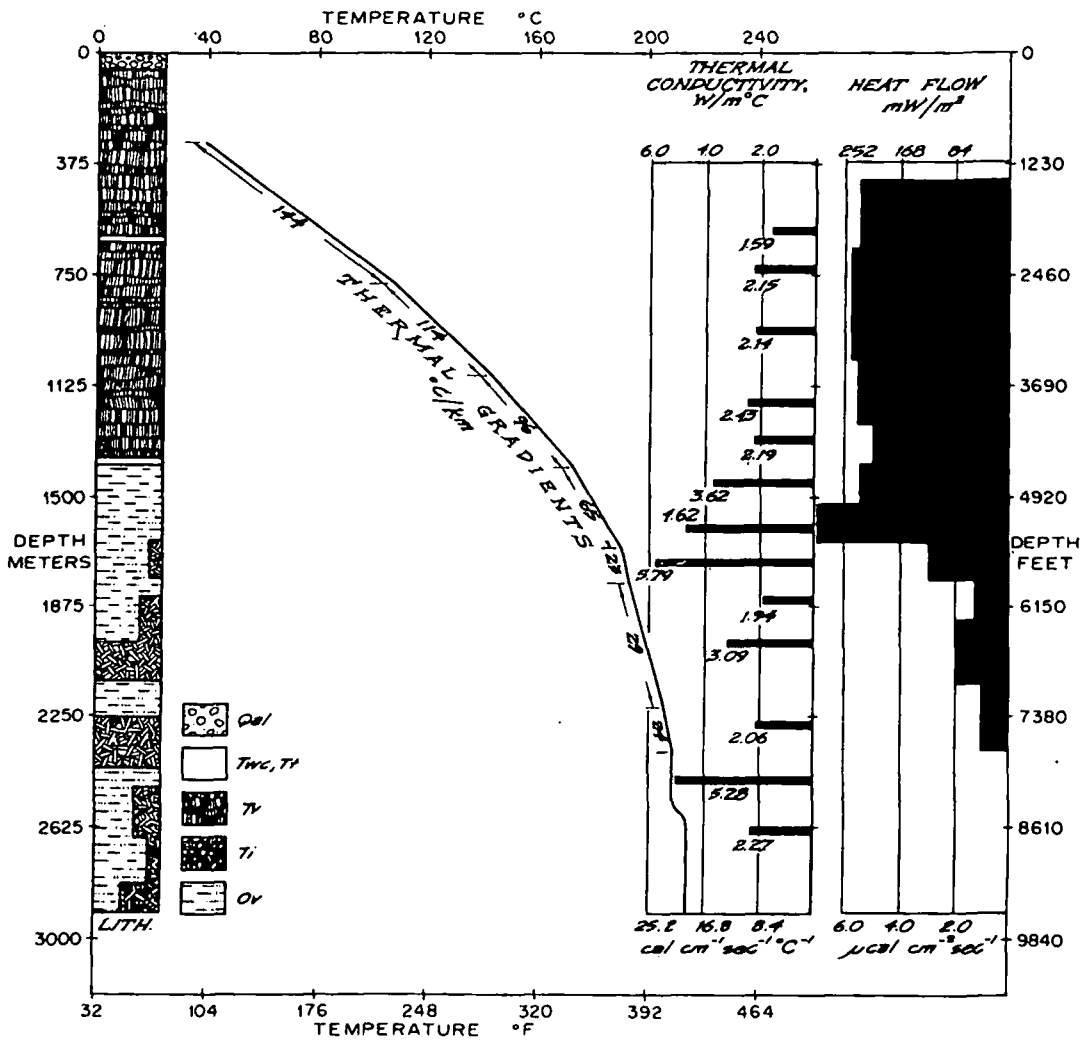

FIG. 10. Generalized lithology, thermal gradients and conductivities, and computed heat flow, Chevron Resources Co. Ginn 1–13 geothermal test well, Whirlwind Valley. Lithologic symbols given in Figure 2.

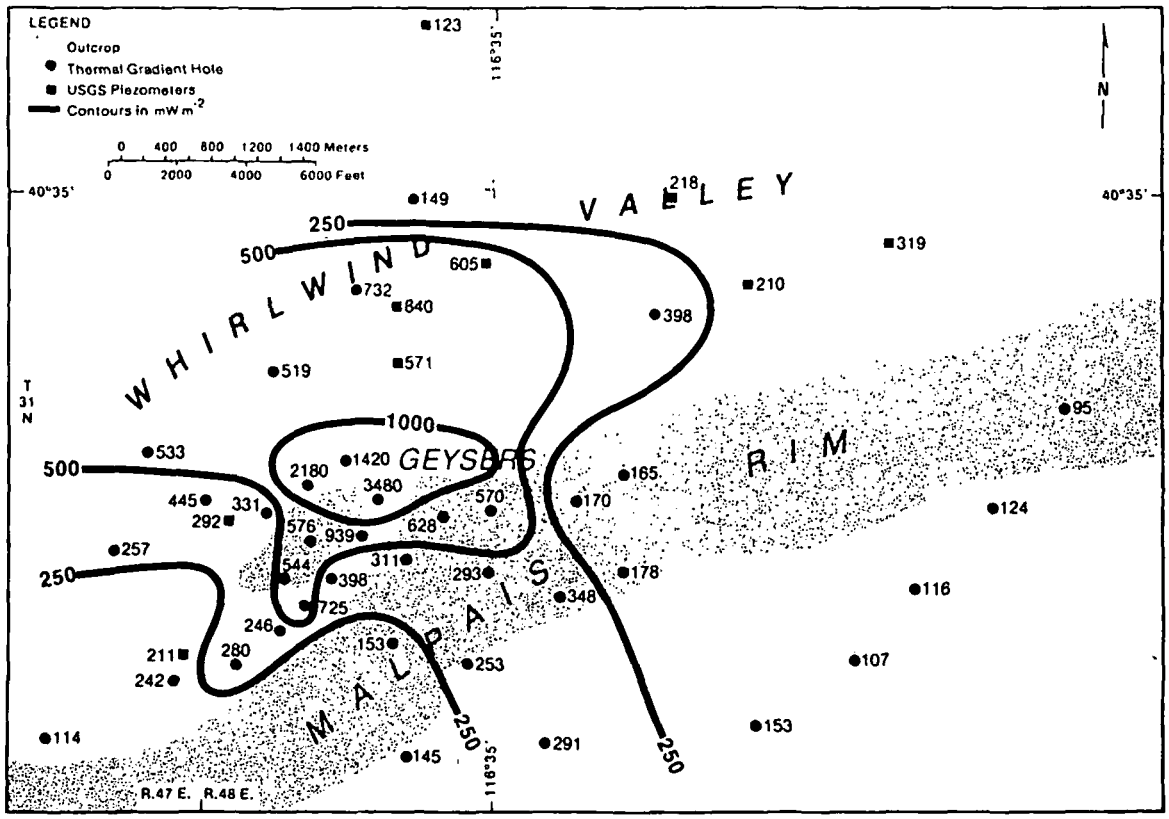

FIG. 11. Map of shallow heat flow, with generalized, variable contour interval in mW/m^2. Discrepancies among neighboring values have been ignored. These differences may be due to the wide range of depths over which the thermal gradient is calculated.

sured for these sedimentary units may be 20–30 percent too large. The matrix porosity of the competent rocks probably averages less than 10 percent and the required correction less than 15 percent.

The low thermal conductivities of the vitrophyric dacite flow and shard-rich tuffaceous sediments reflect their high glass content. The thermal conductivities of the volcanic flow and intrusive rocks cluster around 2 $Wm^{-1}K^{-1}$, but argillization of some of the dacite flows reduces their conductivity significantly. The high thermal conductivity and standard deviation computed for the Valmy formation reflect the preponderance of quartzite in the measured sample and a highly variable lithology.

An equilibrium temperature log of the Ginn 1-13 geothermal test well is shown in Figure 10 (Chevron Resources Co., 1979). The total depth of the well is approximately 2900 m and the bottom-hole temperature 213°C. It is essentially isothermal below a depth of 2400 m within the Valmy formation. Between 1600 and 2400 m, the temperature gradient decreases systematically. The hole either penetrates a hot water-bearing structure or a permeable formation. Given the fractured character of the Valmy (Evans and Theodore, 1978), it is likely that it could contain a high-temperature hydrothermal reservoir.

Above 1600 m, thermal gradients range from 23 to 144°C/km and thermal conductivities from 1.59 to 5.79 $Wm^{-1}K^{-1}$. The inverse relationship between the gradients and conductivities produces a nearly constant conductive heat flow averaging 235 mW/m^2. The uniformity of the heat flow above the inferred deep reservoir indicates that the Tertiary volcanic section acts as a relatively impermeable cap. The thermal water must find permeable structures to rise from depth.

Values of surficial heat flow were computed using linear segments of the shallow temperature-depth profiles like those shown in Figures 6 and 7. As shown in Figure 11, the heat flow generally exceeds the 235 mW/m^2 found in the Ginn test well. Most of the Whirlwind Valley and much of the Malpais Rim appear to receive heat not only from the deep reservoir but also from additional shallower sources. In the Whirlwind Valley, the shallow thermal flow system is a supplemental source of heat.

Along the Malpais Rim, the shallow heat flow exceeds the value from the Ginn well in the area between the two southeast-striking cross faults shown in Figure 1. While it is possible that this area contains conduits for upwelling thermal water, hydraulic head data would be required to resolve whether the fault zone channels water to or away from The Geysers.

A different thermal regime is apparent east of the Dunphy Pass fault zone. Four of the values of heat flow along the Malpais Rim average 110 mW/m^2, near the background value given by Sass et al (1971a) for this portion of the Basin and Range province. The Dunphy Pass fault zone appears to form

the eastern margin of the Beowawe hydrothermal system. The 110 mW/m^2 average value may be realistic for background heat flow.

RECOMMENDATIONS

The hydraulic head of the shallow thermal flow system at Beowawe and most other hydrothermal exploration targets could be readily obtained by converting existing thermal gradient holes to piezometers. The conversion would consist of perforating the casing below the top of the thermal aquifer. In addition, a shallower companion piezometer open below the water table would make it possible to compute the vertical hydraulic gradient at these locations. Even if conduits for upwelling hot water were not located, the hydrologic data would surely augment the existing thermal data and refine the conceptual model of the resource.

Converting ungrouted thermal gradient holes to piezometers may not provide reliable hydraulic head values because of the difficulty of ensuring that the perforated interval is open to only an isolated portion of the aquifer (Benson et al, 1980). However, it should be possible to obtain both hydrologic and thermal data from piezometers that are later converted to thermal gradient holes. In areas where shallow drilling is planned, holes that intersect an aquifer could be initially completed as piezometers. A screen and a wellpoint would be attached to pipe and set at the bottom of the hole, the annulus filled with gravel to the top of the screen and grouted to the surface. After the static hydraulic head is obtained, the screen could be plugged with cement and the hole filled with water, converting it to a thermal gradient hole. Companion piezometers would be needed to obtain vertical hydraulic gradient data. This procedure is recommended as an integral part of future hydrothermal exploration programs.

At any geothermal prospect where drilling encounters water, the water is a source of data. The hydrologic-thermal field procedure recommended here requires repeated site visits and the drilling and completion of additional shallow, thin holes. This expanded exploration program is predicated on the assumption that it is worthwhile to gather as much meaningful data as possible at a reasonable price. The possibility of locating viable deep drilling targets with groundwater hydrology should encourage geothermal exploration managers to incorporate hydrologic data acquisition in their exploration plans.

ACKNOWLEDGMENTS

Funding for this project at the Earth Science Laboratory of the Univ. of Utah Research Institute came from the Dept. of Energy/Division of Geothermal Industry Coupled Program contract DE-AC07-80ID12079. E. M. Struhsacker and J. L. Iovenitti provided geologic guidance. F. H. Olmsted and M. L. Sorey of the U.S. Geol. Survey contributed piezometer data and excellent reviews. Dr. David Chapman and Dr. Leslie Smith of the University of Utah helped develop the ideas about combining thermal and groundwater data.

REFERENCES

Benson, S., Goranson, C., Noble, J., Schroder, R., Corrigan, D., and Wollenberg, H., 1980, Evaluation of the Susanville, California geothermal resource: Lawrence Berkeley lab rep. LBL-1187, 100 p.

Chapman, D. S., Clement, M. D., and Mase, C. W., 1981, Thermal regime of the Escalante Desert, Utah, with an analysis of the Newcastle geothermal system: J. Geophys. Res., v. 82, p. 11735–11746.

Chevron Resources Co., 1979, Open-file data released by Earth Science Laboratory, Salt Lake City.

Evans, S. G., and Theodore, T. G., 1978, Deformation of the Roberts Mountains allochthon in north-central Nevada: U.S.G.S. prof. paper 1060, 18 p.

Freeze, R. A., and Cherry, J. A., 1979, Groundwater: Englewood Cliffs, New Jersey, 604 p., Prentice-Hall, Inc.

Garside, L. J., and Schilling, J. H., 1979, Thermal waters of Nevada: Nevada Bur. Mines Geol., Bull. 91, 163 p.

Getty Oil Co., 1981, Open-file data released by Earth Science Laboratory, Salt Lake City, Utah.

Hubbert, M. K., 1940, The theory of groundwater motion: J. Geology, v. 48, p. 785–944.

Oesterling, W. A., 1962, Geothermal power potential of northern Nevada: Southern Pacific Co. report.

Robinson, E. S., 1970, Relations between geologic structure and aeromagnetic anomalies in central Nevada: GSA Bull., v. 81, p. 2045–2060.

Sass, J. H., Lachenbruch, A. H., Munroe, R. J., Greene, G. W., and Moses, T. H., Jr., 1971a, Heat flow in the western United States: J. Geophys. Res., v. 76, p. 6376–6413.

Sass, J. H., Lachenbruch, A. H., and Munroe, R. J., 1971b, Thermal conductivity of rocks from measurements on fragments and its application to heat flow measurements: J. Geophys. Res., v. 76, p. 3391–3401.

Smith, C., 1979, Interpretation of electrical resistivity and shallow seismic reflection profiles, Whirlwind Valley and Horse Heaven areas, Beowawe KGRA, Nevada: Univ. of Utah Research Inst., Earth Science Lab, rep. no. 25, 43 p.

Sorey, M. L., 1971, Measurement of vertical groundwater velocity from temperature profiles in wells: Water Resources Res., v. 7, p. 963–970.

Stewart, J. H., Walker, G. W., and Kleinhampl, F. J., 1975, Oregon-Nevada lineament: Geology, v. 3, p. 265–268.

Struhsacker, E. M., 1980, The Geology of the Beowawe geothermal system, Eureka and Lander counties, Nevada: Univ. of Utah Research Inst., Earth Science Lab, rep. no. 37, 78 p.

Welch, A. H., Sorey, M. L., and Olmsted, F. H., 1981, The hydrothermal system in Southern Grass Valley, Pershing County, Nevada: U.S.G.S. open-file rep. 81-915, 193 p.

Zoback, M. L. C., 1979, A geologic and geophysical investigation of the Beowawe geothermal area, north-central Nevada: Stanford Univ. Publ., Geological Sciences, v. 16, 79 p.

GEOPHYSICS, VOL. 48, NO. 5 (MAY 1983); P. 618–626, 11 FIGS.

Thermal hydrology and heat flow of Beowawe geothermal area, Nevada

Christian Smith*

ABSTRACT

Inflections in temperature-depth profiles from forty 150 m thermal gradient holes define a shallow thermal flow system in the Whirlwind Valley near the Beowawe Geysers. U.S. Geological Survey hydrologic data reveal the vertical and west-to-east components of cold water flow at the water table above the thermal flow system. The temperature inflections break most abruptly in areas with a downward component of flow at the water table. The inflections are thought to indicate the level where the buoyant thermal water maintains a dynamic equilibrium with the overlying cold water. Combining these geophysical and hydrologic data suggests areas away from The Geysers where thermal water may rise from the deep reservoir into the alluvium. These leakage areas may be viable geothermal exploration targets. Even if the temperatures of the leakage were subeconomic, knowledge of where upwelling occurs could be helpful in assessing the potential for energy production. The systematic acquisition of hydrologic data is recommended as a standard component of hydrothermal resource exploration programs.

Measurements of thermal conductivity from chip samples from the shallow holes and from Chevron Resources Company's Ginn 1-13 geothermal exploration hole (2917 m T.D.) enable inferences based on heat flow. The average heat flow east of the Dunphy Pass fault zone, 110 mW/m^2, may be representative of background in this portion of the Battle Mountain high heat flow province. Thermal gradient and conductivity data from the deep well have a wide range of values (65–144°C/km, 1.59–5.95 $Wm^{-1}K^{-1}$) but produce a relatively constant heat flow of 235 mW/m^2 above a depth of 1600 m. The shallow data indicate that the area with similarly high surficial heat flow extends as far east as the Dunphy Pass fault zone, suggesting that this Miocene rift boundary may form the eastern margin of the Beowawe hydrothermal system.

INTRODUCTION

The geysering action of vandalized wells drilled in the late 1950s for geothermal exploration at Beowawe, Nevada, may have been the most spectacular hydrothermal phenomenon created artificially in the United States. The location of the blowing wells, known as The Geysers, is shown in Figure 1. They were spudded in a 1 km long opaline sinter terrace on the south flank of the Whirlwind Valley in Eureka and Lander Counties, Nevada, approximately 50 km east of the town of Battle Mountain. At this time (spring 1981), The Geysers play intermittently.

Struhsacker (1980) gave the most thorough description of the stratigraphic and structural framework of the Beowawe area. Other recent geologic summaries were given in Zoback (1979) and Garside and Schilling (1979). As shown in Figure 1, The Geysers lie along the Malpais fault zone at the base of the Malpais Rim. The steep fault-scarp slope faces north-northwest towards the Whirlwind Valley. Tertiary lava flows and tuffaceous sediments crop out on the Malpais dip slope. The Malpais scarp exposes an older normal fault system, the Dunphy Pass fault zone, that has a northwest trend. This Oligocene to Miocene fault zone forms the eastern margin of a major northwest-trending graben that is part of the southern extension of a 750 km long linear aeromagnetic and structural feature called the Oregon-Nevada lineament (Stewart et al, 1975).

The Tertiary volcanic section within the graben is approximately 1400 m thick; east of the Dunphy Pass fault zone, it is only 100 m thick. The detailed volcanic stratigraphy of Struhsacker (1980) is included in Figure 2. The underlying Ordovician Valmy formation is a shattered sequence of siliceous eugeosynclinal sediments that are part of the Roberts Mountains thrust sheet. Carbonaceous siltstone, chert, and quartzite of the Valmy formation crop out along the Malpais east of the Dunphy Pass fault zone and are encountered by the deep geothermal test wells in the Whirlwind Valley. Tertiary diabase dikes that intrude both the Valmy and the volcanic rocks are thought to be the source for the pronounced aeromagnetic anomaly associated with the Oregon-Nevada Lineament and

Presented at the 50th Annual International SEG Meeting, November 18, 1980, in Houston. Manuscript received by the Editor April 29, 1981; revised manuscript received June 24, 1982.
*Formerly Earth Science Laboratory, University of Utah Research Institute, Salt Lake City; presently Chevron Resources Co., P.O. Box 7147, San Francisco, CA 94107-7147.

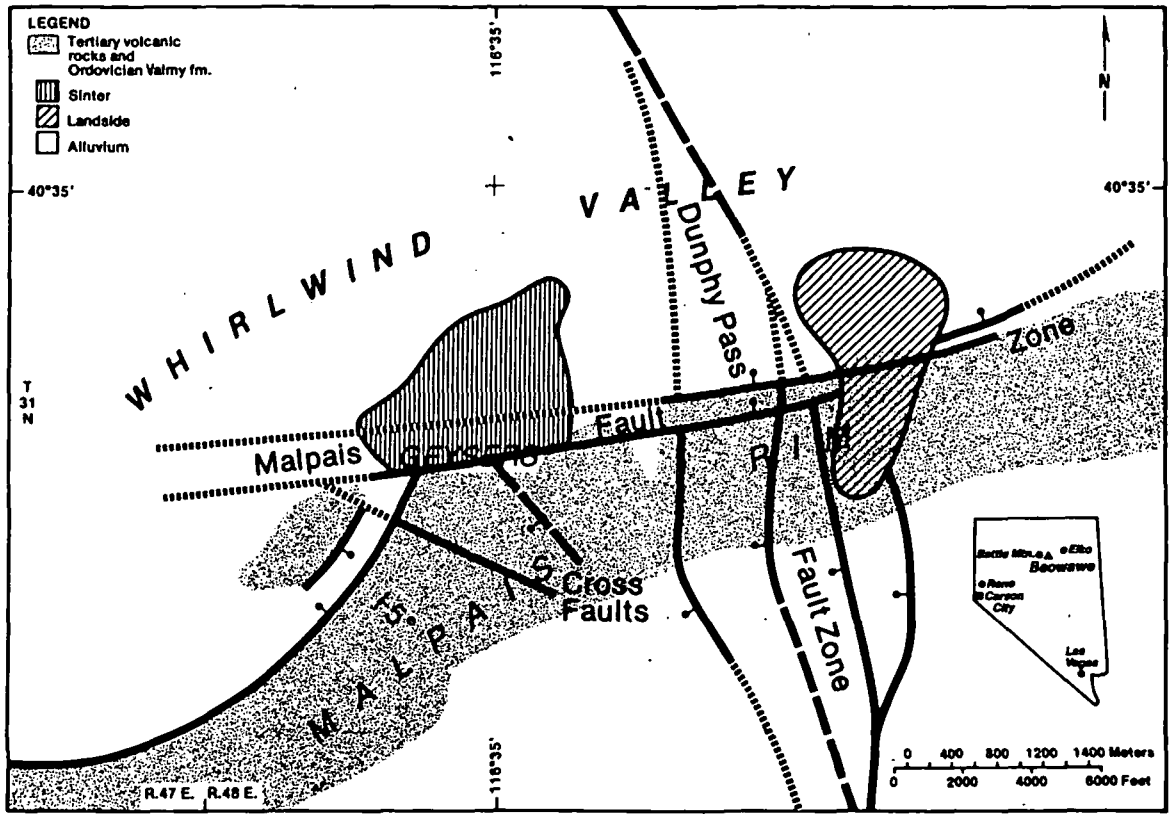

FIG. 1. Location and generalized structure of the Beowawe area (after Struhsacker, 1980).

the feeders for the Tertiary volcanic sequence filling the graben (Robinson, 1970).

In the 1970s, exploration for a hydrothermal resource capable of sustaining electrical power generation was conducted by Chevron Resources Co. and Getty Oil Co. Much of their geophysical data has been acquired and made available through the Dept. of Energy, Division of Geothermal Energy Industry Coupled Program (Chevron Resources Co., 1979; Getty Oil Co., 1981). Included in these data packages are the temperature-depth profiles and drill-chip cuttings from the forty 150 m thermal gradient holes shown in Figure 3. The temperature-depth profiles provide a three-dimensional (3-D) view of the coupled heat and water flow in the shallow subsurface. Mapping these flows can contribute to the exploration effort by locating upflow zones or widespread horizons with enhanced permeability.

THERMAL HYDROLOGY

The geothermal industry has generally neglected to include groundwater studies in their exploration programs even though water is the resource being sought. The typical program has looked at water only with an eye to its chemistry. Geothermal exploration geophysicists can remedy this omission by including piezometers in their shallow drilling plans.

A piezometer is a small-diameter pipe open to a waterbearing formation at one depth only, generally at the bottom, as schematically shown in Figure 4. The annulus between the drilled hole and the pipe or casing is usually grouted to ensure that there can be no vertical fluid flow within the hole. The elevation at which water stands in the piezometer indicates the total hydraulic head at the point of measurement. The hydraulic head H is the sum of two components, the pressure head $P/\rho g$ and the elevation head z:

$$H = z + \frac{P}{\rho g}, \tag{1}$$

where z is the elevation above an arbitrary datum (usually sea level), P is the fluid pressure, ρ the fluid density at ambient temperature, and g the acceleration due to gravity.

Under nonisothermal conditions, observed head values are corrected for density differences. In most groundwater studies these differences are small enough to be neglected. At geothermal areas with cold water aquifers, the less-dense thermal water generally plumes upward to float on the colder water or emerge as hot springs. Where the thermal water is not sufficiently hot and buoyant, the weight of the overlying cold water may hold it down. The result can be a temperature inversion within the aquifer.

Water flows from areas of higher hydraulic head to areas of lower hydraulic head. Figure 4 is a sketch of the relation given

MAP CODE		LITHOLOGIC UNIT	THERMAL CONDUCTIVITY Mean ± Std. Dev. ($W \cdot m^{-1} K^{-1}$)	NUMBER SAMPLES
Qs		Opaline Sinter	——	——
Qls		Landslide	——	——
Qal		Alluvium	1.68 ± 0.11	8
Tv	Tg	Coarse Gravel	1.60	1
	Tb	Basalt	1.60	2
	Twc	Tuffaceous Sediment of White Canyon		
		glassy	1.33 ± 0.12	3
		silty	1.65 ± 0.08	9
	Td	Dacite		
		porphyritic	2.02 ± 0.13	9
		vitrophyric	1.20	2
		argillized	1.67 ± 0.22	4
	Tba	Basaltic Andesite	2.26 ± 0.06	5
	Tts	Early tuffaceous material	1.58 ± 0.01	4
	Tha	Hornblende Andesite	1.90 ± 0.17	5
	Ti	Diabase dikes	2.09 ± 0.17	3
Ov		Valmy Formation	4.44 ± 1.01	6

FIG. 2. Stratigraphy of Beowawe area with measured thermal conductivity values.

by equation (1). The elevations of standing water (corrected for temperature where necessary) in a number of piezometers completed in the same horizon and distributed over an area, as in Figures 5a and 5b, are used to produce maps of hydraulic head. The differences in water levels seen in plan view can be used to compute the horizontal component of hydraulic gradient and, in isotropic media, the direction of water flow.

A cross-section of hydraulic heads can be generated if water levels are measured in adjacent piezometers completed at different depths, illustrated by Figures 5c and 5d. The difference in elevation of standing water in adjacent piezometers can be used to compute the vertical hydraulic gradient. Since elevation is positive upward, a negative vertical hydraulic gradient implies that there is a downward component of groundwater flow at that location. A positive value is computed wherever water rises from depth.

In areas where water flow affects heat flow, hydraulic head data should be able to delineate zones of upwelling hot water. Since hot water is the hydrothermal resource, water levels and vertical hydraulic gradient data should be gathered as part of any geothermal exploration program. Data from Beowawe demonstrate the utility of incorporating groundwater hydrology into thermal gradient surveys.

BEOWAWE GROUNDWATER

The U.S. Geological Survey, Water Resources Division, has drilled piezometers at several northern Nevada geothermal areas (e.g., Welch et al, 1981). Their data for the water table in the Whirlwind Valley are shown in Figure 3. The elevation of the water table appears to decrease systematically down the valley from west to east, reflecting the topography. It is within a few meters of the surface in the center of the valley. Much of the groundwater in the valley is presumably discharged by evapotranspiration at a playa lake beyond the eastern edge of Figure 3. Some may reach the Humboldt River farther to the east.

Water levels in the paired piezometers allow the computation of the vertical hydraulic gradient. Near The Geysers the vertical gradients are negative; water at the water table flows downward as well as toward the center of the valley. The

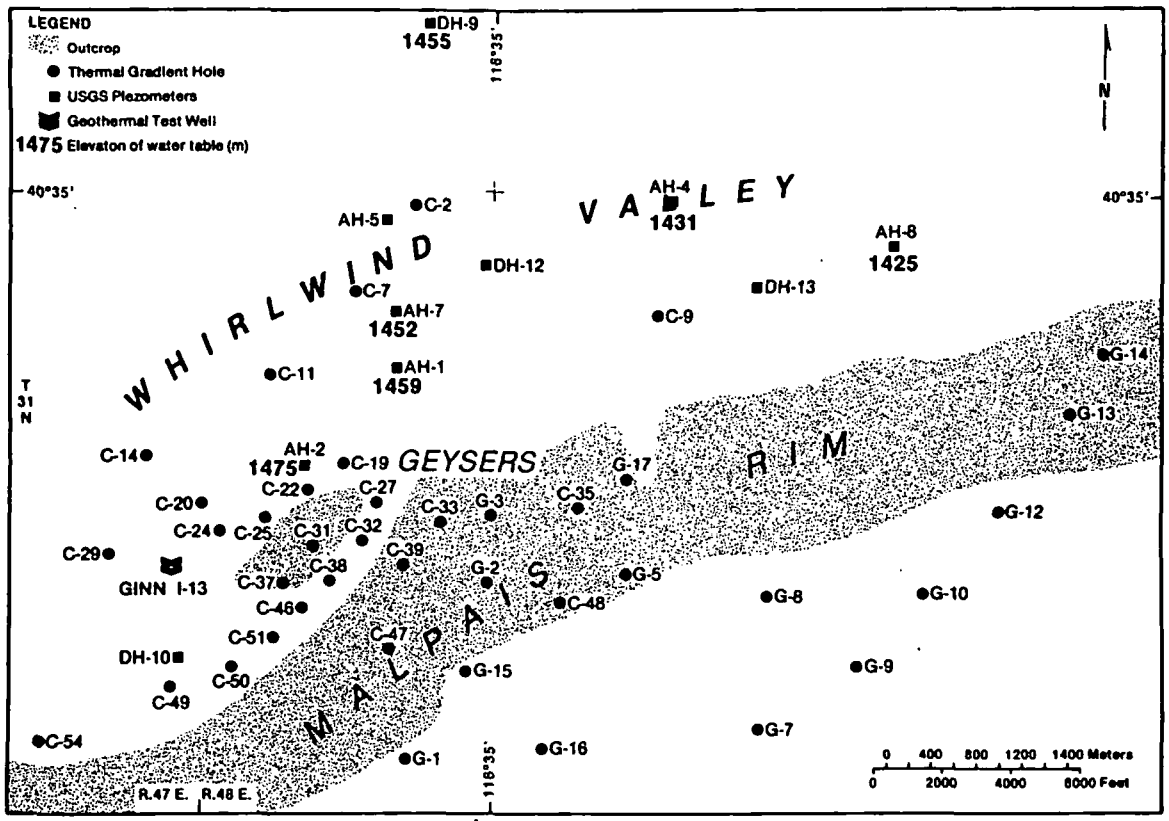

FIG. 3. Map of Beowawe area showing thermal gradient holes, piezometers, and elevation of water table.

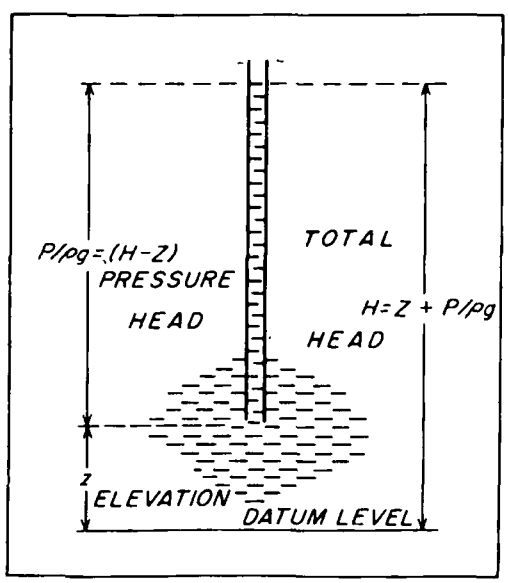

FIG. 4. Relation between total head, pressure head, and elevation (after Hubbert, 1940).

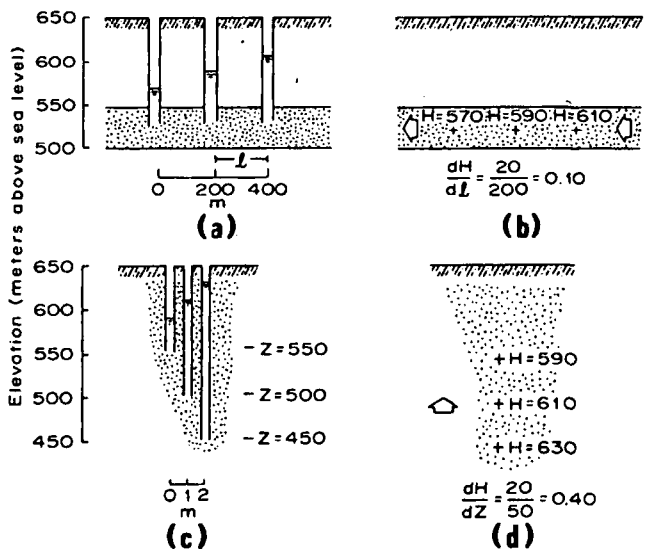

FIG. 5. Theoretical cross-section showing piezometers, head distribution, flow pattern, and hydraulic gradients (after Freeze and Cherry, 1979).

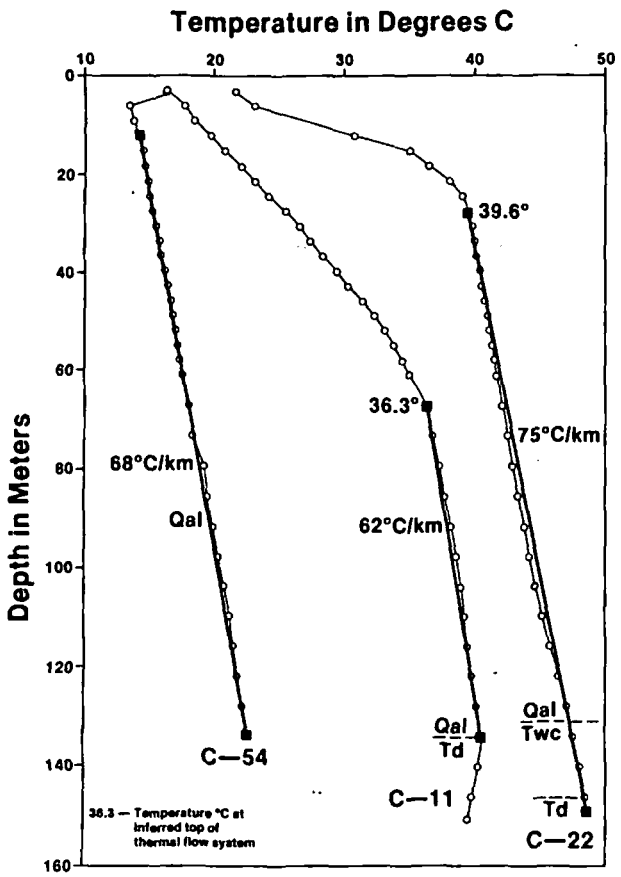

FIG. 6. Temperature-depth profiles with similar thermal gradients, Whirlwind Valley, with inferred depths to top of thermal flow system. Lithologic symbols given in Figure 2.

vertical gradient is positive in the piezometer pairs in the center of the valley. In this area, water flows upward as well as eastward, perhaps responding to evaporation at the water table.

The vertical flow measured in the shallow piezometers is indicated at greater depths by curvature and inflections in temperature-depth profiles. Figure 6 presents examples. Hole C-22 is near piezometer pair AH-2 which has a strong negative gradient; its temperature profile is concave upward, reflecting the downward flow of water (Sorey, 1971). Upward fluid flow is shown by the concave downward profile of hole C-11 near the center of the valley.

The 68°C/km gradient in hole C-54 is similar to those in holes C-11 and C-22, but its linearity for the length of the hole and low temperature are unlike the other profiles in Figure 6. The temperature-depth profile in hole C-54 is one of the few in the Whirlwind Valley that shows little disturbance by groundwater flow and may be representative of regional conductive heat flow. If 68°C/km were a background gradient in alluvium, the regional conductive heat flow would be approximately 118 mW/m^2. This heat flow is within the range of values given by Sass et al (1971a) for this portion of the Basin and Range province, allowing hole C-54 to serve as the reference for an arbitrary definition of *cold* and *thermal* for the Beowawe area: water less than 7°C above the temperature in C-54 at the same

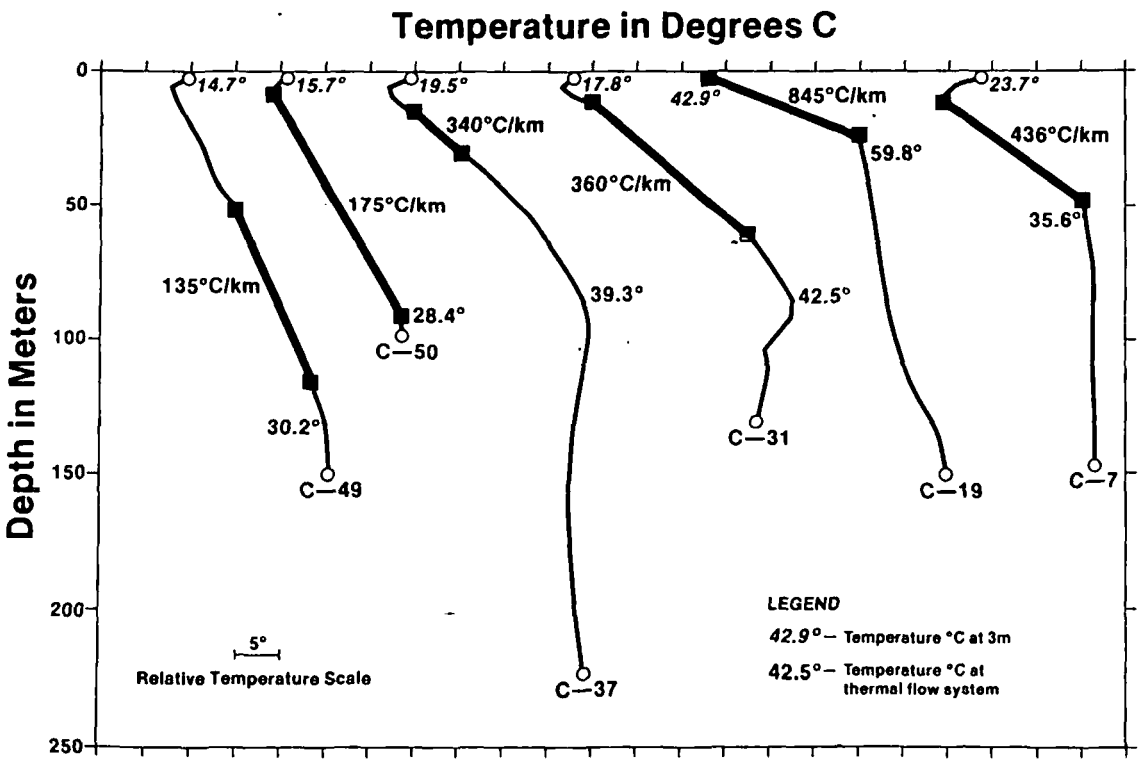

FIG. 7. Representative temperature-depth profiles in Whirlwind Valley.

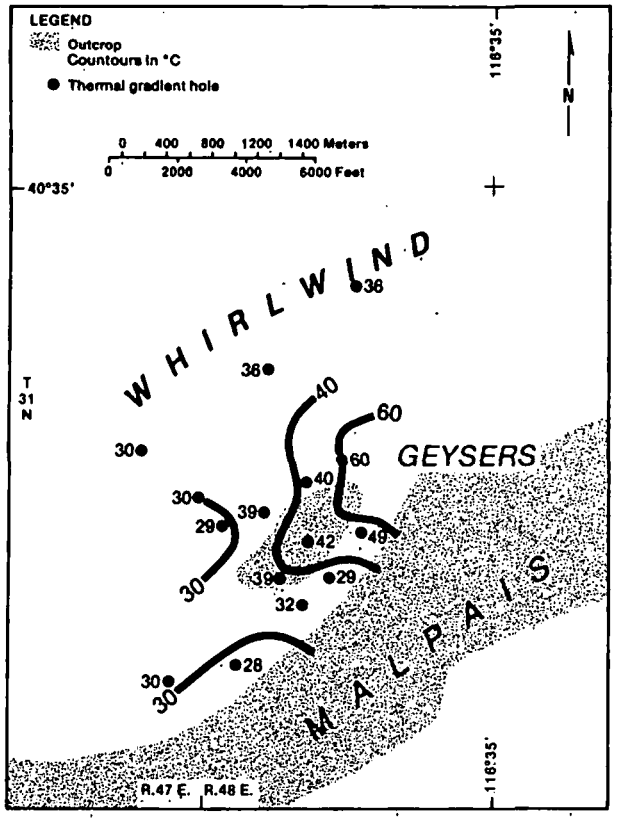

FIG. 8. Map of temperature at top of thermal flow system, contours in °C.

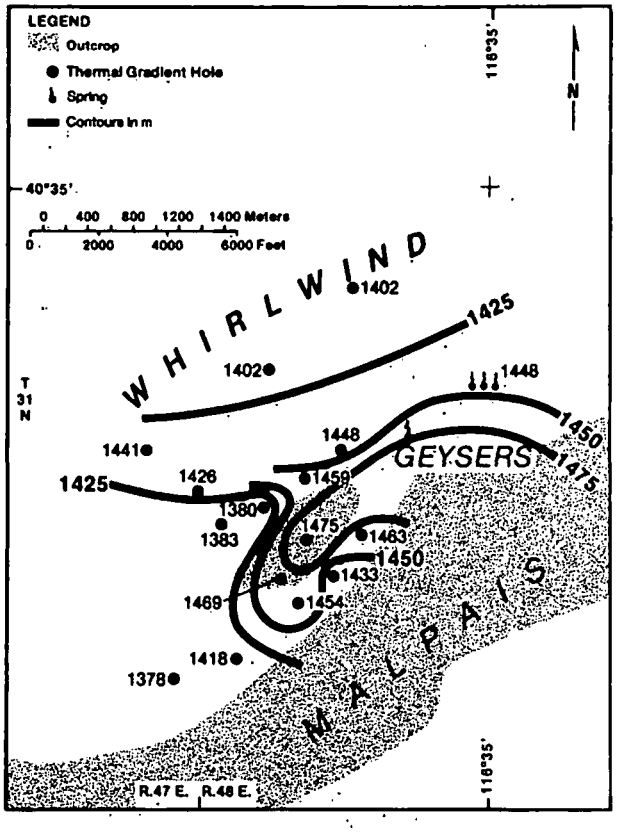

FIG. 9. Map of elevation at top of thermal flow system, contours in meters.

depth is said to be cold; water at higher temperatures is thermal.

Many of the temperature-depth profiles in the Whirlwind Valley contain abrupt downward inflections that are diagnostic of vertical transport of heat by groundwater. The inflections occur at depths ranging between 24 and 134 m and at temperatures from 28°C to 60°C. The relative temperature scale of Figure 7 is used to avoid overlap of several of these profiles. The inflections are keyed with their temperatures. Including the measured temperature at the shallowest depth permits the reconstruction of the actual temperature profiles.

The inflections in the temperature profiles are caused by fluid flow largely within the open annulus of these economically completed exploration holes. To minimize drilling costs, the annulus between the 0.12 m (4.75 inch) drilled hole and the 0.03 m (1 inch) pipe was not grouted. This method of hole completion is not recommended because the open hole forms a conduit for vertical flow. The annulus becomes a poor piezometer, open to the formation over the length of the hole instead of at one isolated interval. Differences in hydraulic head within the formation drive the vertical flow. The temperature inflections are interpreted to occur where the buoyant head of thermal water balances the gravitational head of the column of cold water above. They indicate the level where a dynamic equilibrium is maintained in the hole between rising thermal water and heavier cold water. Their depths probably do not strictly correlate to the top of a particular aquifer or to a true hydraulic head. These data are not optimal but they are usable. They form a mappable horizon interpreted to represent the top of the thermal flow system.

Figure 8 is an illustration of the temperature at the top of the thermal flow system as inferred from inflections like those in Figures 6 and 7. The hot springs around the base of the sinter terrace at The Geysers provide additional data. The near radial symmetry of the temperature distribution suggests that the area of The Geysers contains the principal source of thermal water flowing into the alluvium of the Whirlwind Valley. This symmetry also suggests that the temperature inflections reveal a single, laterally continuous flow system.

The elevation of the top of the thermal flow system is shown in Figure 9. These elevations cannot be corrected for density since the thermal gradient holes are not true piezometers and the inflections are not true hydraulic heads. The contours of Figure 9 reveal the levels to which the buoyant water rises. They reflect neither the radial pattern of the temperature map nor the west-to-east hydraulic gradient of the water table. Thermal water levels are higher within the bedrock southwest of The Geysers than they are in the adjacent alluvium. The high water levels may indicate that upwelling occurs in this area. It is also possible that water from The Geysers is perched above a less permeable horizon of volcanic rock.

Relatively high thermal water levels are sustained within the

alluvium along the buried extension of the Malpais fault zone to the west of The Geysers (Smith, 1979). Since water level and vertical hydraulic gradient data are not available there, it is not possible to decipher the hydrologic system that sustains the high thermal water levels. One plausible flow system would limit the source of thermal water to The Geysers and suggest that it preferentially flows laterally along the fault zone. If this were the case, vertical hydraulic gradient data would probably show only a small vertical component of groundwater flow.

An alternative flow system that would account for the high thermal water levels in the alluvium suggests that the western extension of the Malpais fault zone may be a channel for rising thermal water. If this buried structure were a local source of thermal water, vertical hydraulic gradients along its trace would indicate an upward flow of water.

A few strategically placed piezometers could determine whether the western extension of the Malpais fault zone allows water to rise from depth. If it does, it may prove to be a viable geothermal exploration target or the key to the location of a deep permeable reservoir.

HEAT FLOW

Figure 2 summarizes the mean and standard deviations of the measured thermal conductivities for each of the major rock units in the Beowawe area. All thermal conductivity values were determined using a modified divided bar apparatus at the University of Utah (Chapman et al, 1981). Computations of the thermal conductivities of the 61 drill-chip samples were made using the cell technique of Sass et al (1971b) but were not corrected for in-situ porosity. Uncertainty about the in-situ porosity is the major source of error in the computation of surface heat flow. The porosity of the alluvial and tuffaceous materials may exceed 30 percent; if so, the conductivities mea-

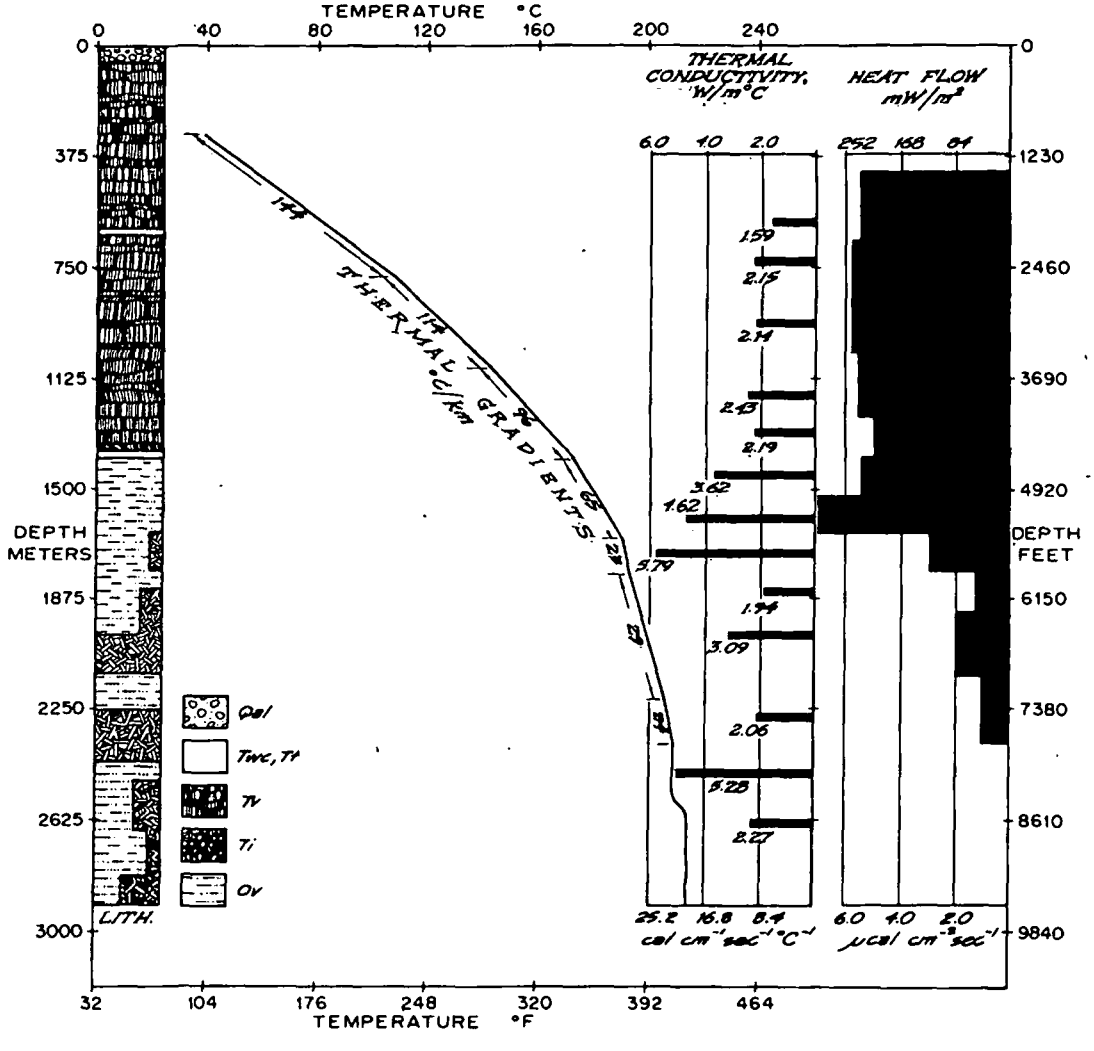

FIG. 10. Generalized lithology, thermal gradients and conductivities, and computed heat flow, Chevron Resources Co. Ginn 1–13 geothermal test well, Whirlwind Valley. Lithologic symbols given in Figure 2.

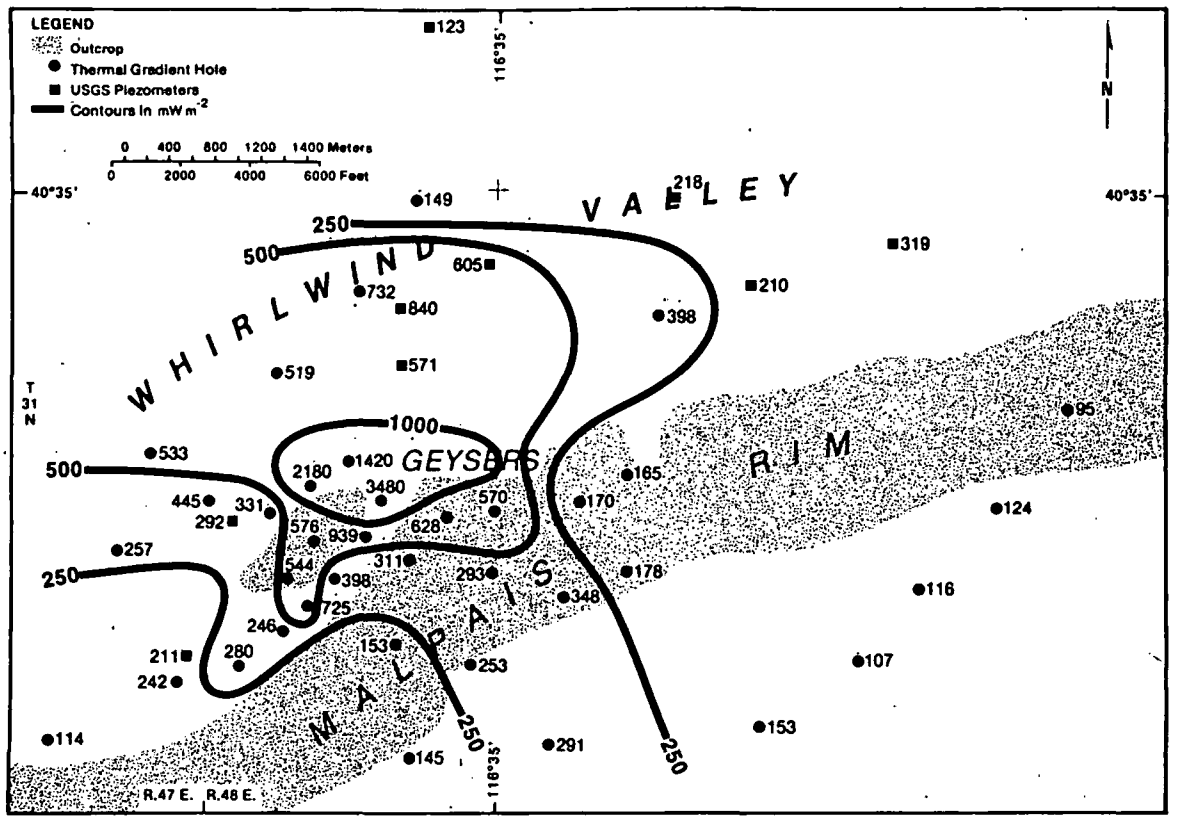

FIG. 11. Map of shallow heat flow, with generalized, variable contour interval in mW/m^2. Discrepancies among neighboring values have been ignored. These differences may be due to the wide range of depths over which the thermal gradient is calculated.

sured for these sedimentary units may be 20–30 percent too large. The matrix porosity of the competent rocks probably averages less than 10 percent and the required correction less than 15 percent.

The low thermal conductivities of the vitrophyric dacite flow and shard-rich tuffaceous sediments reflect their high glass content. The thermal conductivities of the volcanic flow and intrusive rocks cluster around 2 $Wm^{-1}K^{-1}$, but argillization of some of the dacite flows reduces their conductivity significantly. The high thermal conductivity and standard deviation computed for the Valmy formation reflect the preponderance of quartzite in the measured sample and a highly variable lithology.

An equilibrium temperature log of the Ginn 1-13 geothermal test well is shown in Figure 10 (Chevron Resources Co., 1979). The total depth of the well is approximately 2900 m and the bottom-hole temperature 213°C. It is essentially isothermal below a depth of 2400 m within the Valmy formation. Between 1600 and 2400 m, the temperature gradient decreases systematically. The hole either penetrates a hot water-bearing structure or a permeable formation. Given the fractured character of the Valmy (Evans and Theodore, 1978), it is likely that it could contain a high-temperature hydrothermal reservoir.

Above 1600 m, thermal gradients range from 23 to 144°C/km and thermal conductivities from 1.59 to 5.79 $Wm^{-1}K^{-1}$. The inverse relationship between the gradients and conductivities produces a nearly constant conductive heat flow averaging 235 mW/m^2. The uniformity of the heat flow above the inferred deep reservoir indicates that the Tertiary volcanic section acts as a relatively impermeable cap. The thermal water must find permeable structures to rise from depth.

Values of surficial heat flow were computed using linear segments of the shallow temperature-depth profiles like those shown in Figures 6 and 7. As shown in Figure 11, the heat flow generally exceeds the 235 mW/m^2 found in the Ginn test well. Most of the Whirlwind Valley and much of the Malpais Rim appear to receive heat not only from the deep reservoir but also from additional shallower sources. In the Whirlwind Valley, the shallow thermal flow system is a supplemental source of heat.

Along the Malpais Rim, the shallow heat flow exceeds the value from the Ginn well in the area between the two southeast-striking cross faults shown in Figure 1. While it is possible that this area contains conduits for upwelling thermal water, hydraulic head data would be required to resolve whether the fault zone channels water to or away from The Geysers.

A different thermal regime is apparent east of the Dunphy Pass fault zone. Four of the values of heat flow along the Malpais Rim average 110 mW/m^2, near the background value given by Sass et al (1971a) for this portion of the Basin and Range province. The Dunphy Pass fault zone appears to form

the eastern margin of the Beowawe hydrothermal system. The 110 mW/m^2 average value may be realistic for background heat flow.

RECOMMENDATIONS

The hydraulic head of the shallow thermal flow system at Beowawe and most other hydrothermal exploration targets could be readily obtained by converting existing thermal gradient holes to piezometers. The conversion would consist of perforating the casing below the top of the thermal aquifer. In addition, a shallower companion piezometer open below the water table would make it possible to compute the vertical hydraulic gradient at these locations. Even if conduits for upwelling hot water were not located, the hydrologic data would surely augment the existing thermal data and refine the conceptual model of the resource.

Converting ungrouted thermal gradient holes to piezometers may not provide reliable hydraulic head values because of the difficulty of ensuring that the perforated interval is open to only an isolated portion of the aquifer (Benson et al, 1980). However, it should be possible to obtain both hydrologic and thermal data from piezometers that are later converted to thermal gradient holes. In areas where shallow drilling is planned, holes that intersect an aquifer could be initially completed as piezometers. A screen and a wellpoint would be attached to pipe and set at the bottom of the hole, the annulus filled with gravel to the top of the screen and grouted to the surface. After the static hydraulic head is obtained, the screen could be plugged with cement and the hole filled with water, converting it to a thermal gradient hole. Companion piezometers would be needed to obtain vertical hydraulic gradient data. This procedure is recommended as an integral part of future hydrothermal exploration programs.

At any geothermal prospect where drilling encounters water, the water is a source of data. The hydrologic-thermal field procedure recommended here requires repeated site visits and the drilling and completion of additional shallow, thin holes. This expanded exploration program is predicated on the assumption that it is worthwhile to gather as much meaningful data as possible at a reasonable price. The possibility of locating viable deep drilling targets with groundwater hydrology should encourage geothermal exploration managers to incorporate hydrologic data acquisition in their exploration plans.

ACKNOWLEDGMENTS

Funding for this project at the Earth Science Laboratory of the Univ. of Utah Research Institute came from the Dept. of Energy/Division of Geothermal Industry Coupled Program contract DE-AC07-80ID12079. E. M. Struhsacker and J. L. Iovenitti provided geologic guidance. F. H. Olmsted and M. L. Sorey of the U.S. Geol. Survey contributed piezometer data and excellent reviews. Dr. David Chapman and Dr. Leslie Smith of the University of Utah helped develop the ideas about combining thermal and groundwater data.

REFERENCES

Benson, S., Goranson, C., Noble, J., Schroder, R., Corrigan, D., and Wollenberg, H., 1980, Evaluation of the Susanville, California geothermal resource: Lawrence Berkeley lab rep. LBL-1187, 100 p.

Chapman, D. S., Clement, M. D., and Mase, C. W., 1981, Thermal regime of the Escalante Desert, Utah, with an analysis of the Newcastle geothermal system: J. Geophys. Res., v. 82, p. 11735–11746.

Chevron Resources Co., 1979, Open-file data released by Earth Science Laboratory, Salt Lake City.

Evans, S. G., and Theodore, T. G., 1978, Deformation of the Roberts Mountains allochthon in north-central Nevada: U.S.G.S. prof. paper 1060, 18 p.

Freeze, R. A., and Cherry, J. A., 1979, Groundwater: Englewood Cliffs, New Jersey, 604 p., Prentice-Hall, Inc.

Garside, L. J., and Schilling, J. H., 1979, Thermal waters of Nevada: Nevada Bur. Mines Geol., Bull. 91, 163 p.

Geity Oil Co., 1981, Open-file data released by Earth Science Laboratory, Salt Lake City, Utah.

Hubbert, M. K., 1940, The theory of groundwater motion: J. Geology, v. 48, p. 785–944.

Oesterling, W. A., 1962, Geothermal power potential of northern Nevada: Southern Pacific Co. report.

Robinson, E. S., 1970, Relations between geologic structure and aeromagnetic anomalies in central Nevada: GSA Bull., v. 81, p. 2045–2060.

Sass, J. H., Lachenbruch, A. H., Munroe, R. J., Greene, G. W., and Moses, T. H., Jr., 1971a, Heat flow in the western United States: J. Geophys. Res., v. 76, p. 6376–6413.

Sass, J. H., Lachenbruch, A. H., and Munroe, R. J., 1971b, Thermal conductivity of rocks from measurements on fragments and its application to heat flow measurements: J. Geophys. Res., v. 76, p. 3391–3401.

Smith, C., 1979, Interpretation of electrical resistivity and shallow seismic reflection profiles, Whirlwind Valley and Horse Heaven areas, Beowawe KGRA, Nevada: Univ. of Utah Research Inst., Earth Science Lab, rep. no. 25, 43 p.

Sorey, M. L., 1971, Measurement of vertical groundwater velocity from temperature profiles in wells: Water Resources Res., v. 7, p. 963–970.

Stewart, J. H., Walker, G. W., and Kleinhampl, F. J., 1975, Oregon-Nevada lineament: Geology, v. 3, p. 265–268.

Struhsacker, E. M., 1980, The Geology of the Beowawe geothermal system, Eureka and Lander counties, Nevada: Univ. of Utah Research Inst., Earth Science Lab, rep. no. 37, 78 p.

Welch, A. H., Sorey, M. L., and Olmsted, F. H., 1981, The hydrothermal system in Southern Grass Valley, Pershing County, Nevada: U.S.G.S. open-file rep. 81-915, 193 p.

Zoback, M. L. C., 1979, A geologic and geophysical investigation of the Beowawe geothermal area, north-central Nevada: Stanford Univ. Publ., Geological Sciences, v. 16, 79 p.

Geothermal Resources Council, TRANSACTIONS Vol. 6, October 1982

DEVELOPMENT OF DOWNHOLE GEOTHERMAL HEAT FLUX AND THERMAL CONDUCTIVITY TRANSDUCERS

H. F. Poppendiek
D. J. Connelly
A. J. Sellers

Geoscience Ltd
Solana Beach, California 92075

ABSTRACT

Two new downhole geothermal transducers were developed for the Department of Energy* for the purpose of measuring the geothermal heat flux and thermal conductivity in exploration holes without the necessity of taking core samples. One transducer system was based on the principle of quasi steady state two dimensional heat conduction; the transducers consisted of cylindrical rods having thermal conductivities different from the surrounding earth. A second cylindrical transducer system based on transient conduction generated a step function heat flux that was transferred into the earth. Both systems required that the annular space between the transducer and the hole wall be filled with water or a drilling fluid.

This paper describes the new measurement techniques, the field tests and the results.

INTRODUCTION

The common method of determining the geothermal heat flux in exploration holes consists of measuring the thermal conductivity of core or drill chip samples in the laboratory and using in-place vertical temperature profile measurements to obtain the product. The conductivity measurement is generally made in a "divided bar apparatus," which involves the comparison of the rock sample with a specimen whose thermal conductivity is known. This method has some disadvantages. One is the difficulty in acquiring samples for measurement. Further, if drill chips are used, the reconstituted samples may be different from the original rock. The water content of the rock samples may also change during the collection and transportation processes as a result of evaporation, which may affect the measured thermal conductivity.(1) There are more accurate methods of measuring the thermal conductivity of rocks in the laboratory than the divided bar method; (2) however, most of the disadvantages noted still apply.

There are a number of different methods being used by the geothermal community to assess geothermal reserves. Included are the geochemical, magnetic, electrical resistivity, microseismic, acoustic, infrared imagery, and the heat flux methods.(3) Staff members of exploration companies and the U. S. Geological Survey working with thermal techniques feel that heat flux is a logical and appropriate index of the strength of a geothermal reserve. It is felt that the in-situ measurement of heat flux and thermal conductivity using the two transducers described here has several advantages.

In the following sections, descriptions of the new transducers, field test results and interpretations of the results are presented.

DESCRIPTION OF THE MEASUREMENT TECHNIQUES

A. Rod Heat Flux Transducers

Consider the idealized rod heat flux transducer system shown in Figure 1. A steady state heat transfer analysis of this boundary value problem was made which relates the pertinent system parameters (4) (see the Appendix for the analytical closed form functions). The solution contains two unknowns, namely, the thermal conductivity of the earth and the vertical earth temperature gradient. These two unknowns are evaluated by making steady state thermopile voltage measurements with two rod transducers of different but known thermal conductivities. The solution also accounts for the effect of a fluid annulus between the transducer and the borehole wall.

In addition to the closed form solution, a two dimensional cylindrical finite difference solution was performed for a range of system parameters.

The equations for the temperature distribution along the rod heat flux transducers are functions only of the thermal conductivity of the earth, the temperature gradient, and the physical characteristics of the transducers. The equation for one transducer can be divided by the equation for the other. The resulting ratio is then only a function of the earth thermal conductivity because the unknown earth temperature gradient cancels out.

Each rod transducer consisted of a sealed tube (one having a thick aluminum wall and the other a thin stainless steel wall). Both had long internal thermopiles with packing. The output leads

*Contract EG-77-C-03-1318

connected with a two conductor cable that also deployed the sensors. The typical output signals from these transducers range from 0.1 mv to 0.5 mv.

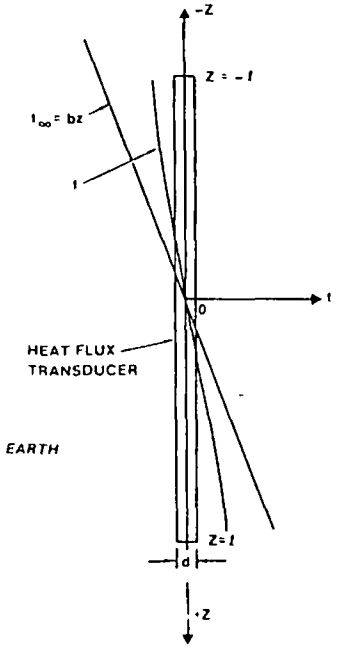

Figure 1. Idealized thin rod transducer system.

B. Thermal Conductivity Probe

Consider the idealized cylindrical thermal conductivity probe system shown in Figure 2. Mathematical heat transfer analyses were used to relate the earth thermal conductivities (and the thermal capacities per unit volume) to the time-temperature measurements, the electrical surface heat addition and the system geometry. Also included was the effect of a fluid annulus between the probe and the borehole wall. The analytical functions are given in the Appendix. (5) (6)

The thermal conductivity probe consisted of a long cylindrical section containing a surface heater over part of its length and a thermopile that measured the temperature rise of the heated surface relative to the unheated surface. Typically, the heater was operated at 0.64 amps and 64 volts. This power level was maintained for a period of about one hour. From a time-temperature recording, while power is applied to the transducer heater, the thermal conductivity and heat capacity per unit volume values can be extracted. At short time periods after the beginning of the constant heating process, the thermal capacity per unit volume controls; for longer time periods after heating initiation, the thermal conductivity controls.

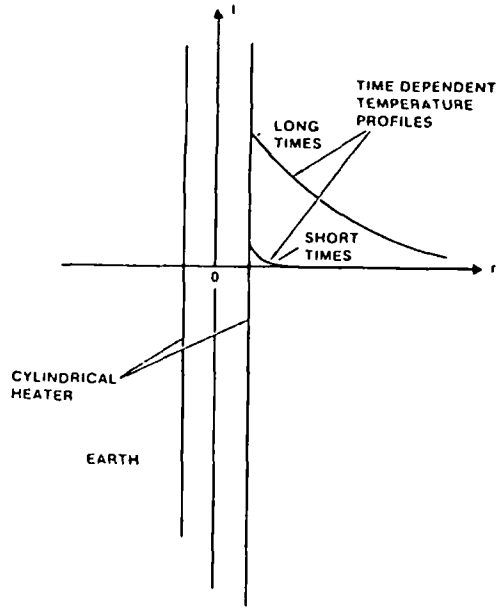

Figure 2. Idealized thermal conductivity probe system.

TEST SITE DESCRIPTION

The well used by Geoscience for these tests was located near Middletown, California. It had been drilled by the Phillips Petroleum Company as a temperature observation well in June of 1977. The drilling log shows that clay and volcanics were the types of earth encountered to a depth of about 122 meters. Deeper than 122 meters, the rock consisted of clay and greenstone to about 305 meters and then principally gabbro to the bottom of the hole. It was almost completely filled with water. The well contained a steel liner surrounded by a thin cement annulus to a depth of about 91 meters; the hole was uncased from 91 meters to the bottom. Both transducer types had an outside diameter of 0.152 meters and a length of about 2.75 meters. The inside diameter of the steel liner of the well was 0.165 meters and the hole diameter of the uncased region was about 0.159 meters.

Geothermal measurements were made at three primary depths. Efforts were made to precondition the two sensor types prior to hole insertion so that equilibration times (to quasi steady state) were not excessive.

RESULTS

A. Rod Heat Flux Transducer

The rod heat flux transducer data were reduced using the equations given in the Appendix of this paper. The thermal conductivities and geothermal heat fluxes at the three primary depths that resulted are given in Table I.

TABLE I

Rod Heat Flux Transducer Results

r_o = 0.91 meter

Depth m	k_∞ W/m·K	q/A (HFU) μ-cal/sec cm^2
52	1.1	2.6
76	1.2	2.3
110	5.1	2.4

B. Thermal Conductivity Probe

The data derived from the thermal conductivity probe were evaluated using the methods given in the Appendix. The data obtained from the thermal conductivity probe were corrected for the small temperature drop across the stainless steel wall of the probe. The results are shown in Table II. The thermal capacity per unit volume ($\rho_\infty c_{p_\infty}$) is shown in Table II, as it is also a parameter in the analysis.

TABLE II

Thermal Conductivity Probe Results

Depth m	$\rho_\infty c_{p_\infty}$ J/m^3·K	k_∞ W/m·K	q/A (HFU) μ-cal/sec cm^2
52	2.0×10^6	1.2	2.6
76	2.3×10^6	1.2	2.3
110	1.1×10^6	3.6	1.9

SOME INTERPRETATIONS

The literature thermal conductivity range for the type of rock described by Phillips Petroleum for its well ranged from approximately $0.5 < k_\infty < 4$ W/m·K; (7) the measured values presented in this document fall within the range of $1 < k_\infty < 5$ W/m·K.

Both sets of data presented indicate that the heat flux did not change significantly for the three depths (as would be expected) yet the thermal conductivity and the thermal capacity per unit volume did change significantly at the 110 meter level. These changes are believed to be related to the different lithology that occurred at that level (as pointed out by Phillips Petroleum staff). Some rock cuttings were obtained from Phillips Petroleum for the 110 meter level and thermal conductivity, specific heat and density measurements were made in the laboratory; the thermal conductivity was found to be approximately 3.3 W/m·K and the specific heat was found to be 750 J/Kg·K. The thermal properties of a reconstituted rock test sample would not be the same as the in-situ rock; thus, the agreement between laboratory and field thermal conductivities and thermal capacities per unit volume found in this study is believed to be reasonable.

The comparison of thermal conductivity and heat flux results as measured by the two different transducers (Table I and Table II) is encouraging at this stage of the transducer development. Both transducers tested can play a role in downhole thermal conductivity and heat flux measurement efforts in future geothermal exploration evaluations.

NOMENCLATURE

A , cross sectional area of the rod

a , thickness of the thin slab

b , undisturbed vertical temperature gradient in the earth

c_{p_∞} , specific heat of the earth

D_1 , thermal diffusivity of the thin slab

D_2 , thermal diffusivity of the semi-infinite solid

k , thermal conductivity of the rod

k_1 , thermal conductivity of the thin slab

k_2 , thermal conductivity of the semi-infinite solid

k_∞ , { thermal conductivity of the infinite solid; thermal conductivity of the earth

ℓ , half length of the rod

P , perimeter of the rod

q , the constant heat release per unit length

$\left(\frac{q}{A}\right)_o$, constant heat flux addition at $x = 0$

r , radial distance from the cylinder centerline

r_i , radius of the rod

r_o , { radius at which the undisturbed linear temperature field in solid exists; radius of the cylinder

R_e , equivalent end thermal resistance of the solid surrounding the rod

R_∞ , equivalent radial thermal resistance of the solid surrounding the rod

t , { temperature; rod temperature (above the rod midpoint temperature datum); *temperature at distance r*

t_∞ , the linear lateral temperature variation (above the rod midpoint temperature datum) in the solid at a radial distance sufficiently great so that the presence of the rod does not effect it

x , distance into the semi-infinite solid measured from the outer surface of the thin slab

z , distance along rod from rod midpoint

θ , time

ρ_∞ , density of the earth

APPENDIX

Recapitulation of the Mathematical Models for the Heat Flux and Thermal Conductivity Transducers

A. Rod Heat Flux Transducers

A heat balance was made on the transducer shown in Figure 1, accounting for vertical conduction along the rod and heat loss to and from its cylindrical surface and its ends, yielding an ordinary second order differential equation. The vertical temperature profile of the undisturbed earth at some distance from the rod is a linear function. Solution of this boundary value problem in terms of the temperature distribution along the rod was (4)

$$t = c_1\left(e^{-\sqrt{C}z} - e^{\sqrt{C}z}\right) + \frac{B}{C}z$$

where

$$C = \frac{P}{R_\infty kA} \quad \text{and} \quad B = \frac{Pb}{R_\infty kA}$$

$$c_1 = \frac{-b}{-\sqrt{C}\left(e^{-\sqrt{C}l} + e^{\sqrt{C}l}\right) + \frac{1}{kR_e}\left(e^{-\sqrt{C}l} - e^{\sqrt{C}l}\right)}$$

$$R_\infty = \frac{r_i}{k_\infty}\ln\frac{r_o}{r_i} \quad \text{and} \quad R_e = \frac{r_i^2\left(\frac{1}{r_i} - \frac{1}{r_o}\right)}{k_\infty}$$

When a transducer is used in a test hole, an annulus of liquid surrounds the transducer. In order to account in the equations for the presence of this layer, the thermal resistance of the fluid annulus, R_{an}, is added to the cylindrical earth resistance to obtain an increased value for R (i.e., $R' = R + R_{an}$). Similarly, the effect of fluid at the end of the transducer is also included, resulting in a modified R'_e (end heat conduction into a two region system).

B. Thermal Conductivity Probe

The transient heat transfer performance of the thermal conductivity probe can be described by the classical step function surface heating boundary condition for a long cylinder (see Figure 2), namely, (5)

$$\frac{4\pi k_\infty}{2.30q}t = \int_{-\infty}^{\log\frac{k_\infty}{\rho_\infty c_{p_\infty}}\theta} e^{4\frac{k_\infty}{\rho_\infty c_{p_\infty}}\theta - \frac{(r_o^2+r^2)}{\frac{k_\infty}{\rho_\infty c_{p_\infty}}\theta}} J_o\left(\frac{ir_o r}{2\frac{k_\infty}{\rho_\infty c_{p_\infty}}\theta}\right) d\left(\log\frac{k_\infty}{\rho_\infty c_{p_\infty}}\theta\right)$$

The addition of a fluid annulus between the thermal conductivity probe and the borehole changes the conduction system into a two region problem. This boundary value problem was first solved by considering the annulus to be a thin slab located adjacent to a semi-infinite solid (the surrounding earth). The transient temperature solution for the annulus region is: (5)

$$t = \frac{\left(\frac{q}{k_0}\right)\sqrt{D_1D_2}}{\sqrt{D_1}k_2+\sqrt{D_2}k_1}\sum_0^n \lambda^n\left[2\sqrt{\frac{\theta}{\pi}}\,e^{-\frac{(2an+x)^2}{4D_1\theta}} - \frac{(2an+x)}{\sqrt{D_1}}\operatorname{erfc}\left(\frac{2an+x}{2\sqrt{D_1\theta}}\right)\right.$$

$$\left. + 2\sqrt{\frac{\theta}{\pi}}\,e^{-\frac{(2an+2a-x)^2}{4D_1\theta}} - \frac{(2an+2a-x)}{\sqrt{D_1}}\operatorname{erfc}\left(\frac{2an+2a-x}{2\sqrt{D_1\theta}}\right)\right]$$

$$+ \frac{\left(\frac{q}{k_0}\right)k_2}{\sqrt{D_1}k_2+\sqrt{D_2}k_1}\left(\frac{D_1}{k_1}\right)\sum_0^n \lambda^n\left[2\sqrt{\frac{\theta}{\pi}}\,e^{-\frac{(2an+x)^2}{4D_1\theta}} - \frac{(2an+x)}{\sqrt{D_1}}\operatorname{erfc}\left(\frac{2an+x}{2\sqrt{D_1\theta}}\right)\right.$$

$$\left. - 2\sqrt{\frac{\theta}{\pi}}\,e^{-\frac{(2an+2a-x)^2}{4D_1\theta}} + \frac{(2an+2a-x)}{\sqrt{D_1}}\operatorname{erfc}\left(\frac{2an+2a-x}{2\sqrt{D_1\theta}}\right)\right]$$

where $\lambda = \dfrac{\sqrt{D_2}k_1-\sqrt{D_1}k_2}{\sqrt{D_2}k_1+\sqrt{D_1}k_2}$ and $n = 0, 1, 2 \ldots$

From the evaluation of this two-slab system it was shown that the temperature difference across the annulus is small in comparison to the transducer surface temperature rise above the initial temperature datum for times greater than the annulus time constant (which is of the order of 0.05 hours for a 0.5 cm thick water layer). Therefore, in the cylindrical coordinate system consisting of the fluid annulus and the surrounding semi-infinite earth, the annulus time constants and temperature drops will likewise be small compared to transducer values. If the water annulus thickness is no more than 15 percent of the probe radius, then one can neglect the annulus effect (for times greater than the annulus time constant).

ACKNOWLEDGMENTS

Support of the following people is acknowledged: A. F. Veneruso, J. A. Coquat, G. W. Crosby, S. D. Johnson, C. M. Sabin, A. C. Reynard, E. M. Boughton, and E. W. Fowler.

REFERENCES

1 Gross, R., and Combs, J., 1975, "Thermal Conductivity Measurement and Prediction from Geophysical Well Log Parameters with Borehole Application," in Proc. Sec. U N Sym. on Devel. and Use of Geoth. Res., Vol 2, p 1019.

2 Kappelmeyer, O., and Haenel, R., 1974, Geothermics, with Special Ref. to Application, Gebruder Borntraeger.

3 Proceedings, Sec. U N Sym. on Devel. and Use of Geoth. Res., 1975, U. S. Gov't. Printing Office.

4 Poppendiek, H. F., and Connelly, D. J., 1977, "A Thin Rod Heat Flux Transducer Positioned in the Earth Having A Uniform Temperature Gradient," GLR-178.

5 Poppendiek, H. F., and Connelly, D. J., 1977, "Cylindrical and Spherical Transient Heat Transfer Solutions and Their Application to Thermal Conductivity Measurements in the Earth," GLR-185.

6 Poppendiek, H. F., and Connelly, D. J., 1977, "The Effects of a Fluid Annulus on the Performance of Thermal Transducers in a Borehole," GLR-189.

7 Jumikis, A. F., Thermal Soil Mechanics, 1966, Rutgers University Press.

TEMPERATURE GRADIENT HOLE RESULTS FROM MAKUSHIN GEOTHERMAL AREA, UNALASKA ISLAND, ALASKA

C.F. ISSELHARDT*, J.S. MATLICK*, P.P. PARMENTIER*, R.W. BAMFORD**

*REPUBLIC GEOTHERMAL, INC.
**SYSTEMATIC–COST EFFECTIVE–RESOURCE DISCOVERY

ABSTRACT

Following geological, geophysical, and geochemical surveys of the Makushin geothermal area, three 1,500±-foot temperature gradient holes (TGH) were sited and drilled. TGH D-1 penetrated andesites and diorite, locally hydrothermally altered, and yielded both convective and conductive thermal profiles. TGH E-1 and TGH I-1 both encountered diorite only. TGH E-1 exhibited high temperatures (195°C) and corresponding geochemical indicia. TGH I-1 was cool (~80°C), but showed geochemistry indicative of a paleogeothermal environment. The high thermal gradients (145°C to 692°C/km), temperatures (195°C), and geochemistry provide strong evidence for the existence of a shallow, high temperature geothermal system.

INTRODUCTION

This paper describes and interprets the geological, thermal, and geochemical data derived from the three temperature gradient holes drilled during 1982 in the Makushin Volcano geothermal area of Unalaska Island in the Aleutian Archipelago of Alaska (Figure 1). The hole locations were chosen on the basis of results derived from preceding geological, geochemical, and geophysical surveys, as well as logistical considerations.

Temperature Gradient Hole D-1

Temperature gradient hole D-1 was drilled on a plateau approximately 1.6 km northwest of the base camp (Figure 1). As shown on Figure 2, the hole was spudded in glacial boulder till 40 feet thick that mantles a sequence of Makushin Volcanics that extended from 40 feet to 1,222 feet. The volcanics are a series of essentially unaltered porphyritic andesite and basaltic andesite flows with interbeds of scoriaceous andesitic cinders, lahars and gravel. Below the volcanics, from 1,222 feet to total depth at 1,429 feet, the hole penetrated a highly altered (propylitized) and fractured, fine-grained to cryptocrystalline diorite, which is cut by an andesite dike from 1,370 feet to 1,393 feet. The diorite is intensely fractured and veined in the upper portion, with most fractures having near-vertical inclinations. Alteration minerals include sulfur, pyrite, kaolinite, calcite, epidote, quartz, anhydrite, and chlorite. Most of these minerals are products of the reaction between the rock and high temperature (>150°C) hydrothermal fluids. The quartz, epidote, anhydrite, and sulfur are primarily found as fracture fillings, although epidote is also found in the groundmass. The andesite dike transecting the diorite is probably related to the young Makushin volcanic sequence.

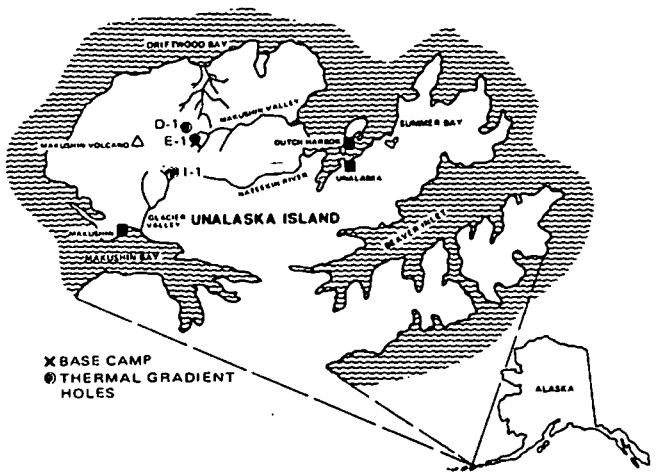

FIGURE 1

Temperature measurements made in TGH D-1 (Figure 2) indicated essentially isothermal convective conditions (ground water circulation) to approximately 700 feet. Below this depth the temperature increases at high rates (from 145°C/km up to 642°C/km) in a conductive (linear) manner to total depth (T.D.). The zone of high temperature gradients corresponds with a self-sealed zone defined by the whole-rock geochemical studies. The gradient over the last 125 feet is 280°C/km. This gradient is still very high (average temperature gradient worldwide is 33°C/km) and it indicates that higher temperatures exist at depth, although the depth to maximum temperature cannot be estimated on the basis of data from this hole alone. The elevated temperature recorded at T.D. (100.2°C), the high gradient over the last several hundred feet of hole, and the high-temperature alteration of the surrounding rock all suggest the presence of a relatively shallow (4,000± feet) hydrothermal system.

C.F. ISSELHARDT, ET AL

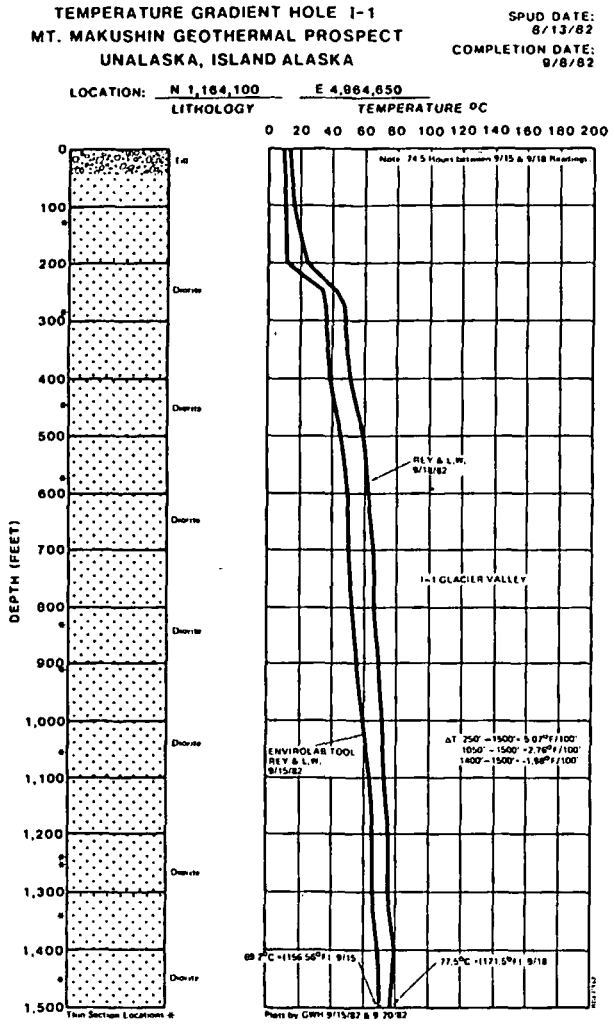

FIGURE 4

about 250 feet to T.D. and appears to be a relatively conductive system with gradients of 49°C/km to 91°C/km and a maximum temperature of 79.8°C (175.6°F) at 1,400 feet. The data in Figure 4 also shows that there is a small temperature reversal (2.3°C) over the last 100 feet of the hole.

The overall temperature regime and profile of this hole indicates that the hole appears to be on the southern edge of the present geothermal system, at least for this depth range, although the intense fracturing and mineralization indicates the previous presence of a high temperature geothermal system. Definition of the boundaries of the present hydrothermal system was one of the uses and goals of the temperature gradient hole program. It appears that TGH I-1 was fortuitously located and that it achieved one of the major project objectives.

As in the other two holes, the general type of chemical anomaly is the same. The upper 700 feet of TGH I-1 contains several zones of Hg, As, S, Li, and F enrichment, some of which correspond with one another and some of which are isolated.

The present temperature regime is considerably cooler than that implied by the geochemistry and there is large-scale artesian flow of cool water above 300 feet (indicating high permeability). The rock chip geochemistry suggests the existence of a self-sealed zone in a paleo-geothermal system that has since been refractured.

Geochemical analysis of the lower 800 feet of hole shows virtually no indication of past or present hydrothermal systems, even though there are old, healed fractures containing minor amounts of quartz, anhydrite and epidote. Thus, TGH 1-1 appears to be located within the limits of an old geothermal system and on the edge or outside of the present hydrothermal system.

SUMMARY AND CONCLUSIONS

It is apparent from the information derived from the temperature gradient holes and other surveys that there is an excellent chance that a liquid-dominated geothermal reservoir with temperatures in excess of 200°C exists on the east flank of the Makushin Volcano at relatively shallow depths (2,000 feet to 4,000 feet). The southern limit of the resource appears to have been defined, but other boundaries have not been determined yet by drilling. By the time this paper is presented, a deeper well will have been drilled in the area to assess the presence of this reservoir, and a fourth gradient hole will have been drilled to the north to better help define the areal extent of the system.

ACKNOWLEDGMENTS

The authors wish to acknowledge the support and cooperation provided by the Alaska Power Authority and the Alaska Geological Survey, Division of Geological and Geophysical Surveys on this project.

BIBLIOGRAPHY

Bamford, R.W., Christensen, O.D., and Capuano, R.M., 1980, Multielement geochemistry of solid materials in geothermal systems and its applications, Part 1: The hot-water system at Roosevelt Hot Springs KGRA, Utah: Earth Sci. Lab., Univ. of Utah Research Inst., ESL-30, p. 168.

Drewes, H., Fraser, G.D., Snyder, G.L., and Barnett, H.F., Jr., 1961, Geology of Unalaska Island and adjacent insular shelf, Aleutian Islands, Alaska: U.S. Geological Survey Bulletin 1028-S, p. 583-669.

Reeder, J.W., 1981, Preliminary assessment of the geothermal resources of the northern part of Unalaska Island: Alaska Dept. Natural Resources, In Press.

GEOPHYSICS, VOL. 46, NO. 1 (JANUARY 1981); P. 76–83, 11 FIGS., 4 TABLES.

In-situ determination of heat flow in unconsolidated sediments

J. H. Sass,* J. P. Kennelly, Jr.,* W. E. Wendt,* T. H. Moses, Jr.,* and J. P. Ziagos‡

Subsurface thermal measurements are the most effective, least ambiguous tools for locating geothermal resources. Measurements of thermal gradient in the upper few tens of meters can delineate the major anomalies, but it is also desirable to combine these gradients with reliable estimates of thermal conductivity, to provide data on the energy flux and to constrain models of the heat sources responsible for the anomalies. Problems associated with such heat flow measurements include the economics of casing or grouting holes, the long waits and repeated visits necessary to obtain equilibrium temperature values, the possible legal liability arising from disturbance of aquifers, the hazards presented by pipes protruding from the ground, and the security problems associated with leaving cased holes open for periods of weeks to months.

We have developed a technique that provides reliable real-time determinations of temperature, thermal conductivity, and hence, of heat flow in unconsolidated sediments during the drilling operation. Temperature, gradient, and thermal conductivity can be measured in one operation in 1 hour using a long (1.5 to 2 m) thin (6-mm diameter) probe containing three thermistors 0.5 or 0.15 m apart in its lowermost 1.2 m. The probe is driven hydraulically through the bit up to 1.65 m into the formation, and a 20- to 25-minute temperature record is obtained for each thermistor, allowing calculation of the equilibrium temperature gradient. A line source heater is then switched on and a 10- to 15-minute temperature record is obtained, allowing calculation of thermal conductivity. Two or three such experiments over the depth range of 50 to 150 m provide a high-quality heat flow determination at costs comparable to those associated with a standard cased gradient hole to comparable depths. The hole can be backfilled and abandoned after drilling, thereby eliminating the need for casing, grouting, or repeated site visits.

INTRODUCTION

Many of the alluvial and lacustrine valleys of the western United States have potential for the exploitation of geothermal energy. Of the various exploration techniques available, heat flow drilling is the most direct and the least ambiguous, and exploration programs involving drilling patterns of holes to depths of between 10 and 500 m are common in geothermal prospecting. Thermal gradients alone generally are sufficient for discovering and delineating thermal anomalies. However, if the thermal conductivity can be characterized, the temperature gradients can be converted to heat flow estimates, which, in turn, provide valuable information concerning the energy budget and can be used to constrain hypotheses on the ultimate sources of the anomalous heat (e.g., Lachenbruch and Sass, 1977; Mase et al, 1978; Olmsted et al, 1975; Ward et al, 1978).

One of the major problems in obtaining useful data on the thermal conductivity of unconsolidated sediments is the high cost and difficulty of recovering suitable core samples. In many prospects, repeated attempts produce little or no core, and what little is recovered may not be representative of the formation. Even when extreme care is taken in handling samples, irreversible changes in their mechanical properties may occur before the conductivity determinations can be made. The conductivities of the solid component can be measured on drill cuttings, but reliable values of porosity are necessary to convert these data into meaningful estimates of formation conductivity.

Another problem in the highly competitive geothermal exploration industry is the security of cased thermal test wells. These holes must be left for at least a few days, and preferably for several weeks to months, to allow the thermal disturbance introduced by the drilling process to subside. During this period, the hole can be entered easily, and "midnight logs" can be made by unauthorized people. A hole that has been left open for a few days to weeks may become artesian, leading to surface damage and contamination of aquifers. Pipes left standing above the ground on playa surfaces may also present a hazard to vehicles.

We describe a downhole heat flow probe which eliminates most of the problems outlined above. It gives satisfactory determinations of both temperature gradient and thermal conductivity and hence of heat flow, in unconsolidated sediments, essentially in real time. Because formation temperatures are measured below the bit during the drilling operation, the hole need not be cased and can be backfilled immediately upon cessation of drilling. Thermal conductivities are measured in situ so that mechanical disturbances to the formation are kept to a minimum.

The first comprehensive field trials of the system were held in the Black Rock Desert (Figure 1) near Gerlach, Nevada, during September, 1978. Holes were drilled in fine-grained unconsolidated Pleistocene or Holocene lake sediments, typically rich in clay, with some sandy layers a few centimeters thick. The results from 29 probe runs in 12 holes (GRA through GRK and GRZ, Figure 1) are described herein and compared with conventional determinations of gradient, conductivity, and heat flow.

The following symbols and units are used:

Manuscript received by the Editor August 17, 1979; revised manuscript received February 25, 1980.
*U.S. Geological Survey, 345 Middlefield Road, Menlo Park, CA 94025.
‡Formerly U.S. Geological Survey, Menlo Park, CA; presently Southern Methodist University, Dallas, TX 75222.
0016-8033/81/0101-0076$03.00.

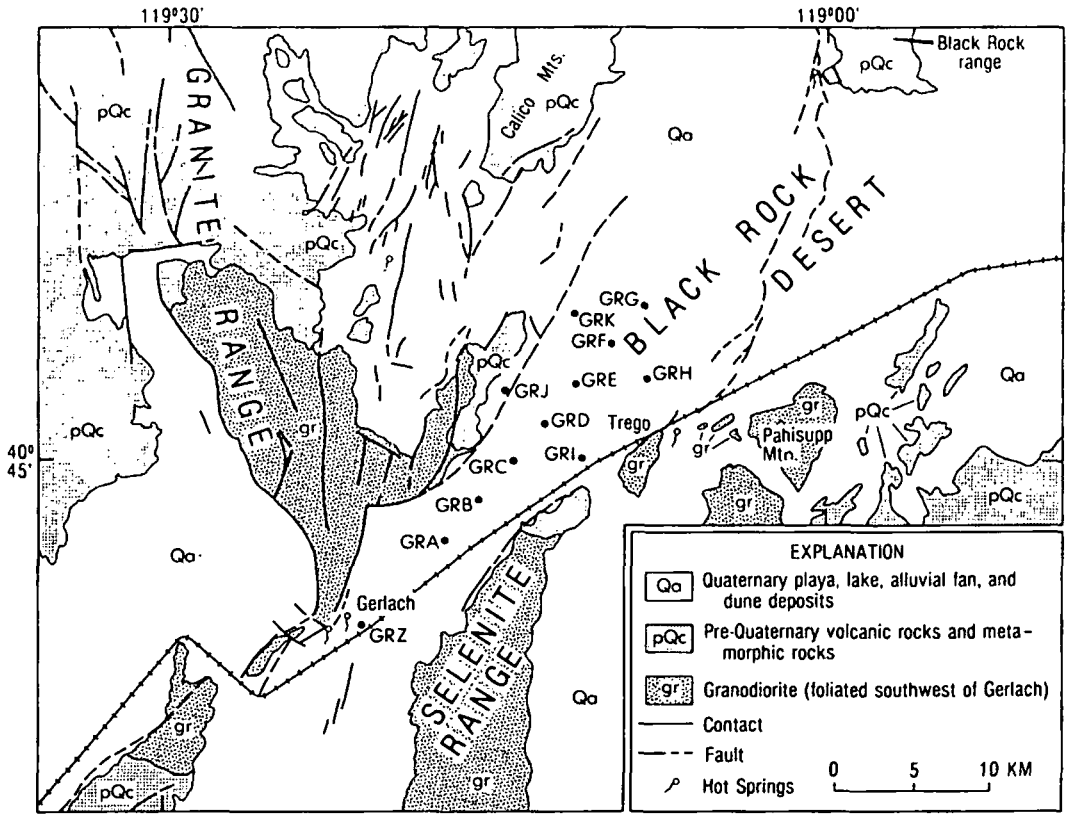

FIG. 1. Geologic sketch map of Gerlach area showing the locations of test wells. Geology and faults generalized from Willden, 1964; Bonham, 1969; Olmsted et al, 1975; and Keller and Grose, 1978.

T = temperature (°C),
t = time (seconds).
K = thermal conductivity (1 HCU = 1 mcal $cm^{-1}s^{-1}°C^{-1}$ = 0.418 $Wm^{-1}K^{-1}$),
q = heat flow (1 HFU = 10^{-6} cal $cm^{-2}s^{-1}$ = 41.8 mWm^{-2}),
Temperature gradient = °C km^{-1} = mKm^{-1},
Pressure = 1 kPa = 0.145 psi.

GENERAL DESCRIPTION OF THE SYSTEM

Figure 2 illustrates the essential features of a downhole probe test. The probe is basically 2.13 m of heat-treated 52100 grade steel, 6.4 mm OD and 3.2 mm ID. It contains three thermistors: thermistor 1, 0.15 m; thermistor 2, 0.65 m; and thermistor 3, 1.15 m above the tip. (A shorter version for use in stiffer materials has the thermistors in the tip, 0.15 and 0.3 m above it, respectively. It was developed subsequent to the trials described here.) A loop of heater wire and four thermistor leads, all mutually insulated and enclosed in heat shrinkable tubing, are placed in the steel tube, and the voids are filled with molten woods metal. The woods metal expands slightly on freezing, thereby facilitating thermal contact among heater, thermistors, and probe wall. The switching instrumentation is attached at the top of the probe, and the entire probe is mated to the 3/16-inch (4.8 mm) OD four-conductor armored logging cable by means of an oil field type well logging cablehead.

At the depth selected for the test, the driller thickens the mud

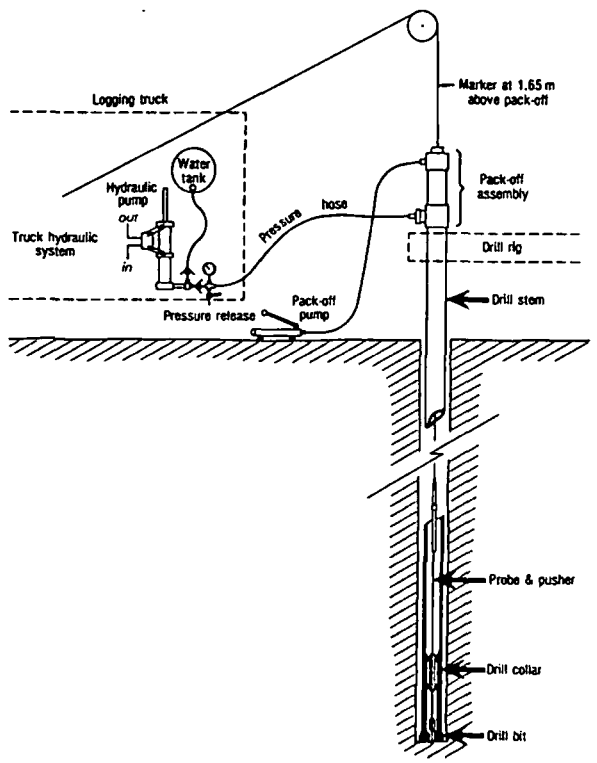

FIG. 2. Schematic diagram of field setup for downhole probe experiment.

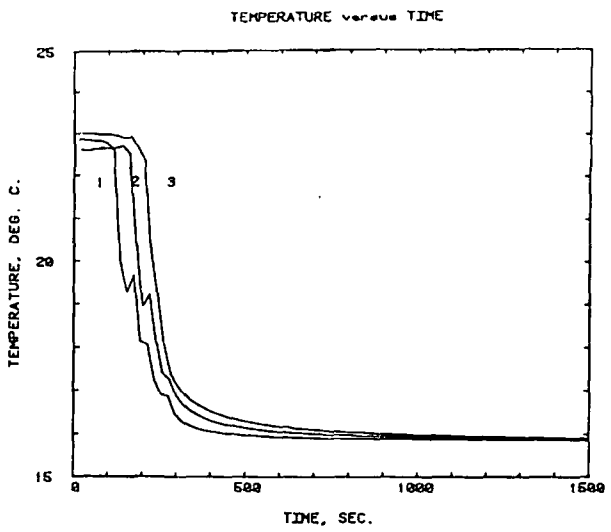

FIG. 3. Temperature-time graph obtained during and after complete penetration of the downhole probe in hole GRE. Solid lines connect discrete temperature observations at 20-second intervals. Numbers refer to probe thermistors (1, lowermost). Thermistor 1 is 0.15 m, thermistor 2, 0.65 m, and thermistor 3, 1.15 m above the tip. In this case, the drilling fluid is several degrees warmer than the formation.

column and circulates for a few minutes to flush the cuttings out of the hole. The bit is then placed on bottom, and a wireline pack-off assembly is connected to the drill string just above the rotary table. The probe is lowered into the drill stem until the piston on the driving mechanism ("pusher") enters the smooth-bored drill collar immediately above the bit (Figure 2; also Appendix C, Sass et al, 1979). The hydraulic pump on the logging truck then is activated, delivering water from an ~150-liter capacity tank to the drill column. At the same time, the pack-off pump is used to tighten the packer assembly (Figure 2) to the point where only a small amount of fluid is leaking out of the top of the pack-off. The pusher portion of the piston consists of a series of ball bearings which roll up a ramped sleeve and compress the outer wall of the probe when pressure is applied to the drill column, allowing the piston to drive the probe into the formation. When the cable moves downward a few centimeters, the water pressure is released to allow the return springs to move the pusher up the probe and the column is pressurized again. This process is repeated until 1.65 m of penetration is achieved or until the pressures approach the mechanical strength of the probe (~15,000 kPa). During this period, the electrical resistance of each thermistor is monitored at 20-second intervals and converted to temperature by the data-reduction program. The temperature-time data are stored on magnetic tape, and a graph similar to that shown in Figure 3 is generated in real time by the digital $x - y$ plotter. The passive temperature record is run for 1500 seconds, typically allowing 1000 to 1200 seconds for the decay of the thermal transient resulting from the friction between probe and formation. This time interval is not nearly sufficient to achieve thermal equilibrium, but when a smooth record is obtained (as in Figure 3), the data may be extrapolated to equilibrium values in a manner similar to that employed for the Bullard type of oceanic heat flow probe (Bullard, 1954; Langseth, 1965). One simple extrapolation scheme involves plotting temperature (T) as a function of $1/t$ (see Table 1, Lachenbruch and Brewer, 1959) where t is the elapsed time reckoned from approximately the midpoint of the penetration interval (about 225 seconds for Figure 3). This reduction is illustrated in Figure 4 for the corresponding curves in Figure 3. For time t large relative to the time taken to penetrate the formation, the curves should be linear, and indeed they are (Figure 4). Note also that even though the final measured temperatures are in reverse order (i.e., thermistor 3 hotter than 2 hotter than 1), the extrapolation to $1/t = 0$ provides (at least qualitatively) the expected increase in temperature with depth.

Upon completion of the passive temperature run (Figure 3), a constant current of about 100 mA is applied to the heater loop, the specific resistance of which is about 700 Ωm^{-1}. The heat input to the formation is thus about 7 watts per meter of probe length. Representative temperature-log time curves are shown in Figure 5. The differences in temperature among the three thermistors are the result of differences in contact resistance between the heater and probe wall. The temperatures plotted in Figure 5 are not corrected for the rate of downward drift resulting from the decay of the thermal transients associated with frictional heating during penetration. This drift rate was calculated at the midpoint of the conductivity run ($t \cong 2000$ sec) from the slope of the T-versus-$1/t$ lines (e.g., Figure 4) and a correction was applied to the observed temperature. This resulted in a small but significant increase in the slope of the T-versus-log t line (e.g., Figure 5). Consequently,

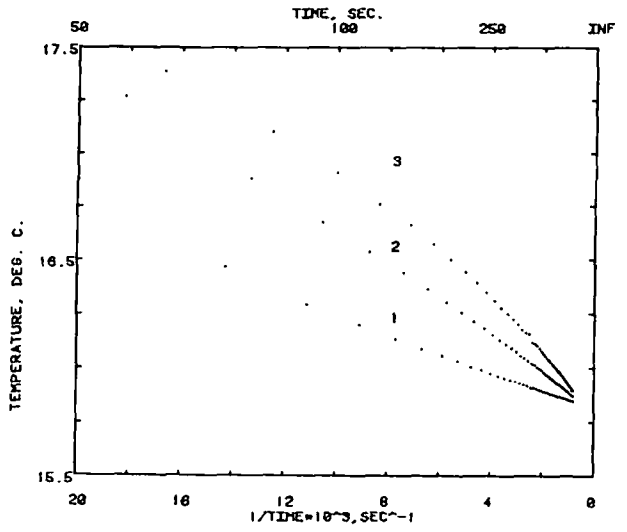

FIG. 4. Temperature-versus-1/time for the probe test shown in Figure 3. The time origin relative to Figure 3 is 225 sec.

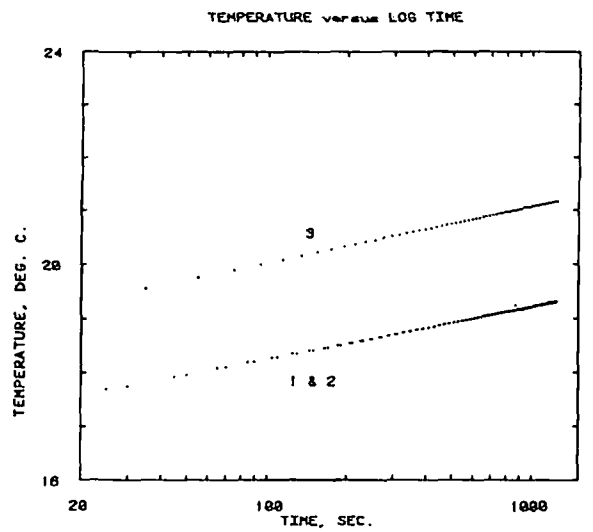

FIG. 5. Temperature-versus-log time data for conductivity run corresponding to the downhole test shown in Figure 3.

Table 1. Summary of downhole probe experiments, Hole GRF, Black Rock Desert, Nevada.

Depth (m)		Penetration (m)	Temperature (°C)		Gradient (°C/km)		Conductivity (HCU)	Heat flow (HFU)	
Bit	Thermistor		Probe	Log	Probe	Log		Probe	Log
61		1.65							
	61.5		16.241	16.258			2.69		
					62				
	62.0		16.272	16.303			2.70		
					98				
	62.5		16.321	16.332					
					80	76	2.70	2.16	2.05
121.9		1.65							
	122.4		21.627	21.656			2.41		
					113				
	122.9		21.665	21.703			2.39		
					76				
	123.4		21.721	21.752			2.44		
					95	95	2.41	2.29	2.29
							Mean	2.23	2.17
Interval heat flow									
62-123 m					88.7	89.0	2.55	2.26	2.27
Least-squares intervals									
42-83 m					74.4±0.3		2.70±0.01	2.01±0.02	
84-126 m					92.5±0.2		2.41±0.02	2.23±0.02	
							Best value	2.2±0.1	

there was a decrease of 1 to 5 percent in the conductivity which is calculated from this slope based on

$$T(t) = \frac{Q}{4\pi K} \ln t + 0\left(\frac{1}{t}\right) \qquad (1)$$

where Q is the rate of heating and K, the thermal conductivity (Lachenbruch, 1957; Jaeger, 1958; Von Herzen and Maxwell, 1959). The terms of the order of $1/t$ become unimportant in equation (1) within two minutes for this probe, and sufficient redundancy of data is achieved after a few hundred seconds (Figure 5). Upon completion of the conductivity test, the probe is removed by raising the entire drill string until the probe is completely out of the formation. Thereafter, the probe is raised to the surface by reeling in the cable and drilling is resumed.

In the first few holes, many probe tests were performed and cores were obtained to provide comparisons with in-situ determinations of thermal conductivity. As the study progressed, however, we dispensed with coring and settled on a scheme whereby probe tests were made at depths of 61 and 91 m (200 and 300 ft). Total time required for insertion, 25-minute drift test, 10- to 15-minute conductivity test, and retrieval of the probe was about an hour, or roughly the time required for a coring trip at these depths. At one site (GRF, Table 1), we established that the probe would penetrate fully at ~120 m (400 ft).

COMPARISON OF DOWNHOLE PROBE RESULTS WITH CONVENTIONAL MEASUREMENTS

Introduction

Comparisons between probe and conventional determinations of temperatures, gradients, and thermal conductivities are shown in detail in Appendices A and B of Sass et al (1979). In this section, we discuss briefly the various comparisons and some of their implications. The statistics for the relation $y = Ax$ (where y is the probe value and x the value derived from conventional measurements) are shown in Table 2. Some individual comparisons are made in Tables 1, 3, and 4. For these tables, the first three columns give reference depths; the first gives the approximate depth reached by the bit before the experiment began. The second column refers to the depths of the probe thermistors assuming that the bit depth is accurate. Actually, because of shifting reference levels on the rig relative to the ground surface, the accuracy of the bit-depth estimate is probably no better than ±0.3 m. Temperatures obtained from linear extrapolation of the temperature-versus-$1/t$ time curves (see Figure 4) are compared with those obtained from the most recent temperature logs in columns 4 and 5, and comparisons among other quantities are presented in the remaining columns. The bottom segments of these tables have comparisons between heat flow ("interval heat flows") over intervals of several tens of meters determined from downhole measurements and from subsequent conventional temperature measurements in the cored holes. They also show heat flow estimates obtained by multiplying least-squares gradients from the conventional temperature log by the harmonic mean thermal conductivity over the designated least-squares intervals.

Thermal conductivity

Cores corresponding to the depths of the probe tests were obtained in hole GRZ (the first drilled); then in GRA, GRB, and GRC (Figure 1). At this stage, we were satisfied that the downhole conductivities were, in fact, comparable to those obtained with a needle probe on core, and coring was discontinued (see, for example, the comparison between conductivities, columns 8

Table 2. Coefficients of the least-squares regression line $y = Ax$ for the comparison between thermal parameters derived from downhole probe measurements (y) and those (x) determined by conventional methods.*

Parameter	Correlation coefficient	A	rms residual‡
Conductivity	0.96	1.05	0.12 HCU
Temperature	1.00	1.00	0.04°C
One-meter gradients	0.99	0.94	5.6°C/km
Heat flow (1-m)	0.99	0.96	0.13 HFU
Heat flow (neighboring probe runs)	1.00	1.02	0.05 HFU

*"Equilibrium" temperature logs for temperatures and gradients; needle-probe determinations on core for thermal conductivity.

‡$\left[\sum_{i=1}^{N} (y_i - Ax_i)^2/(N-2)\right]^{1/2}$

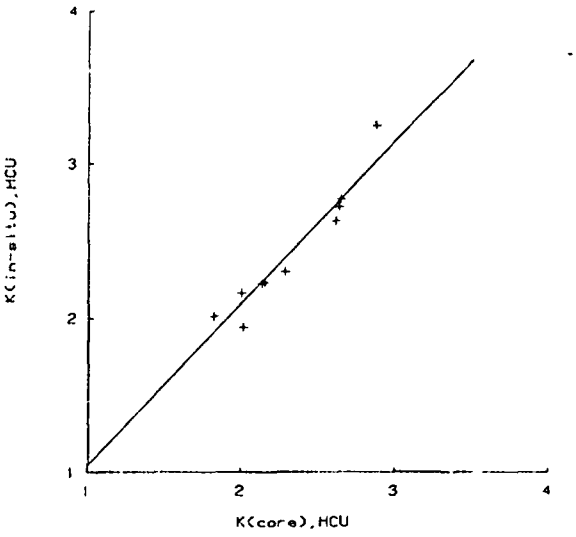

FIG. 6. Comparison between average downhole probe conductivities over 1 m and the corresponding averages for 3 to 6 needle-probe determinations on core. [See Appendix B, Sass et al (1979) for details.]

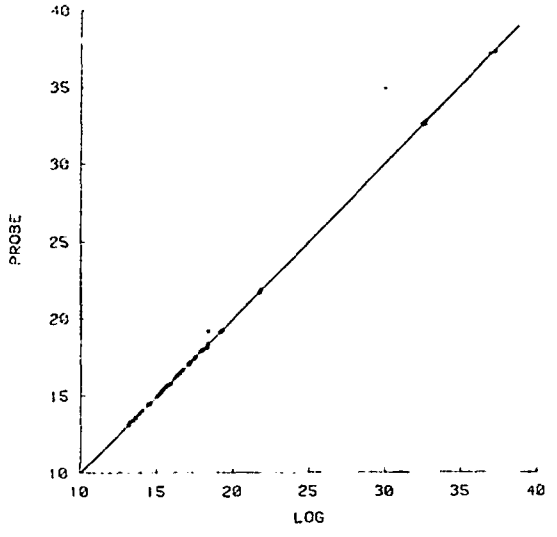

FIG. 7. Formation temperatures (°C) deduced from downhole probe tests versus temperature at the same depth from the most recent temperature log.

Table 3. Summary of downhole probe experiments, Hole GRA, Black Rock Desert, Nevada.

Depth (m)		Penetration	Temperature (°C)		Gradient (°C/km)		Conductivity (HCU)		Heat flow (HFU)	
Bit	Thermistor	(m)	Probe	Log	Probe	Log	Probe	Core	Probe	Log
30.5		1.65								
	31.0		13.596	13.582			1.96	1.83		
					64					
	31.5		13.628	13.620			2.03	1.82		
					88					
	32.0		13.672	13.667			2.03	1.82		
					76	85	2.01	1.82	1.54	1.55
67.10		1.65								
	67.6		16.126	16.125			2.30	2.31		
					50					
	68.1		16.151	16.168			2.24	2.24		
					98					
	68.6		16.200	16.205			2.35	2.30		
					74	80	2.30	2.28	1.70	1.82
91.44		1.40								
	91.7		18.257	18.229			2.23	2.10		
					48*					
	92.2		18.281	18.226			2.23	2.21		
					15*					
	92.7		18.288	18.307			2.21	2.08		
					32*	78	2.22	2.13	(0.7)*	1.66
								Mean	1.62	1.68
Interval heat flows										
32-69 m					66.6	69.3	2.15	2.05	1.43	1.42
69-93 m					86.6	87.2	2.26	2.20	1.96	1.92
32-93 m					76.1	76.4	2.18	2.08	1.66	1.59
Least-squares intervals										
20-40 m					82.8±0.4		1.91±0.1		1.58±0.09	
61-103 m					85.8±0.2		2.23±0.04		1.91±0.04	
30-103 m					76.2±0.3		2.11±0.08		1.61±0.07	
							Best value		1.7±0.2	

*Electrical noise in record. Excluded from means.

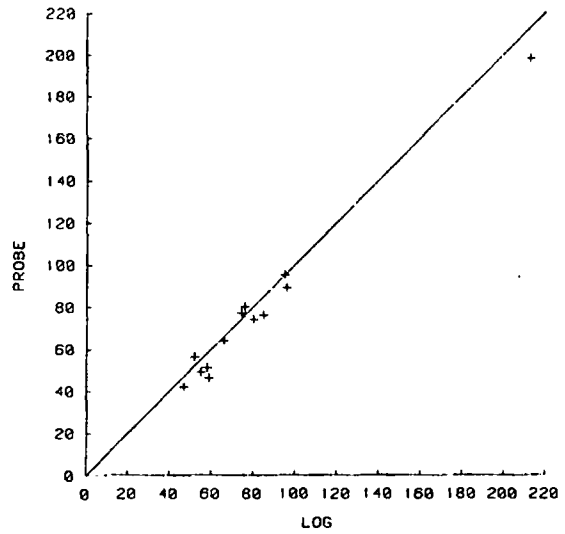

FIG. 8. Temperature gradients (°C/km) over 1 m from downhole probe experiments versus those determined from the most recent temperature log.

and 9, Table 3). The scatter is fairly small (Figure 6). The coefficient of correlation is 0.96, and downhole probe conductivities are systematically higher than those measured on core by about 5 percent (Table 2). We attribute this difference to slight structural changes in the core caused by the removal of the core from its environment, and thus we prefer the downhole values (sufficient conductivities were measured along the axis of the core to confirm that there was no measurable anisotropy). The most striking example of physical changes occurred in the core from 30.5 to 32 m in hole GRA (Table 3). When a hole was drilled into the wall of the core liner to allow access for the needle probe, there was a pop and a muddy slurry was extruded from the core. We see in this instance (conductivity columns, Table 3) that needle-probe conductivities are systematically lower than in-situ values by about 10 percent at this depth.

Formation temperatures

Temperatures obtained from all probe runs by least-squares extrapolation of the later parts of the T-versus-$1/t$ lines (generally for the last 200 to 300 seconds) are plotted against temperatures at the same depth from the most recent temperature log in Figure 7. The correlation is excellent (Table 2), and the value for A of 1.00 tends to confirm our suggestion (Appendix B, Sass et al, 1979) that the temperature differences are random and are caused primarily by the uncertainties in depth measurement that can result in a maximum error of up to 0.1°C.

Gradients over one meter

The largest source of uncertainty in obtaining gradients over a 1-m interval results from the ~0.01°C resolution in relative temperatures between thermistors. Even though individual thermistors were calibrated to within a few millidegrees and the drift rate of each thermistor calibration is slow, small and unpredictable changes in calibration do occur. Calibrations were checked in the field by comparing each thermistor to a single thermistor mounted in a lagged aluminum cylinder. Departures (usually a few millidegrees) from calibration were noted and included in the temperature reduction part of the program so that all thermistor temperatures were relative to a common datum. Even with these procedures, our maximum possible error in the gradient over 1 m is ±20°C/km, clearly not accurate enough for single point determinations of regional heat flow, but certainly sufficiently sensitive to delineate the type of anomaly associated with possible sources of geothermal energy.

Although there is a fairly large scatter (Figure 8), 1-m gradients from the probe experiments correlate very well with those determined from least-squares fits to the six points from the most recent temperature log spanning the 1.5-m interval penetrated by the probe (Table 2). Only results from complete penetrations were used in this comparison. Where only two thermistors entered the

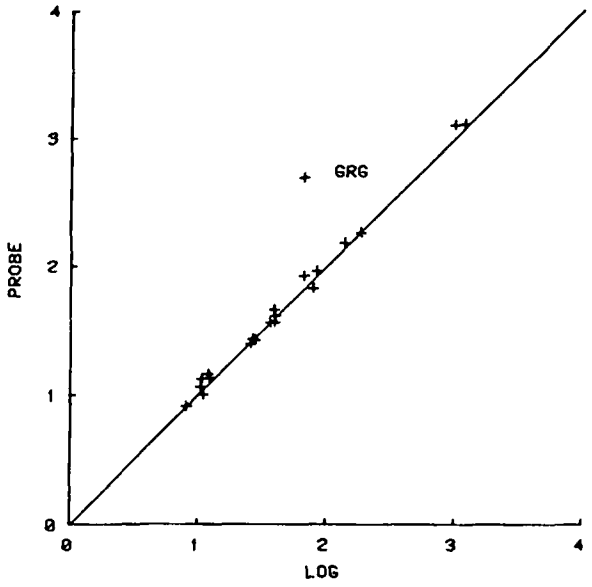

FIG. 9. Heat flow (HFU) over intervals of between 6 and 60 m determined between neighboring downhole probe runs versus heat flows determined over the same intervals from conventional temperature logs.

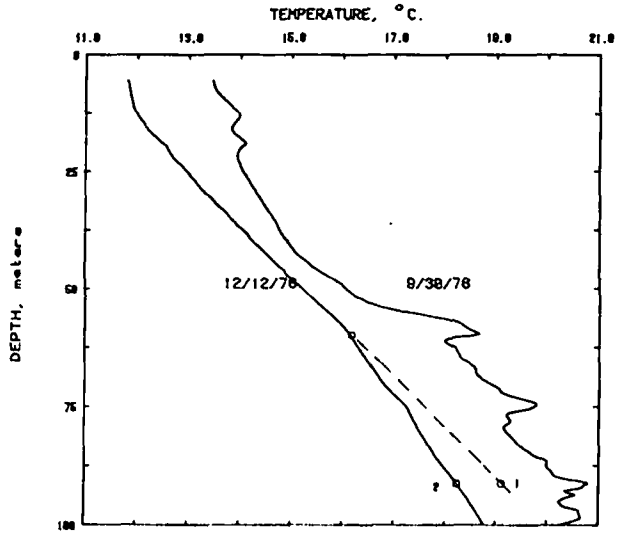

FIG. 10. Temperatures measured at 0.3-m intervals on dates indicated (solid lines) in hole GRG, and downhole probe measurements made during drilling (open circles). Elevated temperatures on the earlier log indicate the interval in which the annulus is filled with cement grout. Numbers beside circles refer to probe thermistors (1 lowermost). The well was drilled on September 27, 1978. Dashed line represents an extrapolation of the upper portion of the profile (between ~30 and 60 m).

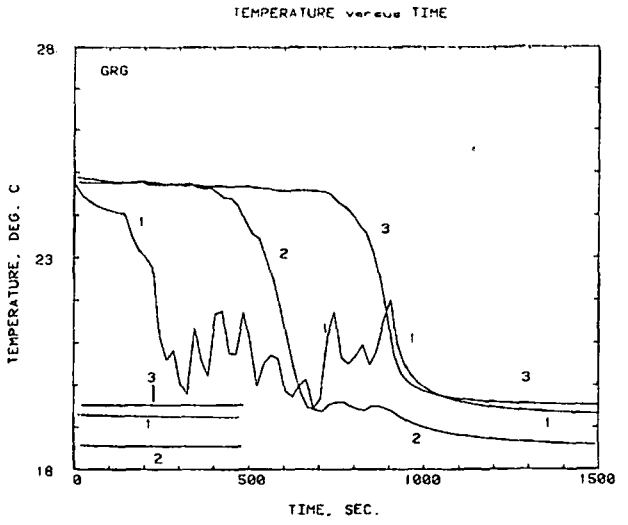

FIG. 11. Penetration record for downhole probe run in Hole GRG, 91 m. Numbers refer to probe thermistors (1 lowermost). Lines at lower left are continuations of the original decay curves ($t_0 \cong 1600$ sec).

formation, the scatter was much greater. This should be expected, as we are attempting to measure the gradient over only 0.5 m and commonly the temperature of the second thermistor is affected by the invasion of drilling fluid.

Heat flow

Since, in most instances, the downhole conductivities were used for both the probe and conventional heat flow estimates over 1 m, the same comments as those made with respect to the 1-m gradient determinations apply to the one-m heat flow determinations. Another approach to heat flow determinations involves computing gradients and mean thermal conductivities over one or more intervals between probe runs ("Interval heat flows" column, Tables 1, 3, and 4). When intervals of a few tens of meters are used, the uncertainties due to reference levels and the errors of ±0.01°C in relative temperatures become negligible. Only one thermistor need penetrate the formation for each run, a requirement that was met in every trial. The interval approach is mandatory when the short probe (all three thermistors in the lowermost 0.3 m) is used. With one exception, the heat flow estimates over the larger intervals agree very well with those calculated from the most recent temperature log (Figure 9). The one exception, hole GRG (Figure 10 and Table 4), suggests that the downhole probe may be the superior technique quite apart from its other advantages.

For the probe test at 91 m in GRG, only two thermistors penetrated well into the formation (thermistor 3 was perhaps 2 cm, at most 5 cm below the bit). When drilling resumed, the driller reported a hard sandy stringer a few centimeters thick just below 61 m. Maximum pressures and a long time (~1000 sec) were required to get the probe into the formation. From the penetration record (Figure 11), thermistor 1 had repeated episodes of frictional heating, whereas the temperature of thermistor 2 dropped immediately as it entered the formation with a cooling curve quite different from either 1 or 3. Thermistor 3 was barely in and its decay curve was probably affected by interaction with the drilling fluid. It is curious and probably not coincidental that the extrapolated equilibrium temperature for thermistor 1 lies on the extension of the very smooth profile in the upper 60 m (Figure 10), whereas that for thermistor 2 lies precisely on the most recent temperature log, which is quite irregular below 60 m. If we interpret the 1-m heat flow at 61 m and the interval heat flow (62–92 m) for thermistor 2 literally (Table 4), then we arrive at a most likely value of between 1.4 and 2 HFU for the heat flow. To reconcile this with the observed gradient of >90°C/km above 60 m, we must assume an implausibly low thermal conductivity of ~2 HCU for the upper part of the hole (see "Least-squares intervals" column, Table 4). If, on the other hand, we assume that the conductivities measured at 61 and 91 m are representative of the entire hole and that, below 60 m, the hole is disturbed, then our preferred heat flow will be about 2.6 HFU, about 30 percent higher than that obtained from the literal interpretation and consistent with the interval heat flow (62.5–92.5 m, Table 4) for thermistor num-

Table 4. Summary of downhole probe experiments, Hole GRG, Black Rock Desert, Nevada.

Depth (m)		Penetration (m)	Temperature (°C)		Gradient (°C/km)		Conductivity (HCU)	Heat flow (HFU)	
Bit	Thermistor		Probe	Log	Probe	Log		Probe	Log
61		1.65							
	61.5		16.162	16.241			2.90		
					26				
	62.0		16.175	16.272			2.85		
					75				
	62.5		16.213	16.302			2.45		
					51	58	2.72	1.39	1.58
91.44		1.16							
	92.0		18.281	18.266			2.63		
					1800				
	92.5		19.167*	18.300			2.85		
					1800*	65	2.74	~49*	1.78
Interval heat flows									
62-92 m					70.2	66.5	2.73	1.92	1.82
62.5-92.5 m					98.5	66.6	2.73	2.69	1.82
Least-squares intervals									
30-56 m					93.5±0.2		2.0? 2.73?		1.87 2.55
60-102 m					66.1±0.2		2.73±0.02		1.80±0.02
							Best value		2.6

*See Figures 10 and 11 and discussion in the text.

ber 1. Since there is no change in lithology between the upper and lower parts of the hole, it seems more probable that the drill opened a channel below ~60 m between two intervals with a slight head difference, and that water has been moving downward in the annulus since that time; this despite the fact that the annulus between casing and wall in the anomalous section of the hole was apparently grouted off (see temperature log for 9/30/78, Figure 10). This explanation might be applicable to other areas in which, within an apparently uniform lithology, an abrupt change in temperature gradient is observed.

SUMMARY AND CONCLUSIONS

A downhole probe capable of precise determinations of formation temperature and thermal conductivity and rough estimates of the thermal gradient over 1 m can be inserted through a drill bit into unconsolidated sediments, activated, and removed in the time normally taken for a coring run. Two or more penetrations of the probe provide a heat flow determination comparable in accuracy to a conventional heat flow measurement without the necessity of casing the hole or relogging it after completion of drilling. The heat flow determination is made during the drilling process; thus, there is no time delay in obtaining data, no surface hazard associated with protruding casing, and no opportunity for unauthorized entry to boreholes in sensitive or competitive prospects. Because the hole need not be cased, grouted, or visited repeatedly, the technique also is very cost effective. The components necessary for a downhole probe system (described in detail by Sass et al, 1979) can be assembled and added to a preexisting digital temperature-logging system at a modest cost (in the neighborhood of $2,000 to $3,000 at 1980 prices).

Useful information was obtained in all 29 runs in the present study, demonstrating the robustness and the reliability of the equipment. In one hole, data obtained with the downhole probe provided evidence that the drilling process altered the thermal regime locally by permitting vertical water movement even though the casing was grouted in.

Many prospectively important geothermal systems are located within or adjacent to the alluvial and lacustrine sedimentary formations of the western United States. Using the technique outlined in this report, it should be possible to obtain 4 or 5 probe runs per day to depths of between 50 and 150 m in these formations, thus allowing two high-quality heat flow data or several reconnaissance heat flow estimates per day. Even if the field conditions and program objectives call for casing the wells, the reliable determinations in situ of thermal conductivity and the real time estimates of heat flow make the downhole probe a valuable adjunct to the standard approach.

ACKNOWLEDGMENTS

Arthur Lachenbruch originally suggested the technique and gave valuable advice at many stages. Our success in the field was due, in no small measure, to the patience and skill of John Clingan and Western Geophysical crew GT-3. Vaughn Marshall, Mary Lou Zoback, and Eugene Smith rendered valuable assistance in the field.

REFERENCES

Bonham, H. F., 1969, Geology and mineral deposits of Washoe and Storey counties, Nevada: Nevada Bur. Mines Bull. 70, 140 p.

Bullard, E. C., 1954, The flow of heat through the floor of the Atlantic Ocean: Proc. Royal Soc. London, A, v. 222, p. 408–429.

Jaeger, J. C., 1958, The measurement of thermal conductivity and diffusivity with cylindrical probes: AGU Trans., v. 39, p. 708–710.

Keller, G. V., and Grose, L. T., 1978, Studies of a geothermal system in northwestern Nevada, part 1: Colorado School of Mines Quart., v. 73, 84 p.

Lachenbruch, A. H., 1957, A probe for measurement of thermal conductivity of frozen soils in place: AGU Trans., v. 38, p. 691–697.

Lachenbruch, A. H., and Brewer, M. C., 1959, Dissipation of the temperature effect of drilling a well in Arctic Alaska: U.S.G.S. Bull. 1083-C, p. 73–109.

Lachenbruch, A. H., and Sass, J. H., 1977, Heat flow in the United States and the thermal regime of the crust, *in* The Earth's Crust—Its Nature and Physical Properties: J. G. Heacock, Ed., AGU monograph series, Washington, D.C., v. 20, p. 626–675.

Langseth, M. G., 1965, Techniques of measuring heat flow through the ocean floor, *in* Terrestrial heat flow: W. H. K. Lee, Ed., AGU monograph series, Washington, D.C., v. 8, p. 58–77.

Mase, C. W., Chapman, D. S., and Ward, S. H., 1978, Geophysical study of the Monroe-Red Hill geothermal system: Univ. of Utah topical rep. IDO/76-1601-77-17, 89 p.

Olmsted, F. H., Glancy, P. A., Harrill, J. R., Rush, F. E., and VanDenburgh, A. S., 1975, Preliminary hydrogeologic appraisal of selected hydrothermal systems in northern and central Nevada: U.S.G.S. open file rep. 75–56, p. 128–147.

Sass, J. H., Kennelly, J. P., Jr., Wendt, W. E., Moses, T. H., Jr., and Ziagos, J. P., 1979, In-situ determination of heat flow in unconsolidated sediments: U.S.G.S. open-file rep. 79-593, 73 p.

Von Herzen, R. P., and Maxwell, A. E., 1959, The measurement of thermal conductivity of deep sea sediments by a needle probe method: J. Geophys. Res., v. 64, p. 1557–1563.

Ward, S. H., Parry, W. T., Nash, W. P., Sill, W. R., Cook, K. L., Smith, R. B., Chapman, D. S., Brown, F. H., Whelan, J. A., and Bowman, J. R., 1978, A summary of the geology, geochemistry, and geophysics of the Roosevelt Hot Springs thermal area, Utah: Geophysics, v. 43, p. 1515–1542.

Willden, R., 1964, Geology and mineral deposits of Humboldt County, Nevada: Nevada Bur. Mines Bull. 59, 154 p.

GEOPHYSICS, VOL. 46, NO. 1 (JANUARY 1981); P. 76–83, 11 FIGS., 4 TABLES.

In-situ determination of heat flow in unconsolidated sediments

J. H. Sass,* J. P. Kennelly, Jr.,* W. E. Wendt,* T. H. Moses, Jr.,* and J. P. Ziagos‡

Subsurface thermal measurements are the most effective, least ambiguous tools for locating geothermal resources. Measurements of thermal gradient in the upper few tens of meters can delineate the major anomalies, but it is also desirable to combine these gradients with reliable estimates of thermal conductivity, to provide data on the energy flux and to constrain models of the heat sources responsible for the anomalies. Problems associated with such heat flow measurements include the economics of casing or grouting holes, the long waits and repeated visits necessary to obtain equilibrium temperature values, the possible legal liability arising from disturbance of aquifers, the hazards presented by pipes protruding from the ground, and the security problems associated with leaving cased holes open for periods of weeks to months.

We have developed a technique that provides reliable real-time determinations of temperature, thermal conductivity, and hence, of heat flow in unconsolidated sediments during the drilling operation. Temperature, gradient, and thermal conductivity can be measured in one operation in 1 hour using a long (1.5 to 2 m) thin (6-mm diameter) probe containing three thermistors 0.5 or 0.15 m apart in its lowermost 1.2 m. The probe is driven hydraulically through the bit up to 1.65 m into the formation, and a 20- to 25-minute temperature record is obtained for each thermistor, allowing calculation of the equilibrium temperature gradient. A line source heater is then switched on and a 10- to 15-minute temperature record is obtained, allowing calculation of thermal conductivity. Two or three such experiments over the depth range of 50 to 150 m provide a high-quality heat flow determination at costs comparable to those associated with a standard cased gradient hole to comparable depths. The hole can be backfilled and abandoned after drilling, thereby eliminating the need for casing, grouting, or repeated site visits.

INTRODUCTION

Many of the alluvial and lacustrine valleys of the western United States have potential for the exploitation of geothermal energy. Of the various exploration techniques available, heat flow drilling is the most direct and the least ambiguous, and exploration programs involving drilling patterns of holes to depths of between 10 and 500 m are common in geothermal prospecting. Thermal gradients alone generally are sufficient for discovering and delineating thermal anomalies. However, if the thermal conductivity can be characterized, the temperature gradients can be converted to heat flow estimates, which, in turn, provide valuable information concerning the energy budget and can be used to constrain hypotheses on the ultimate sources of the anomalous heat (e.g., Lachenbruch and Sass, 1977; Mase et al, 1978; Olmsted et al, 1975; Ward et al, 1978).

One of the major problems in obtaining useful data on the thermal conductivity of unconsolidated sediments is the high cost and difficulty of recovering suitable core samples. In many prospects, repeated attempts produce little or no core, and what little is recovered may not be representative of the formation. Even when extreme care is taken in handling samples, irreversible changes in their mechanical properties may occur before the conductivity determinations can be made. The conductivities of the solid component can be measured on drill cuttings, but reliable values of porosity are necessary to convert these data into meaningful estimates of formation conductivity.

Another problem in the highly competitive geothermal exploration industry is the security of cased thermal test wells. These holes must be left for at least a few days, and preferably for several weeks to months, to allow the thermal disturbance introduced by the drilling process to subside. During this period, the hole can be entered easily, and "midnight logs" can be made by unauthorized people. A hole that has been left open for a few days to weeks may become artesian, leading to surface damage and contamination of aquifers. Pipes left standing above the ground on playa surfaces may also present a hazard to vehicles.

We describe a downhole heat flow probe which eliminates most of the problems outlined above. It gives satisfactory determinations of both temperature gradient and thermal conductivity and hence of heat flow, in unconsolidated sediments, essentially in real time. Because formation temperatures are measured below the bit during the drilling operation, the hole need not be cased and can be backfilled immediately upon cessation of drilling. Thermal conductivities are measured in situ so that mechanical disturbances to the formation are kept to a minimum.

The first comprehensive field trials of the system were held in the Black Rock Desert (Figure 1) near Gerlach, Nevada, during September, 1978. Holes were drilled in fine-grained unconsolidated Pleistocene or Holocene lake sediments, typically rich in clay, with some sandy layers a few centimeters thick. The results from 29 probe runs in 12 holes (GRA through GRK and GRZ, Figure 1) are described herein and compared with conventional determinations of gradient, conductivity, and heat flow.

The following symbols and units are used:

Manuscript received by the Editor August 17, 1979; revised manuscript received February 25, 1980.
*U.S. Geological Survey, 345 Middlefield Road, Menlo Park, CA 94025.
‡Formerly U.S. Geological Survey, Menlo Park, CA; presently Southern Methodist University, Dallas, TX 75222.
0016-8033/81/0101-0076$03.00.

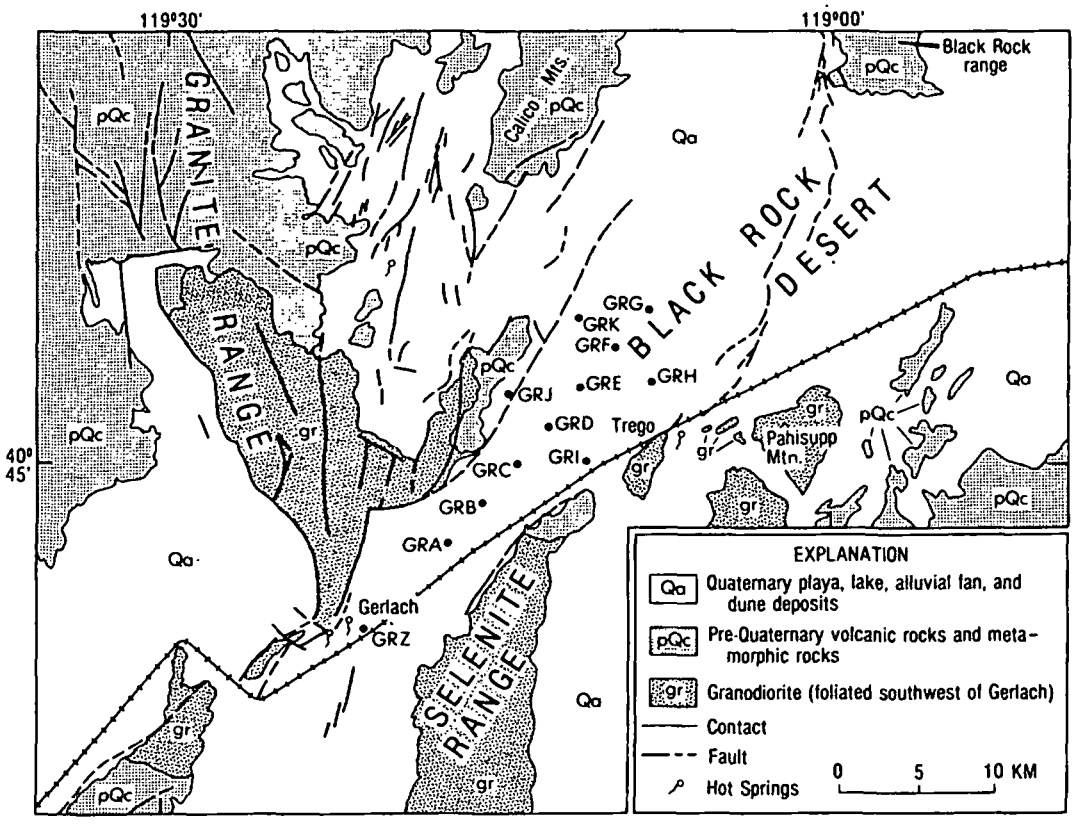

FIG. 1. Geologic sketch map of Gerlach area showing the locations of test wells. Geology and faults generalized from Willden, 1964; Bonham, 1969; Olmsted et al, 1975; and Keller and Grose, 1978.

T = temperature (°C),
t = time (seconds).
K = thermal conductivity (1 HCU = 1 mcal $cm^{-1}s^{-1}°C^{-1}$ = 0.418 $Wm^{-1}K^{-1}$),
q = heat flow (1 HFU = 10^{-6} cal $cm^{-2}s^{-1}$ = 41.8 mWm^{-2}),
Temperature gradient = °C km^{-1} = mKm^{-1},
Pressure = 1 kPa = 0.145 psi.

GENERAL DESCRIPTION OF THE SYSTEM

Figure 2 illustrates the essential features of a downhole probe test. The probe is basically 2.13 m of heat-treated 52100 grade steel, 6.4 mm OD and 3.2 mm ID. It contains three thermistors: thermistor 1, 0.15 m; thermistor 2, 0.65 m; and thermistor 3, 1.15 m above the tip. (A shorter version for use in stiffer materials has the thermistors in the tip, 0.15 and 0.3 m above it, respectively. It was developed subsequent to the trials described here.) A loop of heater wire and four thermistor leads, all mutually insulated and enclosed in heat shrinkable tubing, are placed in the steel tube, and the voids are filled with molten woods metal. The woods metal expands slightly on freezing, thereby facilitating thermal contact among heater, thermistors, and probe wall. The switching instrumentation is attached at the top of the probe, and the entire probe is mated to the 3/16-inch (4.8 mm) OD four-conductor armored logging cable by means of an oil field type well logging cablehead.

At the depth selected for the test, the driller thickens the mud

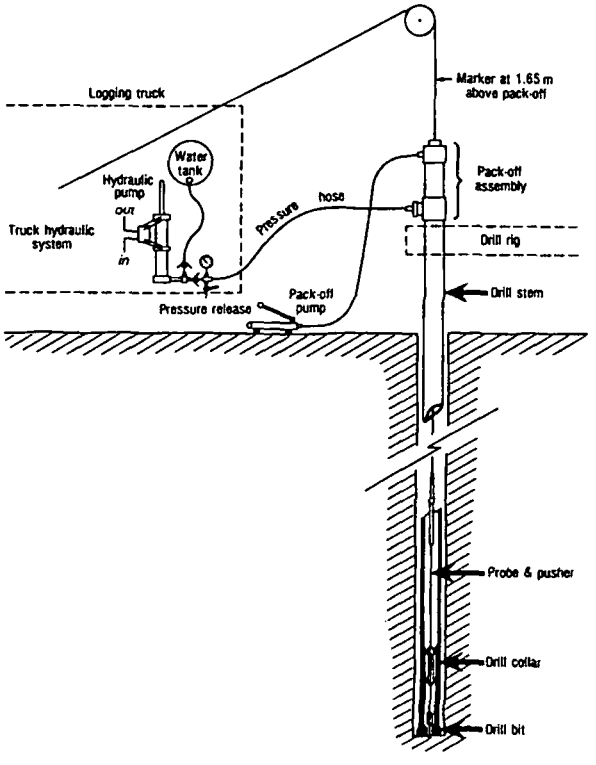

FIG. 2. Schematic diagram of field setup for downhole probe experiment.

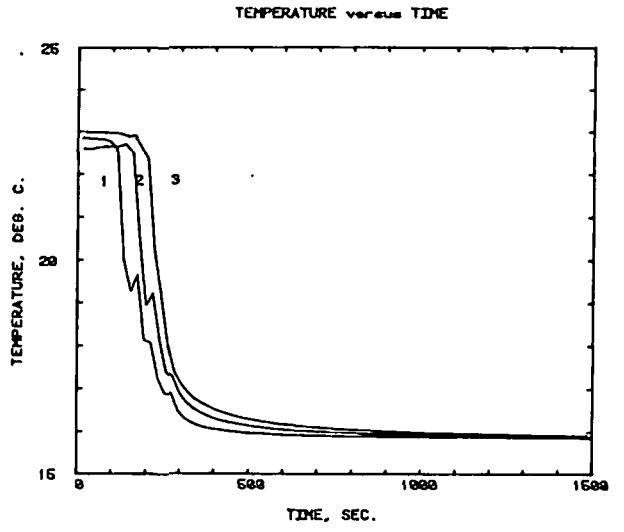

FIG. 3. Temperature-time graph obtained during and after complete penetration of the downhole probe in hole GRE. Solid lines connect discrete temperature observations at 20-second intervals. Numbers refer to probe thermistors (1, lowermost). Thermistor 1 is 0.15 m, thermistor 2, 0.65 m, and thermistor 3, 1.15 m above the tip. In this case, the drilling fluid is several degrees warmer than the formation.

column and circulates for a few minutes to flush the cuttings out of the hole. The bit is then placed on bottom, and a wireline pack-off assembly is connected to the drill string just above the rotary table. The probe is lowered into the drill stem until the piston on the driving mechanism ("pusher") enters the smooth-bored drill collar immediately above the bit (Figure 2; also Appendix C, Sass et al, 1979). The hydraulic pump on the logging truck then is activated, delivering water from an ~150-liter capacity tank to the drill column. At the same time, the pack-off pump is used to tighten the packer assembly (Figure 2) to the point where only a small amount of fluid is leaking out of the top of the pack-off. The pusher portion of the piston consists of a series of ball bearings which roll up a ramped sleeve and compress the outer wall of the probe when pressure is applied to the drill column, allowing the piston to drive the probe into the formation. When the cable moves downward a few centimeters, the water pressure is released to allow the return springs to move the pusher up the probe and the column is pressurized again. This process is repeated until 1.65 m of penetration is achieved or until the pressures approach the mechanical strength of the probe (~15,000 kPa). During this period, the electrical resistance of each thermistor is monitored at 20-second intervals and converted to temperature by the data-reduction program. The temperature-time data are stored on magnetic tape, and a graph similar to that shown in Figure 3 is generated in real time by the digital $x - y$ plotter. The passive temperature record is run for 1500 seconds, typically allowing 1000 to 1200 seconds for the decay of the thermal transient resulting from the friction between probe and formation. This time interval is not nearly sufficient to achieve thermal equilibrium, but when a smooth record is obtained (as in Figure 3), the data may be extrapolated to equilibrium values in a manner similar to that employed for the Bullard type of oceanic heat flow probe (Bullard, 1954; Langseth, 1965). One simple extrapolation scheme involves plotting temperature (T) as a function of $1/t$ (see Table 1, Lachenbruch and Brewer, 1959) where t is the elapsed time reckoned from approximately the midpoint of the penetration interval (about 225 seconds for Figure 3). This reduction is illustrated in Figure 4 for the corresponding curves in Figure 3. For time t large relative to the time taken to penetrate the formation, the curves should be linear, and indeed they are (Figure 4). Note also that even though the final measured temperatures are in reverse order (i.e., thermistor 3 hotter than 2 hotter than 1), the extrapolation to $1/t = 0$ provides (at least qualitatively) the expected increase in temperature with depth.

Upon completion of the passive temperature run (Figure 3), a constant current of about 100 mA is applied to the heater loop, the specific resistance of which is about 700 Ωm^{-1}. The heat input to the formation is thus about 7 watts per meter of probe length. Representative temperature-log time curves are shown in Figure 5. The differences in temperature among the three thermistors are the result of differences in contact resistance between the heater and probe wall. The temperatures plotted in Figure 5 are not corrected for the rate of downward drift resulting from the decay of the thermal transients associated with frictional heating during penetration. This drift rate was calculated at the midpoint of the conductivity run ($t \cong 2000$ sec) from the slope of the T-versus-$1/t$ lines (e.g., Figure 4) and a correction was applied to the observed temperature. This resulted in a small but significant increase in the slope of the T-versus-log t line (e.g., Figure 5). Consequently,

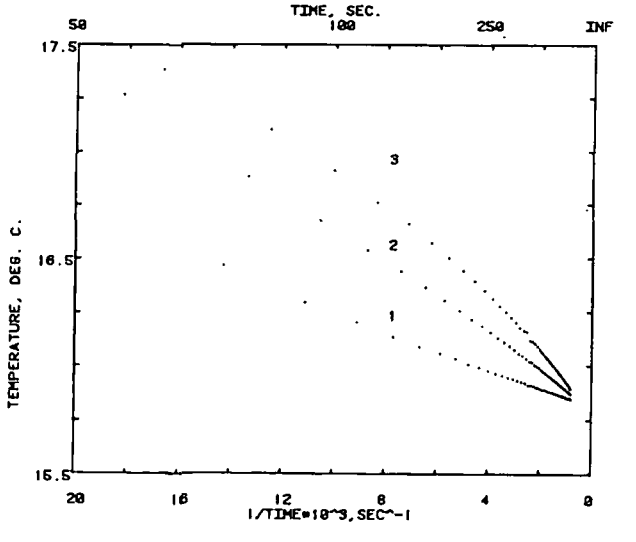

FIG. 4. Temperature-versus-1/time for the probe test shown in Figure 3. The time origin relative to Figure 3 is 225 sec.

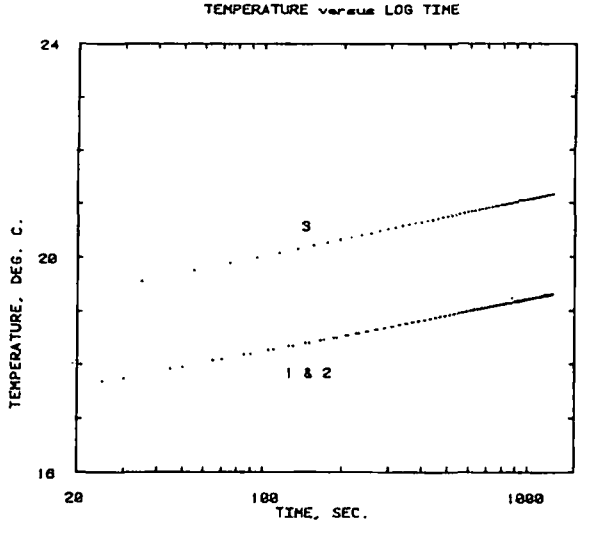

FIG. 5. Temperature-versus-log time data for conductivity run corresponding to the downhole test shown in Figure 3.

Table 1. Summary of downhole probe experiments, Hole GRF, Black Rock Desert, Nevada.

Depth (m) Bit	Depth (m) Thermistor	Penetration (m)	Temperature (°C) Probe	Temperature (°C) Log	Gradient (°C/km) Probe	Gradient (°C/km) Log	Conductivity (HCU)	Heat flow (HFU) Probe	Heat flow (HFU) Log
61		1.65							
	61.5		16.241	16.258			2.69		
					62				
	62.0		16.272	16.303			2.70		
					98				
	62.5		16.321	16.332					
					80	76	2.70	2.16	2.05
121.9		1.65							
	122.4		21.627	21.656			2.41		
					113				
	122.9		21.665	21.703			2.39		
					76				
	123.4		21.721	21.752			2.44		
					95	95	2.41	2.29	2.29
							Mean	2.23	2.17
Interval heat flow									
62-123 m					88.7	89.0	2.55	2.26	2.27
Least-squares intervals									
42-83 m					74.4±0.3		2.70±0.01	2.01±0.02	
84-126 m					92.5±0.2		2.41±0.02	2.23±0.02	
							Best value	2.2±0.1	

there was a decrease of 1 to 5 percent in the conductivity which is calculated from this slope based on

$$T(t) = \frac{Q}{4\pi K} \ln t + 0\left(\frac{1}{t}\right) \qquad (1)$$

where Q is the rate of heating and K, the thermal conductivity (Lachenbruch, 1957; Jaeger, 1958; Von Herzen and Maxwell, 1959). The terms of the order of $1/t$ become unimportant in equation (1) within two minutes for this probe, and sufficient redundancy of data is achieved after a few hundred seconds (Figure 5). Upon completion of the conductivity test, the probe is removed by raising the entire drill string until the probe is completely out of the formation. Thereafter, the probe is raised to the surface by reeling in the cable and drilling is resumed.

In the first few holes, many probe tests were performed and cores were obtained to provide comparisons with in-situ determinations of thermal conductivity. As the study progressed, however, we dispensed with coring and settled on a scheme whereby probe tests were made at depths of 61 and 91 m (200 and 300 ft). Total time required for insertion, 25-minute drift test, 10- to 15-minute conductivity test, and retrieval of the probe was about an hour, or roughly the time required for a coring trip at these depths. At one site (GRF, Table 1), we established that the probe would penetrate fully at ~120 m (400 ft).

COMPARISON OF DOWNHOLE PROBE RESULTS WITH CONVENTIONAL MEASUREMENTS

Introduction

Comparisons between probe and conventional determinations of temperatures, gradients, and thermal conductivities are shown in detail in Appendices A and B of Sass et al (1979). In this section, we discuss briefly the various comparisons and some of their implications. The statistics for the relation $y = Ax$ (where y is the probe value and x the value derived from conventional measurements) are shown in Table 2. Some individual comparisons are made in Tables 1, 3, and 4. For these tables, the first three columns give reference depths; the first gives the approximate depth reached by the bit before the experiment began. The second column refers to the depths of the probe thermistors assuming that the bit depth is accurate. Actually, because of shifting reference levels on the rig relative to the ground surface, the accuracy of the bit-depth estimate is probably no better than ±0.3 m. Temperatures obtained from linear extrapolation of the temperature-versus-1/time curves (see Figure 4) are compared with those obtained from the most recent temperature logs in columns 4 and 5, and comparisons among other quantities are presented in the remaining columns. The bottom segments of these tables have comparisons between heat flow ("interval heat flows") over intervals of several tens of meters determined from downhole measurements and from subsequent conventional temperature measurements in the cored holes. They also show heat flow estimates obtained by multiplying least-squares gradients from the conventional temperature log by the harmonic mean thermal conductivity over the designated least-squares intervals.

Thermal conductivity

Cores corresponding to the depths of the probe tests were obtained in hole GRZ (the first drilled); then in GRA, GRB, and GRC (Figure 1). At this stage, we were satisfied that the downhole conductivities were, in fact, comparable to those obtained with a needle probe on core, and coring was discontinued (see, for example, the comparison between conductivities, columns 8

Table 2. Coefficients of the least-squares regression line $y = Ax$ for the comparison between thermal parameters derived from downhole probe measurements (y) and those (x) determined by conventional methods.*

Parameter	Correlation coefficient	A	rms residual‡
Conductivity	0.96	1.05	0.12 HCU
Temperature	1.00	1.00	0.04°C
One-meter gradients	0.99	0.94	5.6°C/km
Heat flow (1-m)	0.99	0.96	0.13 HFU
Heat flow (neighboring probe runs)	1.00	1.02	0.05 HFU

*"Equilibrium" temperature logs for temperatures and gradients; needle-probe determinations on core for thermal conductivity.

‡$\left[\sum_{i=1}^{N} (y_i - Ax_i)^2/(N-2)\right]^{1/2}$

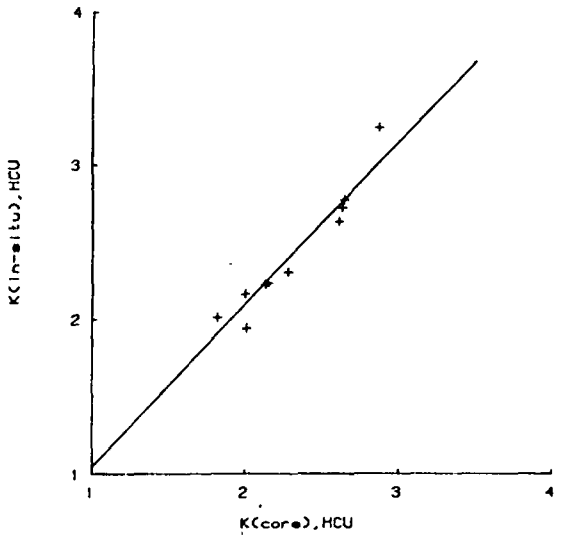

FIG. 6. Comparison between average downhole probe conductivities over 1 m and the corresponding averages for 3 to 6 needle-probe determinations on core. [See Appendix B, Sass et al (1979) for details.]

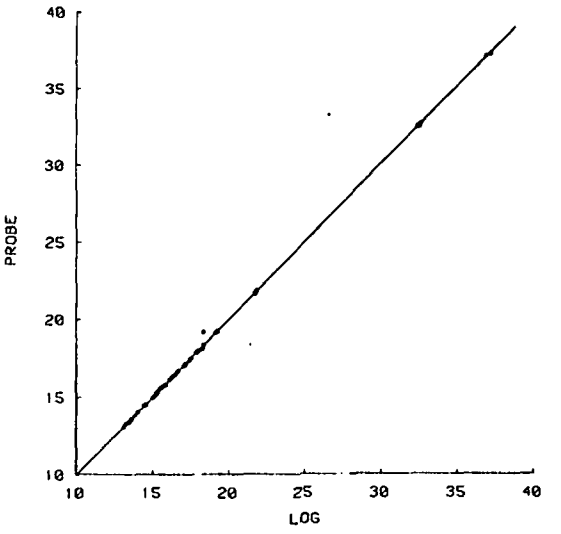

FIG. 7. Formation temperatures (°C) deduced from downhole probe tests versus temperature at the same depth from the most recent temperature log.

Table 3. Summary of downhole probe experiments, Hole GRA, Black Rock Desert, Nevada.

Depth (m)		Penetration (m)	Temperature (°C)		Gradient (°C/km)		Conductivity (HCU)		Heat flow (HFU)	
Bit	Thermistor		Probe	Log	Probe	Log	Probe	Core	Probe	Log
30.5		1.65								
	31.0		13.596	13.582	64		1.96	1.83		
	31.5		13.628	13.620	88		2.03	1.82		
	32.0		13.672	13.667			2.03	1.82		
					76	85	2.01	1.82	1.54	1.55
67.10		1.65								
	67.6		16.126	16.125	50		2.30	2.31		
	68.1		16.151	16.168	98		2.24	2.24		
	68.6		16.200	16.205			2.35	2.30		
					74	80	2.30	2.28	1.70	1.82
91.44		1.40								
	91.7		18.257	18.229	48*		2.23	2.10		
	92.2		18.281	18.226	15*		2.23	2.21		
	92.7		18.288	18.307			2.21	2.08		
					32*	78	2.22	2.13	(0.7)*	1.66
								Mean	1.62	1.68
Interval heat flows										
32-69 m					66.6	69.3	2.15	2.05	1.43	1.42
69-93 m					86.6	87.2	2.26	2.20	1.96	1.92
32-93 m					76.1	76.4	2.18	2.08	1.66	1.59
Least-squares intervals										
20-40 m					82.8±0.4		1.91±0.1		1.58±0.09	
61-103 m					85.8±0.2		2.23±0.04		1.91±0.04	
30-103 m					76.2±0.3		2.11±0.08		1.61±0.07	
							Best value		1.7±0.2	

*Electrical noise in record. Excluded from means.

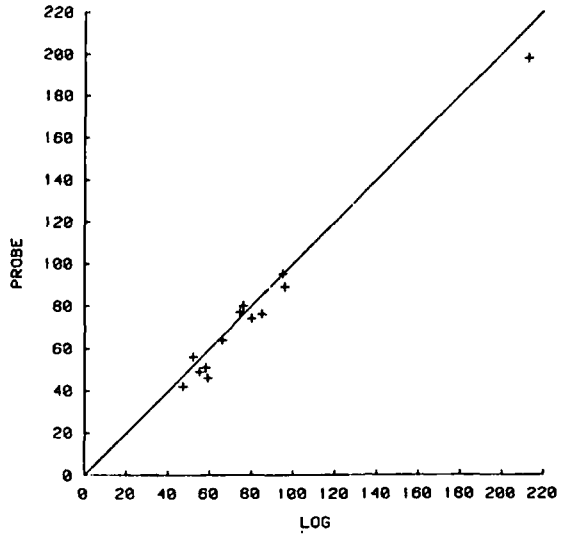

FIG. 8. Temperature gradients (°C/km) over 1 m from downhole probe experiments versus those determined from the most recent temperature log.

and 9, Table 3). The scatter is fairly small (Figure 6). The coefficient of correlation is 0.96, and downhole probe conductivities are systematically higher than those measured on core by about 5 percent (Table 2). We attribute this difference to slight structural changes in the core caused by the removal of the core from its environment, and thus we prefer the downhole values (sufficient conductivities were measured along the axis of the core to confirm that there was no measurable anisotropy). The most striking example of physical changes occurred in the core from 30.5 to 32 m in hole GRA (Table 3). When a hole was drilled into the wall of the core liner to allow access for the needle probe, there was a pop and a muddy slurry was extruded from the core. We see in this instance (conductivity columns, Table 3) that needle-probe conductivities are systematically lower than in-situ values by about 10 percent at this depth.

Formation temperatures

Temperatures obtained from all probe runs by least-squares extrapolation of the later parts of the T-versus-$1/t$ lines (generally for the last 200 to 300 seconds) are plotted against temperatures at the same depth from the most recent temperature log in Figure 7. The correlation is excellent (Table 2), and the value for A of 1.00 tends to confirm our suggestion (Appendix B, Sass et al, 1979) that the temperature differences are random and are caused primarily by the uncertainties in depth measurement that can result in a maximum error of up to 0.1°C.

Gradients over one meter

The largest source of uncertainty in obtaining gradients over a 1-m interval results from the ~0.01°C resolution in relative temperatures between thermistors. Even though individual thermistors were calibrated to within a few millidegrees and the drift rate of each thermistor calibration is slow, small and unpredictable changes in calibration do occur. Calibrations were checked in the field by comparing each thermistor to a single thermistor mounted in a lagged aluminum cylinder. Departures (usually a few millidegrees) from calibration were noted and included in the temperature reduction part of the program so that all thermistor temperatures were relative to a common datum. Even with these procedures, our maximum possible error in the gradient over 1 m is ±20°C/km, clearly not accurate enough for single point determinations of regional heat flow, but certainly sufficiently sensitive to delineate the type of anomaly associated with possible sources of geothermal energy.

Although there is a fairly large scatter (Figure 8), 1-m gradients from the probe experiments correlate very well with those determined from least-squares fits to the six points from the most recent temperature log spanning the 1.5-m interval penetrated by the probe (Table 2). Only results from complete penetrations were used in this comparison. Where only two thermistors entered the

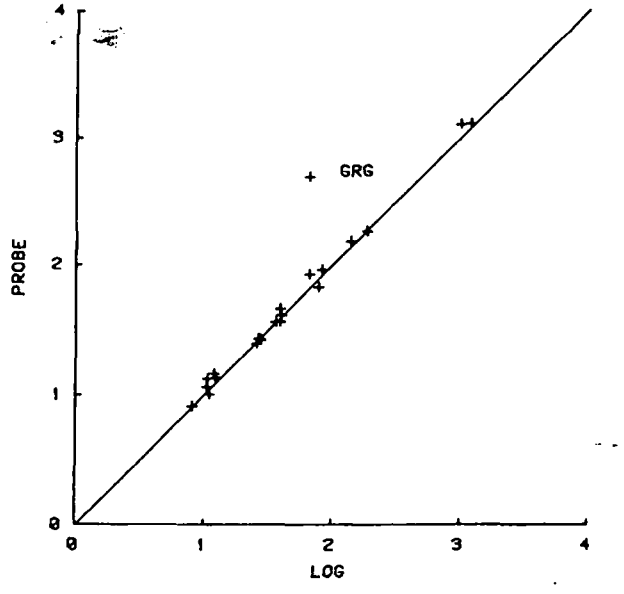

FIG. 9. Heat flow (HFU) over intervals of between 6 and 60 m determined between neighboring downhole probe runs versus heat flows determined over the same intervals from conventional temperature logs.

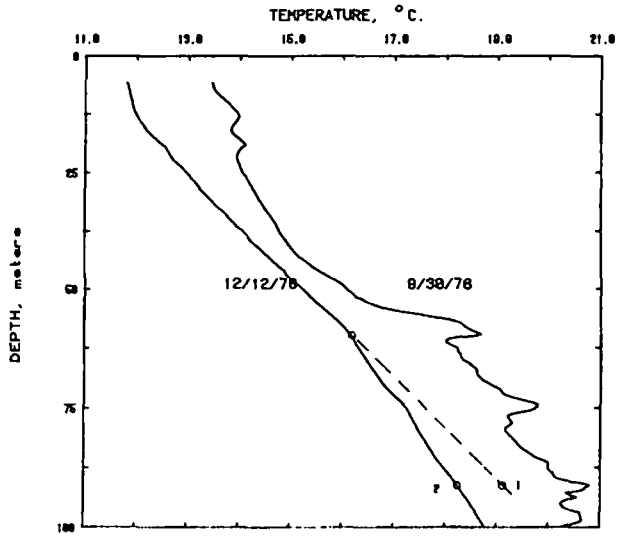

FIG. 10. Temperatures measured at 0.3-m intervals on dates indicated (solid lines) in hole GRG, and downhole probe measurements made during drilling (open circles). Elevated temperatures on the earlier log indicate the interval in which the annulus is filled with cement grout. Numbers beside circles refer to probe thermistors (1 lowermost). The well was drilled on September 27, 1978. Dashed line represents an extrapolation of the upper portion of the profile (between ~30 and 60 m).

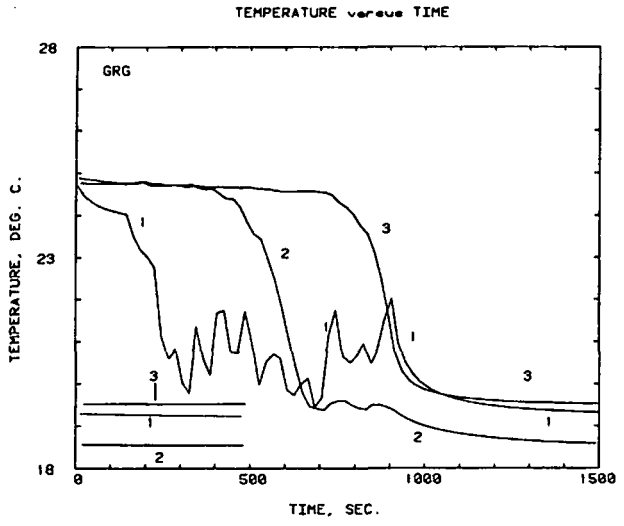

FIG. 11. Penetration record for downhole probe run in Hole GRG, 91 m. Numbers refer to probe thermistors (1 lowermost). Lines at lower left are continuations of the original decay curves ($t_0 \cong 1600$ sec).

formation, the scatter was much greater. This should be expected, as we are attempting to measure the gradient over only 0.5 m and commonly the temperature of the second thermistor is affected by the invasion of drilling fluid.

Heat flow

Since, in most instances, the downhole conductivities were used for both the probe and conventional heat flow estimates over 1 m, the same comments as those made with respect to the 1-m gradient determinations apply to the one-m heat flow determinations. Another approach to heat flow determinations involves computing gradients and mean thermal conductivities over one or more intervals between probe runs ("Interval heat flows" column, Tables 1, 3, and 4). When intervals of a few tens of meters are used, the uncertainties due to reference levels and the errors of ±0.01°C in relative temperatures become negligible. Only one thermistor need penetrate the formation for each run, a requirement that was met in every trial. The interval approach is mandatory when the short probe (all three thermistors in the lowermost 0.3 m) is used. With one exception, the heat flow estimates over the larger intervals agree very well with those calculated from the most recent temperature log (Figure 9). The one exception, hole GRG (Figure 10 and Table 4), suggests that the downhole probe may be the superior technique quite apart from its other advantages.

For the probe test at 91 m in GRG, only two thermistors penetrated well into the formation (thermistor 3 was perhaps 2 cm, at most 5 cm below the bit). When drilling resumed, the driller reported a hard sandy stringer a few centimeters thick just below 61 m. Maximum pressures and a long time (~1000 sec) were required to get the probe into the formation. From the penetration record (Figure 11), thermistor 1 had repeated episodes of frictional heating, whereas the temperature of thermistor 2 dropped immediately as it entered the formation with a cooling curve quite different from either 1 or 3. Thermistor 3 was barely in and its decay curve was probably affected by interaction with the drilling fluid. It is curious and probably not coincidental that the extrapolated equilibrium temperature for thermistor 1 lies on the extension of the very smooth profile in the upper 60 m (Figure 10), whereas that for thermistor 2 lies precisely on the most recent temperature log, which is quite irregular below 60 m. If we interpret the 1-m heat flow at 61 m and the interval heat flow (62–92 m) for thermistor 2 literally (Table 4), then we arrive at a most likely value of between 1.4 and 2 HFU for the heat flow. To reconcile this with the observed gradient of >90°C/km above 60 m, we must assume an implausibly low thermal conductivity of ~2 HCU for the upper part of the hole (see "Least-squares intervals" column, Table 4). If, on the other hand, we assume that the conductivities measured at 61 and 91 m are representative of the entire hole and that, below 60 m, the hole is disturbed, then our preferred heat flow will be about 2.6 HFU, about 30 percent higher than that obtained from the literal interpretation and consistent with the interval heat flow (62.5–92.5 m, Table 4) for thermistor num-

Table 4. Summary of downhole probe experiments, Hole GRG, Black Rock Desert, Nevada.

Depth (m)		Penetration (m)	Temperature (°C)		Gradient (°C/km)		Conductivity (HCU)	Heat flow (HFU)	
Bit	Thermistor		Probe	Log	Probe	Log		Probe	Log
61		1.65							
	61.5		16.162	16.241			2.90		
					26				
	62.0		16.175	16.272			2.85		
					75				
	62.5		16.213	16.302			2.45		
					51	58	2.72	1.39	1.58
91.44		1.16							
	92.0		18.281	18.266			2.63		
					1800				
	92.5		19.167*	18.300			2.85		
					1800*	65	2.74	~49*	1.78
Interval heat flows									
62-92 m					70.2	66.5	2.73	1.92	1.82
62.5-92.5 m					98.5	66.6	2.73	2.69	1.82
Least-squares intervals									
30-56 m					93.5±0.2		2.0?		1.87
							2.73?		2.55
60-102 m					66.1±0.2		2.73±0.02		1.80±0.02
							Best value		2.6

*See Figures 10 and 11 and discussion in the text.

ber 1. Since there is no change in lithology between the upper and lower parts of the hole, it seems more probable that the drill opened a channel below ~60 m between two intervals with a slight head difference, and that water has been moving downward in the annulus since that time; this despite the fact that the annulus between casing and wall in the anomalous section of the hole was apparently grouted off (see temperature log for 9/30/78, Figure 10). This explanation might be applicable to other areas in which, within an apparently uniform lithology, an abrupt change in temperature gradient is observed.

SUMMARY AND CONCLUSIONS

A downhole probe capable of precise determinations of formation temperature and thermal conductivity and rough estimates of the thermal gradient over 1 m can be inserted through a drill bit into unconsolidated sediments, activated, and removed in the time normally taken for a coring run. Two or more penetrations of the probe provide a heat flow determination comparable in accuracy to a conventional heat flow measurement without the necessity of casing the hole or relogging it after completion of drilling. The heat flow determination is made during the drilling process; thus, there is no time delay in obtaining data, no surface hazard associated with protruding casing, and no opportunity for unauthorized entry to boreholes in sensitive or competitive prospects. Because the hole need not be cased, grouted, or visited repeatedly, the technique also is very cost effective. The components necessary for a downhole probe system (described in detail by Sass et al, 1979) can be assembled and added to a preexisting digital temperature-logging system at a modest cost (in the neighborhood of $2,000 to $3,000 at 1980 prices).

Useful information was obtained in all 29 runs in the present study, demonstrating the robustness and the reliability of the equipment. In one hole, data obtained with the downhole probe provided evidence that the drilling process altered the thermal regime locally by permitting vertical water movement even though the casing was grouted in.

Many prospectively important geothermal systems are located within or adjacent to the alluvial and lacustrine sedimentary formations of the western United States. Using the technique outlined in this report, it should be possible to obtain 4 or 5 probe runs per day to depths of between 50 and 150 m in these formations, thus allowing two high-quality heat flow data or several reconnaissance heat flow estimates per day. Even if the field conditions and program objectives call for casing the wells, the reliable determinations in situ of thermal conductivity and the real time estimates of heat flow make the downhole probe a valuable adjunct to the standard approach.

ACKNOWLEDGMENTS

Arthur Lachenbruch originally suggested the technique and gave valuable advice at many stages. Our success in the field was due, in no small measure, to the patience and skill of John Clingan and Western Geophysical crew GT-3. Vaughn Marshall, Mary Lou Zoback, and Eugene Smith rendered valuable assistance in the field.

REFERENCES

Bonham, H. F., 1969, Geology and mineral deposits of Washoe and Storey counties, Nevada: Nevada Bur. Mines Bull. 70, 140 p.

Bullard, E. C., 1954, The flow of heat through the floor of the Atlantic Ocean: Proc. Royal Soc. London, A, v. 222, p. 408–429.

Jaeger, J. C., 1958, The measurement of thermal conductivity and diffusivity with cylindrical probes: AGU Trans., v. 39, p. 708–710.

Keller, G. V., and Grose, L. T., 1978, Studies of a geothermal system in northwestern Nevada; part 1: Colorado School of Mines Quart., v. 73, 84 p.

Lachenbruch, A. H., 1957, A probe for measurement of thermal conductivity of frozen soils in place: AGU Trans., v. 38, p. 691–697.

Lachenbruch, A. H., and Brewer, M. C., 1959, Dissipation of the temperature effect of drilling a well in Arctic Alaska: U.S.G.S. Bull. 1083-C, p. 73–109.

Lachenbruch, A. H., and Sass, J. H., 1977, Heat flow in the United States and the thermal regime of the crust, *in* The Earth's Crust—Its Nature and Physical Properties: J. G. Heacock, Ed., AGU monograph series, Washington, D.C., v. 20, p. 626–675.

Langseth, M. G., 1965, Techniques of measuring heat flow through the ocean floor, *in* Terrestrial heat flow: W. H. K. Lee, Ed., AGU monograph series, Washington, D.C., v. 8, p. 58–77.

Mase, C. W., Chapman, D. S., and Ward, S. H., 1978, Geophysical study of the Monroe-Red Hill geothermal system: Univ. of Utah topical rep. IDO/76-1601-77-17, 89 p.

Olmsted, F. H., Glancy, P. A., Harrill, J. R., Rush, F. E., and VanDenburgh, A. S., 1975, Preliminary hydrogeologic appraisal of selected hydrothermal systems in northern and central Nevada: U.S.G.S. open file rep. 75–56, p. 128–147.

Sass, J. H., Kennelly, J. P., Jr., Wendt, W. E., Moses, T. H., Jr., and Ziagos, J. P., 1979, In-situ determination of heat flow in unconsolidated sediments: U.S.G.S. open-file rep. 79-593, 73 p.

Von Herzen, R. P., and Maxwell, A. E., 1959, The measurement of thermal conductivity of deep sea sediments by a needle probe method: J. Geophys. Res., v. 64, p. 1557–1563.

Ward, S. H., Parry, W. T., Nash, W. P., Sill, W. R., Cook, K. L., Smith, R. B., Chapman, D. S., Brown, F. H., Whelan, J. A., and Bowman, J. R., 1978, A summary of the geology, geochemistry, and geophysics of the Roosevelt Hot Springs thermal area, Utah: Geophysics, v. 43, p. 1515–1542.

Willden, R., 1964, Geology and mineral deposits of Humboldt County, Nevada: Nevada Bur. Mines Bull. 59, 154 p.

Heat Flow

ON SHALLOW-HOLE TEMPERATURE MEASUREMENTS— A TEST STUDY IN THE SALTON SEA GEOTHERMAL FIELD

TIEN-CHANG LEE*

Shallow-hole (<13 m) temperature measurements made at various depths and/or times may yield reliable values of geothermal gradient and thermal diffusivity if the groundwater table is shallow (a few meters) such that the effect of time-dependent moisture content and physical properties is negligible. Two numerical methods based on nonlinear least-squares curve fitting are derived to remove the effect of annual temperature wave at the ground surface. One method can provide information on the gradient and diffusivity as a function of depth while the other gives average value over the depth interval measured.

Experiments were carried in six test holes cased with 2 cm OD PVC pipes in the Salton Sea geothermal field. A set of 5 to 7 thermistors was permanently buried inside the individual pipes with dry sand. Consistent gradient determinations have been obtained with both numerical methods from six monthly observations. By linearly extrapolating the depths to the 100°C and 200°C isotherms from the calculated gradients and mean ground temperatures, we have found good agreement with the nearby deep-well data for four holes. Discrepancy is found for two holes, one of which is located near the field of CO_2 mud volcanoes and the other near the volcanic Red Hill, reflecting complicated local hydrologic conditions.

INTRODUCTION

Heat-flow measurements on land are usually made in boreholes deeper than 30 m in order to avoid the influence of annual temperature variation on the ground surface. Water-filled holes are preferred to the air-filled holes for better thermal contact between the temperature sensor and the surrounding rocks. Here we present two mathematical methods to find geothermal gradient from temperature measurements made within the depth range which is penetrated by the annual temperature wave; and we report the results from six test holes located in the Salton Sea geothermal field (Figure 1) where the groundwater table is 1 to 2 m below the ground surface.

Shallow-temperature measurements have been used to locate and delineate near-surface geologic structures. However, interpretations of the data are often inconclusive. Most debates focus on how the raw data are obtained and how they are reduced to useful formats. Successful case histories have been reported by Poley and Van Stevenick (1970) for outlining salt domes, by Carr (1966) for finding gravel deposits within a clay till, and by Birman (1969) for groundwater exploration. The measurements were made usually below one skin-depth (~1.5 m) of the diurnal solar temperature wave. A set of data is routinely collected within a short time span (1–2 weeks) in order to avoid appreciable temperature change from the annual solar temperature wave which has a skin depth ~20 m. These "contemporaneous" data may reflect the difference in thermal conductivities and, thus, geologic structures. The target thermal anomaly is 1 – 2°C with an error ≥ 0.2°C as estimated by repeated measurements due to air temperature fluctuation in the shallow drill hole and poor thermal contact between the temperature sensor and wall rocks. Since the normal geothermal gradient is around

Manuscript received by the Editor March 15, 1976; revised manuscript received October 4, 1976.
* University of California, Riverside, CA 92502

to be tolerated for gradient and/or heat-flow measurements. The resolution of temperature sensors and precision of depth estimates necessitate gradient measurement be made preferably at depth intervals greater than 1 m. No reliable heat-flow measurements have been reported for drill holes <2 m deep, except in deep sea environments where there are nearly isothermal bottom waters and the sedimentation or erosion rates are small.

The feasibility of using shallow-hole (<20 m) temperature measurements to deduce deeper geothermal gradient has been appraised by Lovering and Goode (1963). If the thermal diffusivity of rocks is known, they can use the graphical method to calculate the gradient from two sets of measurements made at sufficiently separated times. On the other hand, if the diffusivity is unknown but the temperature on ground surface as a function of time or the times when the temperature reaches the annual mean temperature are known, the gradient and diffusivity can be estimated in situ. Either approach requires prior knowledge of the ground temperature characteristics or rock property, and an uneconomically large time span of observation. Furthermore, graphical solutions obtained from sparsely spaced data can hardly exclude personal bias.

The methods presented in this study are based on a nonlinear least-squares fitting and requires no prior knowledge of the thermal diffusivity and the surface temperature as a function of time. A by-product of the methods is a means to estimate in-situ thermal diffusivity. Parasnis (1974) has used an iteration scheme to calculate in-situ diffusivity. His method requires an initial guess on the values of four parameters and neglects geothermal gradient in the calculation. Since the objective of this study is to find the geothermal gradient, different procedures are needed.

MATHEMATICAL FORMULATION

Suppose that the earth within a small area can be approximated by a homogeneous half-space in which the temperature distribution is governed by

$$\frac{\partial T}{\partial t} = \mu \frac{\partial^2 T}{\partial Z^2}, \qquad (1)$$

where T = temperature, t = time, μ = thermal diffusivity, and Z = distance with positive direction pointing into the ground. Suppose further that the temperature on the ground surface is

[heat flux from the earth] where k = thermal conductivity and g = geothermal gradient. Then, the temperature distribution in the ground is

$$T = T_s + gZ + A\, e^{-Z\sqrt{\omega/2\mu}} \sin[\omega(t - t_0) - Z\sqrt{\omega/2\mu}], \qquad (2)$$

where ω is the frequency of the annual temperature wave and A is its amplitude at $Z = 0$, and t_0 is the time when the temperature crosses its mean temperature (twice a year). Perturbation from this idealized distribution will be discussed later.

The gradient g is the quantity to be sought in the shallow-hole temperature measurements. It can be easily calculated if the temperature is measured at a given (t, Z), and other parameters T_s, A, T_0, and μ are previously known. In practice these parameters are unknown and need to be estimated in addition to g. Since T is a nonlinear function of (t, Z, μ), the linear least-squares method cannot be used directly to find g and other parameters. With suitable transformation of variables, however, equation (2) can be linearized.

Direct method

The first method requires measurements be made at two given depths at different times. Since no assumption is made, this method is herein called the direct method.

At given depth Z_i, equation (2) becomes, after trigonometric expansion,

$$T_{j,i} = \alpha_i + \beta_i x_j + \gamma_i y_j, \qquad (3)$$

where the new parameters

$$\alpha_i = T_s + g Z_i,$$

$$\beta_i = A\, e^{-Z_i\sqrt{\omega/2\mu}} \cos(\omega t_o + Z_i\sqrt{\omega/2\mu}), \qquad (4)$$

and

$$\gamma_i = -A\, e^{-Z_i\sqrt{\omega/2\mu}} \sin(\omega t_o + Z_i\sqrt{\omega/2\mu}),$$

are determined by (linear least-squares) fitting the dependent variable $T_{j,i}$ to the "independent" variables $x_j = \sin \omega t_j$ and $y_j = \cos \omega t_j$, with subscript j representing discrete observation times, $j = 1, 2, \ldots, n$ $(n \geq 4)$. Another set of measurements at depth Z_{i+1} provides a means to calculate the gradient

$$g_{i+1/2} = (\alpha_{i+1} - \alpha_i)/(Z_{i+1} - Z_i), \qquad (5)$$

and thermal diffusivity

Subscript $i + 1/2$ indicates a quantity determined for the depth range from z_i to z_{i+1}. Other parameters can be subsequently obtained from (4) but are omitted for lack of interest here.

One of the basic assumptions regarding the temperature distribution (2) is the homogeneity of the medium. If temperatures are measured at more than two depths, any pair of data sets will yield values of g and μ. Deviations of the individual g and μ from their means indicate their depth dependencies, even for the same type of sediments or soils since thermal conductivity is expected to increase with depth owing to compaction. The gradient decreases and diffusivity increases accordingly with depth. More involved mathematical procedures based on multilayered models can a finer solution in this study.

Indirect method

The second method requires temperature measurements be made at more than five depths at one given time. It needs to scan through the range of all possible values for one of five parameters: T_s, g, A, μ, and t_0. Since the range of thermal diffusivity for common rocks is small (2×10^{-7} to 2×10^{-6} m^2sec^{-1}) as compared to other parameters, it is chosen for scanning. This method is herein called the indirect method.

At a given time t_j, equation (2) becomes after trigonometric expansion

$$T_{j,i} = T_s + gZ_i + \delta x_i + \epsilon y_i , \qquad (7)$$

where the parameters T_s, g,

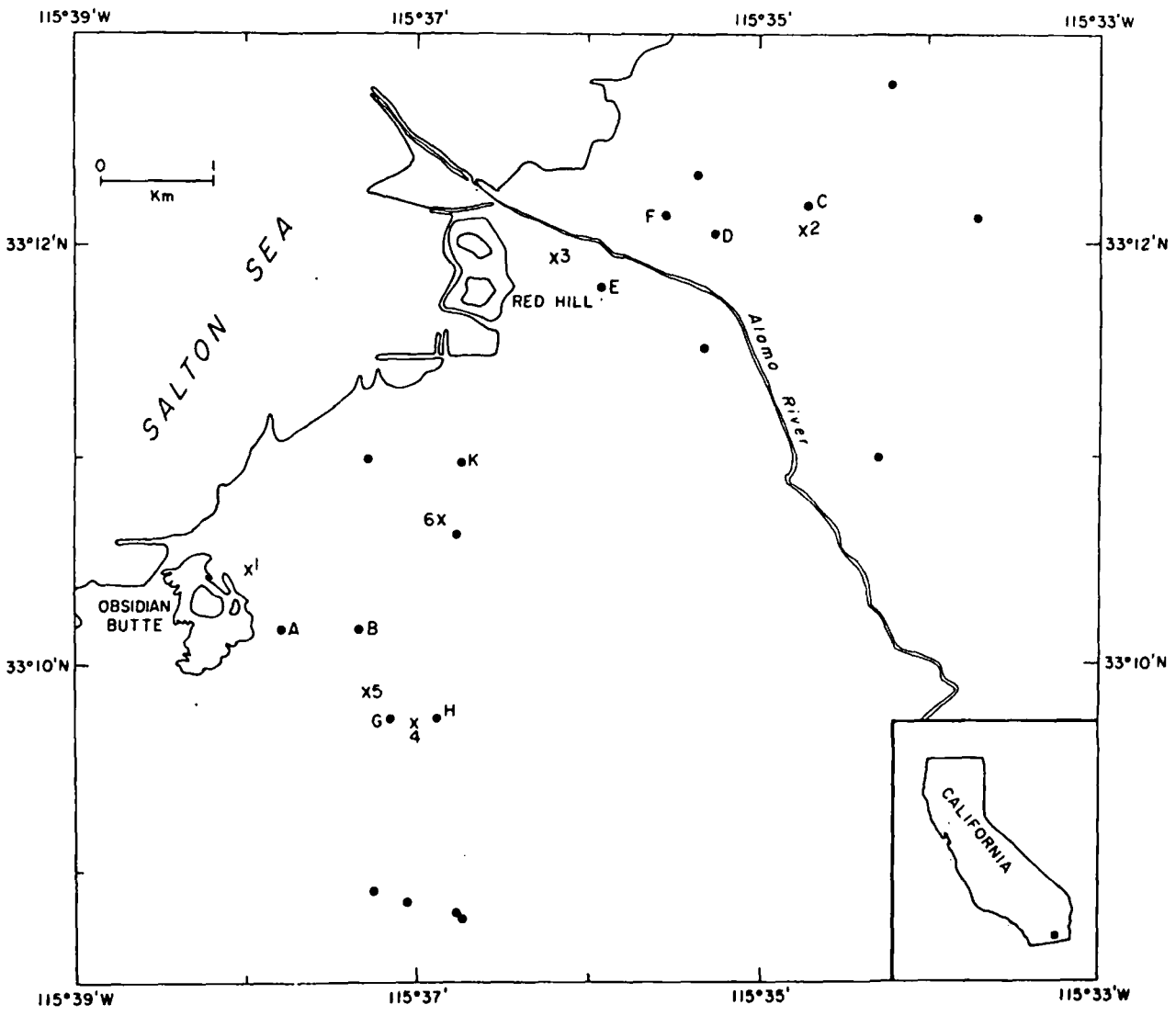

FIG. 1. Locations of shallow holes (×) and deep wells (solid circles). Numbers refer to hole names, UCR-SSS-1 to UCR-SSS-6 series; letters refer to well names cited in Table 3.

$$\epsilon = A \cos \omega(t - t_o)$$

are determined by fitting the dependent variable $T_{j,i}$ to the "independent" variables Z_i,

$$x_i = e^{-z_i \sqrt{\omega/2\mu}} \cos (Z_i \sqrt{\omega/2\mu}),$$

and

$$y_i = e^{-z_i \sqrt{\omega/2\mu}} \sin (Z_i \sqrt{\omega/2\mu}),$$

with $i = 1, 2, \ldots, m$ and $m \geq 5$. By scanning through the possible values of μ at an increment of 2.5×10^{-8} $m^2 sec^{-1}$, a minimum in the misfit as indicated by the standard deviation will emerge. Since $m = 4$ gives an exact fit to determine four parameters, $m \geq 5$ is needed to find the minimum. The μ for this minimum is taken as the weighted average of the thermal diffusivity in the depth range covered. Then the gradient g is one of the parameters directly determined from the least-squares method for the chosen μ.

A comparison of the two methods is in order. The indirect method has the advantage of saving time because it requires measurement at one given time, whereas the direct method requires observations over several months. However, longer observations are indispensable for a shallow-hole temperature survey in a given area in order to see possible temperature perturbations and to provide confidence limit on the estimated gradients. Direct methods give information on depth dependencies but indirect method gives the weighted average only.

EXPERIMENT

To test the applicability of the two methods for finding geothermal gradients we made several monthly observations in six shallow holes, which were drilled in the Salton Sea geothermal field (Figure 1). These holes range in depth from 7 to 13 m, reflecting the different degree of difficulty in drilling at various places. Each hole was cased with a 3/4 inch OD PVC pipe to prevent the spacing of thermistors from changing during installment of the sensors. A set of seven thermistors, each housed respectively in a 1/8 inch OD stainless steel tube 6 inches long, was hung permanently inside the pipe with the lead wires. The rest of the pipe was filled with dry, fine sand in order to improve thermal contact and minimize air convection inside the pipe; and both ends of

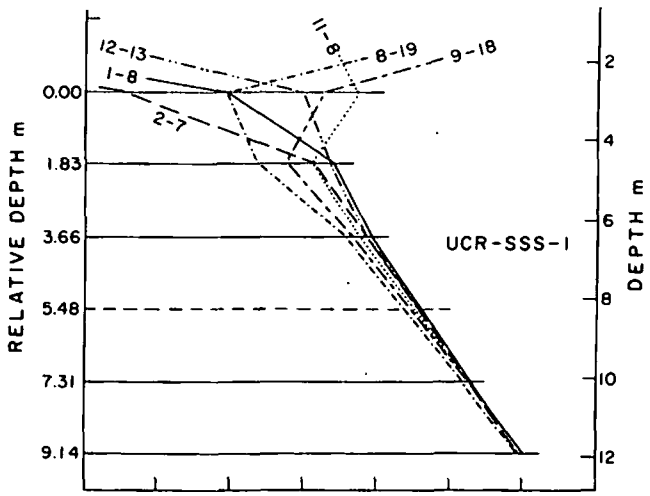

FIG. 2. Temperature vs depth as a function of time near the Obsidian Butte, UCR-SSS-1. Horizontal lines indicate depths of measurements (dashed line indicates a malfunctioned thermistor). Depth refers to the ground surface and relative depth refers to the second thermistor from the top.

the pipe were sealed to keep water from seeping into thermistor probes even though the probe has been shown to be waterproof for 10 hours of laboratory test. The lead wires were connected to a terminal board outside the collar, which was buried ~30 cm below the ground surface. Only the terminal board was exposed for monthly measurements.

The thermistors used were of Fenwall GB32M2 with a nominal resistance around 2000 Ω at room temperature (~4000 Ω is recommended for future work, so that the resistance of thermistor stays about a few kΩ at borehole temperature of 50°C). The largest lead wire resistance is ~1Ω, hence no compensation was made for it. All thermistors together with their protective probes were calibrated in a constant temperature bath (Neslab TE70) from 5°C to 45°C at an increment of 5°C against a quartz thermometer (Hewlett Packard 2800 A) of which the calibration was traceable to the U.S. Bureau of Standards. A calibration curve of the type $T = B + C \ln R + D (\ln R)^3$ was fitted to the calibration points (see Appendix) where T = temperature in °K, R = resistance in ohms, and B, C, D are coefficients to be determined from calibration. For laboratory calibrations and field measurements, the same Wheatstone bridge, standard decade resistor, and null meter were used. Resistance was read to the nearest 0.1 Ω; and the calibration constants B, C, and D were used to convert a resistance reading into its

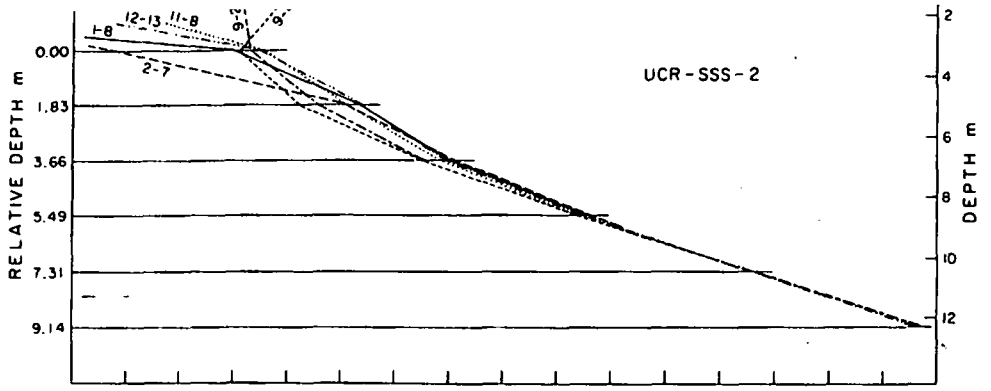

FIG. 3. Temperature vs depth as a function of time near the mud volcanoes, UCR-SSS-2. Horizontal lines indicate depths of measurements (dashed line indicates a malfunctioned thermistor). Depth refers to the ground surface and relative depth refers to the second thermistor from the top.

equivalent temperature. The precision was a few 0.001°C, and accuracy was around 0.01°C because of calibration error, lead wire resistance, thermistor drifting, and other errors in measurement.

Because the thermal conductivity of sediments cannot be estimated in situ with the suggested methods, we have used the needle probe method (Von Herzen and Maxwell, 1959) to measure thermal conductivities of the sediments brought up during drilling.

DATA ANALYSIS

The temperature data obtained from six monthly observations are shown in Figures 2 to 7 for holes UCR-SSS-1 to UCR-SSS-6, respectively. The first set of measurements in each hole was made at least 11 days after the hole was drilled. According to equation (63) of Jaeger (1965), the transient temperature disturbance due to drilling will die away within 5 days for a drilling time of 3 hours and a hole radius of 3 cm. Disturbance due to PVC-pipe casing is negligible. Our measurements thus represent values at equilibrium with the ambient temperature. Both the direct and indirect methods have been used to fit these data, except that recorded by the topmost thermistor in each hole, because its relative depths to other thermistors are not accurately known. The differences between the observed temperature and the values calculated from the coefficients of least-squares fit are smaller than the graphical resolution. We have therefore omitted the fitted curves drawn from equation (2) and connected the discrete observation points only with line segments to demonstrate temperature as a function of time and depth. All thermistors installed appear to behave properly as of the last measurements in February 1976 (except for one thermistor at UCR-SSS-1 one month after installment).

Table 1 summarizes the results of data reduction with the indirect method. Because the iteration scheme of this method requires more than 5 depth points, the geothermal gradient and thermal diffusivity cannot be determined for UCR-SSS-5, where only 4 thermistors are usable. The standard deviations of the geothermal gradients in individual holes are less than 1.2 percent of their

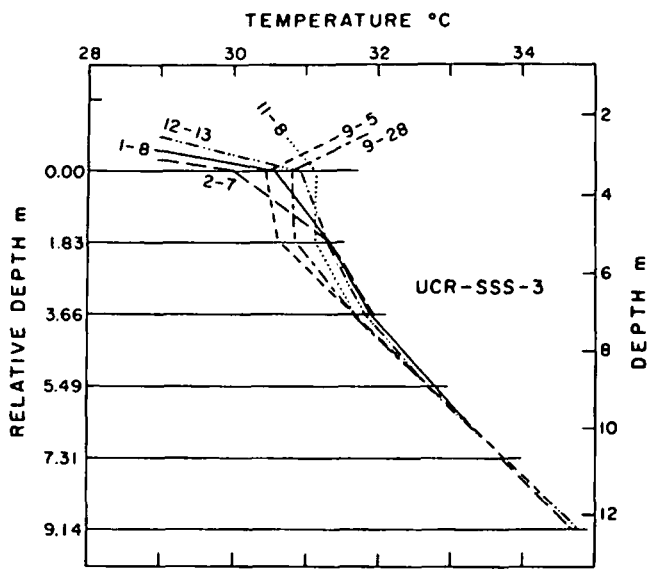

FIG. 4. Temperature vs depth as a function of time, east of the Red Hill, UCR-SSS-3. Horizontal lines indicate depths of measurements (dashed line indicates a malfunctioned thermistor). Depth refers to the ground surface and relative depth refers to the second thermistor from the top.

Holes	A	B	n	m	Δ	μ	g
1	08/08/75	08/19/75	5	7	0.001	2.19 ± 15%	0.401 ± 1.0%
2	08/09/75	08/29/75	6	7	0.012	3.96 ± 42%	1.658 ± 0.9%
3	08/09/75	08/19/75	6	8	0.004	2.69 ± 32%	0.561 ± 0.4%
4	08/18/75	09/03/75	6	6	0.010	7.88 ± 24%	0.356 ± 1.1%
6	08/19/75	09/03/75	6	6	0.021	4.56 ± 10%	0.334 ± 1.2%

[1] Date A = drilling date; Date B = date of first temperature measurements; n = number of thermistors used in data reduction; m = number of monthly measurements; μ = mean thermal diffusivity in units of 10^{-7} m^2s^{-1}; g = weighted mean geothermal gradient in units of $°Cm^{-1}$; Δ = mean of the standard deviations for the individual monthly measurements in unit of °C. Uncertainties ± in μ and g are standard deviations from the means.

respective means. They are negligibly small but the maximum standard deviations (≤0.02°C) of temperature fittings are about twice the maximum error in our thermistor calibration. Errors in the individual determinations of thermal diffusivity may reach as much as 42 percent of the mean. An examination of the gradients corresponding to different diffusivity values, which are a few increments (2.5×10^{-8} m^2sec^{-1}) more or less than the chosen value, indicates that uncertainty in the in-situ determination of diffusivity may lead to an error of ≤0.008°C m^{-1} in the reduction of gradient. This error is ~2 percent of the gradient in the Salton Sea geothermal field and ~10 percent in the areas of normal geothermal gradient (~0.060°C m^{-1} in unconsolidated sediments).

The results of data reduction with the direct method are summarized in Table 2. In general, the standard deviations of temperature fittings with the direct method are greater than those with the indirect method. Except at UCR-SSS-1 and UCR-SSS-3 where the thermistor sets were buried at relatively greater depth, fittings at relative depth 0.0 m are here considered unacceptable (standard deviation >0.03°C). The gradient and diffusivity reduced from such unacceptable least-squares fit are starred in Table 2 and excluded from the calculation of the mean geothermal gradient and mean diffusivity. An unreliable determination in diffusivity is usually recognized by data which indicate that the amplitude of annual temperature wave is slightly greater at deeper level. Such cases are doubly starred in Table 2. Excluding the starred values, there is no systematic variation in either the geothermal gradient or diffusivity with depth.

Geothermal gradients reduced from both the direct and indirect methods are listed in Table 3. The mean value derived from the direct method is slightly less than that derived from the indirect method except at UCR-SSS-6. For a given hole, the "direct mean gradient" and "indirect gradient" differ no more than 8 percent from each other. Also given in Table 3 are the mean interval gradients averaged over six monthly observations determined from the bottom-most two thermistors in a hole. Mean bottom gradients agree very well with the indirect gradient. However, systematic time variation in the bottom gradients have been observed in areas of relatively high thermal diffusivity. For example, at UCR-SSS-5, the bottom gradient cannot be estimated from the raw data because of the large time variation in temperature. Standard deviations of the direct gradients are greater than that of indirect gradients. Since the former reflects the variations of gradient with depth as well as times, while the latter reflects time variations, greater standard deviations do not imply that the direct method is inferior to the indirect method. If heat flux at a given locality is

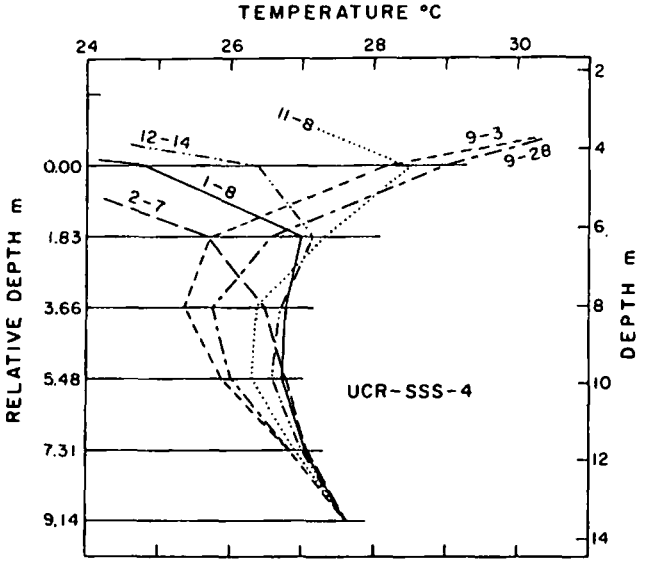

FIG. 5. Temperature vs depth as a function of time, UCR-SSS-4. Horizontal lines indicate depths of measurements (dashed line indicates a malfunctioned thermistor). Depth refers to the ground surface and relative depth refers to the second thermistor from the top.

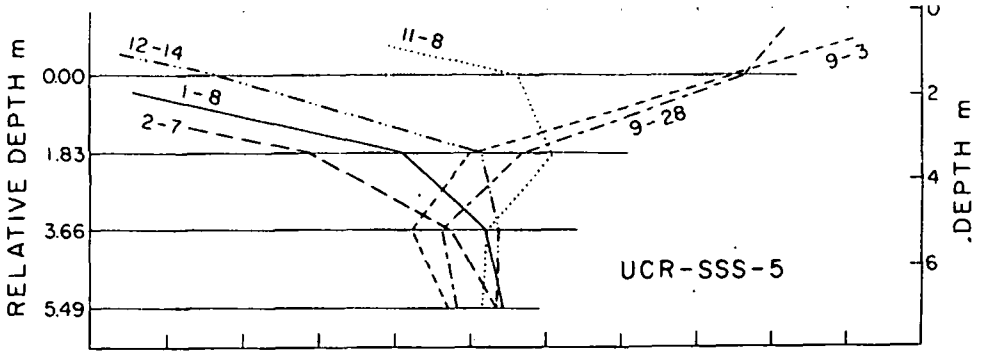

FIG. 6. Temperature vs depth as a function of time, UCR-SSS-5. Horizontal lines indicate depths of measurements (dashed line indicates a malfunctioned thermistor). Depth refers to the ground surface and relative depth refers to the second thermistor from the top.

constant, variation in gradient should be accompanied by conductivity variation. The mean thermal conductivity of sediments in the five individual localities (Table 3, Figure 1) range from 1.05 to 1.90 Wm^{-1} °C. The latter appears unusually high for unconsolidated sediments but it is not impossible for saturated soils and deep-sea sediments with high quartz content (Clark, 1966; Kasameyer et al, 1972). Conductivity variation is also consistent with the variation in the in-situ measured diffusivity. Such variations suggest that the gradient variation with depth as determined by the direct method may be real. At present, we do not have sufficient data to substantiate depth variations.

To test whether the shallow hole temperature measurements can be used to estimate qualitatively the depths to the geothermal reservoir, we have calculated the depths to 100°C and 200°C isotherms by linear extrapolation using the geothermal gradient and the calculated mean temperature at relative depth 0.0 m. The results are listed on Table 3 and compared to the data obtained from two deep wells located nearest to the individual shallow holes (Figure 8). Below 200°C isotherm convection may play a major role in the heat transfer processes so that further extrapolation based on conduction is invalid (convection may occur at temperature less than 200°C, too, depending upon reservoir conditions). Deep well

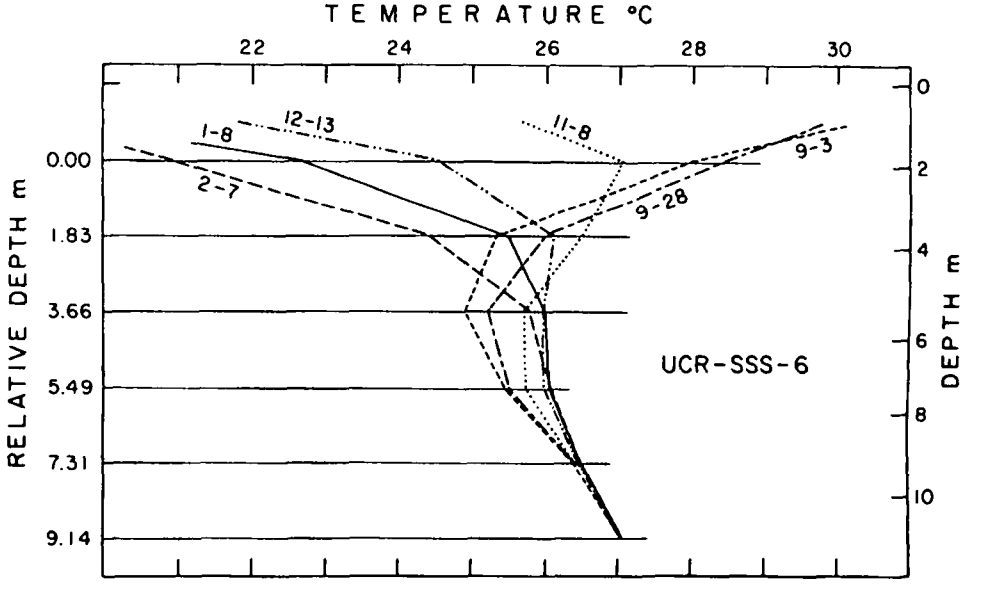

FIG. 7. Temperature versus depth as a function of time, UCR-SSS-6. Horizontal lines indicate depths of measurements (dashed line indicates a malfunctioned thermistor). Depth refers to the ground surface and relative depth refers to the second thermistor from the top.

Hole	Depth	Δ	μ	g
1	0.00	0.010		
			1.50*	0.920*
	1.83	0.022		
			2.27	0.575*
	3.66	0.007		
			4.90	0.400
	7.31	0.003		
			**	0.398
	9.14	0.002		
	mean		3.58	0.399
2	0.0	0.067		
			2.59*	1.656*
	1.83	0.032		
			6.39	1.160*
	3.66	0.010		
			1.58	1.518
	5.49	0.003		
			**	1.687
	7.32	0.008		
			**	1.664
	9.14	0.007		
	mean		3.98	1.623
3	0.0	0.008		
			3.91	0.530
	1.83	0.010		
			1.94	0.517
	3.66	0.008		
			1.92	0.521
	5.49	0.006		
			**	0.541
	7.32	0.008		
			**	0.572
	9.14	0.008		
	mean		2.36	0.536
4	0.0	0.122		
			*	0.140*
	1.83	0.015		
			5.36	0.282
	3.66	0.007		
			7.08	0.292
	5.49	0.007		
			4.10	0.366
	7.32	0.002		
			2.44	0.357
	9.14	0.003		
	mean		4.74	0.324
5	0.00	0.181		
			5.07*	0.363*
	1.83	0.020		
			4.22	0.494
	3.66	0.024		
			4.02	0.406
	5.49	0.015		
	mean		4.12	0.450
6	0.0	0.117		
			6.18*	0.217*
	1.83	0.010		
			3.38	0.426
	3.66	0.012		
			5.58	0.302
	5.49	0.005		
			2.47	0.385
	7.32	0.009		
			2.80	0.325
	9.14	0.003		
	mean		3.56	0.360

[1] Depth = relative depth in units of *m*, used in fitting at a given depth; μ = thermal diffusivity in units of 10^{-7} m^2 sec^{-1}; Δ = standard deviation of temperature fitting, in °C.
* Data may be affected by diurnal wave.
** Unreliable determination in diffusivity.

data are interpolated from temperature profiles compiled by Randall (1974).

The extrapolated depths to the 100°C and 200°C isotherms for UCR-SSS-1, -4, -5, and -6 are within 30 m of the respective depths observed in the nearest deep wells and within 160 m for the second nearest wells (Figures 1 and 8). These discrepancies are comparable in magnitude to the depth variations of a given isotherm observed in the deep wells, i.e., 40 m and 160 m for the 100°C and 200°C isotherms, respectively (excluding River Ranch data). Shallow hole data and their extrapolation are therefore acceptable in the vicinity of these four sites.

Large discrepancies occur, however, at UCR-SSS-3 in the volcanic Red Hill and at UCR-SSS-2 near the active CO_2 mud volcanoes. The extrapolated depths to the 200°C isotherm are, respectively, 210 m and 430 m shallower than the nearby deep well data. If the River Ranch data are used for comparison, the discrepancies become larger. The shallower isotherm (380 m) was measured in 1964 near the time the River Ranch was flowed, and the deeper isotherm (730 m) was measured in 1968 about two years after the well was last flowed for 254 days. Both values are probably not representative of the thermal regime there. High geothermal gradient at UCR-SSS-2 reflects very likely that hot fluid has moved to shallow depth recently. We saw mud bubbling up during drilling, but activity of mud volcanoes was weak then and there was no surface manifestation of previous activity around the site of our measurement. In the Red Hill, bubbling did not occur during drilling.

Heat-flow data based on the calculated gradient

		Gradient	K	Q	Depth	Dist	Depth	Well name	
1	Direct	0.399 ± 0.3%	1.15	460(11)	180/430	0.6	210/440	Magmamax 2	A
	Indirect	0.401 ± 1.0%		460(11)	180/430	1.1	210/400	Magmamax 3	B
	Bottom	0.399 ± 0.4%		460(11)	180/430				
2	Direct	1.623 ± 5.6%	1.10	1870(45)	45/105	0.3	230/730 /380	River Ranch	C
	Indirect	1.658 ± 0.9%		1910(46)	40/100	0.8	210/530	Sportsman 1	D
	Bottom	1.678 ± 1.7%		1930(46)	40/100				
3	Direct	0.536 ± 4.1%	1.05	560(13)	130/320	0.5	210/520	IID 2	E
	Indirect	0.561 ± 0.4%		590(14)	125/300	1.1	210/540	IID 1	F
	Bottom	0.571 ± 1.5%		600(14)	120/300				
4	Direct	0.324 ± 13.4%	1.90	620(15)	235/545	0.2	170/360	Magmamax 1	G
	Indirect	0.356 ± 1.1%		680(16)	215/495	0.2	/490	Woolsey 1	H
	Bottom	0.362 ± 18.5%		690(16)	210/490				
5	Direct	0.450 ± 13.8%	1.87	840(20)	170/390	0.3	170/360	Magmamax 1	G
6	Direct	0.360 ± 15.7%	1.41	510(12)	210/490	0.5	200/500	Elmore 1	K
	Indirect	0.334 ± 1.2%		470(11)	230/530	0.2	210/400	Magmamax 3	B
	Bottom	0.334 ± 13.0%		470(11)	230/530				

[1] Gradient in units of °C m^{-1}; K = conductivity in units of Wm^{-1} C^{-1}; Q = heat flux in units of 10^{-3}W m^{-2}, number in parenthesis in units of 10^{-6} cal/cm^2sec; depth = depth to 100°C and 200°C isotherms, respectively, in meters; Dist = distance from shallow hole to deep well, in kilometers; letters after the well name refer to well location on Figure 1.

and measured conductivity are listed in Table 3. The conductivities were measured for three samples in each hole except that the average of all data is assumed to be the conductivity at UCR-SSS-6. The highest flux is 1943 mWm^{-2} (46 μ cal/cm^2sec) at UCR-SSS-2 near the mud volcanos and lowest flux 460 mWm^{-2} (11 μcal/cm^2sec) at UCR-SSS-1 near the Obsidian Butte.

DISCUSSION

Our data reduction from shallow-hole temperature measurements is based on an idealized temperature distribution, equation (2). Perturbations from that may be caused by time-dependent boundary conditions on the ground surface besides the annual wave. Although diurnal variations are attenuated to 37 percent of their ground values at one skin depth (~1.5 m) where the relative depth 0.0 m is roughly set for each hole, a couple of degrees change at the ground surface is still significantly large for the accuracy required in the shallow hole heat-flow measurements. Poor temperature fitting at relative depth 0.0 m at UCR-SSS-4 through UCR-SSS-6 (Table 2) results very likely from the contamination of diurnal variations. At next depth level (1.83 m), the fitting error is reduced to ~10–12 percent of that at the depth 0.0 m. Consistent with the theory, the attenuation of diurnal variation over equal depth interval are greater for area of low thermal diffusivity. Fitting error at 0.0 m in UCR-SSS-1 and UCR-

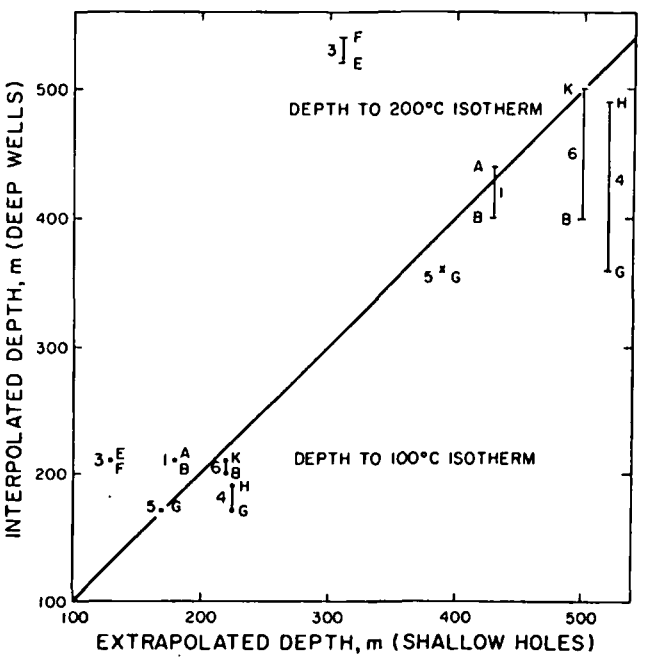

FIG. 8. Depths to 100°C and 200°C isotherms. Diagonal line represents ideal agreement between extrapolation and interpolation. Vertical bar indicates the range of depths to a given isotherm observed in the two deep wells closest to individual shallow holes. Numbers and letters refer to hole and well locations in Figure 1 and Table 3.

the diffusivity is also relatively smaller compared to other sites, but the cause of greater error at 1.83 m in UCR-SSS-1 cannot be attributed to the diurnal effect. At 1.83 m in UCR-SSS-2, the error which is ~50 percent of that at 0.0 m may be caused by the diurnal effect if the measured high thermal diffusivity is reliable. It is noted that this high diffusivity layer is underlain by a low diffusivity layer and that the average of the two values obtained from the direct method is the same as the weighted mean value determined with the indirect method.

Our sampling intervals in time and depth are too large to resolve the effect of diurnal variation. At relative depth 1.83 m or greater, the fitting error is about the same order of magnitude of experimental error. The diurnal effect cannot be estimated and removed from the error analysis of attenuation. Some interval gradients which may be affected by diurnal variation therefore have been starred in Table 2 and excluded from averaging. In this sense, the mean geothermal gradient determined with the direct method is free of interference from diurnal effect but the indirect gradient may be contaminated. However, the interference is probably negligible because the indirect gradient does not differ more than 8 percent from the average direct gradient in each hole.

Annual temperature variation on the ground surface is an imperfect sinusoidal wave: its period may not be exactly one year, its amplitude may be time dependent, and its peak may not be exactly six months from its trough. Our measurements are results of aperiodic annual and diurnal waves coupled with long-term climatic variations and irregular temperature change due to natural causes or human activities. The amplitude of long period climatic variation is very unlikely to exceed two percent in the Salton Sea geothermal field (heat flux >420 × 10^{-3} Wm^{-2} or 10 μcal/cm^2sec), although our observation time and depth were insufficient to detect these effects. Abrupt temperature change could have happened at UCR-SSS-4 owing to the development of the geothermal field from the crop field. Our six-month observations with the indirect method show only 1.1 percent variation (Table 3) and hence did not differentiate the effect of a step-function-like event which had occurred two to three years before the hole was drilled.

A fluid column in a vertical hole may become Gretener, 1967; and references therein),

$$\left(\frac{\Delta T}{\Delta Z}\right)_{cri} = \frac{g\alpha T}{C_p} + \frac{B\nu\kappa}{g\alpha r^4},$$

where

g = gravitational acceleration,
α = volume coefficient of thermal expansion,
T = absolute temperature,
C_p = specific heat,
B = constant (216 for a tube whose length >> diameter),
k = thermal conductivity,
ρ = density,
$\kappa = k/\rho c$ = thermal diffusivity,
ν = kinematic viscosity, and
r = radius of the hole.

For a 2-cm hole (r = 1 cm) which was used in this study, the critical gradient is 0.87°C/m for pure water and 2.14°C/m for dry air. In areas of normal geothermal gradient (~0.030°C/m), stable temperature measurements in either the water-filled or air-filled holes are expected. In the Salton Sea geothermal field, however, the geothermal gradient may locally exceed the critical gradient (e.g., UCR-SSS-2), and temperature oscillation due to convection on the order of 0.01°C with period ranging from minutes to hours, as reported by Diment and Gretener elsewhere in large diameter wells, may have occurred. To avoid the development of temperature oscillation, the cased holes were filled with dry sand to reduce the effective hole radius and hence increase the critical values. Convection might have developed in the holes filled with porous sand, but we have not yet detected its existence.

Groundwater movement outside the holes may affect the temperature measurement either directly or indirectly by changing the physical properties of sediments and soils. Because the thermistors used were located below the groundwater table, the effect of the vertical movement of water or vapor is probably negligible. A detailed discussion on this diurnal effect has been presented by Lettau (1951, 1954).

Nonuniform "steady-state" temperature distribution on the ground surface may influence the heat-flow values determined from shallow holes such that they do not represent the values at deeper level. Topographic effect is negligible because the ground is essentially flat in this part of

poses some problems for linear extrapolation to greater depth. No attempt has been made to correct those effects. By comparing to the deep-well data, we have established the feasibility of using shallow-hole temperature measurements to deduce the depths to the 200°C isotherm, which is probably within the regime dominated by conduction heat transfer.

Discrepancy between the extrapolated and interpolated depths to the 100°C and 200°C isotherms at UCR-SSS-2 and UCR-SSS-3 suggests that there are probably two thermal and/or hydrographic regimes separated by a NW-trending fault near Red Hill. Existence of such a fault is also suggested but not yet confirmed conclusively by a resistivity survey and a seismic refraction profile. Degassing of CO_2 and activity of mud volcanoes appear to have been restricted to the northeast of the proposed fault. A detailed study is now taken to resolve whether there are two regimes; in one area the shallow hole data can be used for extrapolation whereas in another area the extrapolated values are not reliable.

CONCLUSIONS

We have demonstrated the applicability of shallow-hole temperature measurements in geothermal study by (1) showing consistency in gradient determinations with the direct and indirect methods, and (2) comparing the linearly extrapolated depths to 100°C and 200°C isotherms with the direct interpolation from deep well data. Success in gradient determination is due in part to favorable hydrological conditions in the study area because a shallow groundwater table (1 ~ 2 m) prevents drastic time-depth oscillation in thermal conductivity and diffusivity which may arise from an oscillating change of moisture contents in the sediments. Our methods are based on the assumptions of medium homogeneity and time-independent physical properties of sediments.

Depths to 100°C and 200°C isotherms for four shallow-holes are found to agree with nearby deep-well data, but disagreements appear in the remaining two holes. In case of discrepancy the estimated depths are invariably shallower than the observed depths. The discrepancy is due to complicated local hydrological conditions near the carbon-dioxide mud volcanoes (UCR-SSS-2) and possibly near the volcanic Red Hill too (UCR-SSS-3).

their comments on this manuscript and to W. Grinyer, S. Lauber, and P. Laurin for their laboratory and field assistance. This work is sponsored by NSF-RANN grant AER 72-03551.

REFERENCES

Bennett, A. S., 1972, The calibration of thermistors over the temperature range 0° ~ 30°C: Deep-Sea Res., v. 19, p. 157–163.

Birman, J. H., 1969, Geothermal exploration for groundwater: Bull. GSA, v. 80, p. 617–630.

Carr, D. D., 1966, Temperature variation at a depth of 30 cm in clay till and outwash sand and gravel: Proc. 4th Sympos. Remote Sensing of Environ., Ann Arbor, Mich., p. 203–214.

Clark, S. P., Jr., 1966, Thermal conductivity, *in* Handbook of physical constants: S. P. Clark, Jr., ed., GSA Mem. 97.

Diment, W. H., 1967, Thermal regime of a large diameter borehole: Instability of the water column and comparison of air- and water-filled condition: Geophysics, v. 32, p. 720–726.

Goss, R. D., 1974, Empirical relationships between thermal conductivity and other physical parameters in rocks: Ph.D. dissertation, Univ. California, Riverside, 216 p.

Gretener, P. E., 1967, On the thermal instability of large diameter wells—an observational report: Geophysics, v. 32, p. 727–738.

Jaeger, J. C., 1965, Application of the theory of heat conduction to geothermal measurements, *in* Terrestrial heat flow: W. H. K. Lee, ed., AGU Mongr. 8, p. 7–23.

Kasameyer, P. W., Von Herzen, R. P., and Simmons, G., 1972, Layers of high thermal conductivity in the North Atlantic: J. Geophys. Res., v. 77, p. 3162–3167.

Lettau, H., 1951, Theory of surface-temperature and heat-transfer oscillations near a level ground surface: Trans. AGU, v. 32, p. 189–200.

——— 1954, Improved models of thermal diffusion in soil: Trans. AGU, v. 35, p. 121–132.

Lovering, T. S., and Goode, H. D., 1963, Measuring geothermal gradients in drill holes less than 60 feet deep, East Tintic District, Utah: U.S.G.S. Bull., v. 1172, 48 p.

Parasnis, D. S., 1974, Estimates of in situ thermal diffusivity of the ore-bearing rocks in some drillholes in the Skellefte field (N. Sweden) using the annual temperature wave: J. Geophys., v. 40, p. 83–95.

Poley, Ph. J. and Van Steveninck, J., 1970, Geothermal prospecting—delineation of shallow salt domes and surface faults by temperature measurements at depth of two meters: Geophys. Prosp., v. 18, p. 666–700.

Randall, W., 1974, An analysis of the subsurface structure and stratigraphy of the Salton Sea geothermal anomaly, Imperial Valley, California: Ph.D. dissertation, Univ. California, Riverside, 92 p.

Steinhart, J. S., and Hart, S. R., 1968, Calibration curves for thermistors: Deep-Sea Res., v. 15, p. 497–503.

Von Herzen, R. P., and Maxwell, A. E., 1959, The measurements of thermal conductivity of deep-sea sediments by a needle-probe method: J. Geophys. Res., v. 64, p. 1557–1563.

absolute temperature T qualitatively by

$$R = A\, e^{-E/T}, \qquad \text{(A-1)}$$

where E and A are constants. However, a calibration curve of the form (with an additional term for second order correction),

$$\ln R = \alpha + \beta/T + \gamma/T^2, \qquad \text{(A-2)}$$

does not meet the precision required for temperature measurement. Polynomial curves of the form,

$$T = \sum_{i=1}^{n} \alpha_i R^{i-1}, \qquad \text{(A-3)}$$

have been claimed to be acceptable for calibration by Goss (1974) for $n = 5$ and Parasnis (1974) for $n = 3$.

According to Steinhart and Hart (1968), who have tried many forms of calibration curve, the form

$$1/T = \alpha + \beta \ln R + \gamma)\ln R)^2 + \delta(\ln R)^3, \qquad \text{(A-5)}$$

may deteriorate the fitting.

Contrary results have been reported by Bennett (1972) who claims that (A-5) will improve fitting to the same data set as used by Steinhart and Hart. Results of our curve fittings show that (A-5) is not necessarily superior to (A-4). For some thermistors (A-5) improves the fitting, but for others (A-5) deteriorates the fitting. This conclusion is also true for the published data sets as used by Steinhart and Hart, and Bennett.

The controversy about (A-4) and (A-5) probably results from truncation errors in different numerical algorithms used for solving the normal equations. Since both (A-4) and (A-5) fit the data equally well, we have chosen the form with fewer coefficients, although (A-5) is independent of the resistance units used (Bennett, 1972).

Heat Flow

The Calorimetry of Steaming Ground in Thermal Areas

R. F. BENSEMAN

Department of Scientific and Industrial Research
Dominion Physical Laboratory,
Private Bag, Lower Hutt, New Zealand

Abstract—A portable calorimeter that measures heat output from the steaming ground found in areas of natural thermal activity is described. With a minimum of disturbance to the site, heat flow is measured in a range from 10 to 70 $\times$ 10^{-3} cal/cm² sec with an accuracy better than 10 per cent. Below this range, the accuracy decreases. The relationship of heat output to the soil temperatures measured at a depth of 35 cm is shown for measurements at 27 different sites.

Introduction—The total natural output of heat from a thermal region can be a useful guide to its potentialities as a source of underground steam for the generation of electric power. The main thermal regions of New Zealand occur in country formed of very permeable pumice breccia, and they are characterized by extensive tracts of ground through which steam slowly percolates. The amount of heat lost in this way is comparable to the heat output of the more obvious features such as geysers and hot springs. The present apparatus is considered to be the best of a number of calorimeters that have been used in New Zealand to measure the heat output from steaming ground. Important features are (1) it does not require the ground surface to be smoothed or leveled, and it does not produce a partial vacuum over the site; therefore there is good reason to suppose that the flow of steam is unaffected by the presence of the calorimeter, and (2) being light and portable, the instrument is suited to use in rugged and bush-covered country.

Description of apparatus—The calorimeter is essentially a box, formed of sheet aluminum on a light frame, and having an open bottom 25 by 80 cm. The box is pressed slightly into the ground so as to seal off the portion of ground below it. Ports in the top allow a fan to draw air through the box at a measured rate, and the temperature and humidity of the air are measured as the air enters and leaves the box. From these measurements the flow of heat into the box can be calculated.

Air enters at *A* (Fig. 1) past differential thermocouples which detect the wet-bulb and dry-bulb temperatures. It passes a hot-wire anemometer and then traverses the chamber *S*

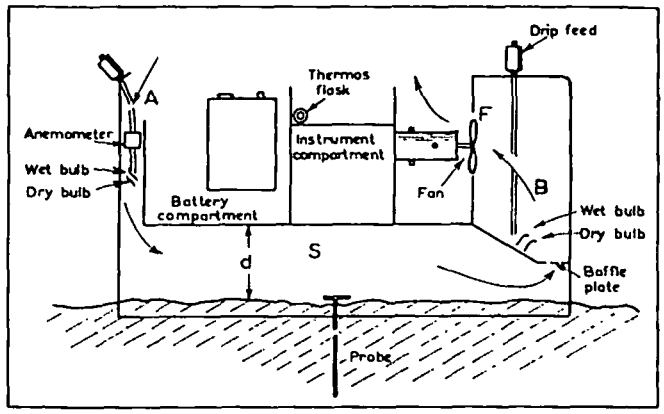

FIG. 1—Schematic section of calorimeter box

where it gains heat from the ground. It is exhausted from the system by the fan *F* after passing a second set of thermocouples at *B*. To reduce heat transfer through the sides and top of the chamber *S*, these are lined with quarter-inch cork sheet. The fan and the anemometer heater are powered by the battery shown, and the instrument compartment includes a multi-position switch that selects the circuit whose emf is to be measured. Figure 2 is a photograph of the calorimeter box and the portable potentiometer used for measuring the emfs.

Design details—Previous calorimeters had shown that steaming ground may emit as much as 50 $\times$ 10^{-3} cal/cm² sec, and it was estimated that the present calorimeter would need to pass seven liters of air per second if the dry-bulb temperature were not to rise by more than 20°F in the most unfavorable weather conditions (85°F and 80 pct relative humidity). Using entry and exit ports of area 100 cm² it was found that this rate of flow produced no measurable pressure deficiency in the sampling chamber. The chamber was made 12 cm deep so that the air velocity would not exceed one mile an

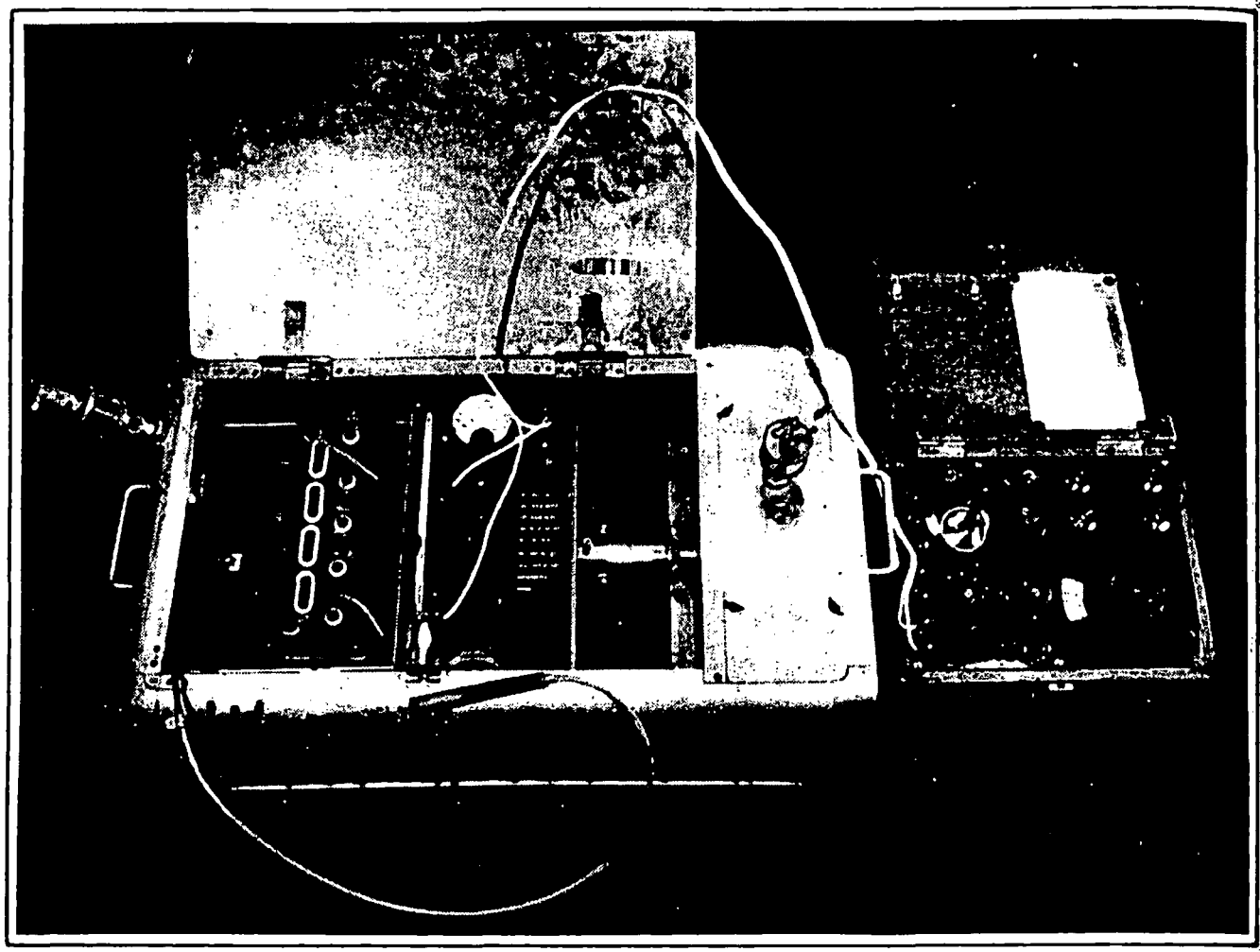

FIG. 2—Completed box with its potentiometer

hour, comparable to the wind speed on a calm day.

The hot-wire anemometer has been described by *Benseman* and *Hart* [1955]. Briefly it consists of a short length of one inch square-section tubing in which is an electrically heated grid flanked by a differential thermopile. As the air speed through the tube varies, so does the emf generated by the thermopile. This anemometer has proved superior to more conventional types since it has no moving parts, retains its calibration after rough handling, and is most sensitive at very low rates of air flow. It was calibrated *in situ* by drawing air through the box at known rates, the fan and motor having been removed.

The wet-bulb and dry-bulb temperatures at inlet and outlet were each measured by five copper-constantan thermojunctions spaced across the air stream and held rigidly on suitable brackets. The wet junctions were provided with muslin envelopes kept moist by drip attachments fixed to the body of the box. In the present apparatus the air speed does not exceed 3 ft/sec, so humidity is deduced from tables used by the Meteorological Office for wet- and dry-bulb temperatures observed within a screen.

The reference junctions of all the thermocouples are embedded, together with a mercury-in-glass thermometer, in paraffin wax within a small vacuum flask housed in the top of the box. All temperatures can therefore be determined absolutely, but in practice it is convenient to read (1) the temperature of the mercury thermometer, (2) the emf of the dry thermopile at the inlet, (3) the differential emf between dry thermopiles at inlet and outlet, and (4) the differential emf between wet and dry thermopiles at the inlet and at the outlet.

Laboratory tests—Tests in which moisture and heat were presented to the calorimeter in a variety of proportions showed that it would account for heat flows in the range 10 to 70 $\times$ 10^{-3} cal/cm^2 sec with an accuracy better than ten per cent. Below 10 $\times$ 10^{-3} cal/cm^2 sec the accuracy was $\pm 1 \times 10^{-3}$ cal/cm^2 sec.

Use in the field—An area of steaming ground was chosen which could be reached only by boat and was therefore unlikely to be disturbed by casual visitors. Fourteen sites were pegged at ten-meter intervals in a straight line over ground that was not too active to support some stunted trees and bushes. Thirteen additional sites were chosen on a patch of very hot ground that grew only a little moss. These thirteen sites were surveyed on only one occasion, for it proved difficult to repeat individual measurements; the ground surface was soft and sticky, and merely walking over it seemed to affect the heat output at sites nearby. The 14 cooler sites were re-measured on a number of occasions spread over more than a year.

The temperature of the ground 35 cm below the surface was recorded also, for it was hoped that measurements at this depth might prove to be related to the heat flow. It is to be expected from theoretical arguments [*Benseman*, 1956] that the flow of steam through the ground should control the gradient near the surface.

The measurements are fully reported and discussed in a report that is available from this Laboratory on request [*Benseman*, 1958]. Here it is sufficient to summarize the conclusions.

Operational notes and results of measurements—The following summary comments are made:

(1) The calorimeter box is easily set in place, but it may take an hour before a steady reading can be obtained. During this time the fan must be in continuous action.

(2) Measurements of heat output made in the afternoon tend to be a little higher (10 to 15 pct) than measurements made in the morning. This extra heat is probably that fraction of the solar heat that the surface of the box fails to reflect.

(3) Winds can bring gusts of warm and cold air past the site of the measurements. The resulting fluctuations in the outputs of the thermocouples make work difficult except in calm weather or in light winds. Some thermal lagging of the thermocouples might reduce this difficulty.

(4) Heat outputs at the 14 sites showed large daily and monthly changes, half of the changes between readings exceeding 30 pct. These variations suggested a redistribution of steam flow in the ground rather than a significant change in total flow. No correlation was found between the heat-flow variations and weather conditions, such as wind, cloud, rainfall, and barometric pressure or rate of change of pressure.

(5) The scatter diagram of Figure 3 shows

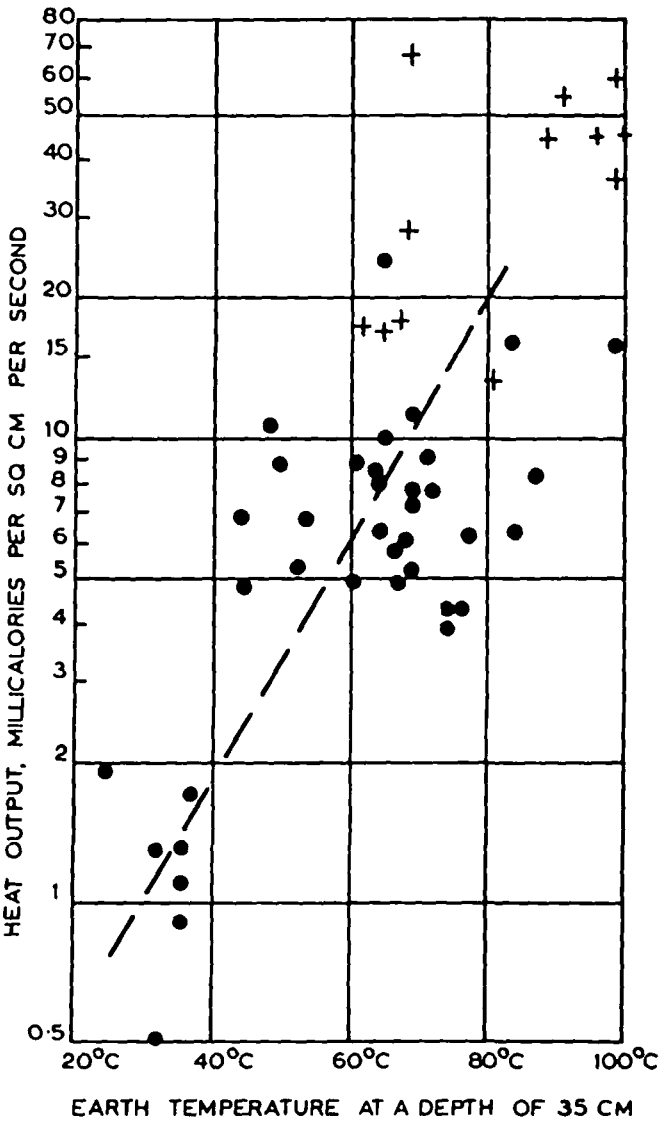

FIG. 3—A scatter diagram relating the heat output of each site with the temperature at 35 cm; crosses indicate sites in the hotter area, circles refer to sites in the cooler area

the connection between the heat output at a site and the temperature at a depth of 35 cm below the surface. Earth temperatures can be measured much more quickly than the heat output, and in spite of the lack of exact correlation between these variables, the measurements of earth temperatures may be a rapid and sufficiently accurate means of estimating an overall heat flow. Figure 3 cannot of course be expected to apply to other thermal areas where the soil has a very different texture or permeability

References

BENSEMAN, R. F., AND H. R. HART, A thermocouple anemometer, *J. Sci. Instr.*, 32, 1–17, 1955.

BENSEMAN, R. F., The natural heat output of Orakei Korako, *Tech. Rep. R258*, Dominion Phys. Lab., Dep. Sci. Ind. Res., Wellington, New Zealand, pp. 11–12, 1956.

BENSEMAN, R. F., Measurements of heat output from steaming ground, *Tech. Note 119*, Dominion Phys. Lab., Dep. Sci. Ind. Res., Wellington, New Zealand, pp. 1–17, 1958.

(Manuscript received August 18, 1958.)

HEAT FLOW IN THE NORTHERN BASIN AND RANGE PROVINCE

David D. Blackwell

Department of Geological Sciences
Southern Methodist University
Dallas, Texas 75275

ABSTRACT

The heat flow in the Basin and Range province of northern Nevada is extremely complex. It is a product of superposition of the regional effects of extension and volcanism/intrusion modified by the local conductive effects of thermal refraction (complicated structural settings), variations in radioactive heat production, erosion and sedimentation. In addition to these conductive effects, groundwater flow, both on a local and a regional basis, affects heat-flow measurements. Typical heat-flow values for the Basin and Range province average 85 ± 10 mWm^{-2}. The higher estimates are probably based on biased sets of heat-flow measurements, and actual averages are on the order of 100 ± 10 mWm^{-2}. Geothermal systems appear to be related to deep fluid circulation in an active tectonic setting rather than to young silicic volcanic rocks. Young volcanoes occur along the borders of the Basin and Range province, but not in the part of northern Nevada discussed in this paper.

INTRODUCTION

The Basin and Range province of the western Cordillera of the United States is an exceedingly complex area resulting from the superposition of 600 million years of recurring tectonic and volcanic activity. In the late Cenozoic, the already highly fragmented geology of the Basin and Range was further disrupted by the subsidence and covering of approximately half the province by alluvial deposits in the valleys and by the exposure of different stratigraphic and structural levels in adjacent ranges. The heat flow in the Basin and Range province reflects this complicated tectonic development in both regional and detailed ways.

The object of this paper is to discuss the distribution of, and controls on, heat flow in the part of the Basin and Range province in northwestern Nevada from an observational point of view. Thermal variations may not have as distinctive an imprint as structural and stratigraphic evolution; however, certainly the varied thermal events during the mid and late Cenozoic have left their marks. Furthermore, the interaction between the present-day thermal background and the detailed structural and hydrologic settings is complex. Consequently, even with a relatively high density of heat flow data, compared to many areas of the earth, there are still many uncertainties and unknowns in the actual magnitude of the background, the detailed geographic and vertical distribution, and the way in which variations relate to structural geology, hydrology and volcanic history.

The history of heat flow studies in the Basin and Range province dates back to the late 1960s. Reconnaissance data in the Basin and Range were discussed by Roy et al. (1968b) and Sass et al. (1971). The most recent detailed heat flow map of northwestern Nevada was presented by Sass et al. (1981, Fig. 1). Sass et al. (1971) divided the Basin and Range province in Nevada into three heat flow regimes: a region of heat flow typical of the province average (surface heat flow values of about 85 ± 10 mWm^{-2}*); a region of above average heat flow (surface heat flow values of 100 + mWm^{-2}) which was designated the Battle Mountain Heat Flow High; an area of below average heat flow values which was named the Eureka Heat Flow Low (surface heat flow values of less than 60 mWm^{-2}). These heat flow subdivisions were maintained in later discussions by Lachenbruch and Sass (1977, 1978). In contrast, Blackwell (1978) argued that the highest overall energy loss within the Basin and Range province was along the eastern and western boundaries near the Wasatch and the Sierra Nevada Mountains, and not within the Battle Mountain Heat Flow High.

Extensive heat flow or subsurface temperature data have become available for many geothermal systems subsequent to the major discussions in 1978, especially in northern and northwestern Nevada. These data have yet to be integrated into the pre-existing regional data set. Neither space nor time permit the integration of these data in this paper, but some salient aspects of these studies which have a bearing on the current understanding of heat transfer in the Basin and Range province will be discussed. The order of the discussion in the paper proceeds more or less according to Table 1, a list of major effects on the heat flow pattern in the Basin and Range province. Following a brief summary of the

TABLE 1. THERMAL EFFECTS

Volcanism and Intrusion
Extension
Thermal Refraction-Structure
Radioactive Heat Production
Erosion and Deposition
Local Groundwater Flow
Geothermal Systems

* 41.84 mWm^{-2} = 1 x 10^{-6} cal/cm^2 sec = 1 HFU

observations, the regional effects on heat flow will be discussed. These regional effects are grouped as thermal effects related to extension and to volcanism. Following this discussion, the more local effects which may cause heat flow variations on the scale of a few kilometers will be discussed. The effects specifically to be discussed include the conductive effects of variation of basement radioactivity, effects of structure (i.e., lateral variations of thermal conductivity), erosion and deposition, and the effects of regional and local convective geothermal fluid-flow systems.

OBSERVED HEAT FLOW DISTRIBUTION

The regional heat flow data described by Sass et al. (1981) are shown in Figure 1. A total of 93 heat-flow measurements for the Nevada portion of the Basin and Range province are shown. The spacing of heat-flow stations is quite dense for a continental region, but as will subsequently become obvious, it is not dense enough to determine many of the characteristics of the heat-flow pattern. Superimposed on the heat-flow map are the contours of the Eureka Heat Flow Low and Battle Mountain Heat Flow High. Heat-flow values generally exceed 100 mWm^{-2} within the area identified as the Battle Mountain Heat Flow High. Elsewhere within the Basin and Range province, heat-flow values are typically 85 ± 10 mWm^{-2}. The thermal boundaries of the Basin and Range province are very sharp against the Wasatch Mountains-Colorado Plateau region on the east (Bodell and Chapman, 1982; Keller et al., 1979; Reiter et al., 1979) and the Sierra Mountains on the west (Roy et al., 1968b, 1972; Sass et al., 1971). To the north there is no distinct thermal boundary with the Columbia Plateau region and, in fact, contours of the Battle Mountain Heat Flow High include part of the High Lava Plains in Oregon, and the Snake River Plain region in Idaho (see Brott et al., 1978, 1981).

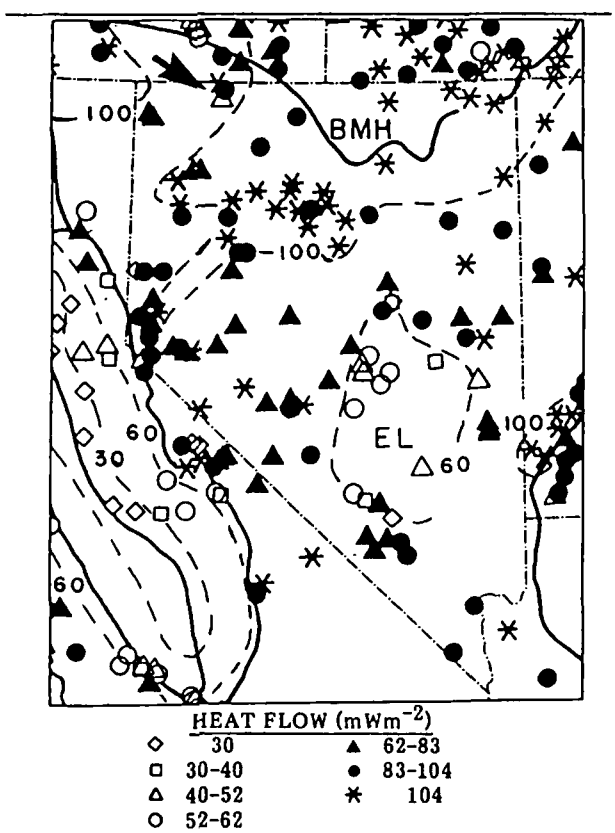

FIGURE 1. Heat flow in Nevada and surrounding areas, after Sass et al. (1978). Contours are from Lachenbruch and Sass (1978). Arrow in northwestern Nevada indicates three holes in granite discussed in text.

In addition to the "regional heat flow" data set, an extensive data set including 10 to 100 times as many holes as shown on Figure 1 is available from exploration activities associated with individual geothermal systems. In general, these data are not included in Sass et al. (1981), nor in earlier descriptions of heat flow in the Basin and Range province. The existence of this new data set gives an additional complexity to the heat-flow character, poses many interesting questions, and also opens the possibility of investigating in more detail local conditions affecting observation.

Most of the geothermal exploration drilling has been along the boundaries between a range and valley, or within a valley. On Figure 1, no "regional" heat flow data from the valleys are shown, so the two data sets do not overlap geographically or geologically, and it cannot necessarily be anticipated that the geothermal regimes will be the same in the ranges and in the valleys. Another important aspect of the geothermal systems is the maximum temperature of the system, which is controlled by the depth and rate of circulation. No systematic summary of such temperatures based on drilling has yet been described. Edmiston (1982) has presented a map showing the location of deep geothermal tests and the geothermal tests which have been successful (i.e., have found temperatures in excess of 200°C). Analysis and integration of the new data set with regional data will take effort, but has the potential to greatly refine our understanding of the heat flow distribution in the Basin and Range province.

REGIONAL CONTROLS ON HEAT FLOW

Introduction. The two dominant regional thermal effects are mechanical-thermal effects associated with the late Cenozoic extension, and the thermal effects of mid and late Cenozoic intrusion and volcanism. Although these two effects will be discussed separately, in fact they are interrelated, and individual components are difficult to identify separately.

Thermal Effects of Extension. There has been an emphasis on extension effects on the thermal pattern because the extensional activity is so prominent in the most recent history of the Basin and Range province. Lachenbruch and Sass (1977, 1978) have developed a model for the thermal regime in the Basin and Range province emphasizing extension. The primary thermal effect of extension is to move deeper, hotter material to shallower depths as the lithosphere is stretched. However, there are definite limits to the enhancement of surface heat flow by this mechanism if the spreading does not lead rapidly to ocean basin formation, so the favored models discussed by Lachenbruch and Sass (1978) actually depend on basalt intrusion to supply a large part of the high heat flow observed at the surface. Indeed, the Lachenbruch and Sass (1978) models have a one-to-one correlation between extension rate and intrusive emplacement. These models were also applied to areas of large-scale silicic volcanism such as Yellowstone and Long Valley. In these areas, much more of the anomalous

surface heat flow is associated with intrusion than with extension!

Limits on the amount of extension are related to isostatic effects. As stretching occurs, continental crustal material is replaced by mantle material with a large increase in density and, consequently, subsidence. The subsidence is offset to some extent by thermal effects of extension. A comparison of these two quantities is shown in Table 2. The heat-flow model includes one-dimensionsal time-dependent stretching (Jarvis and McKenzie, 1980). Example extension rates, total extension associated with a 17 M.Y. period of extension in the form of ratios (βs), the amount of mechanical subsidence which would be associated with extension of an originally 40 km thick continental crust, the amount of thermal uplift, and the difference between the mechanical subsidence and the thermal uplift (a net subsidence) are shown in Table 2. The associated heat flow anomaly for each case is also shown. This model includes a time-dependency, so the heat flow values are slightly lower than would be the case if extension had occurred long enough for thermal equilibrium to be attained (see Figure 2). The 17 M.Y. period was chosen as it is the maximum period of time of extension in the northern Basin and Range province during the late Cenozoic, and was the period of time of extension assumed in the analysis of Lachenbruch and Sass (1978).

Typical extension proposed (Lachenbruch and Sass, 1978) ranges from 50 to over 100%, corresponding to β values of 1.5 to 2. Taking isostatic effects into account, a net subsidence of 1.5 to 2.4 km is associated with the required heat-flow anomaly of 40 to 60 mWm^{-2}. These observations can be compared to the mean topographic height of the Basin and Range province in Nevada at the present time (from 1.5 km in the Lahontan and Bonneville Basins to over 2 km in the center of the province), and the regional elevations of approximately 2 to 2.5 km in the Wasatch Range and the Sierra Nevada Mountains. Unless the Basin and Range province started at an extraordinarily great elevation, it seems unlikely that the total subsidence could exceed 0.5 km, as the Basin and Range province still stands at a high elevation. The results of this analysis suggest that extension is not the main mechanism responsible for high heat flow in the Basin and Range province.

Figure 2 shows more detail of the heat-flow contribution associated with a transient thermal event as summarized in Table 2. In this calculation, an initial lithospheric thickness of 94 km and a background heat flow of 40 mWm^{-2} were assumed. Extension rates in percent per million years are shown for each curve. The dashed line on the plot is the locus of points with a β value of 1.5.

These results may be compared to the various heat flow subregions in the Basin and Range province. A typical background heat flow in the Basin and Range is approximately 85 mWm^{-2}. The reduced or mantle heat flow (the heat flow from below the upper crustal radioactivity layer) is 59 mWm^{-2}, approximately 50% of

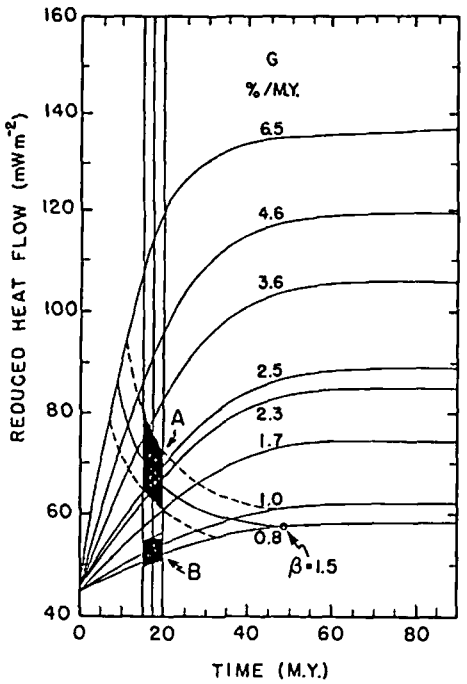

FIGURE 2. Thermal effect of extension calculated using model of Jarvis and McKenzie, 1980. Age range of extension in the Basin and Range province is shown by the vertical lines (17 ± 2 M.Y.). G is extensional strain rate in %/M.Y. Shaded area A is the region of the graph corresponding to reduced heat flow values typical of the Battle Mountain Heat Flow High. Shaded area B is the region of the graph consistent with present crustal thickness.

TABLE 2. COMPARISON OF MECHANICAL SUBSIDENCE AND THERMAL UPLIFT IN BASIN AND RANGE PROVINCE FOR 17 M.Y.

Extensional Strain Rate (%/M.Y.)	β (17 M.Y.)	Mechanical Subsidence (km)	Thermal Uplift (km)	Net Subsidence (km)	Surface Heat Flow (mWm^{-2})
0.8	1.14	0.67	0.24	0.43	78
1.7	1.29	1.33	0.54	0.79	84
2.5	1.43	1.83	0.73	1.10	93
3.6	1.61	2.43	0.91	1.52	104
4.6	1.78	2.87	1.02	1.85	117
5.6	1.95	3.25	1.11	1.11	128
6.5	2.11	3.54	1.17	2.37	140

which is anomalous with respect to a thermally "normal" continental lithosphere (Roy et al., 1968a, 1972). Heat flow values in the Battle Mountain Heat Flow High range from 100 to 150 mWm^{-2}, and the reduced heat flow in the Battle Mountain Heat Flow High according to Lachenbruch and Sass (1977, 1978) ranges from 85-100 mWm^{-2}, or approximately 30-45 mWm^{-2} in excess of the normal Basin and Range reduced heat flow, and 60-75 mWm^{-2} in excess of a "normal" continental reduced heat flow.

It is clear from the consideration of Table 2 and Figure 2 that the magnitude of heat flow observed in the Battle Mountain Heat Flow High cannot be associated with the thermal effects of extension alone. To add emphasis to this conclusion, it is clear that the present-day distribution of active earthquake zones in the Basin and Range province is not coincident with the highest heat flow. One zone of earthquake activity extends north through the Battle Mountain Heat Flow High, but much of the heat-flow high is essentially aseismic at the present time (Smith, 1978). Other zones of active seismicity along the Sierra Nevada-Basin and Range transition and along the Colorado Plateau-Basin and Range transition are not apparently characterized by quite as high surface heat flow (see Lachenbruch and Sass, 1978; Blackwell, 1978).

Thermal Effects of Intrusive and Volcanic Activity. There is no difficulty in generating high heat flow values in association with volcanic and intrusive activity, although many of the highest values are obviously associated with geothermal systems rather than with conductive heat flow from magma chambers. A correlation between the age of volcanic activity in a particular area and the heat flow, especially in the case of the continental crust characterized by rhyolitic volcanic activity, might be expected. A generalized volcanic age map for the area shown in Figure 1 is shown in Figure 3. The pattern has been discussed by many people, recently including Stewart and Carlson (1978) and Snyder et al. (1976). The areas of oldest, or lack of, Cenozoic volcanism are in southern Nevada and in east-central Nevada. Most of the rest of Nevada is characterized by volcanism in the age range 6-17 M.Y. and only along the margins of the province are younger, extensive silicic volcanic features found.

Various types of volcano/thermal models have been discussed, including the extension/intrusion models of Lachenbruch and Sass (1978). If volcanism is not associated one-to-one with extension, then the event will lead to some sort of heating of the crust followed by cooling after the end of the volcanic/intrusive event. The peak heat flow will depend on the actual distribution of magma within the crust and lithosphere. However, after 1-5 M.Y. or so of cooling, all models approach the same sort of behavior. The long time asymptote of the cooling depends on the assumption of the background heat flow. The general sort of behavior is shown in Figure 4. The curves in Figure 4 are shown to cool off to three different backgrounds, depending on the assumed steady-state mantle heat flow. These models are discussed in more detail by Blackwell (1978). On Figure 4, the typical heat flow in the Basin and Range province and the heat-flow range for the Battle Mountain Heat Flow High are shown. Based on these results, it would appear that the higher estimates of heat flow in the Battle Mountain Heat Flow High are too high to be explained by the volcanic model if no silicic volcanism in the area is

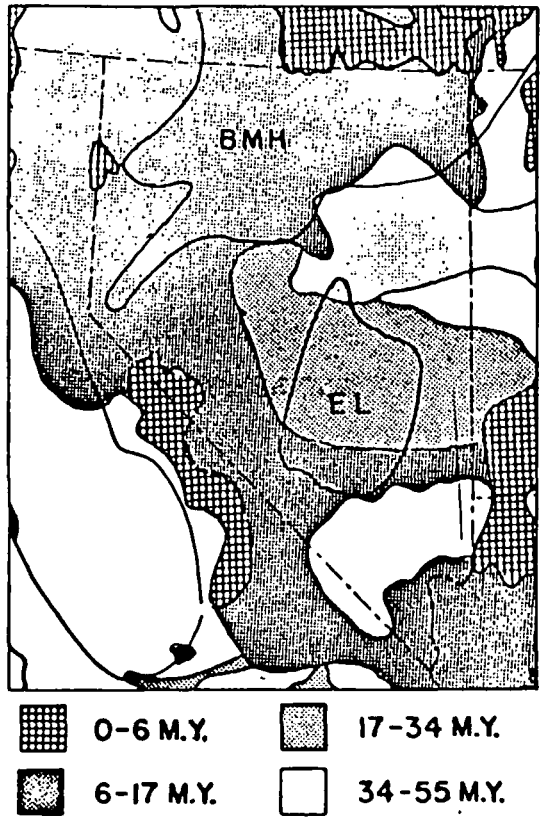

FIGURE 3. Age of silicic volcanism (generalized from Stewart and Carlson, 1978). Light lines are 60 mWm^{-2} heat-flow contours.

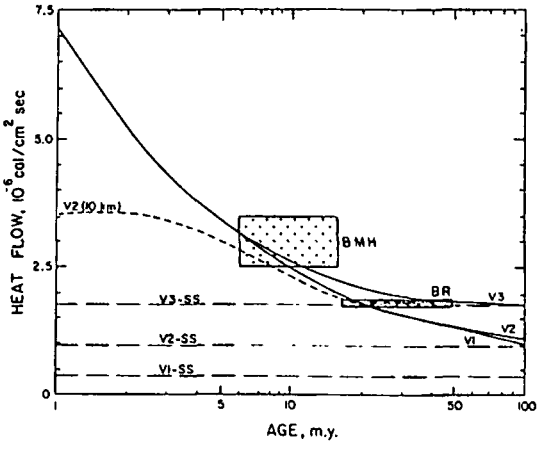

FIGURE 4. Thermal models for regional volcanic and intrusive events in the Basin and Range province. Observed heat-flow ranges for the models are explained by Blackwell (1978). SS indicates the steady-state asymptotic heat-flow values.

younger than 6 M.Y. Because the heat flow is also too high to be explained by extension, the apparent magnitude of the regional heat flow pattern is somewhat difficult to explain.

LOCAL CONDUCTIVE HEAT FLOW EFFECTS

Radioactive Heat Production. If the geology of the Basin and Range province were similar to the Sierra Nevada Mountains, and consisted of a large, homogeneous, relatively unfractured, granitic terrain, then the heat flow evaluation would be relatively straightforward. The surface heat flow within the granite would show a linear correlation with the local heat production of the rocks from uranium, thorium and potassium. In this simple case, local lateral heat-flow variations due to sub- and intracrustal sources, groundwater flow, thermal refraction and so forth, would not have significant effects on the heat flow distribution. Such linear arrays have been observed in many places throughout the world (Roy et al., 1968a; 1972). Early studies of heat flow versus heat production for the Basin and Range province indicated a regional linear relationship with an intercept heat flow of approximately 59 mWm^{-2} and a slope of approximately 9.4 km (Roy et al., 1968a). Subsequent studies of the relationship between heat flow and heat production in granitic rocks in the Basin and Range have led to a considerably more complicated pattern.

A summary of the available data is shown in Figure 5. This figure was presented by Lachenbruch and Sass (1978), but the detailed data on which this figure is based have not been published. It is difficult to identify a linear relationship between heat flow and heat production

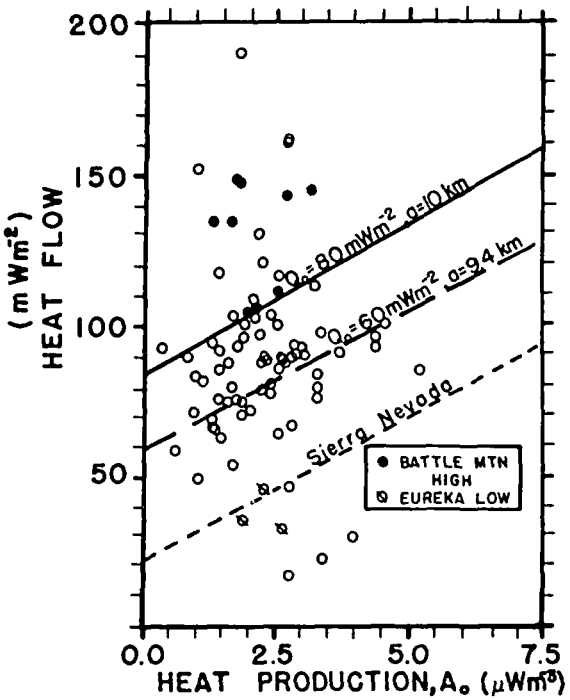

FIGURE 5. Surface heat flow as a function of surface heat production (after Lachenbruch and Sass, 1977).

in this data set, although most of the data lie between two lines with intercept values of 50 mWm^{-2} and 90 mWm^{-2} (with slopes of 9.4 to 10 km).

In the Basin and Range province, unlike the Sierra Nevada Mountains, it is not possible to avoid systematic effects on the heat flow data, even by drilling heat-flow holes only in granitic rocks, in large part because granitic rocks represent only a small fraction of the exposed bedrock of Nevada (2.8%, Archbold, 1972). Therefore, the data shown in Figure 5 have all sorts of extraneous (from the regional point of view) effects present in the measurements. The difficulties of attempting to use these data to determine regional quantities are illustrated by three points in granite in close proximity in north-central Nevada (see arrow in Figure 1). The radioactive heat production values are approximately the same for the three points, and yet the heat-flow values are respectively 45, 85 and 150 mWm^{-2}. These points are within a few km of one another, and all are in granite. If only one of the three holes were available, it might be inferred that this area had heat flow typical of (1) the Eureka Heat Flow Low, (2) normal Basin and Range, or (3) the Battle Mountain Heat Flow High.

The sites are close to the Baltazor geothermal system (Earth Power Prod. Co., 1980), and it is possible that there is some interaction between the fluid convection represented by the geothemal system and the extreme variation in heat-flow values shown by these three data points. Thus it seems quite clear that both high and low heat flow values are associated with convection systems, as concluded by Lachenbruch and Sass (1977).

Because of the very noisy data set, the heat flow-heat production relationship for various parts of Nevada and its relationship to other known continental patterns is not presently resolvable in an accurate way. It is clear that heat flow determinations in granitic rocks in Nevada, without considerable attention to each individual measurement, are insufficient for the determination of typical regional heat-flow values and heat-flow distribution in contrast to standard practice in some geologic terrains.

Thermal Effects of Structure: Refraction. In an ideal case, to avoid anomalies due to the spatial distribution of thermal conductivity, the thermal conductivity of the rocks should either be uniform or should vary only in the vertical direction. If there are variations only in the vertical direction, then a hole penetrating various units will show an inverse correlation between the thermal conductivity of the rock and the geothermal gradient, resulting in constant heat flow with depth. However, the geologic structure of the Basin and Range province is anything but layer cake. In order to investigate possible systematic effects of thermal conductivity on heat flow, determinations from the Battle Mountain Heat Flow High are plotted as a function of thermal conductivity in Figure 6. Most of the early heat-flow determinations in the Battle Mountain Heat Flow High were made in very high thermal conductivity sedimentary rocks. Average thermal conductivities at these sites are over 4 $Wm^{-1}K^{-1}$. The thermal conductivity of the granites where subsequent heat-flow values were obtained is typically about 3 $Wm^{-1}K^{-1}$ (Sass, personal communication, 1980). Typical thermal conductivities from some of the basins are 1-1.5 $Wm^{-1}K^{-1}$. The basin data are primarily from the Black Rock Desert, which has been extensively studied (Sass et al., 1979; Mase and Sass, 1980), and the Grass Valley area (Sass et al., 1976; Welch et al., 1981). A strong positive correlation between the heat flow and thermal conductivity is demonstrated in Figure 6. This correlation suggests that thermal refraction is important in the results; consequently, heat-flow

values from any one geologic terrain may not represent true regional values.

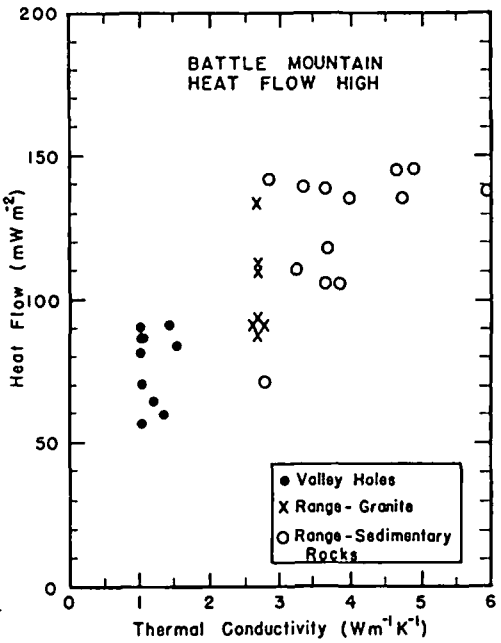

FIGURE 6. Comparison of heat flow and thermal conductivity from heat-flow sites in the Battle Mountain Heat Flow High. Data from reference in text and from J.H. Sass (personal communication, 1980).

Another way to investigate systematic effects between heat flow and thermal conductivity is to look at variations in gradient. Measurements in granite, in pre-Tertiary sedimentary rocks, and in valley fill are shown by separate patterns in Figure 7. The gradient distribution from both the granite and the sedimentary rock lithologies overlap, with the range of values being 25-40°C/km. The fact that there is a correlation between heat flow and thermal conductivity, but not between heat flow and gradient, also suggests that structural effects are controlling the variation of the heat-flow values. The reasoning proceeds as follows: if the measurements had been made in horizontal units of varying thermal conductivity (the ideal case), then the gradients would be inversely proportional to the thermal conductivity, there would be no correlation between heat flow and thermal conductivity, and there would be good correlation between gradient and conductivity. In fact, the reverse situation is observed in each case.

Also shown in Figure 7 is a histogram of gradient values from the Basin and Range province of Arizona. This data set includes values recently published by Shearer and Reiter (1981). The Basin and Range province in Arizona has a considerably larger percent of granitic bedrock, generally lower relief, fewer known geothermal systems, and older volcanic rocks. Thus some of the geologic complexities of the northern Basin and Range in Nevada are more subdued in the part of the Basin and Range province in Arizona. A histogram of gradients from the ranges in Arizona shows almost identical distribution to that in the Battle Mountain Heat Flow High, whereas an average of the heat flow values in the

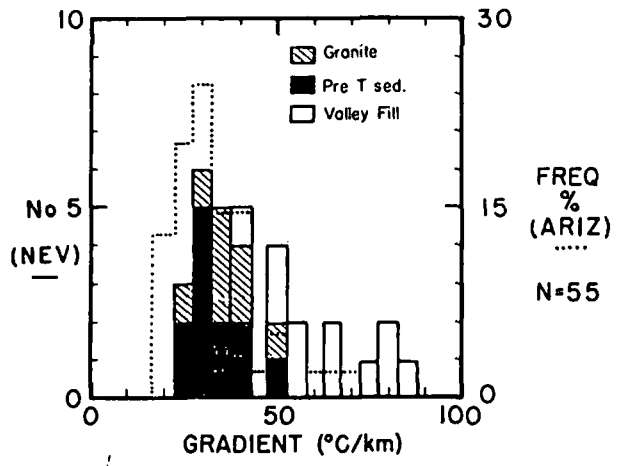

FIGURE 7. Histograms of gradient in Battle Mountain Heat Flow High and Arizona Basin and Range province (dotted lines). Arizona data from Shearer and Reiter (1981) and Sass et al. (1982).

two provinces differs by 25 to 50% (lower in Arizona). Figure 8 shows a plot of thermal conductivity versus heat flow for the Arizona data. Included in this plot are the data from several holes in the valleys in Arizona which are, as in the case of Nevada, undersampled in the present data set. The correlation between thermal conductivity and heat flow is weak, and there is a large overlap between the data from the Battle Mountain Heat Flow High and from central Arizona, excluding the very high heat flow values in the high thermal conductivity sedimentary rocks in the northern Basin and Range province. The conclusion of this discussion is that there may be a bias in heat flow toward too-high values if data only from the ranges (including the high thermal conductivity sedimentary rocks) are used to calculate province average values.

Of course, detailed evaluation of the structural effects on heat flow has to be considered individually for each hole. However, there is one large-scale effect which needs to be considered in this discussion. This thermal effect is the large-scale distortion of heat flow by Basin and Range structure. In general, the valleys are 10-20 km wide and 1-2 km deep. They are generally filled with low thermal conductivity Cenozoic sedimentary rocks. In the ranges, older sedimentary, igneous and metamorphic rocks generally have thermal conductivity values two to three times greater. As a result of this contrast, heat flows preferentially into the ranges, resulting in systematically high values in the ranges, and systematically low values in the valleys with respect to the regional mean value. This large-scale effect of a valley is sometimes modeled as a single, semi-elliptical or semi-circular cylinder embedded in an otherwise uniform media (see Jaeger, 1965). In this case, for typical geometries observed in the Basin and Range province, there would be no appreciable expected effect of thermal refraction except in the immediate proximity of a range-bounding fault, where higher-than-normal values would be observed in the range side, and lower-than-normal values would be observed on the basin side. Two effects are not considered in this simple model. The first of these is that the basins and ranges repeat, so that it is not appropriate to consider only a single valley

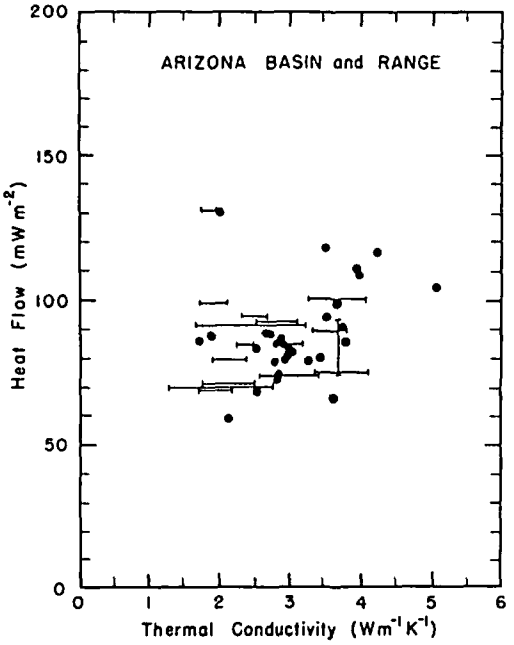

FIGURE 8. Comparison of heat flow and thermal conductivity at heat-flow sites in Arizona. The bars represent ranges of values as observed in specific holes or areas.

to consider only a single valley embedded in an otherwise semi-infinite media with conductivities typical of the ranges. The effect of repeated ranges and valleys is interaction (Lee and Henyey, 1974), so that larger refraction effects than calculated from the single ellipse model of Jaeger (1965) are observed.

Another complexity not considered in either of these models is the fact that the heat source is within the crust. The boundary condition for the models is that there is constant heat flow from "great depth" and the heat flow is allowed to adjust at great depths below the inhomogeneity. In the Basin and Range province the heat sources (extension effects and magma) may be in the mid- to upper levels of the crust, and there may be interaction between the heat source and the variations in thermal conductivity, with even more heat being forced through the ranges (and less heat forced through the valleys) than calculated assuming a constant heat flow at great depth. In the extreme limit, the model would be characterized more by constant temperature than by constant heat flow, in which case (except again in the immediate vicinity of the boundaries of the inhomogeneities) the mean heat flow would be simply proportional to the integrated thermal resistance from the constant temperature plane to the surface.

A typical model is shown in Figure 9. A Basin and Range valley filled with rocks having a thermal conductivity of 1.7 $Wm^{-1}K^{-1}$ is embedded in material with a conductivity of 3.35 $Wm^{-1}K^{-1}$. The geometry of the model is constant into and out of the paper, and repeats that shown side-to-side. In a steady-state case, it is assumed that the heat flow is uniform at great depth. If the average regional heat flow is assumed to be 72 mWm^{-2}, then the heat flow observed in the valley away from the bounding fault would be 60 mWm^{-2}, while the heat flow observed in the range away from the bounding fault would be 80 mWm^{-2}; this represents a 25% variation between the high and low heat-flow values and an error in regional heat-flow determination (if the range value is used) of about +12%. If heat-flow determinations were made in the ranges without avoiding areas close to the bounding fault, however, the mean observed heat flow would be 16% higher than the true mean. Therefore, based on this simple model, a random set of measurements in the ranges would be 16% higher than the regional average, and would be greater than 25% higher than the values measured in the adjoining valleys.

These results are consistent with the distribution of gradients shown in Figure 7, and to some extent with the distribution of heat-flow values shown in Figure 6, if the most thermally conductive sedimentary rocks are not considered typical and the values in the granites are used for comparison instead. It is iteresting to note that peak heat-flow values associated with the boundary of the range would be 96 mWm^{-2}, or 25% high with respect to the average in a steady-state case. Since the amount of the granitic exposure in the northern Basin and Range

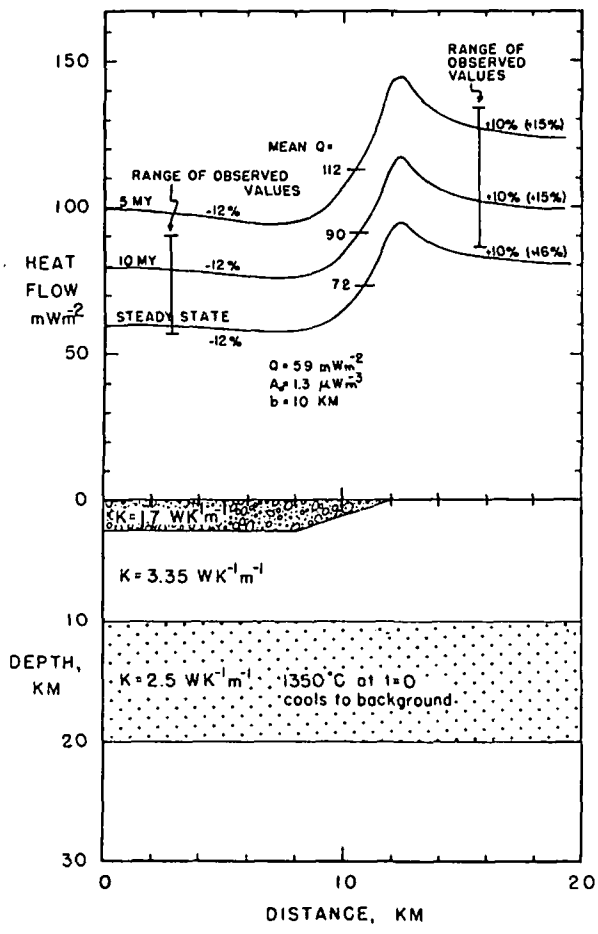

FIGURE 9. Surface heat flow effects of Basin and Range structure and a crustal intrusive. Range of observed values refers to Battle Mountain Heat Flow High.

province is so limited, it is argued that use of these sites for the determination of regional heat-flow values may have a large bias.

Effects of Erosion and Deposition. The thermal effects associated with erosion of mountain ranges and the deposition of sediments in basins have been discussed by numerous authors (including Jaeger, 1965; England and Richardson, 1980). The general effect is to decrease observed heat-flow values in the sedimenting basins as the colder sediments deposited in the basin are heated up, and to increase heat-flow values in the ranges as hotter rocks are exposed by erosion. In view of the great tectonic relief developed in the last few million years in the Basin and Range province, significant perturbations from these effects may exist in the heat-flow data set. Unfortunately, there are not sufficient data to estimate these corrections in general. However, it is possible that systematic effects of up to 10 or 20% of the observed values could be related to the systematic differences in the erosional and depositional environments of the ranges and valleys. These effects might or might not be superimposed on the refraction effects in an additive way, depending on the detailed timing of the development of the basins and ranges, and of the thermal conductivity contrast associated with various structural settings. The sense of these effects is in the same direction as the structural effects, i.e. values would appear to be higher than the true regional value in the ranges and lower than the true regional value in the valleys.

CONVECTIVE HEAT-FLOW EFFECTS

Shallow Groundwater Aquifers. The effects of subsurface water movement on heat flow can be many, complex, and on different scales. The most common effect is that of water table fluid flow, which is probably present in varying degrees at almost all sites. Water movement in very large aquifers may affect the heat flow so severely that it is virtually impossible to use holes of any reasonable depth to do classical heat-flow studies. An example of this situation is the Snake River Plain aquifer in Idaho, where heat flow values are much subnormal over an area 50 km wide by 200 km long (Brott et al., 1981). Because of the rapid flow rates in the aquifer (up to 1000 m/year), about 75% of the total amount of heat conducted into the bottom of the Snake Plain aquifer is advected out the end of the aquifer, leaving only about 25% of the heat to be measured by conductive heat-flow studies. On the other end of the scale, if the aquifer moves slowly enough that no heat is actually advected at the discharge zone of the aquifer, then the overall heat budget would remain the same as in the conductive heat-flow case, but the distribution would reflect the downflow and upflow parts of the system. This situation has been modeled by Domenico and Palciauskas (1973) and applied to basins in the Rio Grande rift by Morgan et al. (1981).

Mifflan (1968, 1983) has discussed in detail the hydrology of the Basin and Range province. The dominant hydrologic system in the Basin and Range province is a range-to-valley flow system. Aquifer heads are typically highest in the ranges and lowest in the valleys. As drill holes are deepened in the ranges, each successive aquifer usually has a lower head, and as drill holes are deepened in the valleys, each successive aquifer usually has a higher head. This observation implies recharge in the ranges and discharge in the valleys of the groundwater flow systems. Thus low heat-flow values would be observed in the ranges and high heat-flow values would be observed in the valleys, if this effect dominates the shallow heat transfer.

In the Battle Mountain Heat Flow High, no low heat-flow values which might be characteristic of recharge areas in the ranges have been described. Even if the regional heat flow is high, it seems likely that some evidence of local circulation would have been discovered, particularly in the sedimentary rocks.

Superimposed on the local hydrologic pattern are (in some situations) complex interbasin groundwater flow systems. These interbasin groundwater flow systems are particularly characteristic of the carbonate terrain in eastern and south-central Nevada. This phenomenon may be related to the existence of the Eureka Heat Flow Low (Sass et al., 1971).

Geothermal Systems. There is also abundant evidence, in the form of many geothermal anomalies, for large-scale water flow in northern Nevada. If water flow goes deep enough, high temperatures and a commercially attractive geothermal system may result. The depth of circulation required is a function of the permeability of the rocks (rate of fluid flow) and the background geothermal gradient. These geothermal convective systems can be local or they can be regional. Near many active volcanic and intrusive centers, the water flow systems may have lateral dimensions of only a few kilometers. On the other hand, some geothermal systems may involve fluid which moves across ranges and valleys (for example, the Desert Peak geothermal anomaly; Yeamans, 1983). The characteristics of some of the geothermal systems in the Basin and Range province have been discussed by Blackwell and Chapman (1977), Sass et al. (1976), Benoit et al. (1983), and Benoit and Butler (1983). Extensive thermal data are now available from many areas, in too great a number to be discussed in detail here. Many of these data were collected through DOE-Industry coupled geothermal programs, and are available from the Earth Science Laboratory of the University of Utah. Brief discussions of many of these areas are given in papers of the Geothermal Resources Council Transactions. References to discussions of thermal data from areas in northern Nevada are listed in Table 3.

Mase and Sass (1980) have discussed an extensive heat-flow study in the Black Rock Desert area of northern Nevada (Figure 10). This area includes several geothermal systems, one of which is Gerlach Hot Springs, but in addition areally extensive data outside the geothermal systems were also calibrated. Typical heat-flow values in the Black Rock Desert are 40-60 mWm^{-2} along the axis of the valley, rising to 80-100 mWm^{-2} at the margins of the valley. Several large high heat-flow anomalies are identified, particularly north of Gerlach along the east side of the Granite Range, along the southeast margin of the Black Rock Desert against Pahisupp Mountain, and along the west side of the Black Rock Range. In addition, MacFarlane's Hot Spring (Swanberg and Bowers, 1982) is just off the map to the east. The major gap in the data is that few values are available from the ranges to compare to the basin. A heat-flow value measured in the granite of Pahisupp Mountain was 188 mWm^{-2}, clearly much in excess of any possible regional value, and affected in some way by a geothermal system.

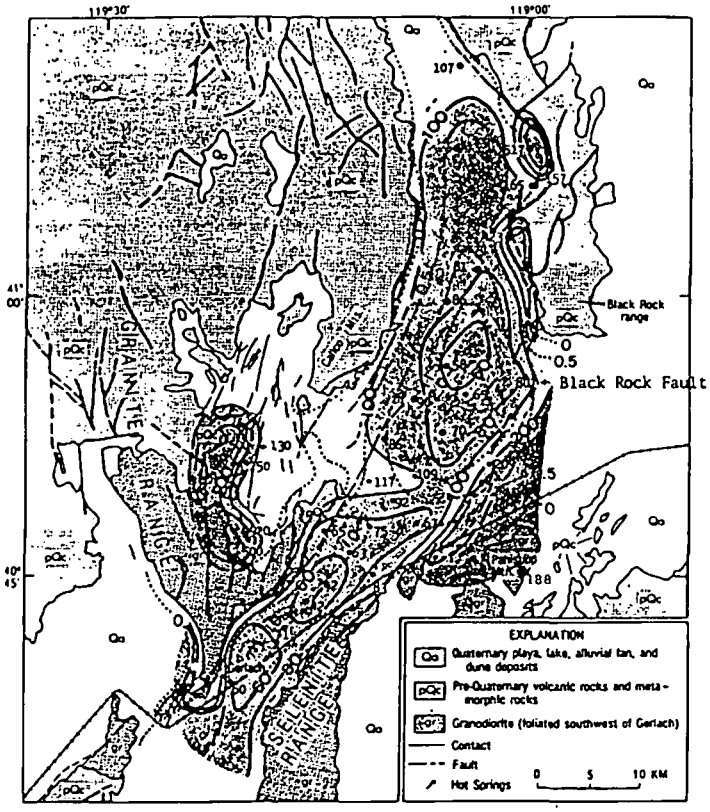

FIGURE 10. Heat-flow contours (solid line: 60, 80, 100, 200,300, 500 mWm^{-2}) and depth-to-basement contours (dotted line: 0,0.5, 1.0, 1.5, 2.0, 2.5 km) in the western Black Rock Desert. Location of heat-flow points (solid circles) for reference. Major normal faults are also indicated. After Mase and Sass (1980).

TABLE 3. Geothermal systems and published geothermal gradient/heat flow studies or data reports.

Location	Geothermal System	Reference
Black Rock Desert	McFarland H.S. Gerlach H.S.	Swanberg and Bowers, 1982 Sass et al., 1979 Sass et al., 1976
San Emedio Desert	San Emedio West	Mackelprang et al., 1980
Humbolt Sink	Colado Humbolt House	Mackelprang, 1982
Carson Sink	Desert Peak Brady H.S. Stillwater Soda Lake Fallon-NAS	Benoit et al., 1982 Hill et al., 1979
Clan Alpine Mts. Pueblo Mountains Steamboat Hills Buena Vista Valley	McCoy Baltazor H.S. Steamboat H.S. Kyle H.S.	Olson et al., 1979 Earth Power Prod. Co., 1980 White, 1968 McMannes et al., 1981
Crescent Valley	Beowawe H.S.	Smith, 1983
Independence Valley	Tuscarora	Pilkington et al., 1980
Grass Valley	Leach H.S. Parker Canyon	Sass et al., 1977 Welch et al., 1981 Mase and Sass, 1980
Buffalo Valley		Sass et al., 1976

Superimposed on the heat-flow values are the depth-to-basement contours, also from Mase and Sass (1980). There is a good correlation between the heat-flow values and the depth to basement, with the lowest heat-flow values being associated with the deepest part of the basin. Mase and Sass (1980) suggested that regional downflow is occurring in the valleys with upflow along the margins of the valleys. The proposed hydrologic circulation would be counter to the "normal" hydrologic circulation pattern of downflow in the ranges and upflow in the valleys (Mifflan, 1968). Unfortunately, the lack of data in the ranges does not allow a complete test of the Mase and Sass (1980) hypothesis. Furthermore, geothermal systems are often associated with the contact between the valleys and the ranges and may be controlled by hydrologic barriers between the ranges and the valleys. In this case, if water flow were down in the range, it might be expected to come back up again along the bounding fault so that the whole system would be contained within the range. This particular circulation pattern seems to be characteristic of the Roosevelt area in southeastern Utah (Ward et al., 1978). The data of Mase and Sass (1980) not immediately adjacent to geothermal systems are included in Figure 6, and it is clear that the gradients and heat flow values in the Black Rock Desert are consistent with those observed in the Battle Mountain Heat Flow High, if an allowance is made for the refractive effect of the low thermal conductivity sedimentary basins, and no absorption of heat by fluid downflow in the basins is necessary to make the heat flow consistent with the inclusion of this area as part of the Battle Mountain Heat Flow High. Mase and Sass (1980) included this area in the Battle Mountain Heat Flow High based on addition of the total amount of energy lost in the geothermal systems to the actual observed heat-flow values in the valleys. If refractive effects are significant, as is implied by Figure 6, then the observed values are consistent with such an association, without hypothesizing any large-scale water flow effects on the heat-flow data. An additional complexity associated with the geothermal systems is that flow is usually transient. Temperature gradient reversals with depth in exploration holes are almost the rule rather than an exception (see Benoit et al., 1982). Ziagos and Blackwell (1980, 1983) have discussed modeling of temperature-depth curves where this phenomenon is observed, to determine aquifer characteristics and flow regimes.

There is no doubt that the fluid flow patterns are extremely complicated and have a major effect on heat flow at some locations in the Basin and Range province. However, the nature of these patterns remains to be sorted out, as in no place are there sufficient heat-flow data to thoroughly investigate the total geographic extent of a water flow system. There is evidence for many different kinds of flow patterns from the geothermal systems themselves. Many of the geothermal systems are associated with the range-valley contacts; however, some systems appear to be confined to the valley side, some to the range side, some to the faults, and some involve intrabasin/range fluid flow. Consequently, convective systems can be imagined which might involve flow in ranges only, valleys only, ranges and valleys, and perhaps even only along the normal faults. At the present time, neither the data nor the interpretations are sufficiently constrained to allow description of the nature of a "typical" geothermal flow system in the Basin and Range province.

DISCUSSION

The object of this paper has been to investigate the effects and interactions that make the thermal pattern in the Basin and Range province so complex. The basic observations of geothermal gradient (Figure 7) are probably the most reliable and useful information. The heat-flow pattern remains to be explained.

A very simple conceptual model of heat flow in a Basin and Range setting is shown in Figure 9. The model includes the effects of a crustal thermal disturbance and refraction in the Basin and Range setting. The thermal source is approximated by a body at a temperature of 1350°C emplaced between 10 and 20 km. The 1350°C includes the regional background, which was calculated for a Basin and Range heat flow of 80 mWm^{-2} at the surface, and a mantle heat flow of 59 mWm^{-2}. The temperature corresponds approximately to the emplacement temperature of basalt with some allowance for the latent heat effects. The model is similar to the one used for the western Snake River Plain by Brott et al. (1978). The model was designed to investigate the effects of refraction and a thermal anomaly.

Heat-flow values as a function of position are shown at 5 M.Y. and 10 M.Y. after emplacement of this sort of a body (Figure 9). The basic heat-flow pattern is not much affected by the source, even though it is within the crust. If such a source had been emplaced 5 M.Y. ago, then the mean heat flow would be 112 mWm^{-2}, with a variation from below 100 to over 120 mWm^{-2}, except in the vicinity of the range-bounding faults, where variations would be more extreme. If the intrusive has cooled for a period of 10 M.Y., then the mean heat flow drops to 90 mWm^{-2} while the heat flow varies from about 80 mWm^{-2} in the valleys to 100 mWm^{-2} in the ranges. The variation of observed heat-flow values for the valleys and the ranges in the Battle Mountain Heat Flow High, ignoring the extremely high heat-flow values in the sedimentary rocks and those that are certainly associated with geothermal systems, is shown on the plot. The heat-flow pattern associated with a cooling period of 10 ± 5 M.Y. would approximate the midpoint of the range of observed data. There is slightly larger variation in heat flow than is predicted by this model between the ranges and the valleys, which might suggest some superimposed small effects of fluid circulation. The calculated age has little significance because the model is very approximate, and if extension effects are superimposed on a magmatic effect, the heat flow might be maintained at high values for some period of time after it would ordinarily have dropped. At the same time less extension would be required to keep the heat flow at a high level.

The conclusion is that a reasonable heat-flow model for the northern Basin and Range province involves a background heat flow which in superposition of a late Cenozoic thermal (intrusive and extrusive) event followed by regional extension active to within the last 1 M.Y. In the northern Nevada region, intrusive or extrusive silicic rocks of young age are not involved with the geothermal systems. The actual distribution of values is profoundly affected by the thermal conductivity contrasts between the ranges and the valleys. A combination of a very high permeability crust (due to the extension) with relatively high gradients due to high regional heat flow results in the observed pattern of heat flow and geothermal systems. Geothermal manifestations are associated in many cases with range-bounding faults, although there is

no simple relationship between the faults and the geothermal systems. Some of the geothermal systems are on the range side, some are on the valley side, some involve ranges and valleys, and some may be within the fault system itself. Although there are a lot of heat-flow data available, much analysis remains before we thoroughly understand the heat-flow pattern. Drilling in the geothermal systems has added a new set of data which gives information on areas which have not been previously included in the regional data set, and need to be included for complete understanding of the heat flow pattern. Future studies will need to thoroughly assimilate these data, so that a more realistic and accurate pattern of heat-flow distribution and the controls on that distribution in the Basin and Range province can be developed.

ACKNOWLEDGMENTS

The calculations illustrated in Table 2 and Figure 2 were carried out by S. Chockalingam. The calculations in Figure 9 were made by Charles A. Brott. Heat-flow values from some U.S. Geological Survey studies in Nevada, published only as points on maps, were made available by J.H. Sass.

REFERENCES

Archbold, N.L., 1972, Modified geologic map of Nevada, Nevada Bur. Mines and Geol. Map 44.

Benoit, W.R. and D. Butler, 1983 (this volume).

Benoit, W.R., J.E. Hiner and R.T. Forest, 1982, Discovery and geology of the Desert Peak geothermal field: a case history, Nevada Bur. Mines and Geol. Bull. 97, 81 pp.

Blackwell, D.D., 1978, Heat flow and energy loss in the western United States, pp. 175-208 in Cenozoic Tectonics and Regional Geophysics of the Western Cordillera, Memoir 152, Smith, R.B. and G.P. Eaton (eds.), Geol. Soc. Amer., Boulder, Colorado.

Blackwell, D.D. and D.S. Chapman, 1977, Interpretation of geothermal gradient and heat flow data for Basin and Range geothermal systems, Trans. Geothermal Resources Council, 1, 19-20.

Bodell, J.M. and D.S. Chapman, 1982, Heat flow in the Northern Central Colorado Plateau, Jour. Geophys. Res., 87, 2869-2884.

Brott, C.A., 1978, Tectonic implications of the heat flow of the western Snake River Plain, Idaho, Geol. Soc. Amer. Bull., 89, 1697-1707.

Brott, C.A., D.D. Blackwell and J.P. Ziagos, 1981, Thermal and tectonic implications of heat flow in the eastern Snake River Plain, Jour. Geophys. Res., 86, 11709-11734.

Domenico, P.A. and V.V. Palciauskas, 1973, Theoretical analysis of forced convective heat transfer in regional ground-water flow, Geol. Soc. Amer. Bull., 84, 3803-3814.

Earth Power Prod. Co., 1980, Geochemical map, geologic cross section, sulfate map, microearthquake survey map, DOE Industry Coupled Program, Earth Science Laboratory of University of Utah Research Institute Open-File Rept. NV/BAL/EPP-7.

Edmiston, R.C., 1982, A review and analysis of geothermal exploratory drilling results in the northern Basin and Range geologic province of the USA from 1974 through 1981, Trans. Geothermal Resources Council, 6, 11-14.

England, P.C. and S.W. Richardson, 1980, Erosion and the age dependence of continental heat flow, Geophys. Jour. Royal Astr. Soc., 62, 421-437.

Hill, D.G., E.B. Layman, C.M. Swift and S.H. Yungul, 1979, Soda Lake, Nevada thermal anomaly, Trans. Geothermal Resources Council, 3, 305-308.

Jaeger, J.C., 1965, Application of the theory of heat conduction to geothermal measurements, pp. 7-23 in Terrestrial Heat Flow, Geophys. Mono. Ser., 8, Lee, W.H.K. (ed.), Amer. Geophys. Union.

Jarvis, G.T. and D.P. McKenzie, 1980, Sedimentary basin formation with finite extension rates, Earth Planet. Sci. Lett., 48, 42-52.

Keller, G.P., L.W. Braile and P. Morgan, 1979, Crustal structure, geophysical models, and contemporary tectonism of the Colorado Plateau, Tectonophysics, 61, 131-148.

Lachenbruch, A.H., and J.H. Sass, 1977, Heat flow in the United States and the thermal regime of the crust, pp. 626-675 in The Earth's Crust, Geophys. Mono. Ser., 20, Amer. Geophys. Union, Heacock, J.G. (ed.).

Lachenbruch A.H. and J.H. Sass, 1978, Models of extending lithosphere and heat flow in the Basin and Range province, pp. 209-250 in Cenozoic Tectonics and Regional Geophysics of the Western Cordillera, Memoir 152, Smith, R.B. and G.P. Eaton (eds.), Geol. Soc. Amer., Boulder, Colorado.

Lee, T.C. and T.L. Henyey, 1974, Heat-flow retraction across dissimilar media, Geophys. Jour. Royal Astr. Soc., 39, 319-333.

Mackelprang, C.E., 1982, Interpretation of geophysical data from the Colado KGRA, Pershing County, Nevada, Univ. Utah Res. Inst. Rept. DOE/ID/12079-58, ESL-71, 27 pp.

Mackelprang, C.E., J.N. Moore and H.P. Ross, 1980, A summary of the geology and geophysics of the San Emedio KGRA, Washoe County, Nevada, Trans. Geothermal Resources Council, 4, 221-224.

Mase, C.W. and J.H. Sass, 1980, Heat flow from the western arm of the Black Rock Desert, Nevada, U.S. Geol. Surv. Open-File Rept. 80-1238, 38 pp.

McMannes, D., B. Quillin and D. Butler, 1981, Granite Mountain, Nevada geothermal prospect: a case history, Trans. Geothermal Resources Council, 5, 107-110.

Mifflan, M.D., 1968, Delineation of groundwater flow systems in Nevada, Desert Research Institute, Center for Water Resources Research Tech. Rept. Ser., Pub. 4.

Mifflan, M.D., 1983 (this volume).

Morgan, P., V. Harder, C.A. Swanberg and P.H. Daggett, 1981, A groundwater convection model for Rio Grande Rift geothermal resources, Trans. Geothermal Resources Council, 5, 193-196.

Olson, H.J., F. Dellechaie, H.D. Pilkington and A.L. Lange, 1979, The McCoy geothermal prospect, status report of a possible new discovery in Churchill and Louder Counties, Nevada, Trans. Geothermal Resources Council, 3, 515-518.

Pilkington, H.D., A.L. Lange and F.E. Barkman, 1980, Geothermal exploration of the Tuscarora prospect in Elko County, Nevada, Trans. Geothermal Resources Council, 4, 233-236.

Reiter, M., A.J. Mansure and C. Shearer, 1979, Geothermal characteristics of the Colorado Plateau, Tectonophysics, 61, 183-195.

Roy, R.F., D.D. Blackwell and F. Birch, 1968a, Heat generation of plutonic rocks and continental heat flow provinces, Earth Planet. Sci. Lett., 5, 1-12.

Roy, R.F., E.R. Decker, D.D. Blackwell and F. Birch, 1968b, Heat flow in the United States, Jour. Geophys. Res., 73, 5207-5221.

Sass, J.H., A.H. Lachenbruch, R.J. Munroe, G.W. Green and T.H. Moses, Jr., 1971, Heat flow in the western United States, Jour. Geophys. Res., 76, 6356-6431.

Sass, J.H., F.H. Olmsted, M.L. Sorey, H.A. Wollenberg, A.H. Lachenbruch, R.J. Munroe and S.P. Galanis, Jr., 1976, Geothermal data from test wells drilled in Grass Valley and Buffalo Valley, Nevada, U.S. Geol. Surv. Open-File Rept. 76-85.

Sass, J.H., J.P. Ziagos, H.A. Wollenberg, R.J. Munroe, D.E. diSomma and A.H. Lachenbruch, 1977, Application of heat-flow techniques to geothermal energy exploration, Leach Hot Springs area, Grass Valley, Nevada, U.S. Geol. Surv. Open-File Rept. 77-762, 125 pp.

Sass, J.H., M.L. Zoback and S.P. Galanis, Jr., 1979, Heat flow in relation to hydrothermal activity in the southern Black Rock Desert, Nevada, U.S. Geol. Surv. Open-File Rept. 79-1467, 39 pp.

Sass, J.H., R.J. Munroe and C. Stone, 1981, Heat flow from five uranium test wells in west-central Arizona, U.S. Geol. Surv. Open-File Rept. 81-1089, 42 pp.

Sass, J.H., D.D. Blackwell, D.S. Chapman, J.K. Costain, E.R. Decker, L.A. Lawver and C.A. Swanberg, 1981, Heat flow from the crust of the United States, pp. 503-548 in Physical Properties of Rocks and Minerals, McGraw-Hill/CINDAS Data Series on Material Properties, Vol. II-2, Touloukian, Y.S., W.R. Judd and R.F. Roy (eds.), McGraw-Hill.

Shearer, C. and M. Reiter, 1981, Terrestrial heat flow in Arizona, Jour. Geophys. Res., 87, 6249-6260.

Smith, C., 1983, Thermal hydrology and heat flow of Beowawe geothermal area, Nevada, Geophysics, 48, 618-626.

Smith, R.B., 1978, Seismicity, crustal structure, and intraplate tectonics of the interior of the western Cordillera, pp. 111-144 in Cenozoic Tectonics and Regional Geophysics of the Western Cordillera, Memoir 152, Smith, R.B. and G.P. Eaton (eds.), Geol. Soc. Amer., Boulder, Colorado.

Snyder, W.S., W.R. Dickinson and M.L. Silberman, 1976, Tectonic implications of space-time patterns of Cenozoic magmatism in the Western United States, Earth Planet. Sci. Lett., 32, 91-106.

Stewart, J.H. and J.E. Carlson, 1978, Generalized maps showing distribution, lithology, and age of Cenozoic igneous rocks in the western United States, pp. 263-264 in Cenozoic Tectonics and Regional Geophysics of the Western Cordillera, Memoir 152, Smith, R.B. and G.P. Eaton (eds.), Geol. Soc. Amer., Boulder, Colorado.

Swanberg, C.A. and R.L. Bowers, 1982, Downward continuation of temperature gradients at MacFarlane's Hot Spring, northern Nevada, Trans. Geothermal Resources Council, 6, 177-180.

Ward, S.H., W.T. Parry, W.P. Nash, W.R. Sill, K.L. Cook, R.B. Smith, D.S. Chapman, F.H. Brown, J.A. Whelan and J.R. Bowman, 1978, A summary of the geology, geochemistry and geophysics of the Roosevelt Hot Springs thermal area, Utah, Geophys., 43, 1515-1542.

Welch, A.H., M.L. Sorey and F.H. Olmsted, 1981, The hydrothermal system in southern Grass Valley, Pershing County, Nevada, U.S. Geol. Surv. Open-File Rept. 81-915, 193 pp.

White, D.E., 1968, Hydrology, activity and heat flow of the Steamboat Springs thermal system, Washoe County, Nevada, U.S. Geol. Surv. Prof. Paper 458-C, 109 pp.

Yeamans, 1983 (this volume).

Ziagos, J.P. and D.D. Blackwell, 1981, A model for the effect of horizontal fluid flow in a thin aquifer on temperature-depth profiles, Trans. Geothermal Resources Council, 5, 221-224.

Ziagos, J.P. and D.D. Blackwell, 1983, A model for the transient temperature effects of horizontal fluid flow in geothermal systems, Jour. Geophys. Res., in press.

GEOPHYSICS, VOL. XXXII, NO. 4 (AUGUST, 1967), PP. 720–726, 7 FIGS., 1 TABLE

THERMAL REGIME OF A LARGE DIAMETER BOREHOLE: INSTABILITY OF THE WATER COLUMN AND COMPARISON OF AIR- AND WATER-FILLED CONDITIONS†

WILLIAM H. DIMENT*

Temperatures were measured as a function time and depth in a borehole before and after it had been filled with water. The hole is 25 cm in diameter, 340 m deep, and effectively sealed from influx of ground water. The measurements reveal that: (1) Temperature differences between the air-filled hole and the water-filled hole (after dissipation of the water injection disturbance) do not exceed 0.05° C at the same depth. (2) Temperatures in the water-filled hole exhibit oscillations at all depths where temperature increases downward but are stable at the bottom and near the surface where temperature decreases with depth. (3) The temperature oscillations have periods ranging from several minutes to several hours. (4) The amplitudes of the oscillations are several hundredths of a degree, and are roughly proportional to the geothermal gradient near the point of measurement, thus suggesting that the size of cells or eddies are rather constant and that the distance of water movement is no more than several times the inner diameter of the casing. (5) No oscillations were detected in the air-filled hole, but because the time constants of the instrument are long in an air-filled hole, the possibility of short period oscillations cannot be excluded.

INTRODUCTION

Hales (1937) has shown that a fluid column in a vertical tube becomes unstable when the temperature gradient exceeds a certain critical value which depends on the properties of the fluid and the size of the tube. Krige's (1939, p. 451) formulation of this is commonly cited (Misener and Beck, 1960, Garland and Lennox, 1962, Beck, 1965):

$$G_c = \frac{g\alpha T}{C_p} + \frac{Cvk}{g\alpha a^4}$$

where G_c is the critical gradient, g the acceleration due to gravity, T the absolute temperature, α the coefficient of thermal expansion, C_p the specific heat, v the kinematic viscosity, k the thermometric conductivity (diffusivity), a the radius of the tube, and C is a constant which has the value 216 for a tube whose length is great compared with its diameter.

The first term in this expression is the adiabatic gradient which is about 0.2°C/km for water and about 10°C/km for dry air at 20°C. Clearly, adiabatic gradient is exceeded in almost all water-filled holes. The second term is much larger for water-filled holes than for air-filled holes and is particularly sensitive to the effect of hole diameter. According to this formulation, the smaller diameter (2–3 cm) diamond drill holes are usually stable, the larger ones (6–8) cm close to instability or unstable, and almost all of the large diameter holes (10 cm or more) are unstable when filled with water.

Although Hales' theory provides a condition for instability, it does not indicate how the fluid will move or to what extent it will influence the distribution of temperature within the hole. The theory for predicting such effects does not seem to be complete (Donaldson, 1961). Evidently, the effects of the movements are not large. Hallock (1894) found no significant differences between temperatures measured in a 25 cm dry hole and in the same hole after it had filled with water. Van Orstrand (1924) found no evidence for convection in water-filled holes less than 20 cm in diameter. Krige (1939), in comparing results in theoretically stable and unstable parts of holes, found no evidence of a convective disturbance. Diment and Robertson (1963) found no significant differences between temperatures in a 7.5 cm hole and those in the same hole after 2.5 cm casing had been cemented into place.

In recent years, thermistor probes with response times of several minutes or less have been widely used, and small temperature oscillations have undoubtedly been observed by many. We have observed them, A. H. Lachenbruch and R. F. Roy have mentioned them in connection with their studies and have noted the contrasts in

† Manuscript received by the Editor 30 October 1966; revised manuscript received 11 January 1967

stability between large and small diameter holes. However, with exception of the recent reports of Gretener (1967) and Diment and Werre (1966) we find no published record of the phenomenon, probably because there is usually some question as to whether the oscillations are a consequence of the inherent instability of the water column or the result of exchange of water between the hole and the surrounding rocks.

EXPERIMENTAL DETAILS

The U. S. Bureau of Mines maintains an experimental drill hole at its Petroleum Research Laboratory near Morgantown, West Virginia. This vertical hole was drilled and completed by cable-tool methods in 1952. Temperature and stratigraphic data are given in Figure 1. The innermost of several "strings" of steel casing is 25 cm inside diameter and extends from the surface to 360 m where it is plugged with 7 m of cement. The annuli between the centered strings of casing, as well as that between the outer string and rock, are filled with cement. These measures, along with the fact that no water seeped into the hole during the year prior to experiment, assure us that we have no disturbance due to entrance of ground water and suggest that no significant thermal disturbance results from exchange of water between aquifers through any openings that may exist between the cemented casing and the rock.

Conventional components were used for the temperature measurements: five-dial bridge, electronic null-detector (10 μv full scale), disc or glass-encapsulated bead thermistors, and a strip chart recorder (one volt/cm). Two types of cables were used: system A—disc thermistors molded or taped into a multi-conductor cable and spaced at 15 or 30 m intervals; system B—a single glass-encapsuled thermistor in a brass pod. An extra lead was provided in each cable to detect changes in lead resistance. The response characteristics of the two cables are shown in Figure 2. Additional characteristics of the disc thermistors are given by Robertson et al. (1966) and Raspet et al. (1966). Both systems were calibrated several times before and after their use in the hole.

An outline of the experiment is as follows. System B was employed in the dry hole on 19 August 1964 and then removed. System A was installed in the hole on 20 August 1964, and a series of observations were made until 28 August 1964, when the hole was filled with water in 40 minutes. Thereafter, temperatures were monitored at discrete intervals until 12–14 July 1965, when strip chart recordings of temperature were made for one hour at each depth. System A was then removed from the hole and a series of similar recordings made with system B on 15–16 July 1965.

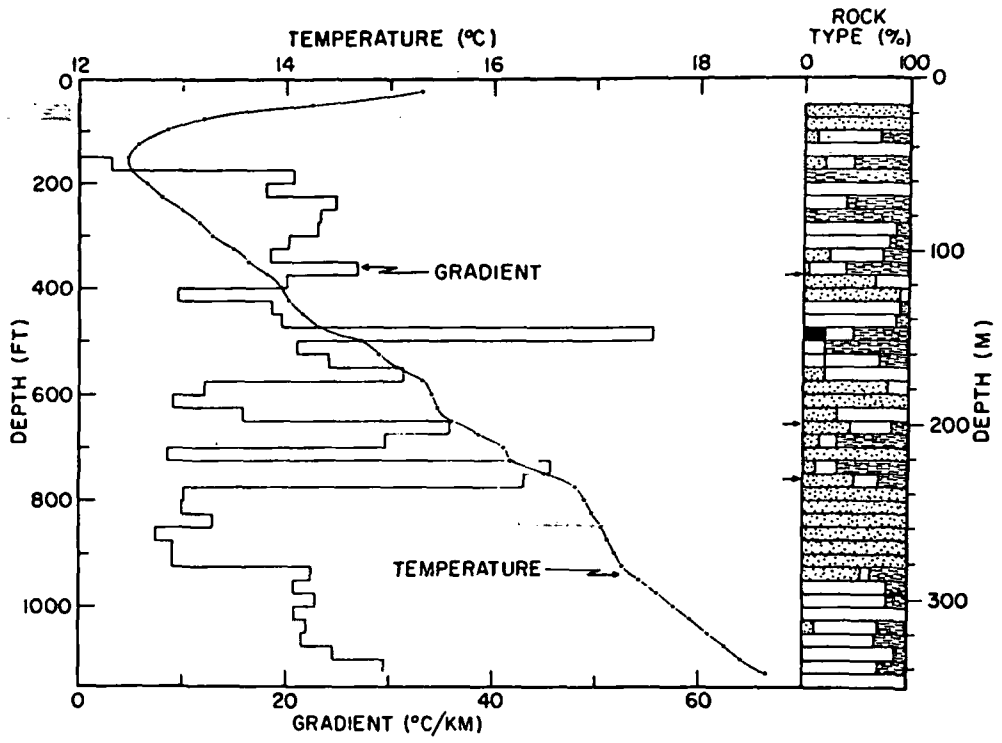

FIG. 1. Temperature and temperature gradient versus depth. Key to rock type: white-limestone, stipled-sandstone, dashed-shale, black-coal. Arrows represent thin coal seams of unreported thickness. Lithologic log compiled

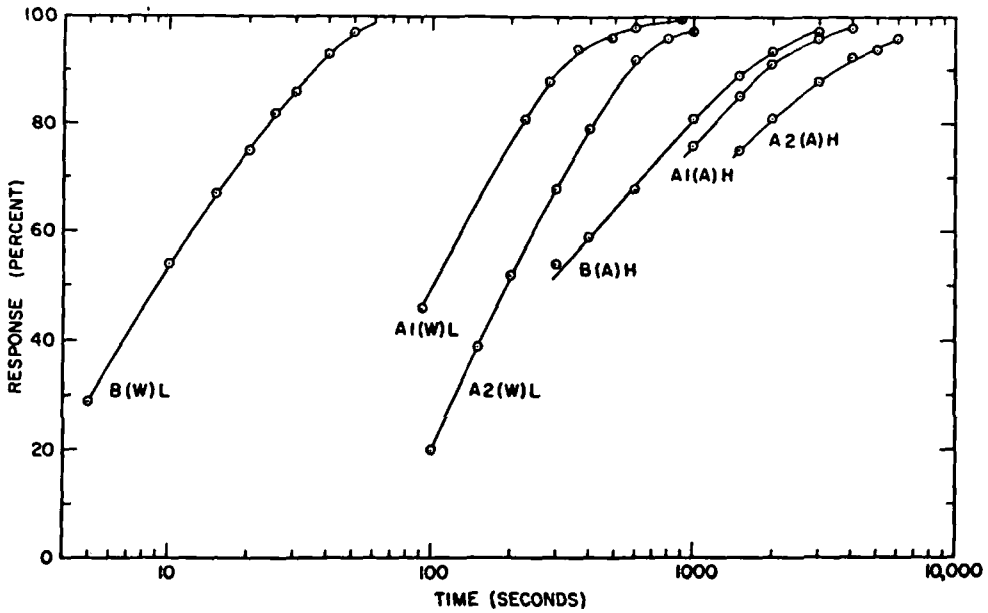

FIG. 2. Response of instruments to a step increase in temperature. First letter indicates the system (A or B). Number, if any, indicates whether thermistor was molded into cable (1) or taped (2) into cable. The letter in parentheses indicates the medium air (A) or water (W). The last letter indicates whether the response was measured in the laboratory (L) or in the hole (H).

CHARACTERISTICS OF OSCILLATIONS

Recordings of the variation of temperature with time at various depths in the water-filled hole are shown in Figures 3 and 4. The multisensor cable used in system A had been in the same position for 11 months prior to the recording; thus, there is no question of the oscillations being caused by movement of the cable. The single thermistor cable (system B) used for obtaining the recordings in Figure 4 was lowered to each position at the zero time on the left of the drawing. Therefore, there is a transient disturbance in the first ten minutes. This transient is much longer than the time constant of the probe and and much too large to be the effect of change of temperature of the lead wires, and, consequently, must be regarded as disturbance of the water column.

There are no temperature oscillations at those depths where temperature decreases downward. Furthermore, there is no oscillation at the bottom of the hole. Therefore, we can conclude that oscillations observed in the remaining part of the hole are real variations in temperature and represent motion of water in the hole.

The form of the oscillations is complex, with periods of rapid change followed by periods of relatively little activity. When several hours of records are examined, waveforms of the same general type are observed repeatedly but they differ in detail and are quasi-periodic at best

record and obtained a Fourier amplitude spectrum of the whole interval as well as each quarter of it. The results indicate no marked periodicity. However, the waveforms suggest that amplitude and period may be coupled somehow. A more sophisticated analysis might be warranted if longer records were available.

Another view of the variation of temperature with time during this nine hour period can be seen in Figure 5. Here we have averaged the tempera-

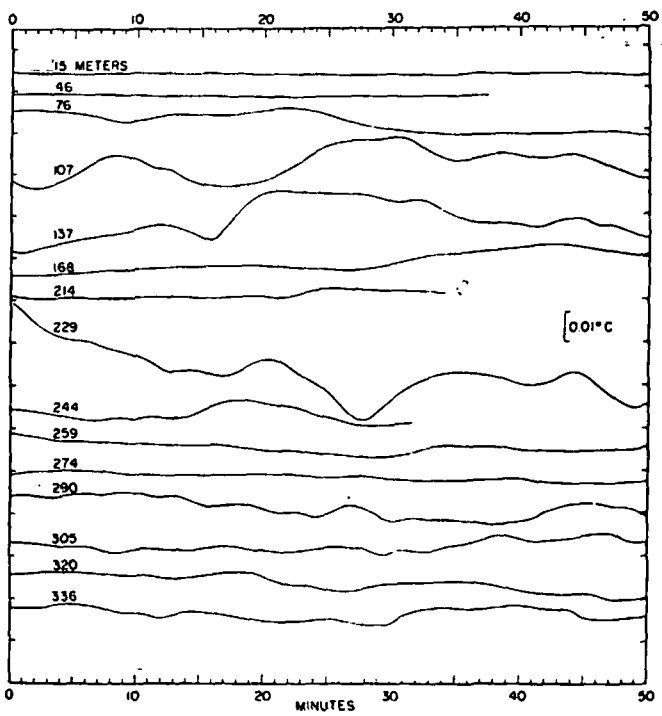

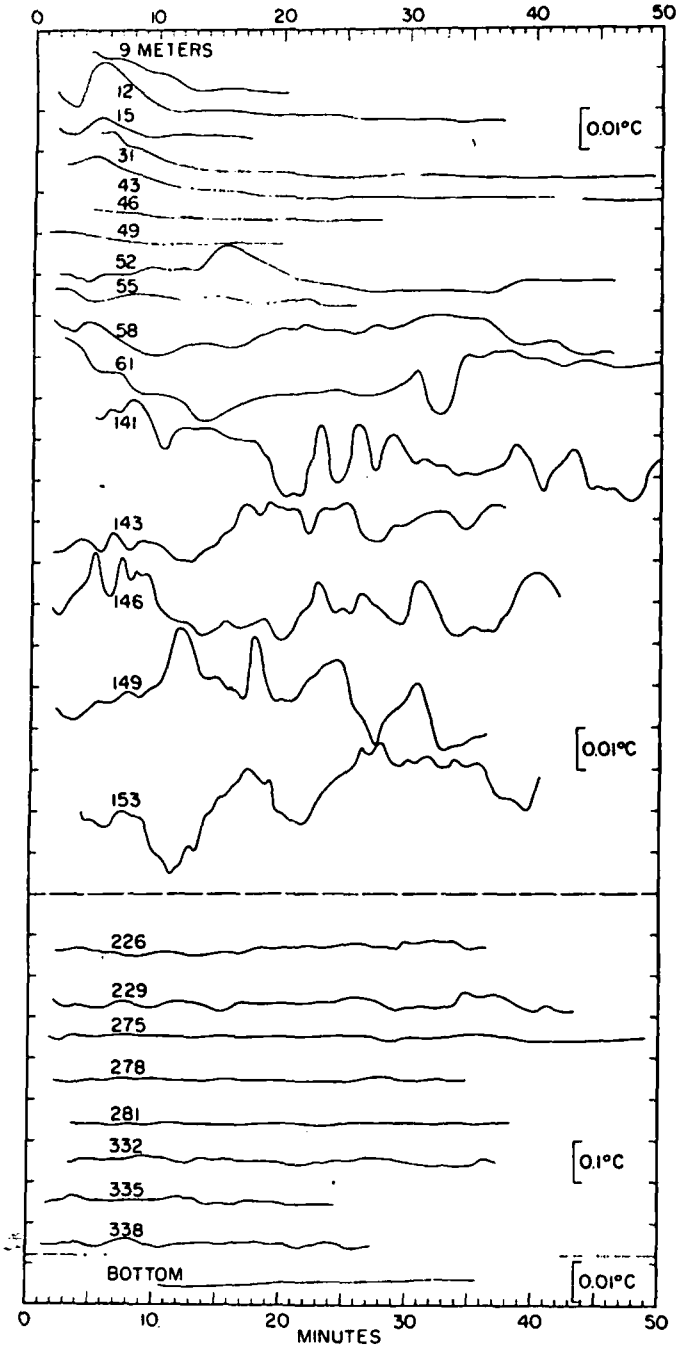

FIG. 4. Time-variation of temperature at various depths in water-filled hole as recorded with system B. Note that the temperature scale for the recordings for depths 226 through 338 m are a tenth of those at other depths.

ture values over various intervals of time (5, 10, 20, 40 minutes) and plotted the averages as a function of time. These moving or running averages are roughly equivalent to filtering. Aside from illustrating certain characteristics of the temperature variation, the averages indicate that there is little to be gained by averaging unless periods over several hours are utilized.

Examination of the details of the temperature variation at depth between 141 and 153 m in

of discrete steps at intervals on the order of a minute and of amplitude on the order of 10 cm and that the large variations of temperature represent a superposition of such movements. This is a reasonable supposition if the time constants of both the probe and the hole (water, steel casing, and surrounding cement and rock) are considered in viewing the form of the oscillation.

RELATION TO GEOTHERMAL GRADIENT

The amplitude of the temperature oscillation does not exceed about 0.05°C and seems to be roughly porportional to the gradient at the depth of measurement. An attempt to examine this proportionally is given in Figure 6. Here the maximum variation of temperature (range) within a ten minute period, as viewed over a total time interval of 50 minutes, is plotted against the gradient at the depth of observation. Actually, we do not have the gradient of the point where the range was observed; we have the average gradient over a 3 (system B) or 8 m (system A) interval above and below the point where the range was determined. Therefore, there are two gradients for each range; and where these gradients differ, both are plotted and a horizontal line is drawn between the points. The ratio of the range to the gradient is the vertical distance water must move (assuming no heat loss) to produce the temperature variation observed in a region of given gradient. Thus, the slopes of the dashed lines in Figure 6 indicate distance of water motion.

The splatter of points is partly the result of the complexity of motion, an arbitrary choice as to range, and the use of average gradients over intervals that are large with respect to lithologic variations. Despite these uncertainties, we can conclude that the thermal oscillations represent water movements over a distance of no more than several times the diameter of the pipe. If we were to view the water column as a series of vertically juxtaposed convection cells or eddies, we could say that the height of the cells was no more than several times their width. Clearly, the actual motion is far more complex and probably involves the continual formation and breakdown of irregular eddies which move in response to the local density distribution within the water column.

If the dimensions of the eddies are, in fact, mainly influenced by the diameter of the pipe, we should suspect (if the properties of the water and

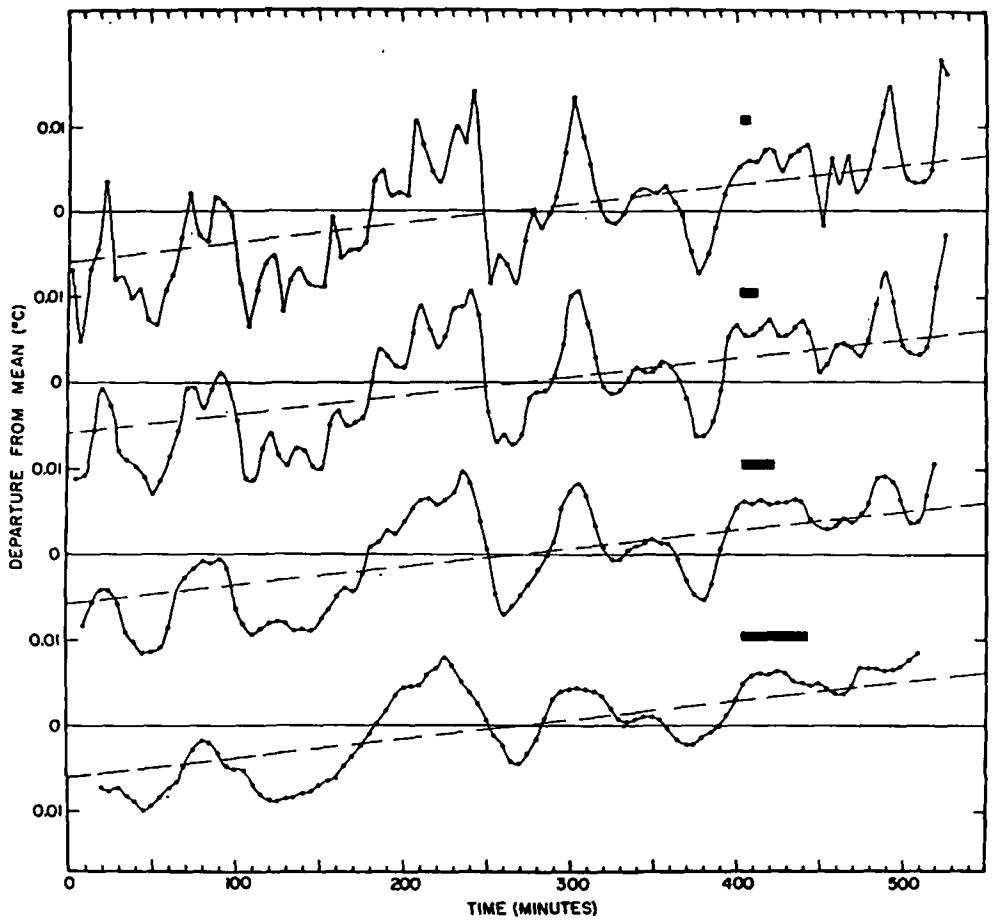

FIG. 5. Moving averages of temperatures recorded at 61 m with system B. Length of bar indicates length of interval averaged. Drift (not removed) caused by change in resistance of test lead is indicated by dashed line.

cells and, hence, amplitude of the oscillation would decrease with decreasing pipe diameter.

STABILITY OF AIR COLUMN

The multi-element thermistor cable (system A) was installed in the air-filled hole on 20 August 1964, where it remained undisturbed until 28 August 1964, when the hole was filled with water. During this interval 25 observations were made at each depth. The average deviation from the mean is less than 0.0005°C and in no case did a single observation deviate more than 0.004°C. Our sensitivity is about 0.002°C; thus, there is no evidence for temperature change.

Temperatures were also measured with a single thermistor probe (system B) at 30 m intervals on 19 August 1964, and again there was no evidence of short period temperature oscillations over the one-hour interval in which the temperatures were monitored at each depth.

This lack of evidence for temperature oscillations, comparable to those found in the water-filled hole, does not necessarily preclude their existence. The time constants of both systems are high frequency components would be greatly attenuated, and we would only expect to see those components having periods greater than an hour. But, we have no evidence for these either.

Even if oscillations existed in the air column, forms similar to those in the water column would not be expected because the response of the hole to a change in temperature of the air would be much quicker (assuming the air to be well stirred). This is a consequence of the fact that the volumetric heat capacity of the air column is less than a hundredth of the heat capacity of the innermost section of casing, whereas the heat capacity of the water column is nearly ten times that of the inner casing.

It might be recalled that the adiabatic gradient in dry air is about 10°C/km and somewhat less in other atmospheres (Hess, 1959). Thus, according to Krige's (1939) formulation, the air-filled hole is much closer to stability than is the water-filled hole, and indeed may be stable in some sections of the hole where the gradient is less than

DIFFERENCE BETWEEN AIR AND WATER TEMPERATURES

The temperatures measured 11 months after the hole was filled with water differ from those in the dry hole by no more than 0.05°C (Table 1). The remaining differences do not involve the water injection disturbance because the decay curves (Figure 7) indicate that it would have dropped to 0.01°C or less in 11 months—a conclusion that can also be reached from theory (Jaeger, 1956). The differences of Table 1 are probably not significant. There is an uncertainty of several hundredths of a degree because of the thermal instability of the water column and the fact that data for less than an hour were averaged to obtain the temperatures. Moreover, anomalous drift rates observed in the laboratory after the experiment suggested that several of the thermistors (results excluded from Table 1) had suffered mechanical or thermal shock when the cable was retrieved from the hole. Conceivably, other thermistors were affected to a less obvious degree.

It seems safe to conclude that the differences between the air- and water-filled holes do not exceed a few hundredths of a degree. The small difference is not surprising, for Hallock (1894) had obtained the same result in a similar experiment. Moreover, if we regard the difference in conditions as one of difference in conductivity, very small differences would be expected from theory (Donaldson, 1959).

Table 1. Difference between temperatures measured in air-filled hole (*Ta*) in August 1964, and in water-filled hole (*Tw*) in July 1965

Depth (meters)	System A *Tw*—*Ta* (Degree centigrade)	System B *Tw*—*Ta* (Degree centigrade)
15	+0.03	
61		−0.02
137	+0.01	
152		−0.03
168	+0.04	
214	−0.05	
259	+0.03	
274	+0.05	−0.03
290	−0.02	
305	−0.01	
321	−0.01	
336	−0.03	−0.03

CONCLUSIONS

The results of this investigation clearly indicate that the water column of a large diameter hole is unstable when the geothermal gradient exceeds a certain value and that this instability manifests itself primarily in vertical water movements of short periods that do not exceed several diameters of the hole. The completely independent investigation of Gretener (1967) yields similar results and, thus, confirms and lends generality to the observation.

A practical result of the instability is that we must expect oscillations of several hundredths of a degree in large diameter holes, the exact amount depending on hole diameter, gradient, and properties of the fluid. Unfortunately, this forms a limit to which the geothermal method can be applied in resolving the details of stratigraphy. Gretener has investigated some ways in which the instability can be reduced.

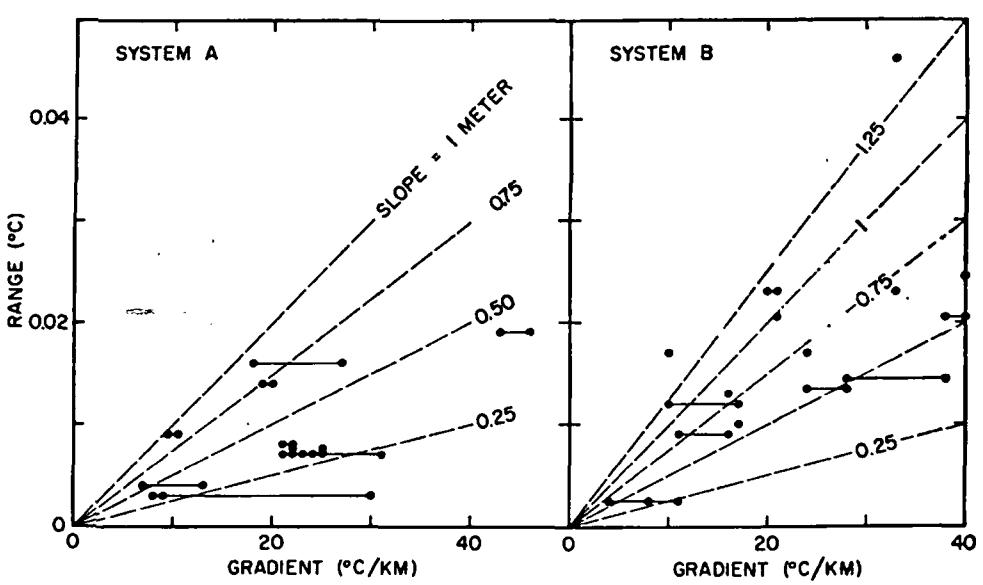

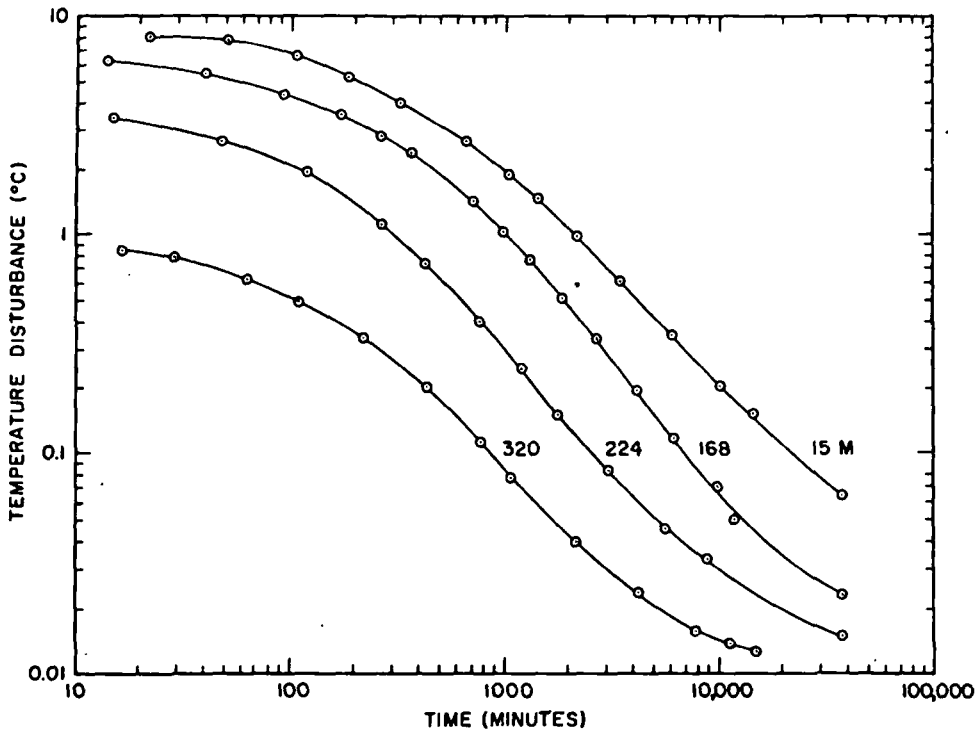

FIG. 7. Typical curves illustrating the decay of the thermal disturbance caused by filling the hole with water. Size of disturbance is based on pre-injection temperatures. Zero time is time at which filling started. Temperatures are uncertain by several hundredths of a degree because of instability of water column.

ACKNOWLEDGMENTS

This work was primarily supported by the U. S. Geological Survey, and I am indebted to A. L. Baldwin, E. D. Saunders, and R. W. Werre of that organization for their assistance in the field and laboratory. G. E. Andreasen, R. A. Robie, D. S. Handwerker, and J. S. Weaver kindly advised computational and programing procedures. S. S. Taylor of the U. S. Bureau of Mines Morgantown Research Center was especially helpful in arranging support for the operation in the field and in providing information on the borehole. I am indebted to P. E. Gretener, A. L. Hales, E. C. Robertson, A. H. Lachenbruch, Gene Simmons, and J. S. Weaver for reading the manuscript.

Publication is authorized by the Director, U. S. Geological Survey.

REFERENCES

Beck, A. E., Techniques of measuring heat flow on land, *in* Terrestrial heat flow: Amer. Geophys. Union, Monograph 8, p. 24–51.

Diment, W. H., and Robertson, E. C., 1963, Temperature, thermal conductivity and heat flow in a drilled hole near Oak Ridge, Tennessee: J. Geophys. Res., v. 68, p. 5035–5047.

Diment, W. H., and Werre, R. W., 1966, Geothermal experiments in a bore hole at Morgantown, West Virginia (abstract): Trans. Amer. Geophys. Union, v. 47, p. 182.

Donaldson, I. G., 1959, Temperature errors introduced by temperature measuring probes: Brit. J. Appl. Phys., v. 10, p. 252–255.

——— 1961, Free convection in a vertical tube with a linear wall temperature gradient: Aust. J. Phys., v. 14, p. 529–539.

Garland, G. D., and Lennox, D. H., 1962, Heat flow in western Canada: Geophys. J., v. 6, p. 245–262.

Gretener, Peter, 1967, On the thermal stability of large diameter wells—an observational report: Geophysics, v. 32, no. 4, p. 727-738.

Hales, A. L., 1937, Convection currents in Geysers: Mon. Not. Roy. Ast. Soc., Geophys. Suppl., v. 4, p. 122–131.

Hess, S. L., 1959, Introduction to theoretical meteorology: New York, Holt, Rinehart, and Winston, 362 p.

Jaeger, J. C., 1956, Conduction of heat in an infinite region bounded internally by a circular cylinder of a perfect conductor: Aust. J. Phys. v. 9, p. 167–179.

Krige, L. J., Bore hole temperatures in the Transvaal and Orange Free State: Proc. Roy. Soc. London, A, 173, 450–474, 1939.

Misener, A. D., and Beck, A. E., 1960, The measurement of heat flow over land, *in* Methods and techniques in geophysics, v. 1: New York, Interscience Publishing, p. 10–61.

Raspet, R., Swartz, J. H., Lillard, M. E., and Robertson, E. C., 1966, Preparation of thermistor cables used in geothermal investigations: U. S. Geol. Survey Bull., 1203-C, p. 1–11.

Robertson, E. C., Raspet, R., Swartz, J. H., and Lillard, M. E., 1966, Properties of thermistors used in geothermal investigations: U. S. Geol. Survey Bull., 1203-B, p. 1–34.

Van Orstrand, C. E., 1924, Temperatures in some springs and geysers in Yellowstone National Park: J. Geol., v. 32, p. 194–225.

GEOPHYSICS, VOL. XXXII, NO. 4 (AUGUST, 1967), PP. 727-738, 17 FIGS., 1 TABLE

ON THE THERMAL INSTABILITY OF LARGE DIAMETER WELLS—AN OBSERVATIONAL REPORT†

PETER E. GRETENER

A fluid in a tube subjected to a thermal gradient will be stable as long as this gradient does not exceed a certain critical value. Observational evidence is presented that the fluid in large diameter wells, such as oil wells, subjected to the normal geothermal gradient is, indeed, unstable as predicted by the theory. Our independent observations support the evidence presented by Diment (1967) in a companion paper.

INTRODUCTION

When a long tube filled with a fluid (or gas) is subjected to a thermal gradient, the fluid will become unstable and start to convect as soon as the gradient exceeds a certain critical value. Hales (1937) treated this problem from a theoretical point of view and derived a formula for the critical gradient. His computation has generally been accepted as a valid criterion (Krige, 1939, Garland and Lennox, 1962, Diment and Robertson, 1963). However, it has often been found (Krige, 1939, Garland and Lennox, 1962) that the theory predicts instability while the measurements indicate stable conditions to prevail. The apparent enigma finds its solution when one looks at the size of the temperature anomalies produced by the instability and the accuracy of earlier temperature measurements. One must keep in mind that Hales' formula only predicts the onset of instability but does not characterize the unstable condition. It is evident that the temperature anomalies produced under unstable conditions will strongly depend on the size of the convection cells set up in the fluid. As long as the individual cells are short, just a few times the diameter of the well, anomalies due to the breaking down and reforming of these cells will be small—too small to be detected by temperature measurements using mercury maximum thermometers. In the following, evidence is presented that this is exactly the situation as encountered in a large diameter bore hole such as an oil well.

Hales' formula reads as follows (in Krige's formulation):

$$\left(\frac{\Delta T}{\Delta Z}\right)_{crit.} = \frac{g\alpha T}{c_p} + \frac{B\nu\kappa}{g\alpha a^4}$$

where

g = acceleration of gravity
α = volume coefficient of thermal expansion
T = absolute temperature
c_p = specific heat
B = constant (216 for a tube where $z \gg 2r$)
λ = thermal conductivity
ρ = density
$\kappa = \lambda/\rho c_p$ = thermal diffusivity
ν = kinematic viscosity
a = radius of the hole

The first term of the above formula gives the onset of convection in the absence of viscosity, whereas the second term takes into consideration the fluid viscosity. For a fluid such as water the first term is usually small, so small that any hole will be unstable under normal geothermal conditions. It is, thus, the second term that is decisive. It contains the well radius to the fourth power in the denominator, which means that the phenomenon of thermal instability is a characteristic of large diameter holes. Table 1 gives a few values for the critical gradient for wells of various diameters. In sedimentary areas the geothermal

† Manuscript received by the Editor 1 November 1966; revised manuscript received 9 January 1967.

* Shell Development Company, Houston, Texas. Now at the Department of Geology, University of Calgary, Calgary, Alberta, Canada.

Table 1. Critical geothermal gradient in °F/100ft

Well Diameter (in inches)		2	5	8
water	77°F	1.6	0.055	0.017
	212°F	0.22	0.004	0.004
crude oil	77°F	55	3.1	0.44
	212°F	5.5	0.22	0.11

gradient is seldom less than 1°F/100 ft and, as a consequence, most oil wells must be thermally unstable.

LOCATION OF TESTS AND INSTRUMENTATION

Our observations were conducted in two wells drilled for oil in the Gulf Coast of Texas, Foster No. 6 and Chapman No. 1 (Figure 1). The former is an abandoned oil well about 50 miles north of Houston, drilled in 1943 to 8289 ft with a 5-inch ID casing. This hole has been idle for many years and was solely used for instrument testing. Chapman No. 1 was drilled in 1962 to 20,800 ft and plugged back to 12,700 ft. It is a dry hole with 8.8-inch ID casing, and at the time of our tests the well had been standing for more than three years. Both wells are, thus, in thermal equilibrium, a fact confirmed by repeated temperature surveys.

Our observations were made with Veco glass bead thermistors (approximately 4500 ohms at 77°F) moulded into a multiconductor Vector cable (Figure 2). Total length of this cable (called X-3) is 1500 ft, and our observations were thus restricted in this regard. The cable contains a total of 14 thermistors spaced over 250 ft. The bottom 4 thermistors are spaced one ft apart while the remaining elements are 25 ft apart.

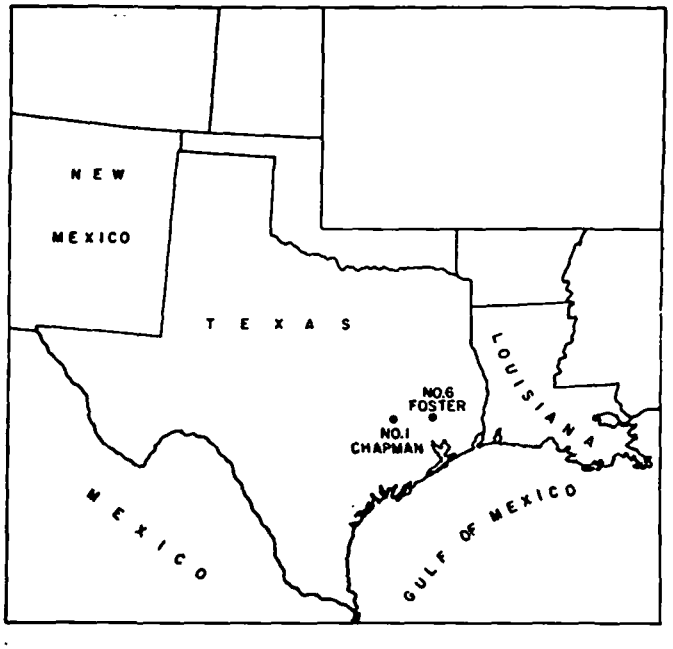

FIG. 1. Location of the test wells.

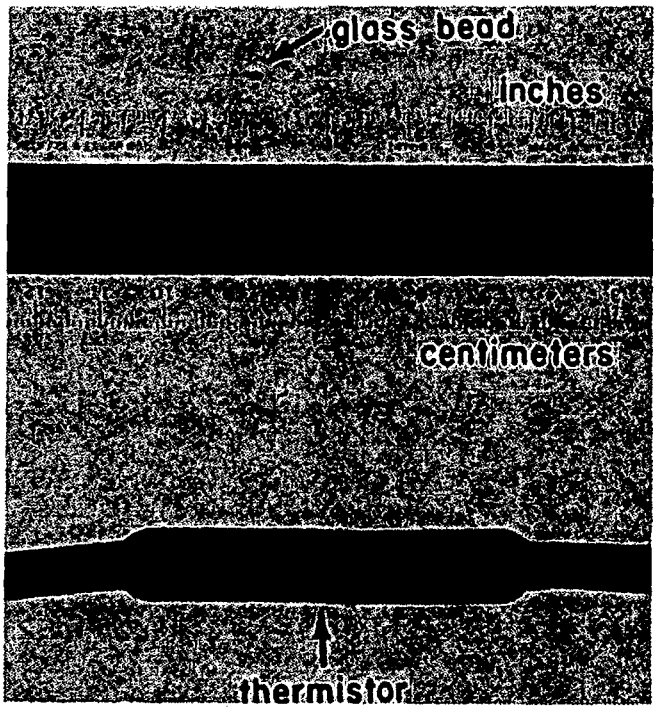

FIG. 2. Veco bead thermistor above scale and moulded into the Vector cable.

Moulding the thermistors into the rubber cable has an adverse effect on the time constant. The response of the thermistors is shown in Figure 3. The response curves were obtained by raising and lowering the cable a certain distance in the hole (a well provides an ideal thermal bath with a thermal gradient). It can be seen that the time required to come within about 5 percent of the new temperature is in the order of three minutes. Temperature variations with a period of less than ten minutes will, thus, not be faithfully recorded.

In order to make our observations, the thermistors were placed at the desired depth in the hole and a permanent record was then made using a four-digit bridge, a Hewlett Packard Nullmeter and a TI Servoriter. The records cover periods of 24 hours or more.

MEASUREMENTS

Observations were made in Foster No. 6 to a depth of 1450 ft. The results of the temperature survey are shown in Figure 4. A large temperature gradient is observed at 600 ft. No explanation is offered as to the cause of this sharp temperature increase. However, the survey has been repeated

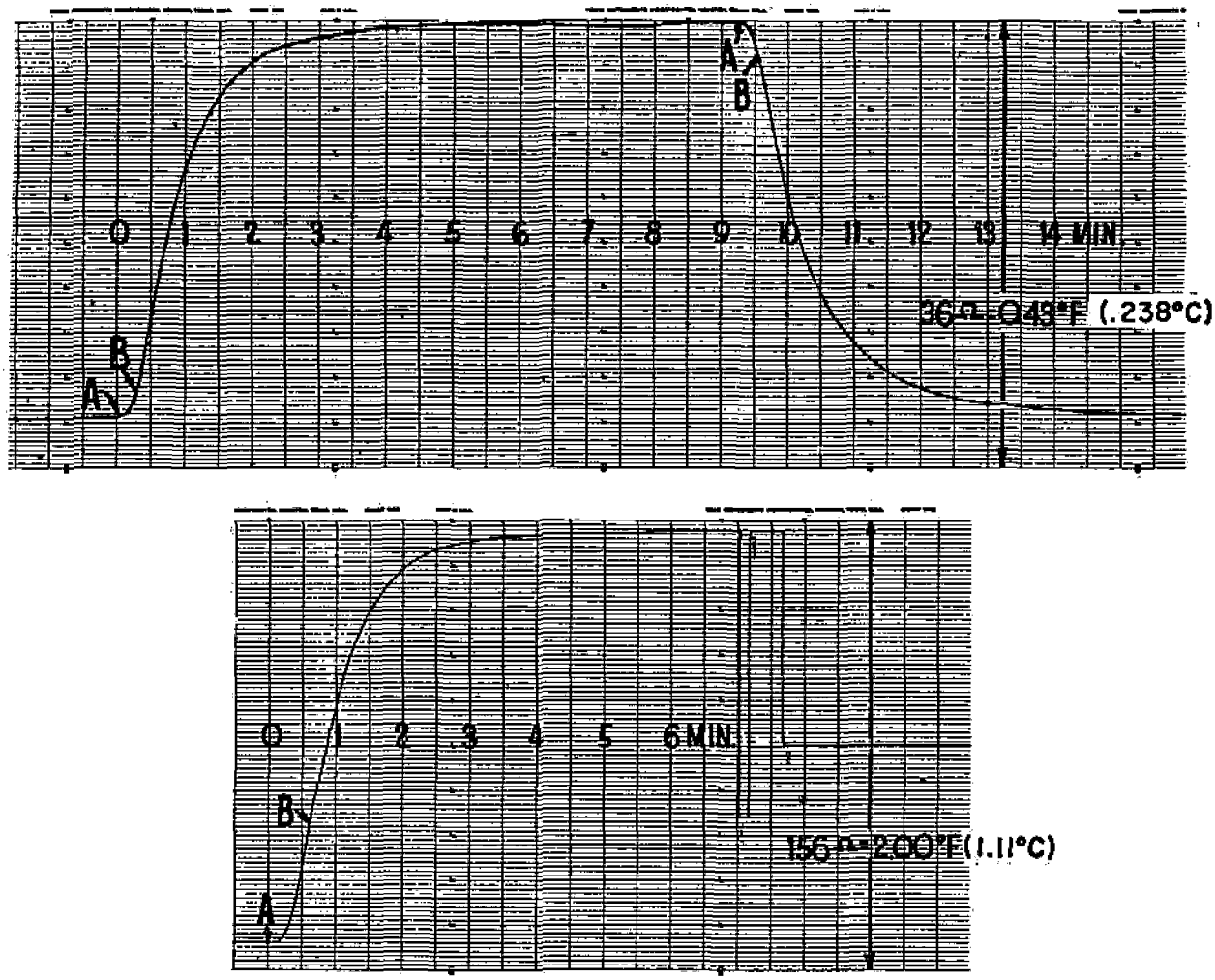

FIG. 3. The time response of the thermistor moulded into the cable. Thermistor no. 17 moved from 381 to 387 m (top); thermistor no. 10 moved from 319 to 349 m (bottom).

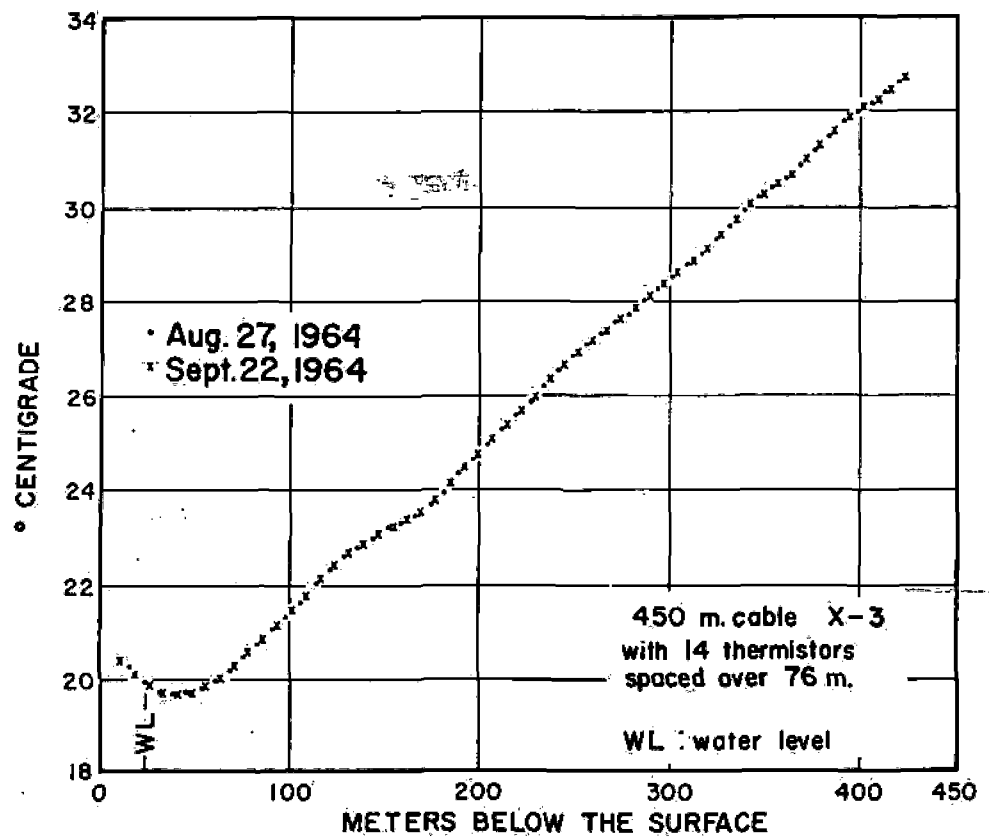

FIG. 4. The temperature depth profile of the well Foster No. 6.

several times over a period of more than a year and the values are fully reproducible within the limits shown below. Figure 5 gives the temperature variations at various levels in the hole while the cable was kept stationary. The fluctuations range from less than 0.02°F to about 0.08°F. The maximum variations are observed in the area of the large temperature gradient.

Figure 6 shows the depth temperature profile for Chapman No. 1. A sharp increase of the temperature with depth is evident at 1200 ft. Again this temperature profile is reproducible. The temperature variations at selected depths in this hole are given in Figures 7 and 8. The maximum variation is again recorded at the depth where the geothermal gradient is largest. Fluctuations range from less than 0.02°F to as much as 0.13°F.

The period of the main fluctuations seems to be in the order of 15 minutes. Longer periods are also indicated in some instances. The shallow records show some drift due to the change of the resistance of the copper wires in response to the varying surface temperature. The change in lead resistance is shown in Figure 9. It is most pronounced for the shallow intervals where most of the cable is on the drum and, thus, exposed to the varying surface temperature. Insulation of the cable will remove any short time changes but not the daily variation as seen in Figure 9. For a depth of 800 ft the double amplitude for 24 hours is about 0.05°F, for the maximum depth of 1450 ft it is less than 0.01°F. Periods of less than ten minutes will

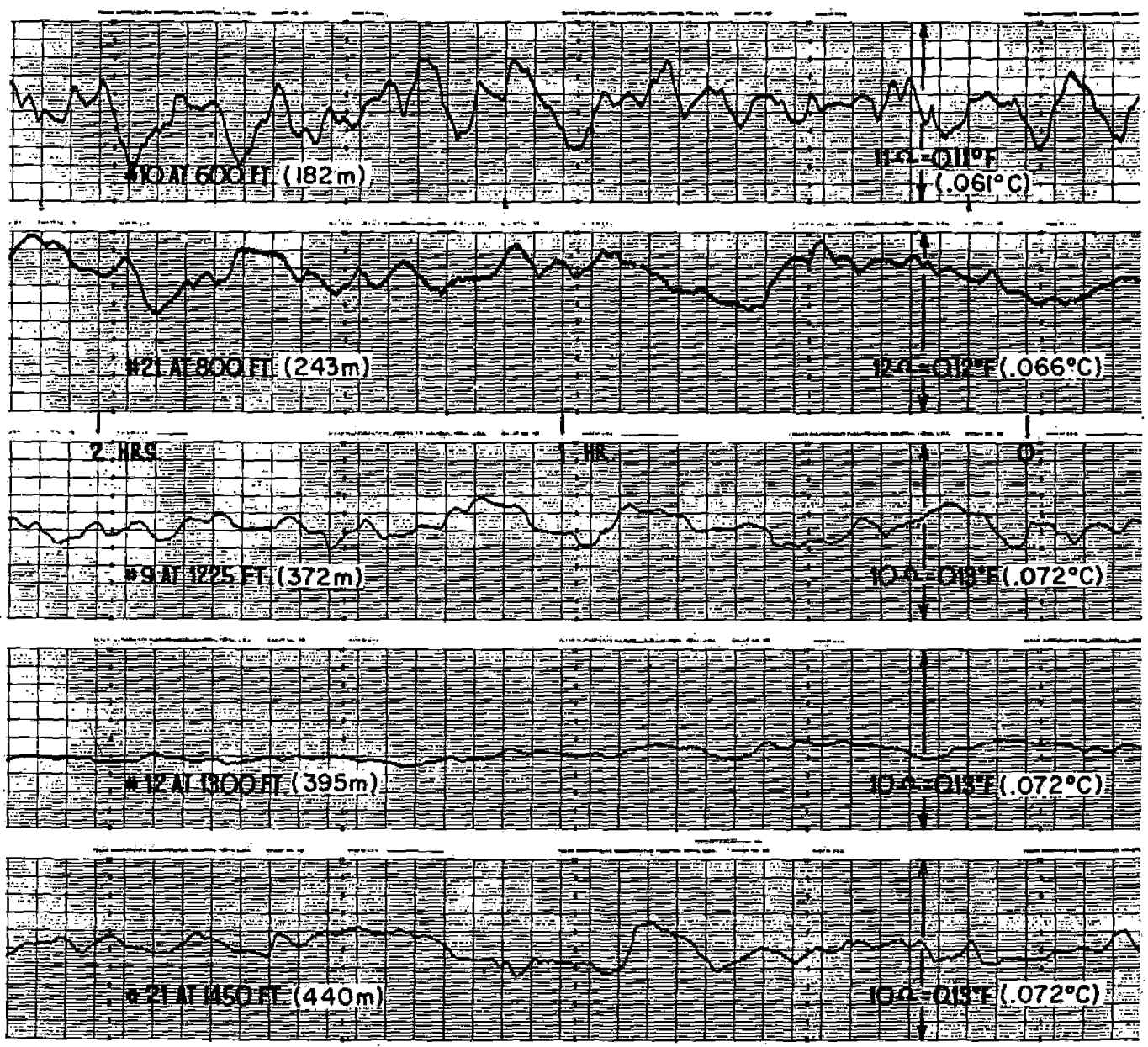

FIG. 5. The thermal fluctuations as recorded at various levels in the well Foster No. 6.

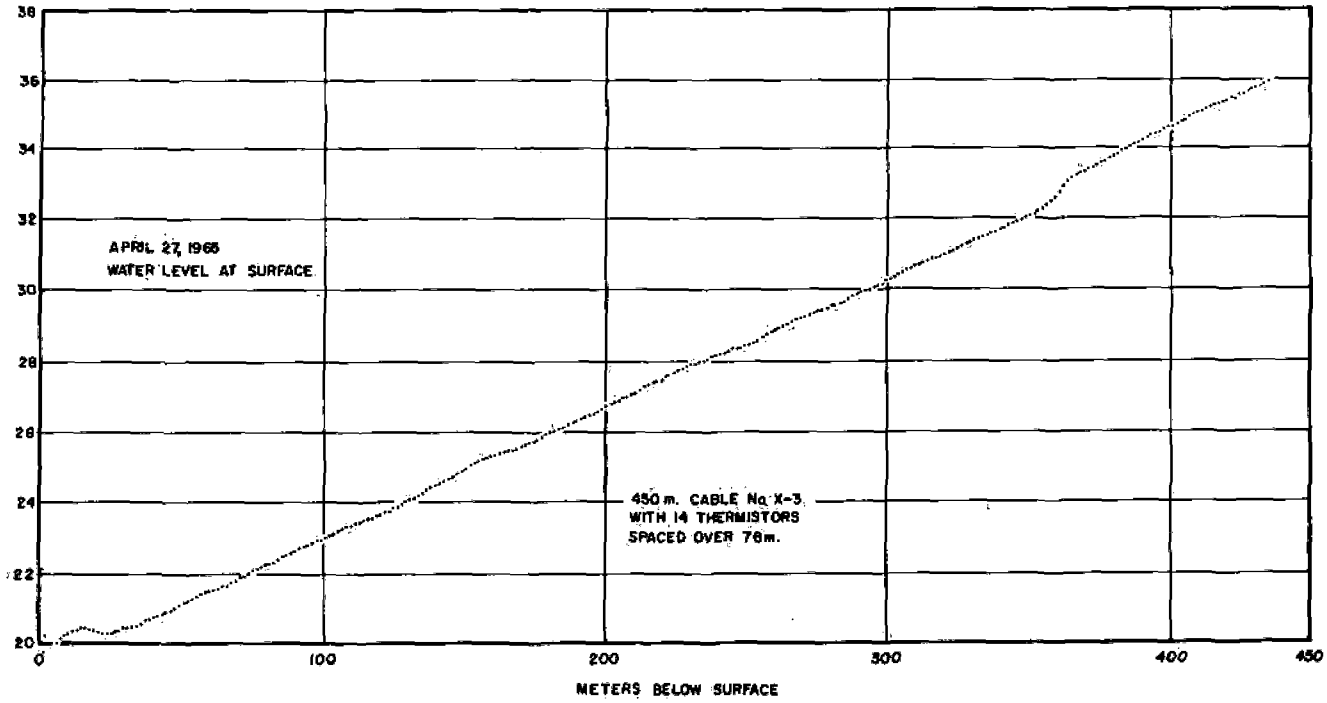

FIG. 6. The temperature depth profile for the well Chapman No. 1.

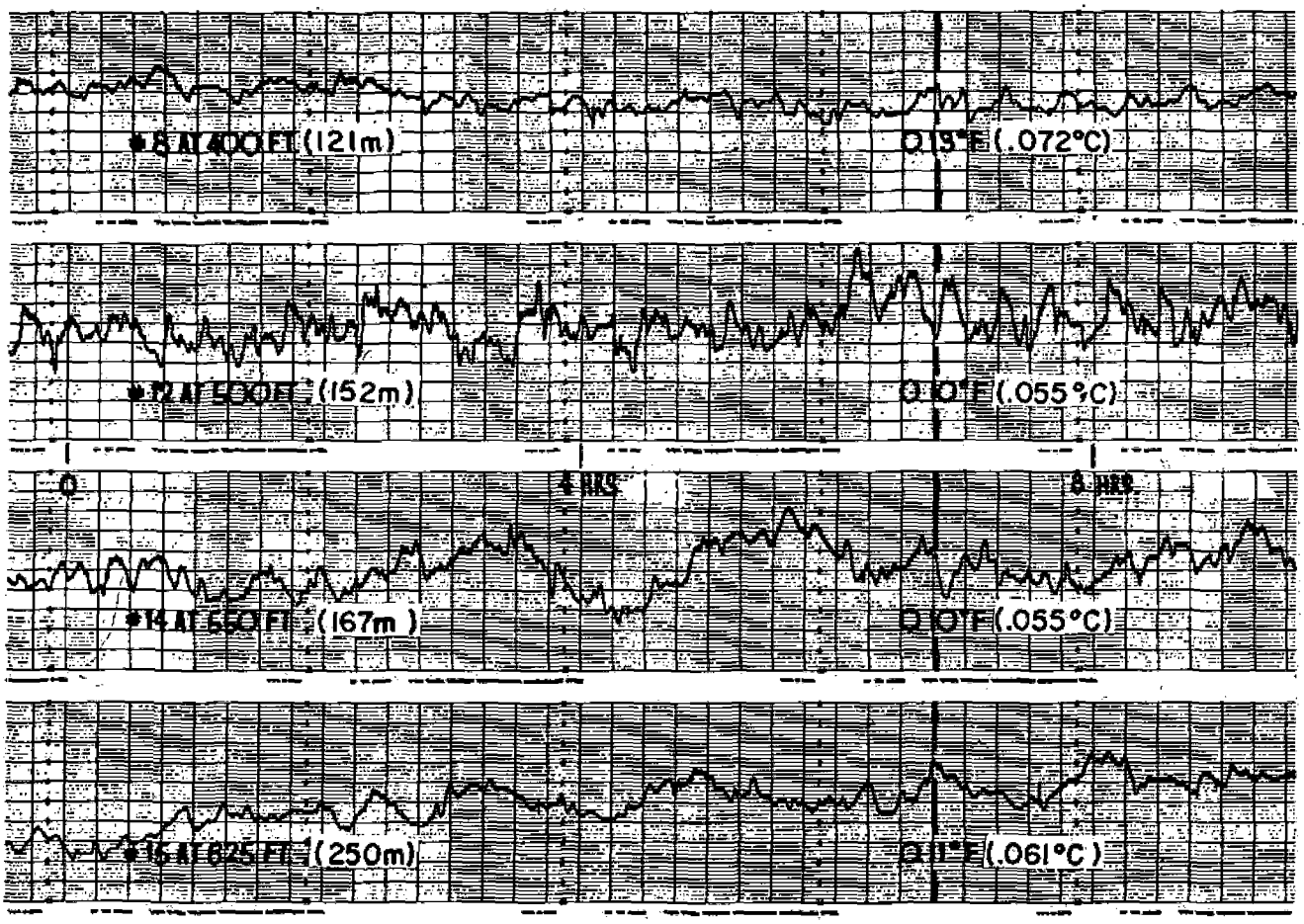

FIG. 7. The thermal fluctuations at selected levels in the well Chapman No. 1.

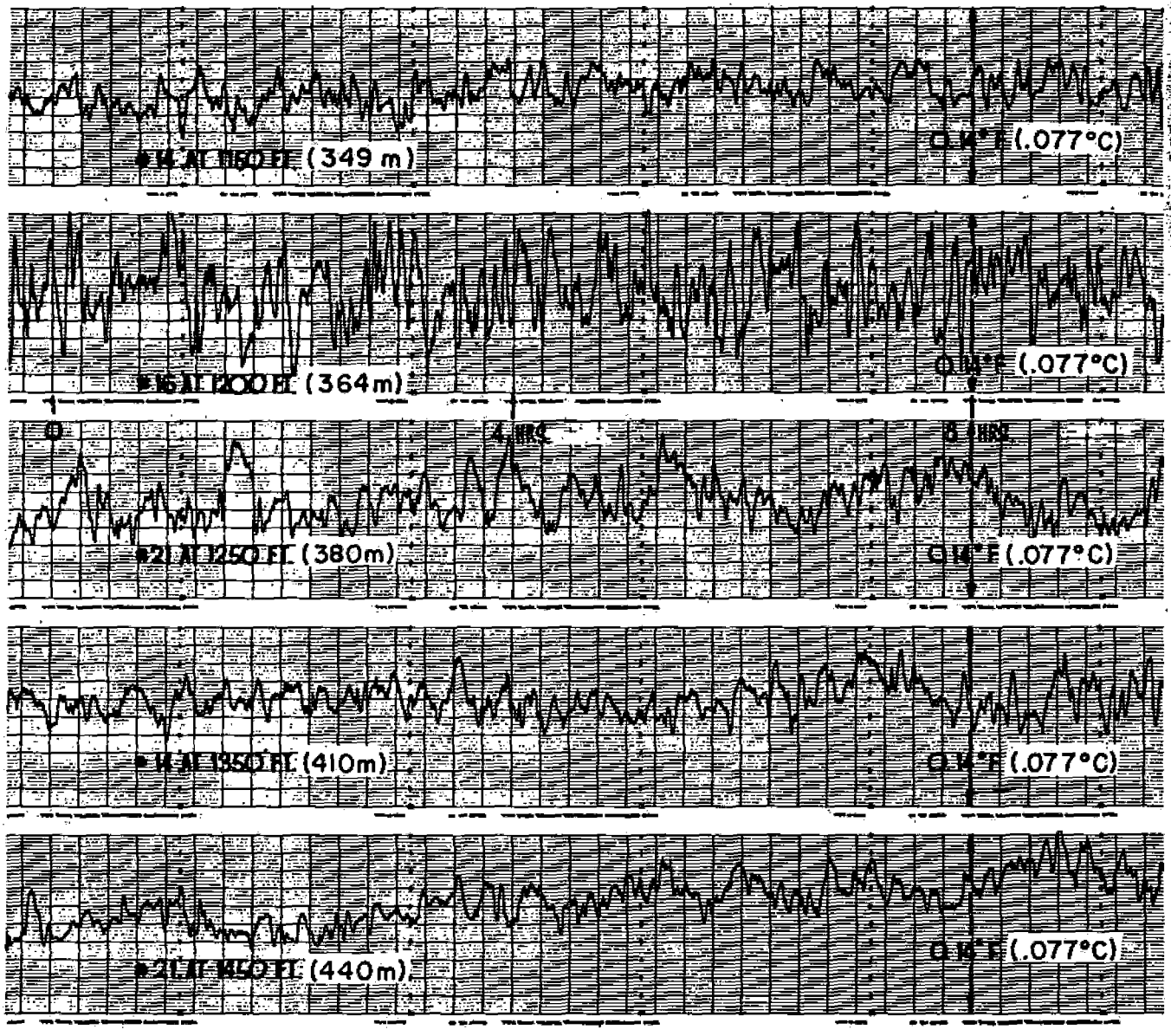

FIG. 8. More thermal fluctuations at selected levels in the well Chapman No. 1.

be increasingly suppressed due to the time constant of the thermistors (Figure 3).

The temperature fluctuations are not induced by the movement of the cable. This is demonstrated in Figure 10 where two records are shown for the same depth with a time interval of eight days, during which the cable remained stationary. No decay of the temperature variations is apparent.

Figure 11 shows a record taken while the thermistor was in an uncontrolled temperature bath. Apart from a slow drift—since the bath is uncontrolled—no fluctuations are registered, thus the system is stable. The observations presented here, thus, truly represent temperature variations within these test holes.

Since some of the thermistors in the cable are spaced very closely, we decided to make some simultaneous recordings with a dual pen recorder. The results are shown in Figures 12 and 13. Figure 12 shows records taken over a distance of three ft, while in Figure 13 we recorded over a distance of one and two ft. In no case is any correlation apparent. In all instances the records run in and out of the phase at random.

STABILIZATION OF THE HOLE

According to Hales' formula, a hole may be stabilized in two ways: either by increasing the fluid viscosity or decreasing the hole diameter. The former requires a complete exchange of the well fluid, a major operation in a deep hole such as our test holes. Thus, we attempted to decrease the hole diameter. For this purpose we lowered the

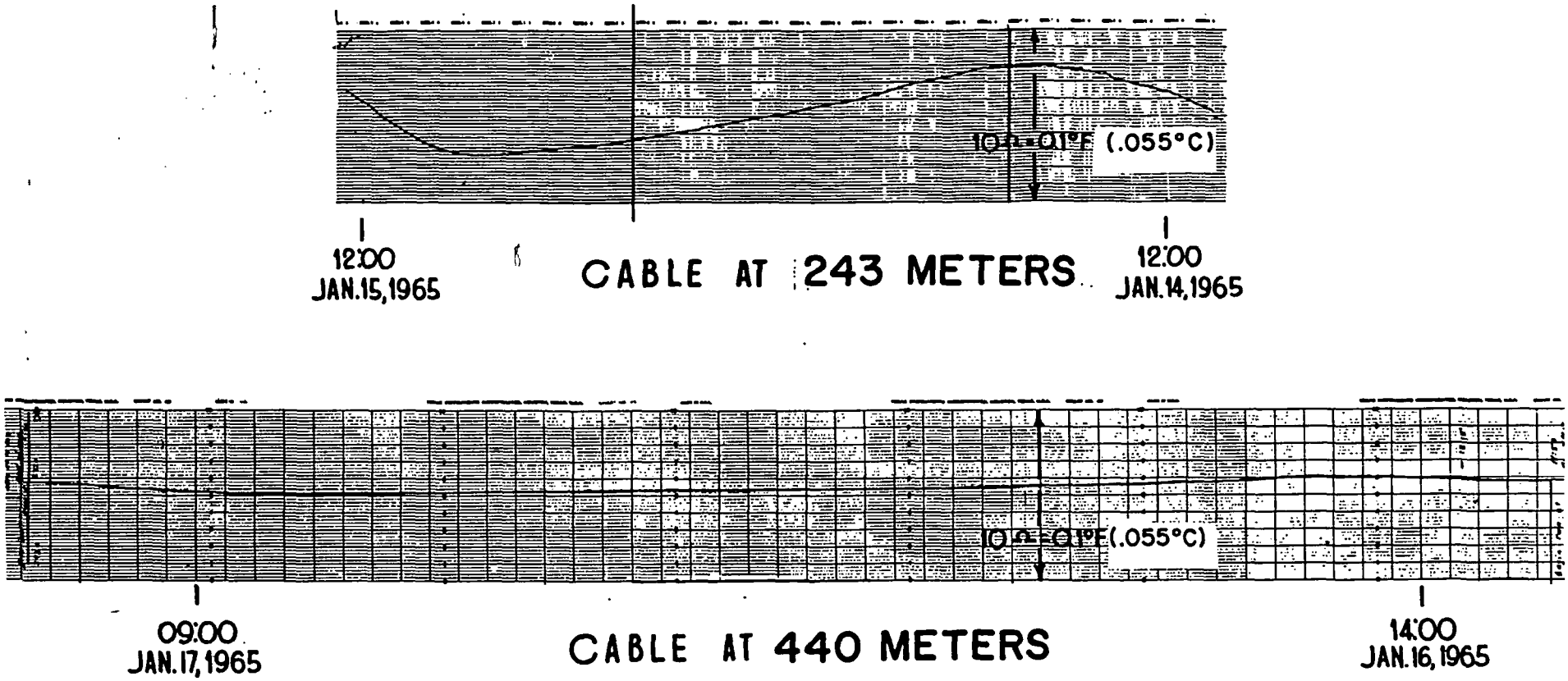

FIG. 9. The change in the lead wire resistance due to the daily temperature variations for different recording levels.

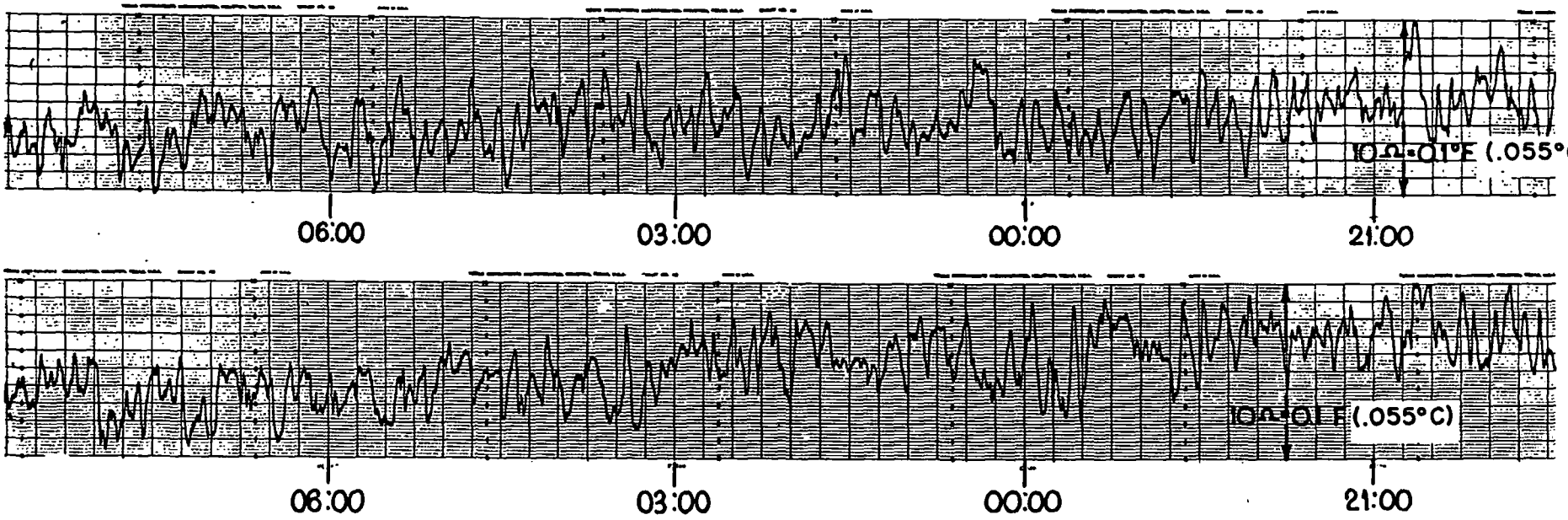

FIG. 10. Temperature variations one and eight days after the installation of the cable at a given depth. Thermistor no. 20 at 182 m; 23, 24 January 1965 (top); 30, 31 January 1965 (bottom).

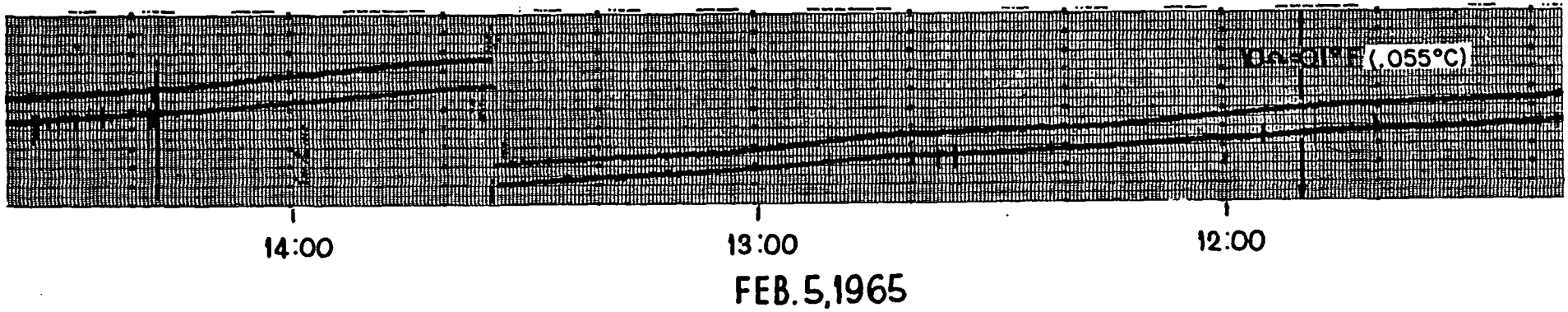

FIG. 11. Thermistors no. 18 and no. 21 in an uncontrolled thermal bath, Feb. 5, 1965.

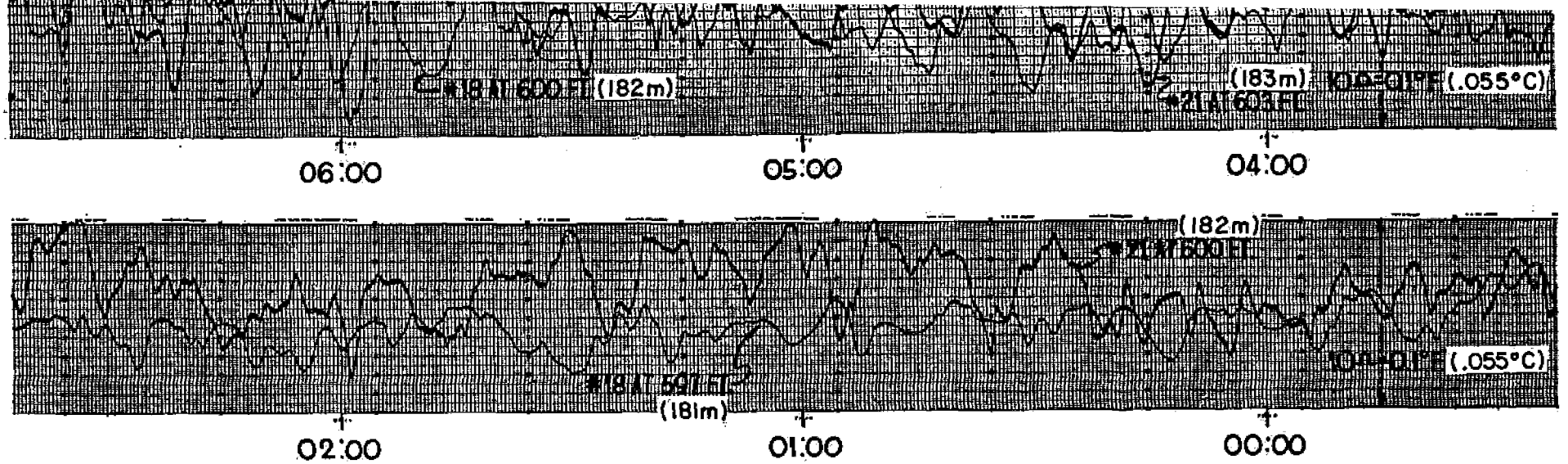

FIG. 12. Records show data obtained simultaneously over a distance of three ft; 3 February 1965 (top); 27 January 1965 (bottom).

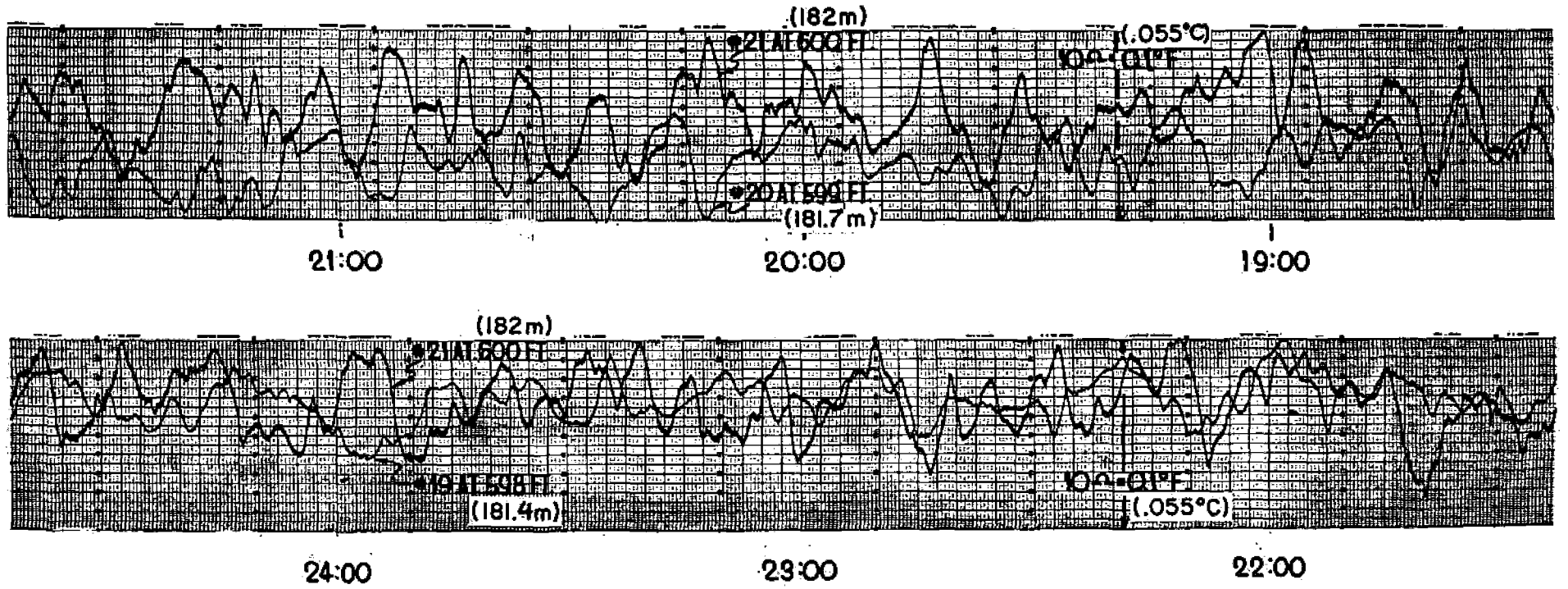

FIG. 13. Recordings taken simultaneously over distances of one ft (25 January 1965, top record) and two ft (29 January 1965, bottom record).

thermistor inside a plastic tube 14 ft long and $1\frac{5}{8}$ inch in diameter. As a test depth we chose 600 ft in Foster No. 6, where previous measurements (Figure 5) had indicated that particularly severe temperature fluctuations existed. Hales' formula indicates a critical hole radius for this part of the well of about one inch. The top record in Figure 14 shows that just previous to our experiment the conditions in the hole were as shown in Figure 5. Lowering the thermistor in the plastic tube reduces the fluctuations to less than half their former value, but stability is not achieved. This is

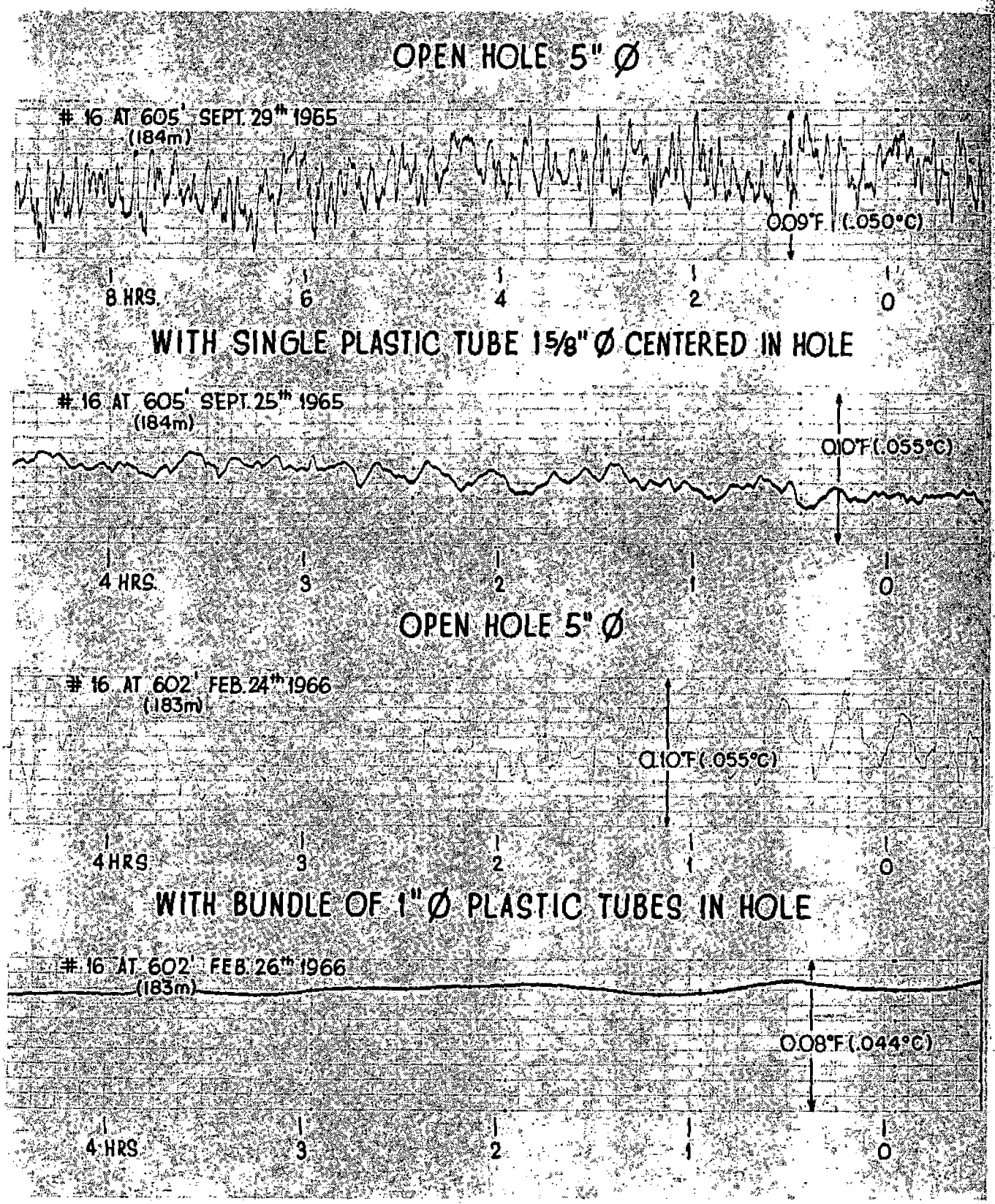

FIG. 14. Stabilization of the well by introducing plastic tubes. Foster No. 6 at 600 ft.

not surprising since the annulus (the plastic tube was equipped with centralizers) is too large to expect stability. In a further attempt, we lowered the bundle of tubes shown in Figure 15. Again the length of the tubes was 14 ft. Record no. 3 in Figure 14 shows that the temperature variations in the open hole are as large as ever. Inserting the bundle of tubes and reducing the hole radius below the critical value leads to stability for all practical purposes (bottom record, Figure 14). Some slight variations of less than 0.01°F and of a period of about one hour might be ascribed to the limited length of our stabilizing equipment, which thus acted as a filter passing some long period disturbances. While the main fluctuations seem to have a period of about 15 minutes, this experiment supports the suspicion that longer period

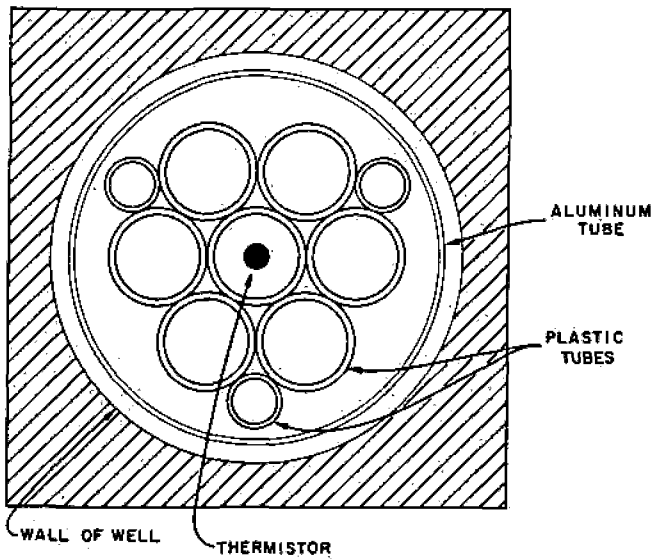

FIG. 15. Cross section of bundle of tubes used to stabilize well. Length of tubes 14 ft.

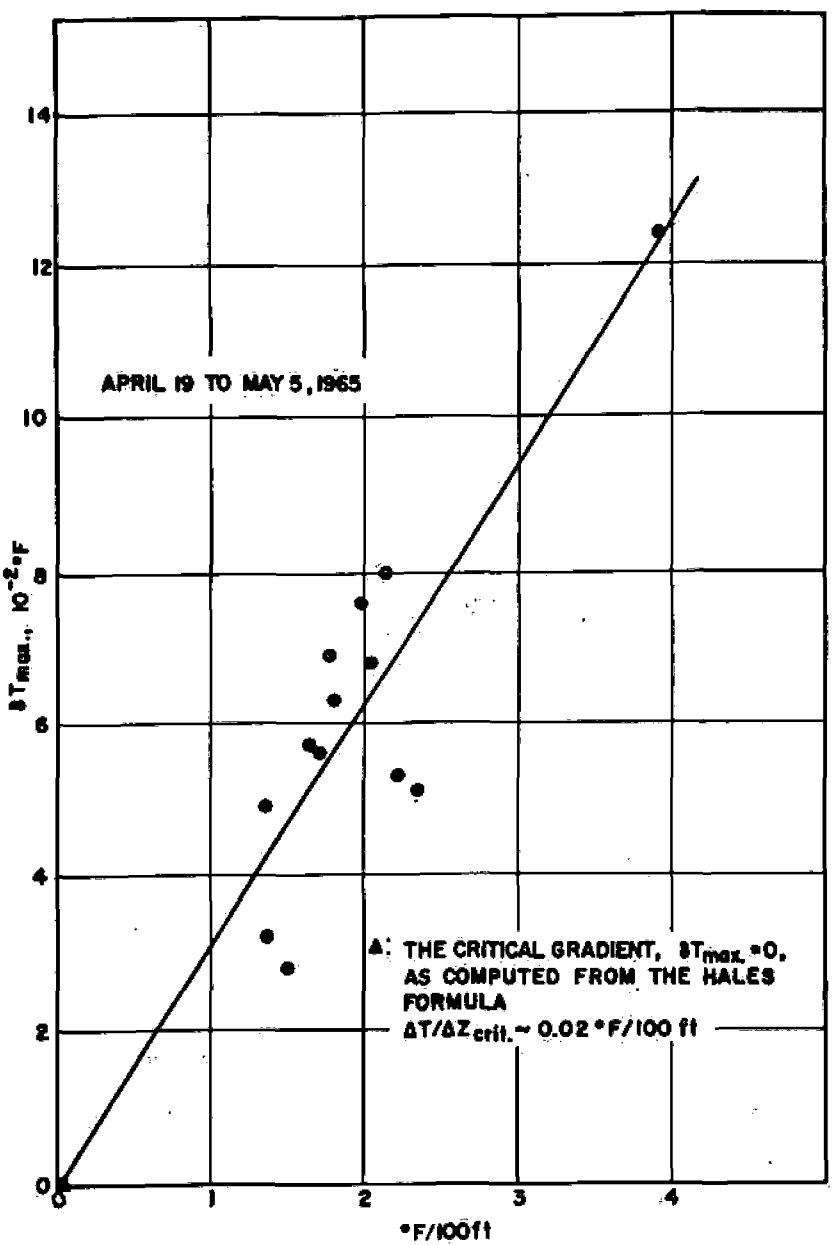

FIG. 16. Plot of the maximum observed temperature variation during any four-hour period on a 24-hour

disturbances are also present. It should be emphasized again that, due to its relatively long time constant, the equipment will not register properly the very short time variations. It is for this reason that no Fourier analysis has been attempted.

INSTABILITY AS A FUNCTION OF THE GEOTHERMAL GRADIENT

In Figures 16 and 17, we have plotted the maximum observed temperature fluctuation within any four hours over a period of 24 hours versus the prevailing geothermal gradient. The correlation factors are 0.90 for Chapman No. 1 and 0.83 for Foster No. 6, indicating a definite correlation, as one would expect. The slopes of the regression lines are 3.12°F/°F/100 ft for Chapman No. 1 and 2.63°F/°F/100 ft for Foster No. 6. This is a small difference in slope considering that the hole diameters differ by a factor of nearly 2. This is explained by the fact that at the time of the measurements Chapman No. 1 was filled with a highly viscous mud while Foster No. 6 contained pure water. The viscosity of the fluid exerts a damping effect as shown in Hales' formula.

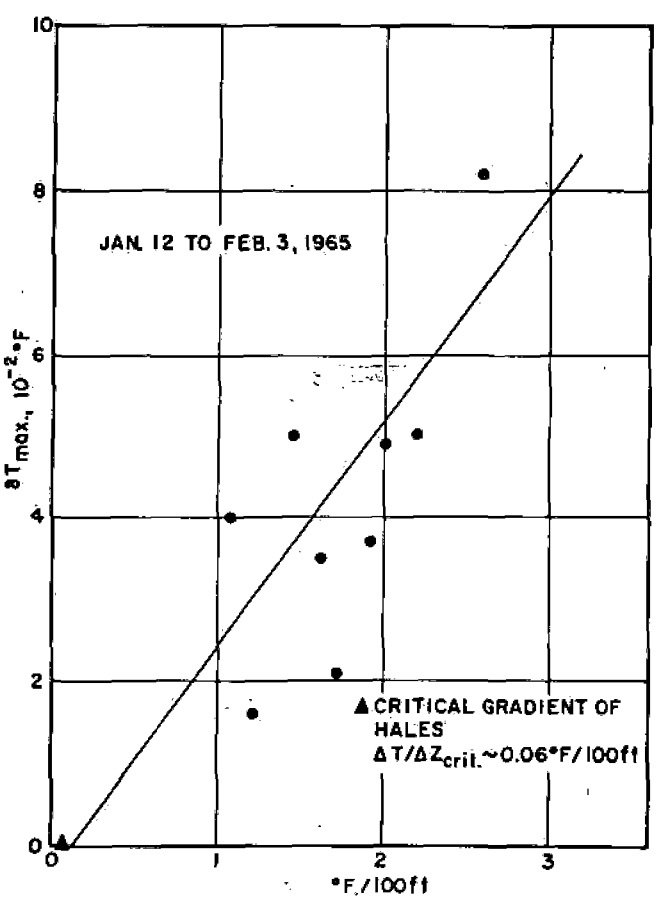

Fig. 17. Same as Figure 16 for Foster No. 6.

Clearly if the described phenomenon is of interest, controlled experiments are needed and not merely casual observations as reported here.

CONCLUSIONS

1. These observations indicate that large diameter wells are thermally unstable as predicted by the theory. Temperature fluctuations are generally small, not exceeding a few hundredths of a degree Fahrenheit.

2. The main period recognized is in the order of 15 minutes. Longer periods seem also to be present. The current equipment did not allow the proper registration of very short period fluctuations.

3. The instability is a function of the geothermal gradient. The double amplitude of the variations increases with increasing gradient for otherwise constant conditions.

4. Simultaneous recordings spaced as closely as one foot did not reveal any correlation in motion.

5. Preliminary experimentation indicates that such holes may be stabilized by either decreasing the well radius or increasing the fluid viscosity.

6. These observations impose a limit on the accuracy to which temperatures may be measured in large diameter wells.

ACKNOWLEDGMENTS

The author wishes to express his appreciation to the Shell Development Company for permission to publish these data. L. D. Park, Jr. has given the author efficient and able assistance in the field and has been responsible for the instrumentation.

REFERENCES

Diment, W. H., and Robertson, E. C., 1963, Temperature, thermal conductivity, and heat flow in a drilled hole near Oak Ridge, Tennessee: J. Geophys. Res., v. 68, no 17, p. 5035–5047.

Diment, W. H., 1967, Thermal regime of a large diameter borehole: instability of the water column and comparison of air and water-filled conditions: Geophysics, v. 32, no. 4, p. 720–726.

Garland, G. D., and Lennox, D. H., 1962, Heat flow in western Canada, Geophys. J., v. 6, p. 245–262.

Hales, A. L., 1937, Convection currents in geysers: Monthly Notices Royal Astron, Soc., Geophys. Supp., v. 4, no. 1, p. 122–132.

Krige, L. J., 1939, Borehole temperatures in the Transvaal and Orange Free State: London, Proc. Royal Soc., A. v. 173, p. 450–474.